Department of Chemistry

Investigation of inhibition processes at sand-deposited surfaces

Vedapriya Pandarinathan

This thesis is presented for the Degree of
Doctor of Philosophy
of
Curtin University

November 2013

Declaration

To the best of my knowledge and belief this thesis contains no material previously published by any other person except where due acknowledgment has been made.

This thesis contains no material which has been accepted for the award of any other academic degree or diploma in any university.

Vedapriya Pandarinathan

Abstract

CO_2 corrosion is an ongoing problem in the oil and gas industry and the deposits present in the production fluids increase the risk of pipeline failures. In this research, the corrosion processes at carbon steel surfaces under mineral deposits in CO_2 environment and their inhibition was investigated. The extent of the corrosion damage was found to be dependent on the deposit characteristics and the deposits increased the risk of localized corrosion both in the presence and absence of the corrosion inhibitors. It was also found that the presence of deposits alters the inhibitor action depending on the chemical nature of the inhibitor. The presence of deposits affected the inhibitor transport through the layer and its availability at the steel surface, hindering the inhibitor from being effective at the steel underneath. Sulphur-containing organic compounds showed low affinity for sand-deposits and subsequently exhibited better inhibition performance at the sand-deposited steels. The behaviour of a corrosion inhibitor directly on the carbon steel surface was monitored by *in-situ* atomic force microscopy, showing surface changes from steel dissolution under uninhibited conditions to the formation of inhibitor aggregates at the surface. The corrosion products formed at sand-deposited steels were identified using synchrotron-sourced infrared microspectroscopy as a mixed layer of chukanovite ($Fe_2(OH)_2CO_3$) and siderite ($FeCO_3$), which is supposed to promote localized attack.

Acknowledgements

My most sincere thanks to my supervisor, Dr. Kateřina Lepková for her greatest support and guidance. Her patience in teaching me every single thing has alone made this thesis possible. I'm thankful to my supervisor Dr. Rolf Gubner for giving me this PhD opportunity and letting me work in his group with large freedom. I thank Dr. Stuart Bailey for his kind acceptance to participate in this research. Thanks to Dr. Thomas Becker for his contribution to the atomic force microscopy work.

I would like to thank Emeritus Professor Wilhelm van Bronswijk and Mr. Peter Chapman for helping me with the spectroscopy work.

Thanks to my friends Amalia, Laura, Mike, Gizelle, Elaine, Karen, Vinod, Varun, Hoda, Mobin and Kod who were such great company. Kriti, Lomas, Jens and Anja are thanked for their support in laboratory.

I thank my parents, little sisters, Brian and Sally and mujju for always being there for me.

Thanks to everyone else who helped me with this research whose contribution has not been possible to mention individually within this space.

Publications

This thesis is assembled by publications, either submitted, under review or accepted which form the individual chapters listed below.

Chapter II

V. Pandarinathan, K. Lepková, S.I. Bailey and R. Gubner "Impact of mineral deposits on CO_2 corrosion of carbon steel" Corrosion 13, NACE International, paper no. 2579 (2013)

Chapter III

V. Pandarinathan, K. Lepková and R. Gubner "Inhibition of CO_2 corrosion of 1030 carbon steel beneath sand-deposits" Corrosion 11, NACE International, paper no. 261 (2011)

Chapter IV

V. Pandarinathan, K. Lepková, S.I. Bailey and R. Gubner "Evaluation of corrosion inhibition at sand-deposited carbon steel in CO_2-saturated brine" Corrosion Science, 72, 108-117 (2013)

Chapter V

V. Pandarinathan, K. Lepková, S.I. Bailey and R. Gubner "Inhibition of under-deposit corrosion of carbon steel by thiobenzamide" Journal of The Electrochemical Society, 160 (9) C432-C440 (2013)

Chapter VI

V. Pandarinathan, K. Lepková and W. van Bronswijk "Chukanovite ($Fe_2(OH)_2CO_3$) identified as corrosion product at sand-deposited carbon steel in CO_2-saturated brine" Corrosion Science, Article in Press

Chapter VII

V. Pandarinathan, K. Lepková, T. Becker, S.I. Bailey and R. Gubner "Adsorption of corrosion inhibitor 1-dodecylpyridinium chloride on carbon steel surface by *in-situ* AFM and electrochemical methods" Industrial & Engineering Chemistry Research, Article in Press

Additional publications relavant to the thesis included in the appendices are listed below.

Appendix 1

V. Pandarinathan and K. Lepková "Investigation of generic inhibitors for general and localized corrosion of sand-deposited carbon steel surfaces under CO_2-saturated conditions" Manuscript to be Submitted

Appendix 2

V. Pandarinathan, K. Lepková, T. Becker and R. Gubner "*In-situ* electrochemical AFM study of CO_2 corrosion of carbon steel" CORSYM 13, NACE International and Gateway India Section, paper no. 38 (2013)

Appendix 3

K. Lepková, W. van Bronswijk, V. Pandarinathan and R. Gubner "Synchrotron infrared microspectroscopy study of the orientation of an organic surfactant on a microscopically rough steel surface" Vibrational Spectroscopy, 68, 204-211 (2013)

I assure that I have obtained, where necessary, permission from all the copyright owners to use any third-party copyright material reproduced in the thesis or to use any of my own published work in which copyright is held by another party.

Statement of Contribution

I, Vedapriya Pandarinathan, as the first author of the publications comprising this thesis was primarily involved in planning and conducting the experiments, data analysis and interpretation of the findings and manuscript preparation. Contributions by the co-authors is mentioned below and the writtten statements from the co-authors are included in Appendix 5.

Kateřina Lepková significantly contributed to the conception of experiments, execution, data interpretation, preparation and appraisal of the manuscripts. Stuart Bailey and Rolf Gubner actively participated in the preparation and critical revision of the manuscripts. Thomas Becker provided technical support for conducting atomic force microscopy (AFM) experiments and contributed to the AFM manuscript preparation. Wilhelm van Bronswijk substantially helped with the experiments conducted at the Infrared Microspectroscopy (IRM) beamline at the Australian Synchrotron, the analysis of results and the preparation of the manuscripts.

The experiments were conducted at the Corrosion Centre for Education, Research & Technology (Corr-CERT) and the Department of Chemistry at Curtin University provided all infrastructures for the project. Australian Synchrotron provided the grants and instrumentation to conduct infrared microspectroscopy experiments. Financial support for this research was offered by Curtin University's International Postgraduate research scholarship (CIPRS) and Woodside Energy Ltd.

Contents

Chapter I

Introduction and Overview

Carbon steel pipelines are widely used for oil and gas transmission and distribution due to the material cost being very economical. These pipelines are subject to internal carbon dioxide corrosion which is a limiting factor for the pipeline integrity.[1,2] Since carbon steels are the preferred option compared to expensive corrosion resistant alloys, great efforts have been made to efficiently use carbon steel and in turn reduce the risk of catastrophic pipeline failures due to corrosion.

In the typical natural gas transportation pipelines, small amount of CO_2 is found due to the co-production of CO_2 gas. In the presence of water, dissolved CO_2 causes the formation of corrosive carbonic acid (H_2CO_3) in oxygen-free, oil field brine solutions.[3] Carbonic acid is very corrosive leading to considerably higher corrosion rates of steel than would be observed in a solution of a strong mineral acid at an equivalent pH.[3] Several reaction mechanisms have been proposed for the dissolution of steel in CO_2-saturated brines[4-6] and the widely acknowledged corrosion reactions are as follows:

$$CO_{2(g)} \rightleftharpoons CO_{2(dissolved)}$$

$$CO_{2(dissolved)} + H_2O_{(l)} \rightleftharpoons H_2CO_{3(aq)}$$

$$H_2CO_{3(aq)} \rightleftharpoons H^+_{(aq)} + HCO_3^-{}_{(aq)}$$

$$Fe_{(s)} \rightarrow Fe^{2+} + 2e^-$$

$$Fe^{2+}_{(aq)} + HCO_3^-{}_{(aq)} \rightarrow FeCO_{3(s)} + H^+_{(aq)}$$

The main anodic reaction is iron oxidation and the main cathodic reaction is reduction of carbonic acid. The overall reaction leading to the formation of iron carbonate ($FeCO_3$) can be written as:

$$Fe + CO_2 + H_2O \rightarrow FeCO_3 + H_{2(g)}$$

The iron carbonate layer formed at the carbon steel surface could be protective or non-protective against CO_2 corrosion depending on the environmental conditions.[7,8]

Corrosion inhibitor treatment is a cost-effective control measure used to lower the CO_2 corrosion damage of carbon steels to acceptable standards in the oil and gas systems.[9]

Under-deposit corrosion (UDC)

In addition to an aggressive CO_2 environment, most oil and gas fields contain deposits that accumulate at the inner surface of the pipelines with low flow rates or during periods of shutdown, leading to a phenomenon termed under-deposit

corrosion (UDC).[10-13] Figure 1 shows an instance of under-deposit corrosion encountered in the field. Typical pipeline deposits include solids carried in the formation waters (silica sand deposits being the primary constituent), corrosion products, hydrocarbons and bio-films, all of which have an effect on the corrosion reactions. In the recent past, concern has increased to understand the UDC process as it is reported as one of the contributing factors for localized corrosion in the form of pitting or mesa attack, eventually causing pipeline failures.[12-15]

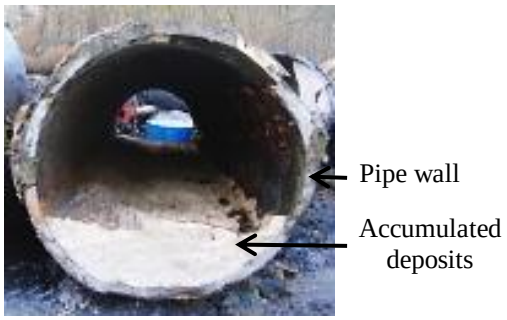

Figure 1. Section of a 12″ diameter pipeline with accumulated deposits.

Though CO_2 corrosion is one of the extensively investigated mechanisms due to its severity and economic impact, corrosion aspects in the presence of deposits have not been largely addressed. Different mechanisms have been proposed for the under-deposit corrosion, the exact principles, however, have not been fully understood. A number of laboratory test methods[12] that differ by design and/or test approach are currently used for UDC testing, but a generally accepted standard method has not been established. Therefore, it is important to develop and standardize test methods that can effectively evaluate the corrosion processes in the presence of deposits.

Test methods used for UDC at ambient pressure

Under-deposit corrosion studies conducted at steel surfaces partially-covered with sand-deposits have proposed that galvanic corrosion occurs due to the sand deposition on part of the steel surface.[13,14] It was shown that the steel area covered with deposit becomes anode and the adjacent area without deposit becomes cathode of the galvanic cell. The potential difference between the anode and the cathode was shown to be the driving force for localized corrosion.[15] In the actual pipeline, since the cathodic area is substantially larger than the anodic area, rapid corrosion takes place at the anodic area under the deposit.

Coupled multi-electrode arrays have also been utilized for UDC studies.[16,17] In this approach, an array of closely-packed smaller electrodes is covered with deposit and coupled to a larger external steel electrode. Steel surface under the deposit was shown to possess more positive corrosion potential than the external electrode. This potential difference was attributed to the locally accelerated corrosion of the electrodes compared to the lower average corrosion rate of the whole array.

In the artificial pit electrode technique used to evaluate the localized corrosion of steel under deposits, galvanic currents were measured between an artificial pit electrode covered with deposits, coupled to a bare electrode without deposits.[18] The galvanic coupling currents were related to the rate of pit propagation.

Studies on carbon steel surfaces completely-covered with deposits[19-22] have shown that the ferrite phase of carbon steel preferentially corrodes leaving behind undissolved iron carbide (Fe_3C). The conductive Fe_3C provides cathodic area and enhances the corrosion of steel under deposits by accelerating the cathodic reactions. The galvanic contact between the Fe_3C lamellae structure and the adjacent steel has been suggested to induce localized corrosion on steels completely-covered with deposits. A decrease in general corrosion rates of steel under deposits compared to the steels without deposits has also been observed. This was related to a combination of surface coverage and mass transfer effects. The deposits reduce the surface area available for corrosion and restrict the diffusion of corrosive species to the steel surface.[21]

This diversity in the UDC test methods and the proposed UDC mechanisms emphasizes the need for further investigations to assess the under-deposit corrosion.

Besides the corrosive environment (with or without deposits) to which the carbon steel surfaces are exposed, another significant factor affecting the corrosion processes is the formation of corrosion products.[7,23] For carbon steel in CO_2-saturated brines, iron carbonate ($FeCO_3$) is the main corrosion product, its formation depending on several factors such as the brine composition, CO_2 partial pressure, temperature, pH, oxygen content, steel microstructure and periods of stagnation. Other corrosion products such as iron oxides (Fe_3O_4), hydroxides ($Fe(OH)_2$), oxy-hydroxides (FeOOH) and hydroxycarbonates ($Fe_2(OH)_2CO_3$) are also likely to form at carbon steel in CO_2 environment.[23-26] However, the corrosion products formed at sand-deposited steels have not been identified to date.

Infrared spectroscopy is one of the analytical techniques used for the corrosion product identification at steel surfaces.[27] With the conventional infrared sources, it is rather difficult to analyse very thin layers of corrosion products and inhibitor films formed at the surface due to the rough and heterogeneous nature of the corroded carbon steel. Application of the high brightness synchrotron radiation is particularly suited for the analysis of thin surface layers and can contribute to the understanding of corrosion principles of carbon steel surfaces.[25,26]

Inhibition of CO_2 corrosion

Injection of film-forming corrosion inhibitors is a common practise to protect the carbon steel pipelines in CO_2 environment, irrespective of the settling of mineral deposits.[28,29] Organic compounds containing nitrogen, oxygen, phosphorous and sulphur are the widely used inhibitors against internal corrosion of carbon steel.[29,30] The basis of the inhibitor action is that the inhibitors form a protective barrier between the steel surface and the corrosive species in pipeline fluids.[30] Inhibitors retard corrosion either by physisorption or chemisorption depending on their chemical structure and the nature of the steel surface. Physisorption is electrostatic interaction between the inhibitor species and the acquired charge on steel surface. Chemisorption involves charge transfer between the inhibitor molecule and the steel surface.

Quaternary ammonium compounds (surfactants) represent one of the most widely used types of CO_2 corrosion inhibitors due to their excellent anti-corrosion ability.[31,32] The performance of quaternary ammonium inhibitors is related to their characteristic structure consisting of a hydrophilic 'head' and a long-chain hydrophobic 'tail'. It is suggested that the inhibitor molecule adsorbs to the anodic or cathodic sites on the steel surface through the head group forming a protective film against corrosion.[31] Surfactant inhibitors exhibit a distinct feature termed the critical micelle concentration (CMC) at which the inhibitor adsorbs at steel as aggregates consisting of monomers.[33] CMC is considered a key parameter in determining the effectiveness of surfactant inhibitors. Figure 2 shows the generally accepted surfactant-inhibitor action at the metal surface.

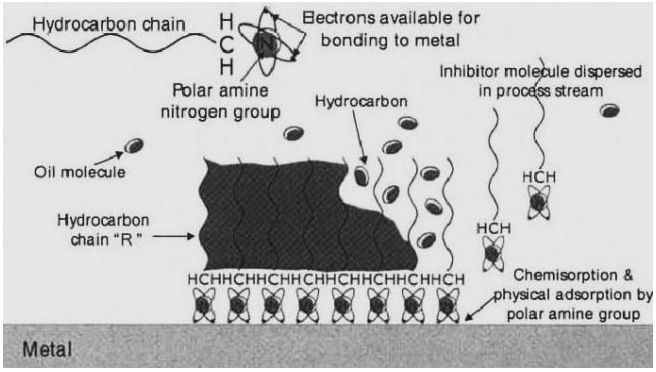

Figure 2. Inhibitor activity at metal surface.[28]

In-situ atomic force microscopy (AFM) is a surface analysis technique utilized for the investigation of surfactant adsorption at model surfaces such as mica and quartz.[34,35] It is one of the mostly sought techniques as the *in-situ* images of adsorbed surfactant aggregates can be acquired with sub-micron resolution. However, the information obtained from surfactant inhibitor behaviour at model surfaces cannot be correlated to its inhibition activity at steel. Therefore, *in-situ* AFM studies at the carbon steel surface as used in the pipelines can determine the adsorbed structures of inhibitors and their relationship to the inhibition effect.

When there are no deposits in the system, CO_2 corrosion inhibitors afford desired level of protection to carbon steel pipelines. In the presence of deposits, inhibitor availability at the steel surface is a critical concern.[36,37] Inhibition failures due to the presence of deposits may lead to higher operational costs and even pipeline shutdown owing to the unpredictable nature of the UDC phenomenon. Therefore, identifying suitable inhibitors to mitigate corrosion under deposits is of great significance to the oil and gas industry.

Corrosion inhibition under deposits largely relies on the diffusion of inhibitors through the deposit layer before the inhibitors can act against the corrosive species. Deposits can reduce the rate of inhibitor transport and/or the inhibitors can preferentially attach to deposit surfaces.[38-43] The impact of mineral deposits on inhibitor performance varies according to the chemical nature and physical characteristics (shape, particle size, porosity, thickness of layer) of the deposits. Corrosion rates are directly proportional to the surface coverage of the steel by the

inhibitor, which in turn is proportional to the concentration of the inhibitor available in the aqueous phase. Parasitic adsorption of inhibitors on deposit surfaces rather than the intended steel surface has been attributed to the enhanced corrosion rates of the deposit-covered steels.[36] Inhibitor application to the steels partially-covered with sand-deposits resulted in the potential difference between the surfaces with and without deposits, accelerating localized corrosion of the deposit-covered surfaces.[13] Corrosion inhibitor performance studies at steels completely-covered with sand-deposits have also showed insufficient inhibition relative to the surface without deposits. This inadequate inhibition was related to the iron carbide (Fe_3C) accumulation at the deposit-covered steels.[20] The variations in the principles proposed for UDC in inhibited systems highlights the need for determining the exact influence of deposits on the inhibitor performance.

The chemical composition and structure of the corrosion inhibitors is another significant factor influencing their behavior at steels in the presence of deposits.[39-43] It has been shown that the corrosion inhibitor formulations with strong affinity for deposit surfaces were depleted from the aqueous phase via adsorption on deposits.[38,39] Adsorption via alkyl chain of the inhibitor's chemical structure on oppositely charged deposit surfaces has been shown for the surface-active corrosion inhibitor compounds.[42,43] However, to better understand the inhibition principles at deposit-covered steels, it is necessary to combine the adsorption studies with the corrosion rate measurements at steel. Therefore, test methods to quantify the extent of inhibitor adsorption on deposits need to be developed and correlated to the inhibitor performance at steels. This approach could aid in identifying the inhibitors that provide sufficient corrosion protection for steels under deposits.

Objectives

The objectives of this research focussing on the inhibition of CO_2 corrosion of carbon steels in the presence of deposits are to:

- determine the effect of mineral deposits on the performance of generic/commercial corrosion inhibitors at carbon steel surfaces exposed to CO_2-saturated brine
- investigate the performance of corrosion inhibitors under sand-deposits for both general and localized corrosion of carbon steel
- develop a test method to determine the extent of inhibitor adsorption on the sand-deposits
- determine the inhibition principles of the best-performing inhibitor compound chosen from the sand adsorption tests
- identify corrosion products formed at the steel surfaces in the presence of sand-deposits using synchrotron-sourced infrared microspectroscopy
- determine if a correlation exists between the adsorbed inhibitor structure and the inhibitor performance at carbon steel using *in-situ* atomic force microscopy

Thesis Outline

This thesis is structured as follows:

Chapter II demonstrates the influence of three types of mineral deposits viz. alumina, silica and calcite on the performance of CO_2 corrosion inhibitors at carbon steel surfaces.

Chapter III shows the performance of a range of generic corrosion inhibitors evaluated at sand-deposited carbon steel surfaces.

Chapter IV presents the test method developed to determine the extent of inhibitor adsorption on the sand-deposits. Correlation between the amount of inhibitor adsorbed on sand deposits and the inhibition effect at the sand-deposited steel surface is also presented.

Chapter V deals with determining the adsorption and inhibition characteristics of the best-performing under-deposit corrosion inhibitor, chosen from the adsorption studies.

Chapter VI presents the synchrotron-sourced infrared microspectroscopy identification of the corrosion products formed at sand-deposited steel surfaces.

Chapter VII shows the relationship between aggregate structure of inhibitor and its performance at the deposit-free steel surface determined using *in-situ* atomic force microscopy.

Additional research findings relevant to the work presented in Chapters II-VII are included in Appendix 1-3.

Appendix 1 presents the evaluation of corrosion inhibitor performance for both general and localized corrosion of sand-deposited carbon steel surfaces.

Appendix 2 presents the preliminary investigation on application of *in-situ* electrochemical atomic force microscopy technique to examine the CO_2 corrosion process at carbon steel surfaces.

Appendix 3 demonstrates the utilization of synchrotron-sourced infrared microspectroscopy to determine the orientation of corrosion inhibitor on the rough carbon steel surfaces.

The test methods used in this research, significance of the study and the main findings are summarized at the end of this chapter along with the suggestions for future work.

Methods

Materials and test solutions

The test material used in this work was carbon steel (1030 grade) with a ferritic-pearlitic microstructure shown in Figure 3. The chemical composition of carbon steel is given in Table 1. Prior to measurements, the steel samples were wet-ground up to 1200 grit SiC abrasive paper, ultrasonically cleaned and dried in nitrogen gas. For *in-situ* surface analysis studies, the steels were ground up to 1200 grit, followed by polishing to < 1 µm using diamond suspensions as required by the sensitivity of the analytical techniques.

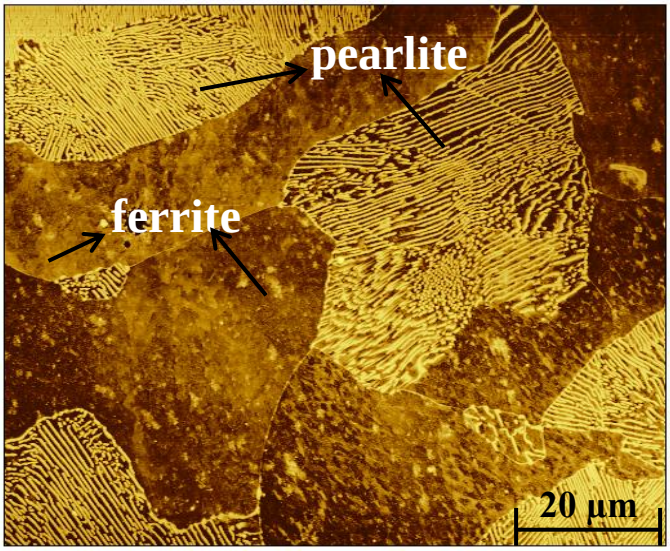

Figure 3. Microstructure of 1030 carbon steel.

Table 1. Chemical composition (weight %) of 1030 carbon steel.

C	Mn	Si	P	S	Cr	Ni	Mo	Sn	Al	Fe
0.370	0.800	0.282	0.012	0.001	0.089	0.012	0.004	0.004	0.010	balance

All the experiments in this study were performed in standard brine solutions comprising of 3 wt% sodium chloride and 0.01 wt% sodium hydrogen carbonate with the corrosion inhibitors added in required concentrations.

The test solutions were saturated with CO_2 (99.99% purity) at atmospheric pressure for 2 h prior to the experiments. The measured initial pH was 4.7 and the dissolved oxygen concentration was less than 20 ppb. This CO_2-saturated test solution was then transferred to the test cell and CO_2 gas was continuously purged throughout the test period. This procedure ensured the removal of oxygen and to sustain dissolved

CO_2 concentration in the test solution. There was no significant change in final pH value measured at the end of the experiments.

Table 2 summarizes the corrosion inhibitors investigated in this study.

Table 2. Chemical formulas and structures of corrosion inhibitors.

Inhibitor	Chemical formula	Chemical structure
1- dodecylpyridinium chloride hydrate (DPC)	$C_{17}H_{30}ClN \cdot H_2O$	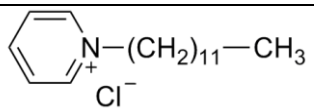
Cetylpyridinium chloride monohydrate (CPC)	$C_{21}H_{38}ClN \cdot H_2O$	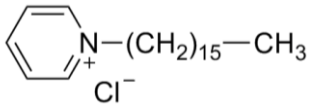
Benzyl dimethyl hexadecyl ammonium chloride (BDHAC)	$C_{25}H_{46}NCl$	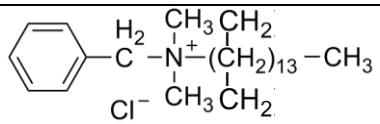
2-mercaptopyrimidine (MPY)	$C_4H_4N_2S$	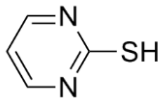
Thiobenzamide (TB)	$C_6H_5CSNH_2$	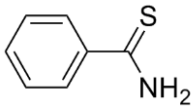

Three different inorganic minerals shown in Figure 4, representative of the major components found in pipeline solids were used as deposits in this study. The deposit characteristics of each mineral are given in Table 3.

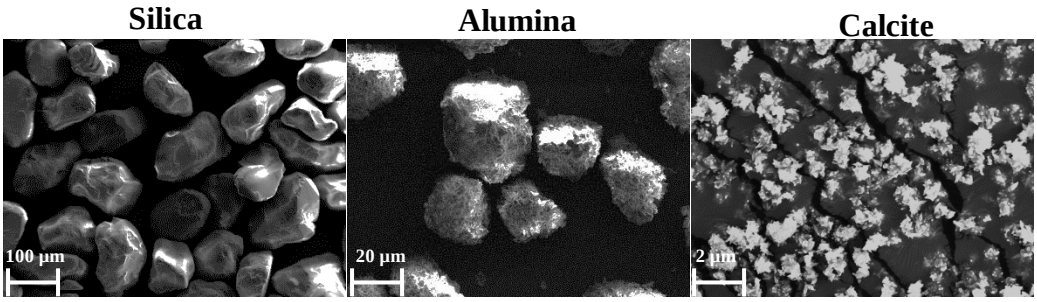

Figure 4. Images of the mineral deposits.

Table 3. Deposit characteristics.

Mineral deposit	Mean particle size µm	Specific surface area m^2g^{-1}
Silica (SiO_2)	303.03	0.055
Alumina (Al_2O_3)	26.88	0.444
Calcite ($CaCO_3$)	2.97	6.412

Experimental techniques

All the experiments were performed separately at carbon steel samples with and without deposits under stagnant CO_2-saturated conditions in the temperature range 30-80 °C.

Electrochemical tests were carried out in a three electrode test cell setup shown in Figure 5. Carbon steel working electrode was soldered to a wire for electrical connection and then embedded in epoxy resin. The exposed surface area of carbon steels samples varied according to the requirements of the experiments. Hastelloy C and saturated Ag/AgCl (3.5 M KCl) with a Luggin capillary were used as counter and reference electrodes, respectively. The sample arrangement at the bottom of the test cell is shown in Figure 6.

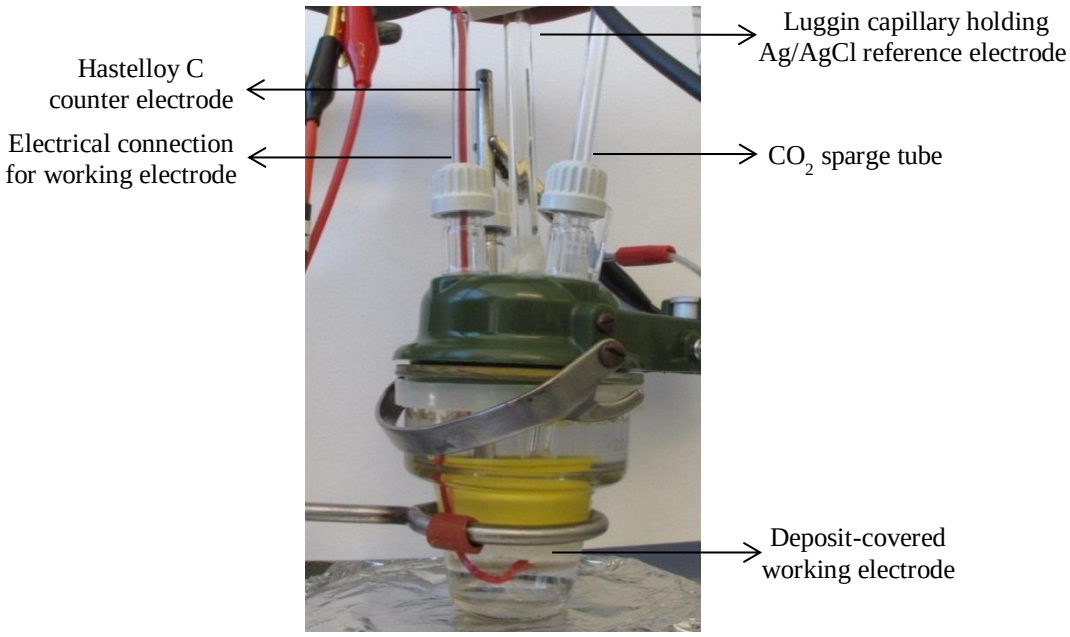

Figure 5. Three-electrode test setup used for the electrochemical measurements.

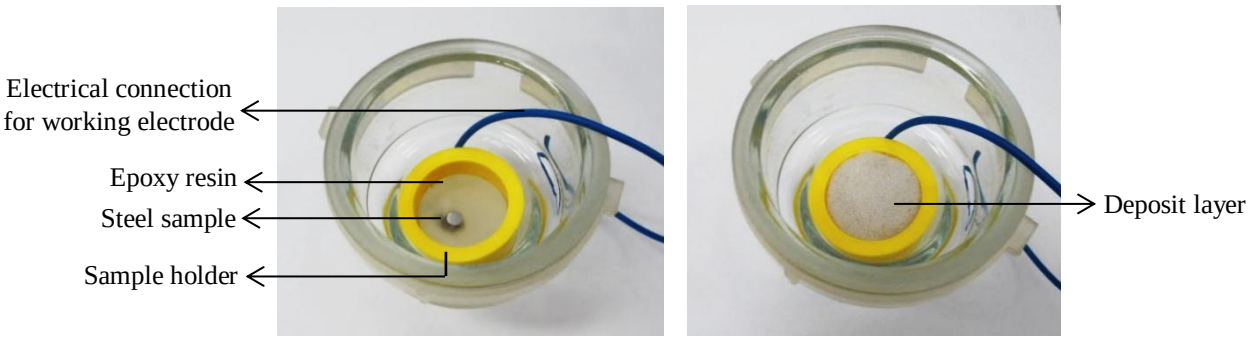

Figure 6. Images of the deposit-free and deposit-covered steel sample arrangement in the test cell.

Electrochemical measurements were conducted to monitor the corrosion rates of steels and to determine the inhibitor efficiencies. Experiments were performed as per the ASTM standard procedures and the techniques used were linear polarization resistance, potentiodynamic and potentiostatic polarization, cyclic voltammetry and electrochemical impedance spectroscopy.

Weight loss measurements were conducted for 15 days and the corresponding corrosion rates were calculated using ASTM standard G1.

Immersion tests were conducted for 29 days. After the exposure period, samples were taken from the solution, dried under nitrogen gas and stored under vacuum until surface analysis.

Scanning electron microscopy and Energy dispersive X-ray spectroscopy were used to analyse the surface morphology and elemental composition of the steels.

Visible-light microscopy was utilized to observe the morphology of the electrochemically treated steel surfaces and to obtain the pit depths and surface roughness values.

Synchrotron-sourced infrared microspectroscopy was used for the identification of corrosion products at steel surfaces and to determine the orientation of adsorbed inhibitor molecules at steel. These experiments were performed at the Infrared Microspectroscopy (IRM) beamline at the Australian Synchrotron.

In-situ atomic force microscopy was utilized to image the aggregate structures of corrosion inhibitor on the steel surface. Contact angle measurements were conducted to determine if the inhibitor adsorbs at the steel surface. Electrochemical atomic force microscopy was employed for *in-situ* monitoring of the corrosion process at the steel-solution interface.

Summary

Corrosion control of carbon steel pipelines is a major concern in CO_2-saturated oil and gas systems, especially in the presence of deposits covering the steel surface. Pipeline deposits negatively impact the corrosion inhibitor performance and promote localized corrosion. This research on the evaluation of CO_2 corrosion inhibitors at the deposit-covered carbon steel surfaces demonstrates that the nature of the mineral deposit influences the effectiveness of the corrosion inhibitors. A test method has been developed to determine the extent of inhibitor adsorption on sand-deposits. Sulphur-containing organic inhibitors exhibited low affinity for sand-deposits and effectively inhibited general corrosion at sand-deposited steels. A relationship between the aggregate structure of a quaternary ammonium inhibitor and its inhibition performance at sand-free carbon steel surface was determined using *in-situ* atomic force microscopy. Chukanovite ($Fe_2(OH)_2CO_3$) was identified using synchrotron-sourced infrared microspectroscopy as the main corrosion product in the mixed layer with siderite ($FeCO_3$) at the sand-deposited steels. The present study contributes to the understanding of under-deposit corrosion of carbon steel in CO_2 environment and its mitigation which is of great significance to ensure reliable operations of the oil and gas systems.

Chapter II examined the effect of mineral deposits alumina, silica and calcite on the corrosion and inhibition processes of carbon steel surfaces. The deposit nature was found to influence the corrosion process and the severity of the corrosion damage of deposit-covered steels was in the sequence alumina-deposited > calcite-deposited > silica-deposited. Electrochemical tests revealed that the general corrosion rates of steels covered with deposits were lower than the steels without deposits. The lower general corrosion rates of deposit-covered steels indicated that deposits block the active surface area on steel and/or act as a diffusion barrier for the corrosive ions from test solution reaching the underlying steel. Surface analysis showed that the steel surfaces covered with deposits had sustained localized attack, irrespective of the nature of deposits.

The inhibitor assessment revealed that the activity of inhibitors beneath the deposits varied with the nature of the deposit as well as the chemical structure of the inhibitor. Thiobenzamide exhibited good inhibition effect at carbon steels under all three deposits and was found to be the most effective inhibitor among the three

compounds tested. Cetylpyridinium chloride and a commercial formulation were less effective at silica and alumina-deposited steels compared to calcite-deposited steels, but their performance was found to improve with increase in inhibitor concentration. This quantifiable difference in the activity of inhibitors beneath the deposits indicated that these compounds adsorbed on the deposits depending upon their chemical nature. A test method developed for the evaluation of the adsorption loss of the inhibitors to deposits is presented in Chapter IV.

In **Chapter III,** the performance of generic corrosion inhibitors at sand-deposited carbon steel surfaces was investigated. The inhibitors tested were two quaternary ammonium compounds (Cetylpyridinium chloride and 1-dodecylpyridinium chloride) and a sulphur-containing compound (2-mercaptopyrimidine). The sulphur-containing compound was found to effectively inhibit general corrosion under sand-deposits. The effectiveness of quaternary ammonium compounds reduced in the presence of sand-deposits. The demonstrated differences in the activity of the tested inhibitors at sand-deposited steels can be related to their chemical nature and the adsorption behaviour at sand-deposits. Chapter II and III prompted the development of a test method to quantify the inhibitor adsorption on sand-deposits.

A test method for determining the extent of inhibitor adsorption on sand-deposits was developed in **Chapter IV**. For this purpose, UV-Vis spectroscopy technique was utilised to measure the concentration of inhibitors in test solutions before and after their contact with silica sand. Based on the amount of the inhibitor adsorbed, its affinity for the deposits was determined. It was found that the sulphur-containing compounds that adsorbed to a lesser extent at the sand-deposit exhibited high inhibition effectiveness at the sand-deposited steels. The quaternary ammonium compounds that adsorbed in large quantities at sand possessed lower inhibition effect due to the concentration loss to sand-deposits. The higher level of adsorption of quaternary ammonium inhibitors on sand-deposits is due to charge attraction and alkyl-group interactions. Contrarily, the lesser or no adsorption of sulphur-containing inhibitors on sand is due to low affinity of those compounds for sand. This shows that the preferential adsorption of inhibitors on sand-deposit is influenced by their chemical nature. It was deemed important to study the best-performing inhibitor in the under-deposit corrosion scenario in detail to better understand the principles of

the UDC inhibition. The results in Chapter IV have shown that thiobenzamide was the most effective inhibitor under sand-deposits. This finding on the suitability of thiobenzamide as under-deposit corrosion inhibitor was substantiated in the study in Chapter V.

Chapter V determined the inhibition principles of thiobenzamide at sand-deposited steels. The mode of inhibition was found to be spontaneous adsorption at the steel surface through the S atom of the thiobenzamide molecule. Thiobenzamide offered sufficient inhibition to steels with and without sand deposits at all concentrations tested. However, inhibition was accomplished in shorter duration when treated with higher inhibitor concentration. The inhibition effect of thiobenzamide was similar for steels surfaces with and without sand deposits at low temperature, while a difference in the inhibition activity was observed at elevated temperature. Surface morphology of corroded steels showed that general corrosion takes place at surfaces without sand deposits. However, localized corrosion was observed at surfaces with sand deposit, both in the presence and absence of thiobenzamide. The results revealed that thiobenzamide is an efficient inhibitor for the mitigation of general corrosion under sand-deposits.

In **Chapter VI,** the corrosion products formed at sand-deposited steels were identified using synchrotron-sourced infrared microspectroscopy. Chukanovite ($Fe_2(OH)_2CO_3$) and siderite ($FeCO_3$) were identified as corrosion products at the sand-deposited steels. In this mixed corrosion product layer, chukanovite was the main product detected. Transformation of chukanovite to siderite was also observed. At steel surfaces without sand-deposit, siderite was the only corrosion product. Both steels with and without sand-deposits exhibited similar general corrosion rates, but localized corrosion was observed at sand-deposited steels. This difference in the corrosion behaviour of the steels with and without sand-deposits is attributed to the presence of sand-deposit which results in the formation of mixed layer of corrosion products (chukanovite and siderite) causing localized corrosion.

Chapter VII presents the investigation of the adsorption behaviour of corrosion inhibitor, 1-dodecylpyridinium chloride (DPC) at carbon steel surface using *in-situ* atomic force microscopy. The adsorption of inhibitor molecules at steel increased the

hydrophobicity of the surface. The results revealed a correlation between the adsorbed aggregate structure of the inhibitor and its inhibition effect. *In-situ* observation of the steel surface in CO_2-saturated conditions showed that DPC adsorbs as hemispherical aggregates when supplied at its critical micelle concentration (CMC) and as cylindrical aggregates at a concentration higher than CMC. The inhibitor performance showed that cylindrical aggregate structure offered better protection compared to the hemispherical structure. It was found that the cylindrical inhibitor aggregates formed faster under the mildly corrosive N_2-saturated conditions compared to the CO_2-saturated conditions.

The investigation in **Appendix 1** is an extension of the CO_2 corrosion inhibition studies at carbon steel surfaces under sand-deposits, with an emphasis on assessing the corrosion inhibitor effectiveness to mitigate general as well as localized corrosion. The study enabled to determine that the sulphur-containing inhibitor, 2-mercaptopyrimidine was efficient against both general and localized corrosion of steel under sand-deposits. It was found that the quaternary ammonium inhibitors (Cetylpyridinium chloride, 1-dodecylpyridinium chloride, Benzyl dimethyl hexadecyl ammonium chloride) which were less effective against general corrosion of sand-deposited steels also sustained localized corrosion attack.

Appendix 2 presents the preliminary results of the application of *in-situ* electrochemical atomic force microscopy (ECAFM) technique for the investigation of the carbon steel surface under CO_2-saturated conditions for the first time. The formation of corrosion product at the steel surface was monitored simultaneously with the corrosion rates. The decrease in corrosion rate corresponded to the protectiveness of the corrosion product film formed at the surface which was identified as iron carbonate. Combination of corrosion rate monitoring capability with the simultaneous imaging of the surface makes *in-situ* ECAFM a powerful technique to investigate the corrosion processes at carbon steels.

There have not been detailed studies regarding the adsorption/orientation of inhibitor species at carbon steel in particular, due to the difficulties in characterizing thin inhibitor films at the heterogeneous and rough carbon steel surfaces. This limitation can be overcome by using synchrotron-sourced surface analysis techniques that have

a superior brightness and signal-to-noise ratio which prompted the investigation shown in Appendix 3.

The objective of the synchrotron infrared microspectroscopy study in **Appendix 3** was to determine the orientation of inhibitor 1-dodecylpyridinium chloride (DPC) at carbon steel surface. It was found that DPC adsorbed at steel through the pyridinium ring positioned parallel to the surface with the aliphatic chain part of the molecule slightly tilted from the perpendicular.

Future work

This work demonstrates that the nature of the mineral deposit uniquely affects the CO_2 corrosion and its inhibition processes at the carbon steel surfaces. Deposits present in the oil and gas fields are usually a complex mixture of several mineral components. Hence, it is essential to determine the combined effect of the mineral components in the actual field deposits. Understanding the impact of the filed deposits on the inhibitor performance will enable to develop efficient corrosion inhibitors for field applications.

The test method developed in this study to determine the extent of inhibitor adsorption on sand-deposits enabled the identification of the inhibitors with low affinity for sand-deposits which were effective at the sand-deposited steels. The test method can be applied to further evaluate the affinity of inhibitors with different chemical structures for various mineral deposits. This will aid in formulating corrosion inhibitors with low adsorption affinity to a particular deposit, thus be an appropriate inhibitor choice to protect deposit-covered steels.

It was evidenced that the deposits affected the inhibition activity under conditions where deposits were present at steels before applying the inhibitors. It would also be useful to investigate the impact of deposits on steel surfaces treated with inhibitors before the introduction of the deposits. This will enable to determine if inhibition can be maintained underneath the deposits.

Despite numerous inhibitor activity studies at model surfaces, investigations at carbon steels are sought-after since carbon steel surface is considered as a realistic representation of the surface used in oil and gas pipelines. *In-situ* atomic force microscopy (AFM) investigation at carbon steel surface in this work demonstrated that the structure of inhibitor aggregates formed at the steel affects its inhibition activity. Application of *in-situ* AFM to determine the relationship between the

aggregate structures of inhibitors and their performance at steel can enable the prediction of efficient inhibitor structures.

A preliminary investigation on the applicability of *in-situ* electrochemical atomic force microscopy (ECAFM) was also conducted in this work and the full capability of the technique for corrosion and inhibition studies at carbon steels is to be further investigated. Successful use of ECAFM can lead to the determination of relationships between the corrosion rates/inhibitor efficiencies and the morphology of the surface layers.

The results obtained from the synchrotron-sourced infrared microspectroscopy in the present study established that the technique enables the identification of thin surface layers and the inhibitor orientation on rough steel surfaces. Further use of synchrotron-sourced infrared microspectroscopy to characterize the carbon steel surfaces can be valuable for determining the orientation of corrosion inhibitors and the assessment of corrosion products formed at the surface.

References

1. M.B. Kermani, A. Morshed, Carbon dioxide corrosion in oil and gas production - A compendium, Corrosion, 59 (8) (2003) 659-683.
2. S. Nesic, Key issues related to modelling of internal corrosion of oil and gas pipelines - A review, Corrosion Science, 49 (2007) 4308-4338.
3. C. DeWaard, D.E. Milliams, Carbonic acid corrosion of steel, Corrosion, 31 (5) (1975) 177-181.
4. S. Nesic, J. Postlethwaite, S. Olsen, An electrochemical model for prediction of corrosion of mild steel in aqueous carbon dioxide solutions, Corrosion, 52 (4) (1996) 280-294.
5. B.R. Linter, G. Burstein, Reactions of pipeline steels in carbon dioxide solutions, Corrosion Science, 41 (1999) 117-139.
6. G. Schmitt, Fundamental aspects of CO_2 corrosion, Advances in CO_2 corrosion, Corrosion 84, NACE International, paper no. 10 (1984).
7. A. Dugstad, Mechanism of protective film formation during CO_2 corrosion of carbon steel, Corrosion 98, NACE International, paper no. 31 (1998).
8. G. Schmitt, M. Horstemeier, Fundamental aspects of CO_2 metal loss corrosion-Part II: Influence of different parameters on CO_2 corrosion mechanisms, Corrosion 06, NACE International, paper no. 112 (2006).
9. J.A. Dougherty, Controlling CO_2 corrosion with inhibitors, Corrosion 98, NACE International, paper no. 15 (1998).
10. M.M. Salama, Influence of sand production on design and operations of piping systems, Corrosion 00, NACE International, paper no. 80 (2000).
11. J. Huang, B. Brown, X. Jiang, B. Kinsella, S. Nesic, Internal CO_2 corrosion of mild steel pipelines under inert solid deposits, Corrosion 10, NACE International, paper no. 379 (2010).
12. J.R. Vera, D. Daniels, M.H. Achour, Under deposit corrosion (UDC) in the oil and gas industry: A review of mechanisms, testing and mitigation, Corrosion 12, NACE International, paper no. 1379 (2012).
13. A. Pedersen, K. Bilkova, E. Gulbrandsen, J. Kvarekval, CO_2 corrosion inhibitor performance in the presence of solids: Test method development, Corrosion 08, NACE International, paper no. 632 (2008).

14. J. Han, Y. Yang, S. Nesic, B. Brown, Roles of passivation and galvanic effects in localized CO_2-corrosion of mild steel, Corrosion 08, NACE International, paper no. 332 (2008).
15. R. Nyborg, Initiation and growth of mesa corrosion attack during CO_2 corrosion of carbon steel, Corrosion 98, NACE International, paper no. 48 (1998).
16. I.G. Winning, A. Linde, G. Jones, E. Gulbrandsen, J. Palmer, C. MacPherson, N. MacAllan, Development of a corrosion inhibitor and comparison of testing methodologies for corrosion mitigation in an export pipeline experiencing localized corrosion under deposits, Eurocorr 07, European Federation of Corrosion, paper no. 1045 (2007).
17. A. Turnbull, G. Hinds, P. Cooling, S. Zhou, A multi-electrode approach to evaluating inhibition of under deposit corrosion in CO_2 environments, Corrosion 09, NACE International, paper no. 445 (2009).
18. A. Turnbull, D. Coleman, A.J. Griffiths, P.E. Francis, L. Orkney, Effectiveness of corrosion inhibitors in retarding the rate of propagation of localized corrosion, Corrosion, 59 (3) (2003) 250-257.
19. J.L. Mora-Mendoza, S. Turgoose, Fe_3C influence on the corrosion rate of mild steel in aqueous CO_2 systems under turbulent flow conditions, Corrosion Science, 44 (2002) 1223-1246.
20. K. Lepková, R. Gubner, Development of standard test method for investigation of under-deposit corrosion in carbon dioxide environment and its application in oil and gas industry, Corrosion 10, NACE International, paper no. 331 (2010).
21. J. Huang, B. Brown, Y.S. Choi, S. Nesic, Prediction of uniform CO_2 corrosion of mild steel under inert solid deposits, Corrosion 11, NACE International, paper no. 260 (2011).
22. J. Been, T.D. Place, B. Crozier, M. Mosher, T. Ignacz, J. Soderberg, C. Cathrea, M. Holm, D. Archibald, Development of a test protocol for the evaluation of under deposit corrosion inhibitors in large diameter crude oil pipelines, Corrosion 11, NACE International, paper no. 263 (2011).
23. J.L. Crolet, N. Thevenot, S. Nesic, Role of conductive corrosion products in the protectiveness of corrosion layers, Corrosion, 54 (3) (1998) 194-203.
24. S. Savoye, L. Legrand, G. Sagon, S. Lecomte, A. Chausse, R. Messina, P. Toulhoat, Experimental investigations on iron corrosion products formed in

bicarbonate/carbonate-containing solutions at 90°C, Corrosion Science, 43 (2001) 2049-2064.

25. R. De Marco, Z.T. Jiang, B. Pejcic, E. Poinen, An in situ synchrotron radiation grazing incidence X-ray diffraction study of carbon dioxide corrosion, Journal of The Electrochemical Society, 152 (10) (2005) B389-B392.
26. B. Ingham, M. Ko, G. Kear, P. Kappen, N. Laycock, J.A. Kimpton, D.E. Williams, *In situ* synchrotron X-ray diffraction study of surface scale formation during CO_2 corrosion of carbon steel at temperatures up to 90°C, Corrosion Science, 52 (2010) 3052-3061.
27. P. Marcus, F. Mansfield, Analytical methods in corrosion science and engineering, CRC Press, Taylor & Francis Group, 2006.
28. J.W. Palmer, W. Hedges, J.L. Dawson, A working party report on the use of corrosion inhibitors in oil and gas production, European Federation of Corrosion Publications (2004).
29. J.W. Palmer, Corrosion control by film forming inhibitors, Corrosion 06, NACE International, paper no. 119 (2006).
30. B. Sanyal, Organic compounds as corrosion inhibitors in different environments-A review, Progress in Organic Coatings, 9 (1981) 165-236.
31. R. Atkin, V.S.J. Craig, E.J. Wanless, S. Biggs, Mechanism of cationic surfactant adsorption at the solid-aqueous interface, Advances in Colloid and Interface Science, 103 (2003) 219-304.
32. D. John, A. Blom, S. Bailey, A. Nelson, J. Schulz, R. De Marco, B. Kinsella, The application of neutron reflectometry in the study of inhibitor films, Physica B: Condensed Matter, 385-386 (2006) 924-926.
33. S. Bosenberg, D. John, T. Becker, S. Bailey, R. De Marco, Resolving the structure of carbon dioxide corrosion inhibitors on surfaces, Australasian Corrosion Association (2007) 819-828.
34. S. Nishimura, P.J. Scales, S.R. Biggs, T.W. Healy, AFM studies of amine surfactant hemimicelle structures at the mica-water interface, Colloids and Surfaces A: Physicochemical and Engineering Aspects, 103 (1995) 289-298.
35. H. Patrick, G.G. Warr, S. Manne, I.A. Aksay, Surface micellization patterns of quaternary ammonium surfactants on mica, Langmuir, 15 (1999) 1685-1692.

36. E. Gulbrandsen, J. Kvarekval, A. Dugstad, Parasitic consumption of corrosion inhibitor by produced solid particles in multiphase flow, Eurocorr 03, European Federation of Corrosion, paper no. 177 (2003).
37. J. McMahon, J.W. Martin, L. Harris, Effects of sand and interfacial adsorption loss on corrosion inhibitor efficiency, Corrosion 05, NACE International, paper no. 274 (2005).
38. J.A.M. de Reus, E.L.J.A. Hendriksen, M.E. Wilms, Y.N. Al-Habsi, W.H. Durnie, M.A. Gough, Test methodologies and field verification of corrosion inhibitors to address under deposit corrosion in oil and gas production systems, Corrosion 05, NACE International, paper no. 288 (2005).
39. W.H. Durnie, M.A. Gough, J.A.M. de Reus, Development of corrosion inhibitors to address under deposit corrosion in oil and gas production systems, Corrosion 05, NACE International, paper no. 290 (2005).
40. B.R. Tian, Y.F. Cheng, Electrochemical corrosion behavior of X-65 steel in the simulated oil sand slurry I: Effects of hydrodynamic condition, Corrosion Science, 50 (3) (2008) 773-779.
41. R.C. Woollam, A. Huggins, C. Mendez, J.R. Vera, W.H. Durnie, Localized corrosion due to galvanic coupling between FeS-covered and uncovered areas: another oilfield myth?, Corrosion 13, NACE International, paper no. 2715 (2013).
42. T. Moon, D.I. Horsup, Relating corrosion inhibitor surface active properties to field performance requirements, Corrosion 02, NACE International, paper no. 298 (2002).
43. B.P. Binks, P.D.I. Fletcher, I.E. Salama, D.I. Horsup, J.A. Moore, Quantitative prediction of the reduction of corrosion inhibitor effectiveness due to parasitic adsorption onto a competitor surface, Langmuir, 27 (2011) 469-73.

Chapter II

V. Pandarinathan, K. Lepková, S.I. Bailey and R. Gubner, Impact of mineral deposits on CO_2 corrosion of carbon steel, Corrosion 13, NACE International, paper no. 2579, Orlando, Florida (2013)

Original Reprint of the Publication

Paper No.
2579

NACE INTERNATIONAL CORROSION 2013 CONFERENCE & EXPO

IMPACT OF MINERAL DEPOSITS ON CO_2 CORROSION OF CARBON STEEL

Vedapriya Pandarinathan, Kateřina Lepková, Stuart I. Bailey and Rolf Gubner
Corrosion Centre for Education, Research and Technology
Department of Chemistry
Curtin University
Perth, Western Australia

ABSTRACT

The present study describes the impact of mineral deposits (SiO_2, Al_2O_3 and $CaCO_3$) on CO_2 corrosion of 1030 carbon steel in a chloride-containing environment. The corrosion process was investigated using electrochemical and weight loss measurements, followed by surface analysis of the corroded steels conducted by visible-light and scanning electron microscopy. It was found that the extent of the corrosion damage is directly related to the nature of the mineral deposits and significant differences were observed in the morphology of the surfaces corroded in the presence/absence of different deposits. The susceptibility of the deposit-covered steels to localized corrosion and the influence of deposits on corrosion inhibition are also discussed and related to the properties of the deposits. The inhibitor performance at deposit-covered steels varied according to the chemical composition of the inhibitor and the nature of the deposit. The study serves to improve the understanding of CO_2 corrosion process in the presence of solid deposits and the findings can be applied to address the under-deposit corrosion in oilfield operations.

Key words: carbon dioxide, carbon steel, mineral deposit, corrosion inhibitor

INTRODUCTION

Carbon steel pipelines in oil and gas systems operating under CO_2 environments frequently encounter mineral deposits transported along with formation fluids, which lead to a range of corrosion problems including under-deposit corrosion (UDC). [1] The deposits found in flow lines are often a combination of silica sand (primary inorganic constituent), clays, alumina, hydrated alumina, calcite, iron oxides, sulphides and carbonates, corrosion products, organic compounds etc. There are numerous consequences to the presence of these deposits such as restricted fluid flow, pressure changes, depletion of inhibitor species and alteration of the corrosion mechanisms. Irrespective of the deposit management strategy applied, significant quantities of deposits will remain depending on the fluids carried through the carbon steel pipelines. The deposits cause UDC of the steel thus eventual pipeline failures. [2-4]

The mineral deposits can also have an adverse effect on the effectiveness of corrosion inhibition operations. [5] The uptake of active inhibitor components from the bulk solution by the deposit particles

hinders the inhibitor activity at the steels, leading to higher corrosion rates than predicted by laboratory tests. In addition to impeding the inhibitor transport to the underlying metal surface, locally accelerated iron dissolution rates due to the presence of deposits can retard the rate of adsorption of inhibitors onto the steel. [6]

In the present paper, we examine the role of major mineral components (SiO_2, Al_2O_3 and $CaCO_3$) of the typical deposits found in the production fluids, on the CO_2 corrosion behaviour of 1030 carbon steel. The comparison of experiments done with and without deposits at steel surface is used to determine the changes in corrosion behaviour introduced by the deposit layer and the susceptibility of the steel beneath deposits to localized and/or uniform corrosion. Since the deposits interfere with the inhibition process, the evaluation studies are conducted incorporating the deposits in the tests so as to determine the optimum inhibition conditions required for UDC mitigation. Our previous studies on UDC inhibition [7] demonstrated that silica sand deposits diminished the inhibitor performance and we present the evaluation of three different corrosion inhibitors' performance at the deposit-covered steels in this paper.

EXPERIMENTAL PROCEDURE

Test materials

The material investigated was UNS G10300 carbon steel. Samples with an exposed surface area of 0.196 cm^2 were embedded in resin. The elemental composition of the steel was: C (0.37%), Mn (0.80%), Si (0.282%), P (0.012%), S (0.001%), Cr (0.089%), Ni (0.012%), Mo (0.004%), Sn (0.004%), Al (0.01%), and Fe (balance). Prior to tests, the steel samples were polished down to 1200 grit SiC[(1)] paper, washed with ethanol and rinsed with ultra-pure water (resistivity – 18.2 MΩ cm) to remove any traces of the solvent. The samples were then dried and immediately placed into the test cell.

The test solution (uninhibited) was standard brine consisting of 30 g/L sodium chloride (NaCl; Ajax Finechem[(2)], analytical reagent, 99.9%) and 0.1 g/L sodium hydrogen carbonate ($NaHCO_3$; Merck[(3)], 99.5%) dissolved in ultra-pure water.

Three corrosion inhibitors were investigated; two were reagent grade pure organic compounds, thiobenzamide ($C_6H_5CSNH_2$; Sigma-Aldrich[(4)]) and cetylpyridinium chloride monohydrate ($C_{21}H_{38}ClN \cdot H_2O$; Sigma-Aldrich) and will be referred to as TB and CPC, respectively. The third referred to as inhibitor CF was a commercial inhibitor formulation supplied by an industry partner and its exact composition is not known. The inhibited test solutions were prepared in standard brine solution at the required concentrations. All experiments presented in this study were carried out under stagnant conditions at 30 °C ± 1 °C at 1 bar CO_2 (<20 ppb oxygen).

Mineral deposit characterization

To represent the major components found in pipeline deposits, three common inorganic minerals of analytical reagent grade (Sigma-Aldrich) were used as deposits in this study. The mean particle size and the specific surface area of the deposits are given in Table 1.

The deposit particles were randomly dispersed on carbon tape and coated with a 3 nm Pt coating to be imaged using the Zeiss[(5)] Evo scanning electron microscope (SEM).

[(1)] Trade name.
[(2)] Trade name.
[(3)] Trade name.
[(4)] Trade name.
[(5)] Trade name.

Table 1
Mean particle size and specific surface area of the deposits investigated

Mineral deposit	Mean particle size	Specific surface area
	μm	m^2/g
Silica (SiO_2)	303.03	0.055
Alumina (Al_2O_3)	26.88	0.444
Calcite ($CaCO_3$)	2.97	6.412

Figure 1 presents the scanning electron micrographs of the mineral deposit particles. The size of the scale bars is given in parenthesis. The silica deposit appears as individual grains with rough surfaces (Figure 1a). The micrograph of the alumina particles shows aggregates of smaller grains (Figure 1b) and calcite particles can be seen as a disordered structure of chunks (Figure 1c).

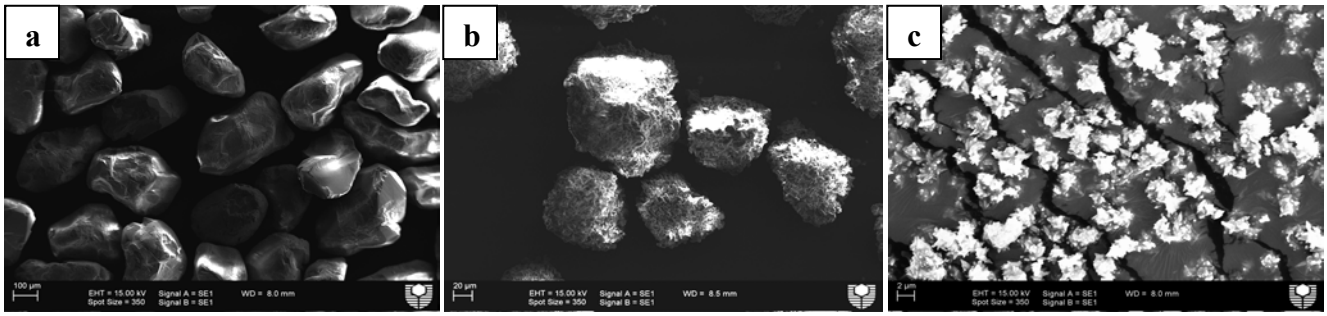

Figure 1: SEM of deposit a) Silica (100μm) b) Alumina (20μm) and c) Calcite (2μm)

In all experiments conducted in the presence of deposits, the polished steel samples were placed at the bottom of the test cell and covered with a deposit layer of consistent thickness ~ 8 mm above the steel (the weight varied for each mineral sample used to form the deposit).

Electrochemical measurements

A three-electrode glass cell setup described elsewhere [7,8] was used to perform the electrochemical measurements using an ACM Gill Potentiostat[(6)]. The counter and reference electrodes used were Alloy UNS N 10276 and saturated Ag/AgCl (3.5 M), respectively.

Linear Polarization Resistance (LPR) measurements of bare steel samples and deposit-covered steels in CO_2 saturated test brine (uninhibited solution) at 30 °C were conducted for 24 h in the potential range of ±10 mV in respect to open circuit potential (OCP). For the inhibitor evaluation tests using the LPR technique, the samples were exposed to test brine solution (uninhibited) for 1 h, after which different concentrations of the selected corrosion inhibitors were dosed into the test solution.

Potentiodynamic polarization measurements of bare steel samples and deposit-covered steels in CO_2 saturated test brine solution at 30 °C were conducted in the potential range of ±0.25 V vs. OCP at 10 mV/min sweep rate. Before each polarization measurement the steels were stabilized at open circuit conditions for 24 h.

The cyclic voltammetry measurements (using Solartron[(7)] 1287 potentiostat) at the bare steel and deposit-covered steels in CO_2 saturated test brine solution at 30 °C were recorded after 300 s at OCP at a sweep rate of 10 mV/s and the detailed measurement procedure is described elsewhere. [7] The

[(6)] Trade name.
[(7)] Trade name.

steel samples after the cyclic voltammetry experiments were rinsed, dried in nitrogen and observed under visible-light infinite focus microscope (Alicona Instruments, Germany) to determine the surface profile parameters such as roughness (Rq) and pit depth. All the electrochemical parameters and the corrosion rates from electrochemical measurements were calculated as per ASTM[8] G102. [9]

Weight loss measurements

Bare carbon steel samples and the deposit-covered steels were immersed in CO_2 saturated test brine solution for a period of 15 days at 30 °C. Four steel coupons were exposed to the test solution under each condition – two samples were used for weight loss measurements and two were taken for surface examination.

After the test period, the weight loss coupons were ultrasonically cleaned for 1 minute, and the weight loss was determined according to the standard chemical cleaning procedure for the corrosion product removal. [10] An analytical balance of ±0.1 mg precision was used to weigh the steel samples before and after the exposure period. The corrosion rates from the weight loss of duplicate coupons (exposed surface area 2.25 cm^2) were determined using the standard ASTM G1 procedure. [10]

The two steel coupons for surface examination were taken at the end of the test duration, rinsed in ultra-pure water, dried in nitrogen gas and stored under vacuum. These samples with the corrosion products were then analysed using the scanning electron microscope (SEM). No chemical treatment was applied to the samples examined under SEM.

RESULTS

Linear polarization resistance measurements

Figure 2 shows the comparison of corrosion rates obtained from the bare steel surface and deposit-covered steels exposed to test brine solution monitored by LPR. The initial corrosion rate of bare steel is higher compared to all three deposit-covered steel surfaces. This can be attributed to the numerous active sites available at the bare steel surface when exposed to corrosive media causing metal dissolution at a faster rate. In the case of the deposit-covered steels, the metal dissolution proceeds slower (i.e. corrosion rates are lower than bare steel) because of the deposit layer acting as a barrier to the transport of corrosive species from the test solution and the release of metal ions from the steel surface. The deposit thus impedes general corrosion at the surface.

The thickness of the deposit layer on the steel was constant, but the layer's characteristics and degree of adherence to the steel will vary according to the nature of the mineral used as deposit. This is reflected in the difference in the corrosion rates between the three deposit-covered steels. In the first hour of exposure to the test solution, the corrosion rates of steels are in the sequence silica-deposited > alumina-deposited > calcite-deposited. The trend is that the corrosion rates are higher for the deposit with the larger particle size. Categorizing the deposits on this basis, it is supposed that the silica deposit is porous, composed of individual grains, compared to a dense homogenous layer of alumina and calcite. Hence, the corrosive ions diffuse quite readily through the porous silica layer contributing to initial higher corrosion rates, less so with alumina, followed by calcite. After 1 h, the corrosion rate of silica-deposited steel gradually decreases and stabilizes at 0.5 mm/yr at the end of 4 h. The corrosion rate of calcite-deposited steel was very low (~ 0.2 mm/yr) for a duration of 4 h which can be ascribed to calcite's closely packed layer above steel surface, restricting the access of reducible species to the steel. Eventually, once the ions have reached the underlying steel (after 4 h), the corrosion rate starts increasing due to the corrosive ions concentrated beneath the calcite deposit. The alumina-deposited steel exhibited higher corrosion rates compared to other two deposits and it kept increasing slowly over

[8] ASTM International, 100 Barr Harbor Dr., West Conshohocken, PA 19428-2959.

the test period of 24 h. It may be associated with the ability of alumina to reduce the pH upon hydrolysis, thus raising the corrosion rate of steel beneath the alumina deposit.

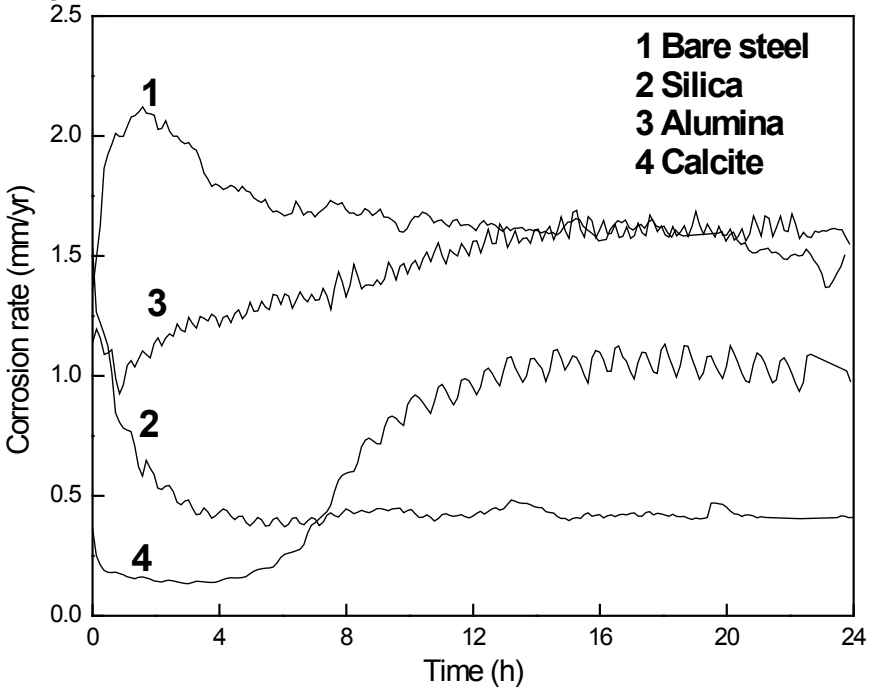

Figure 2: Corrosion rates of bare steel and deposit-covered steels corroded in CO_2 saturated test brine solution at 30 °C

Potentiodynamic polarization measurements

The potentiodynamic curves recorded from bare steel and deposit-covered steels after 24 h (at OCP) exposure to test brine solution at 30 °C are shown in Figure 3.

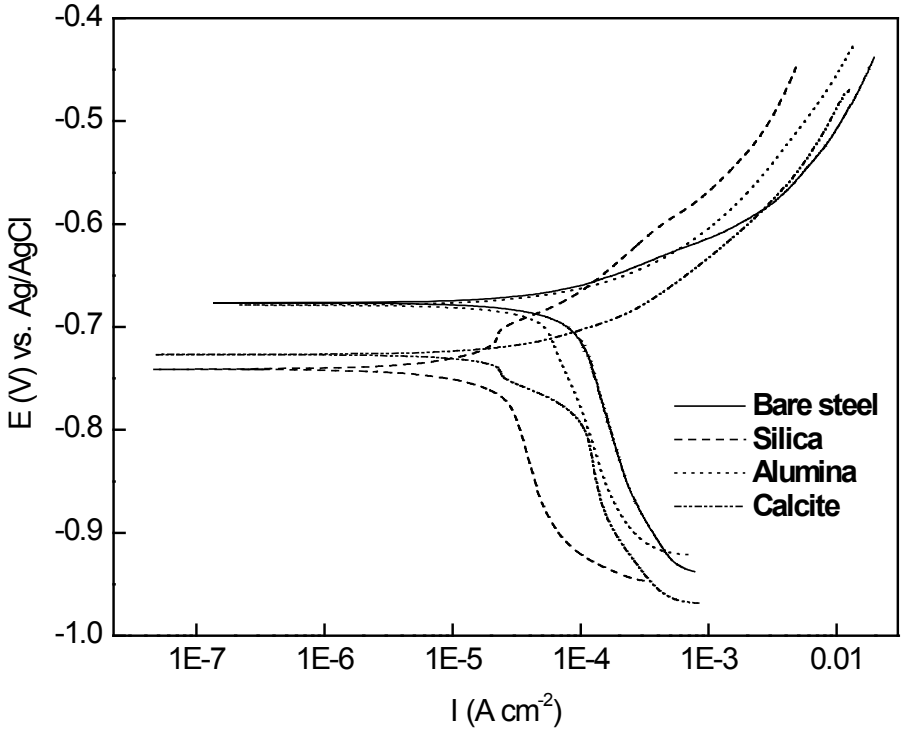

Figure 3: Potentiodynamic curves recorded from bare steel and deposit-covered steels in CO_2 saturated test brine solution at 30 °C after 24 h exposure at OCP.

It can be seen that there is a negative shift in the corrosion potential (E_{corr}) of 64 mV, 2 mV and 50 mV for silica, alumina and calcite-deposited steels, respectively compared to the bare steel surface. This indicates that the cathodic reaction is predominantly suppressed in the presence of deposits at the steel surface. The corrosion current densities (i_{corr}) of silica and calcite-deposited steels decreased in respect to the bare steel, with the silica-deposited surface exhibiting a considerable decrease in both anodic and cathodic domains. The i_{corr} decrease in the presence of these deposits can be related to the deposit particles acting as a physical barrier for the diffusion of reactive ions from the solution to the steel underneath. The polarization curve of alumina-deposited steel is similar to that of the bare steel with a negligible E_{corr} shift indicating that the corrosion reactions are similar to the bare steel surface. The pH of the test solutions was also measured (data not shown) before and after the potentiodynamic polarization tests and no significant change in solution pH during the test period was observed.

Weight loss measurements

The weight loss measurements provided the average corrosion rates of steels over the period of 15 days exposure to CO_2 saturated test brine solution and are presented in Figure 4.

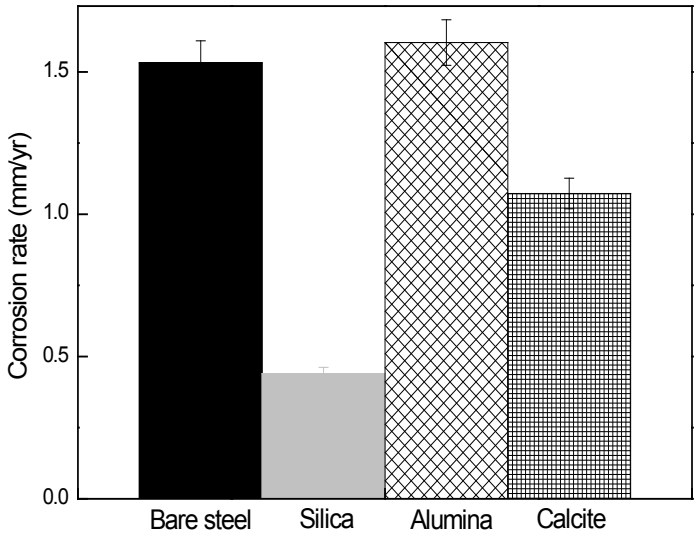

Figure 4: Average corrosion rates determined from weight loss measurements after 15 days exposure of bare steel and deposit-covered steels to CO_2 saturated test brine solution at 30 °C

The presence of silica or calcite deposits at the steel surface lowers the corrosion rate compared to the bare steel samples, whereas the alumina deposit has no significant effect on the corrosion rate. This indicates that silica and calcite deposits hinder the general corrosion process of steel in uninhibited brine test solution. The deposits may reduce the rate of diffusion of aggressive ions from the solution by covering the steel surface, thereby reducing the corrosion rates. The weight loss data are in good agreement with the electrochemical results which showed that the corrosion rate of alumina-deposited steel is similar to the bare steel. For the silica and calcite deposits, the same ordering as shown in Figures 2 and 3 is observed from the weight loss tests.

Scanning electron microscopy (SEM) analysis

Figure 5 shows representative scanning electron microscopy images of the bare steel and deposit-covered steel surfaces after 15 days of exposure to the CO_2 saturated test brine solution.
The bare steel surface (non-deposited) was completely covered with corrosion products (Fe, C and O) detected by Energy Dispersive X-ray Spectroscopy (EDS) and the corrosion is uniform in nature (Figure 5a). The surface morphologies of deposit-covered steels show that localized corrosion is inevitable underneath the deposits irrespective of the nature of the deposit. The deposit-covered steels revealed

severe preferential attack of the iron matrix with pits formed on the surface during the exposure period. No corrosion products could be detected at the deposit-covered steels and the surfaces were mainly composed of Fe and C (determined by EDS).

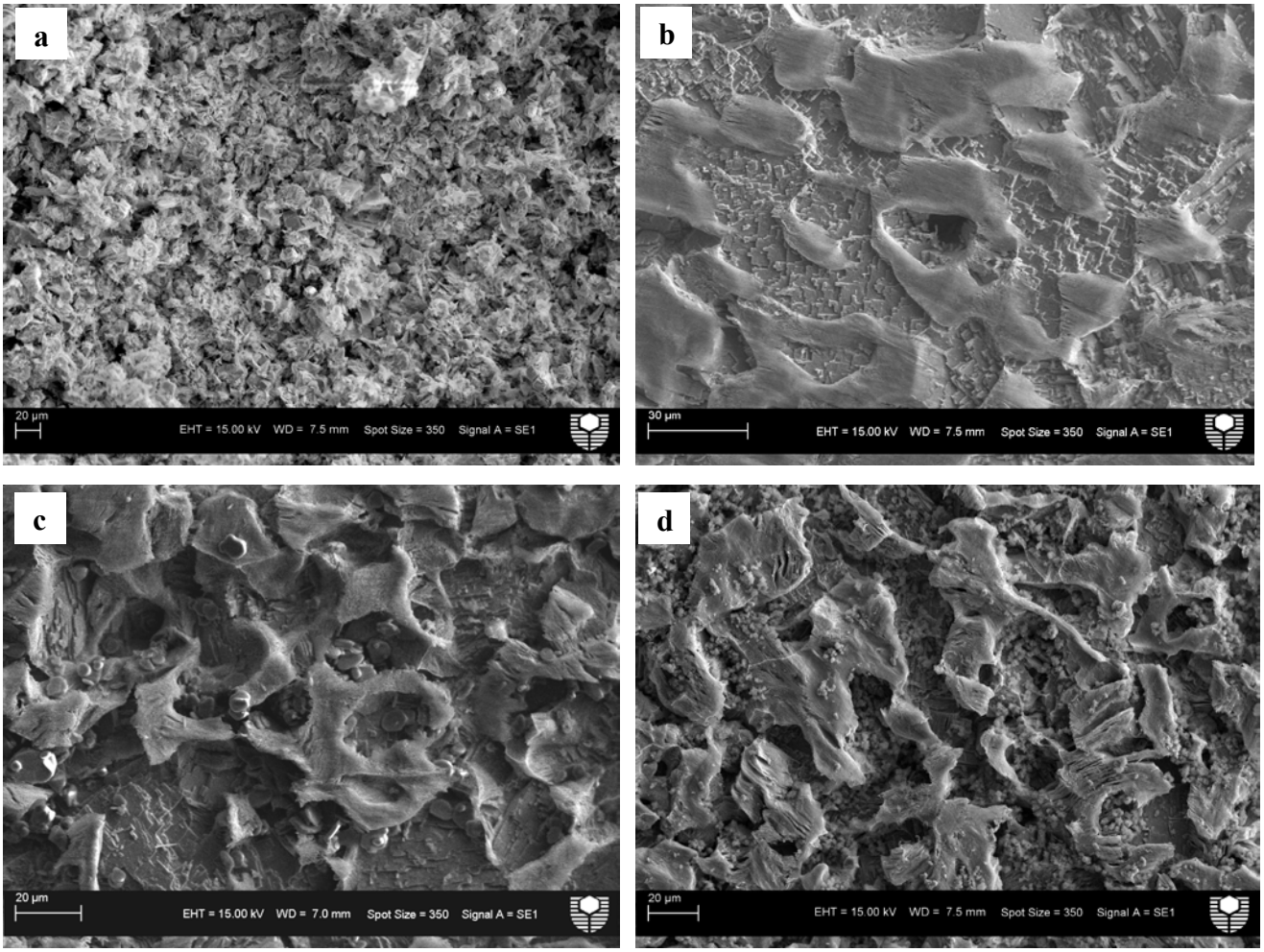

Figure 5: Representative scanning electron micrographs of carbon steel surfaces corroded by 15 days of immersion in CO_2 saturated test brine solution at 30 °C a) bare steel surface b) silica-deposited c) alumina-deposited d) calcite-deposited

In all the deposit-covered steels, residual deposit particles could be identified on the surface of the corroded steel and the surface structure differed according to the nature of the deposit. The smaller the particle size, the greater the quantity of residual particles found at the corroded steel surface. The proportion of calcite deposit (~3 µm average particle size) found on the surface is greater than that of alumina (~27 µm average particle size) (see Figure 5c and 5d). At the silica-deposited steel surface (~303 µm particle size) no silica particles were found (Figure 5b). The SEM results demonstrate that the corrosion process is influenced by the characteristics of the deposits present. The results correspond well with the weight loss observations (Figure 4).

Cyclic voltammetry measurements

The SEM analysis implies that the deposit-covered steels are susceptible to localized corrosion. To investigate the localized corrosion process, cyclic voltammetry experiments were conducted at bare steel samples and deposit-covered steels in test brine solution at 30 °C. Figure 6 presents the anodic polarization scans recorded (scan rate – 10 mV/s) after the steels exposed to test solutions were

stabilized at OCP for 300 s. The 5th scan is shown since the E-I responses were stable after 5 scans during the potential cycle.

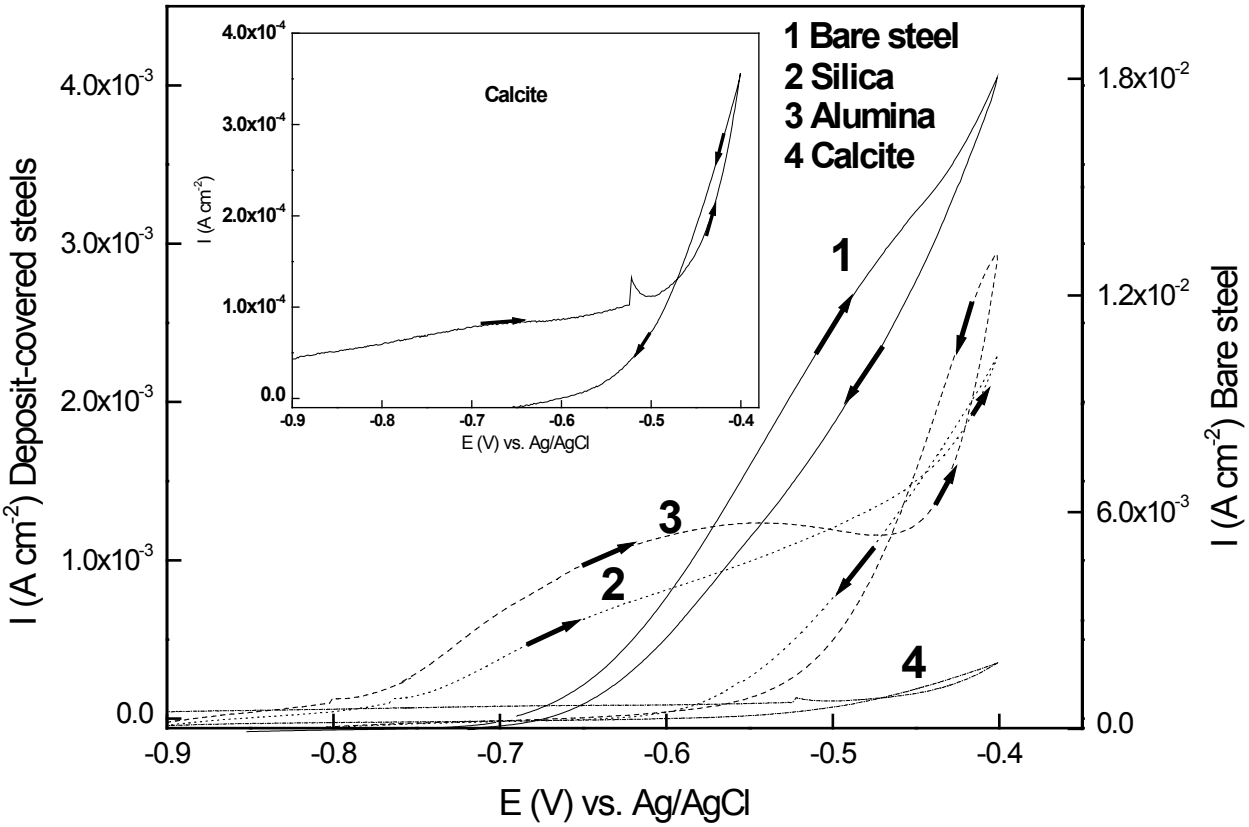

Figure 6: Anodic polarization curves (scan 5) from bare steel and deposit-covered steels in CO_2 saturated test brine solution at 30 °C; inset: calcite-deposited steel

* the y-axis range is different for the bare steel (right) and deposit-covered steels (left)

The cyclic voltammetry response of bare steel surface is typical of a uniform corrosion process indicated by a negative hysteresis where the current densities are less during the reverse scan than at the forward scan, at the same potential. A gradual increase in current density during the forward scan indicates the oxidation of the iron (release of iron ions) and it takes place at a more positive potential compared to deposit-covered steels (Figure 6). In the reverse scan, the current density decreased slowly indicating the formation of corrosion product film at the bare steel surface thereby decreasing the solution concentration of iron ions. This behaviour has been observed in the SEM image of bare steel (Figure 5a).

Unlike the bare steel, the deposit-covered steel surfaces were active at a more negative potential and a sharp increase in current density during the forward scan was observed. However, the current densities are lower (by a factor of 6) for silica and alumina than the bare steel. This indicates that the presence of silica and alumina deposits lowers the rate of anodic oxidation thus suppressing the dissolution of steel. The current density of the calcite-deposited steel (inset in Figure 6) is especially very low (by a factor of 40) compared to the bare steel. This can be related to the dense coverage of the steel surface by calcite deposit, thereby limiting the ion transport to a greater extent. The activity observed from the cyclic voltammetry scans is in accordance with the deposit properties affecting the corrosion process. The voltammograms from deposit-covered steels displayed a positive hysteresis loop which corresponds to the steel undergoing localized corrosion attack beneath the deposits. [11] The current densities during the reverse scan are initially higher and subsequently drop indicating repassivation of the localized corrosion sites developed at the steel surface during forward scan. Previous investigations

at silica sand-deposited surfaces have revealed similar electrochemical behaviour. [7,8] The cyclic voltammetry results support the onset of localized corrosion and formation of pits at the steel surface under deposits.

Visible-light microscopy analysis

The visible-light micrographs of steels after the cyclic voltammetry measurements (Figure 6) are given in Figure 7 and the surface parameters are presented in Table 2.

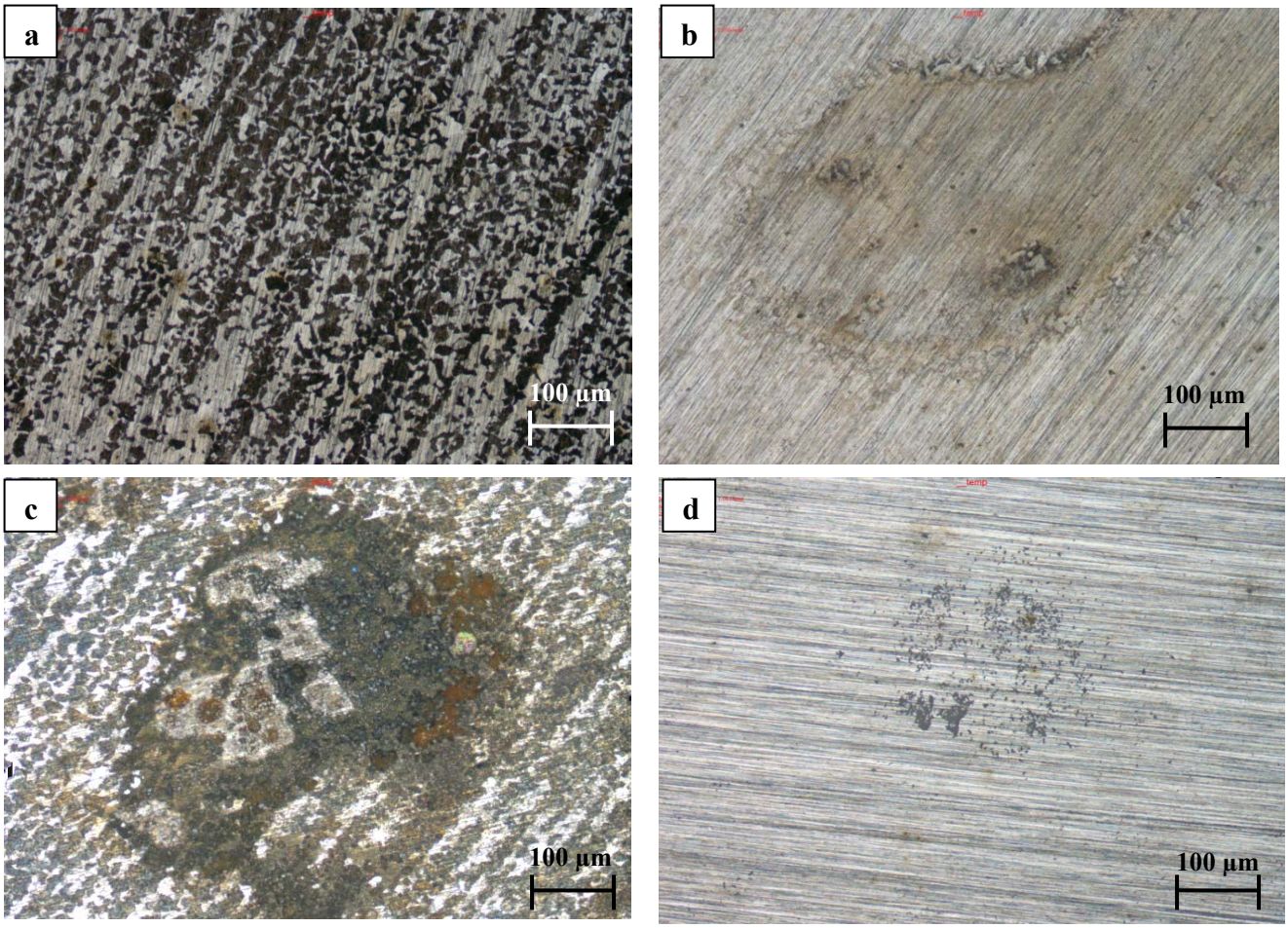

Figure 7: Representative visible-light micrographs of steels corroded by cyclic polarization in CO_2 saturated test brine solution at 30 °C a) bare steel surface b) silica-deposited c) alumina-deposited d) calcite-deposited

Table 2
Estimated surface profile parameters from visible-light microscopy analysis of steel surfaces after cyclic voltammetry measurements in test brine solution at 30 °C

Sample	Roughness (Rq)	Maximum pit depth
	µm	µm
Bare steel	0.97	-
Silica-deposited	1.22	4.77
Alumina-deposited	3.70	16.50
Calcite-deposited	1.59	8.79

The visible-light micrographs confirm that uniform corrosion proceeds at bare steel surfaces and the type of attack is localized at steels underneath deposits. As can be seen from Figure 7a, the bare steel surface exhibits uniform corrosion throughout. The micrographs of deposit-covered steels show that the surface is not uniformly affected like the bare steel, but locally corroded areas were found (Figure 7b, 7c and 7d). This confirms that localized corrosion proceeds under the deposits as seen from the results in the previous sections.

The surface roughness of bare steel was comparatively lower than the deposit-covered steels and no pits were measurable at the surface (Table 2). The roughness of deposit-covered steels is in the sequence, alumina-deposited > calcite-deposited > silica-deposited. Also, the maximum pit depth observed from alumina-deposited steel was higher compared to the other two deposits. This is consistent with the electrochemical, weight loss and SEM results suggesting that the alumina (oxide type deposit) promotes more severe corrosion attack than the other deposits investigated.

Influence of deposits on corrosion inhibitor performance

In all the tests with deposit-covered steels the uniform corrosion rates were less than that of the bare steel samples exposed to the CO_2-saturated test brine solution. In practice, carbon steel pipelines are always protected with chemical inhibitors and so inhibitor evaluation tests at both bare and deposit-covered steels were carried out. The effect of inhibitor addition after 1 h exposure of steels to test brine solution is presented graphically in Figures 8, 9 and 10 for three different corrosion inhibitors. The LPR measurements allowed for monitoring the immediate response of the system while the inhibitors TB, CPC and CF were introduced.

Inhibitor TB

Figure 8 shows that the corrosion rate of bare steel immediately falls below 0.1 mm/yr when inhibitor TB (concentration applied - 100 ppm) was introduced to the test brine. At deposit-covered steels, TB migrates through the deposit layer completely within about 3 h after addition and reduces the corrosion rate to <0.1 mm/yr. This confirms that inhibitor TB was able to reach the steel surface and offered corrosion inhibition beneath all three types of deposits investigated. The activity of TB at deposit-covered steels implies that it is not adsorbing to a large extent at the deposit surface and has greater affinity for the steel surface. The reason for the minimal adsorption of TB on the mineral deposits appears to be due to the electrostatic repulsion between the deposit particles and the electronegative adsorption center (S atom) of thiobenzamide. [12] Further evaluation at higher concentrations was not carried out for inhibitor TB since the corrosion was inhibited sufficiently (<0.1 mm/yr) at the concentration of 100 ppm.

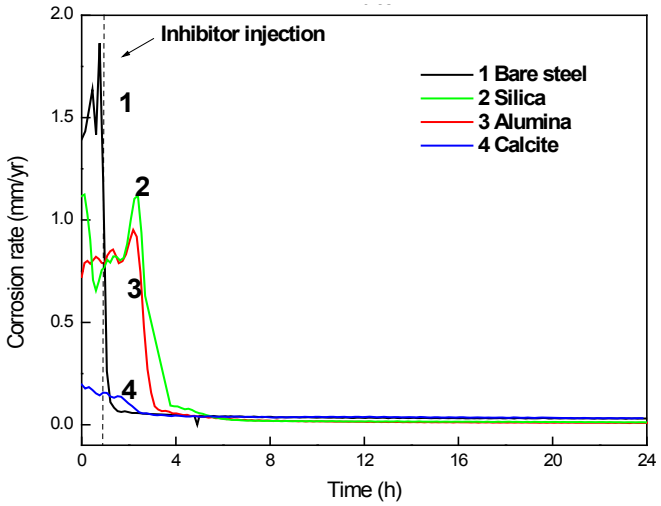

Figure 8: Corrosion rates of bare steel and deposit-covered steels, before and after 100 ppm TB inhibitor addition to the CO_2 saturated test brine solution at 30 °C from LPR measurements

Inhibitor CPC

At the bare steel after inhibitor CPC addition (100 ppm), the corrosion rate continued to decrease slowly for about 7 h which denotes that the inhibitor is adsorbing on the steel surface (Figure 9a). After 7 h, once the surface coverage by inhibitor is complete and is protective, the corrosion rate decreased and remained below 0.1 mm/yr.

At the silica-deposited steel, the corrosion rate decreases gradually after the inhibitor addition and stabilized at ~ 0.5 mm/yr after 3 h. The corrosion rate trend seen in Figure 2 and 9a of the silica-deposited steel is similar, suggesting that CPC addition to the test solution had no inhibition effect. This indicates that inhibitor CPC was selectively adsorbed to the silica deposit, yet corrosion rates decreased slightly because of the deposit itself hindering the corrosion process as it offers resistance to the ions moving towards and away from the underlying steel surface. Despite the initial decrease in corrosion rate, the final value is higher than that recorded in the absence of the inhibitor (see Figure 2) indicating that no corrosion protection was provided by the inhibitor CPC at 100 ppm. It is evident from Figure 9a that at alumina and calcite-deposited steels, 100 ppm of inhibitor CPC was insufficient to provide any corrosion protection underneath these deposits. The corrosion rates increased over time, with alumina-deposited surface undergoing corrosion similar to that of the uninhibited condition (see Figure 2) and the calcite-deposited surface displaying slightly higher value (1.5 mm/yr) than the uninhibited condition (1 mm/yr) at the end of test duration.

Hence, the tests were repeated at a higher inhibitor concentration of 1500 ppm to account for the adsorption loss of the inhibitor to deposits. The results are presented in Figure 9b. It can be observed that the bare steel surface was instantly inhibited with the corrosion rate dropping below 0.1 mm/yr. However, it is interesting to note that the corrosion rate at 1500 ppm dosage at the end of 24 h period was 0.07 mm/yr, which is higher than 0.02 mm/yr obtained from 100 ppm dosage of inhibitor CPC.

At the silica-deposited steel, the corrosion rate decreased gradually to a final value of ~ 0.25 mm/yr after 8 h. At alumina and calcite-deposited steels, even at the high dosage of 1500 ppm, the corrosion rates did not decrease to the desired level below 0.1 mm/yr. This indicates that inhibitor CPC was not accessible at the steel underneath the deposit to provide corrosion protection. This can be explained by the alumina and calcite deposits composed of smaller particles that possess large surface area (see Table 1) available for the inhibitor adsorption. Studies have reported that the presence of cations such as Ca^{2+} (as in calcite) can also reduce the performance of cationic inhibitor compounds. [13]

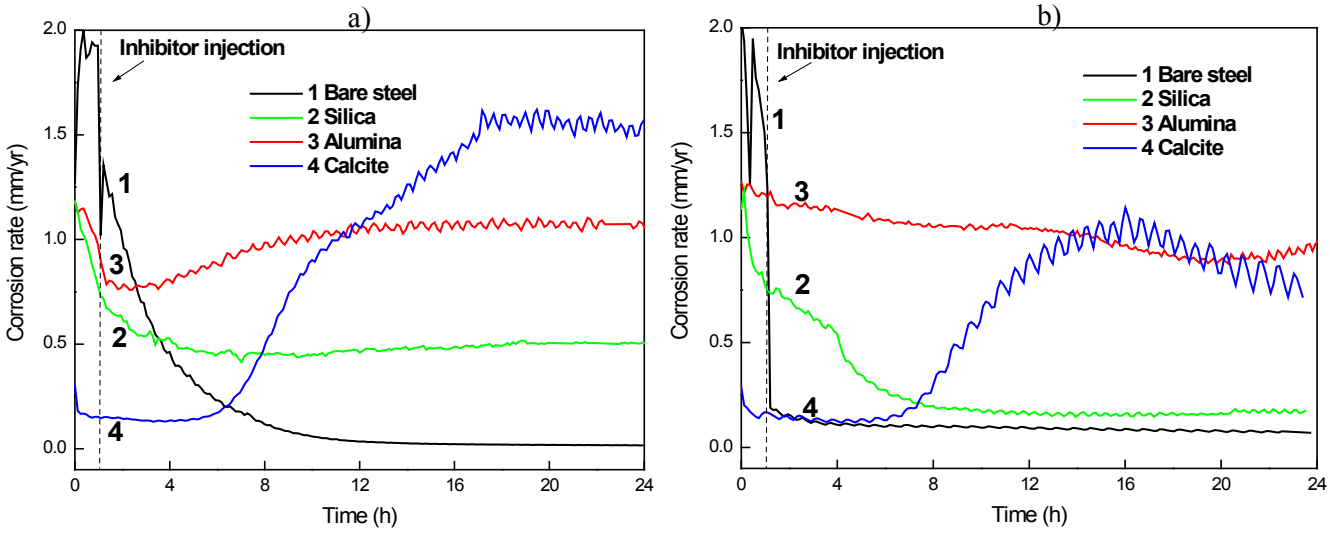

Figure 9: Corrosion rates of bare steel and deposit-covered steels, before and after CPC inhibitor addition to the CO_2 saturated test brine solution at 30 °C from LPR measurements; Inhibitor concentration: a) 100 ppm b) 1500 ppm

The corrosion rates in the presence of the inhibitor CPC suggest that the extent of corrosion is proportional to the level of inhibitor penetrating through the deposit and that an interaction occurring between the deposit and inhibitor can largely affect the inhibitor performance.

Inhibitor CF

The inhibitor CF employed was a commercial formulation (components not revealed by the manufacturer) and tests were conducted at both 100 ppm concentration and 1500 ppm (chemical manufacturer's recommended concentration).

We can see from Figure 10a and 10b that inhibitor CF offers similar level of inhibition (<0.1 mm/yr corrosion rate) at bare steel and calcite-deposited steel at both applied concentrations. In the case of the calcite deposit, it is supposed that improved inhibition is due to the neutralization properties of calcium ions on the steel surface at both concentrations. [14]

In case of silica and alumina-deposited steels, the corrosion rates did not decrease as required at the inhibitor concentration of 100 ppm, indicating that this low concentration was not sufficient enough to inhibit corrosion (Figure 10a). When the inhibitor concentration was raised to 1500 ppm, the corrosion rates gradually dropped over periods of 11 h and 6 h, respectively at silica and alumina-deposited steels (Figure 10b). It is evident that the inhibitor is diffusing through the deposit during this period. The relatively slow rate of inhibitor transport through silica and alumina deposits suggests that the inhibitor adsorption process at steel can be delayed. As a result, dissolution of the underlying steel already takes place while the inhibitor is penetrating through the deposit layer. In general, the inhibitor adsorption on a mineral deposit surface is expected to decrease with increase in particle size (or smaller specific surface area) of the deposit. On this basis, inhibitor transport rate through a silica deposit should be faster than an alumina deposit. By contrast, for inhibitor CF, we notice that the diffusion through silica deposit appears slower than alumina. This can be explained based on intra-particle molecular diffusion process. For a deposit with smaller particle size (alumina), the internal diffusion distance may be smaller. [15] Hence, it is considered that inhibitor CF transits through alumina faster than silica where the inhibitor should be transported a larger distance to reach the steel sites beneath the deposit. If this intra-particle diffusion is limiting the adsorption rate, apparently the corrosion inhibition will be less effective at silica-deposited steel than alumina.

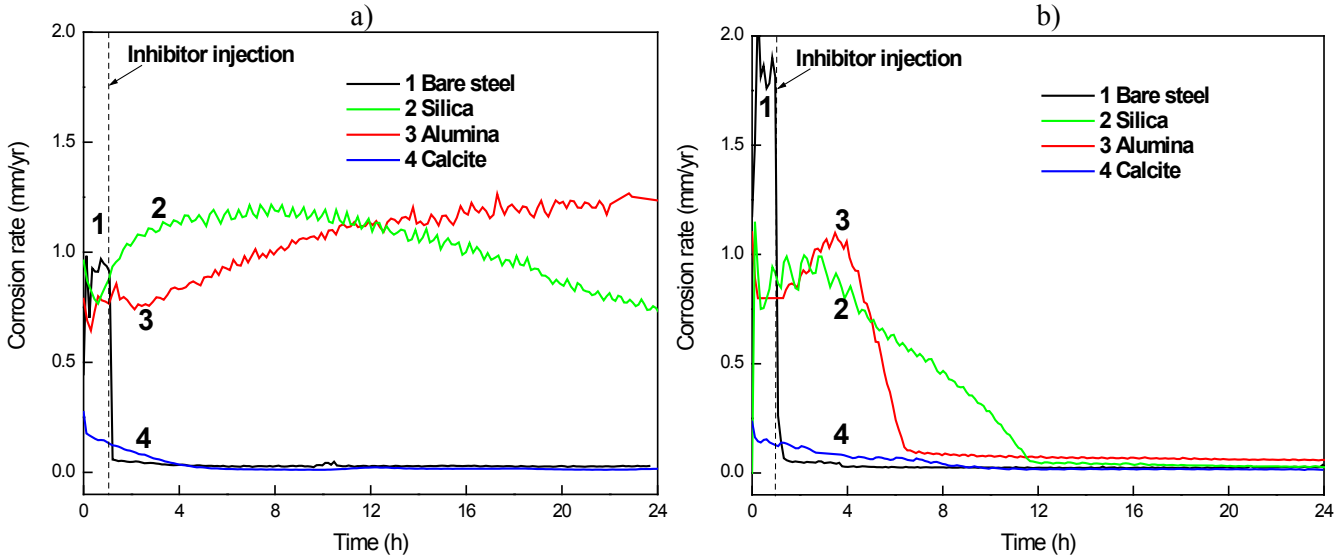

Figure 10: LPR corrosion rates of bare steel and deposit-covered steels, before and after CF inhibitor addition to the CO_2 saturated test brine solution at 30 °C from LPR measurements; Inhibitor concentration: a) 100 ppm b) 1500 ppm

The corrosion rates at bare steel demonstrate that inhibitor CF is a very effective formulation if it is dosed before the deposits enter the pipeline (even at 100 ppm). The inhibitor's performance can be disrupted or slowed down if it is added after the deposit layers are established. Despite this, inhibitor CF offers acceptable corrosion inhibition to steels if the dosage levels are high (1500 ppm).

The LPR results clearly differentiate the performance of different inhibitors at various deposit-covered steels. The transport of inhibitors through the deposit depends on the chemical nature of the inhibitor and its affinity for adsorption at the deposit surface. The results also allow determination of the concentration required to inhibit corrosion satisfactorily under the conditions studied.

Corrosion rates determined by potentiodynamic polarization

The potentiodynamic polarization tests were carried out at bare steel and deposit-covered steels after 24 h exposure (at OCP) to the inhibited test solutions at 30 °C (curves not shown). The corrosion rates calculated by Tafel extrapolation of the potentiodynamic curves are given in Figure 11.

The corrosion rates obtained from potentiodynamic results are in good agreement with the trend observed from LPR measurements. It is evident that the inhibitor performance at deposit-covered steels is dependent on the chemical composition of the inhibitor. The corrosion rates increase with decrease in average particle size of the deposit. This tendency is observed from all inhibitors (except for the calcite deposited steel at 1500 ppm CPC and CF at both concentrations), indicating that the degree of inhibitor penetration through the deposit is dependent on the particle size.

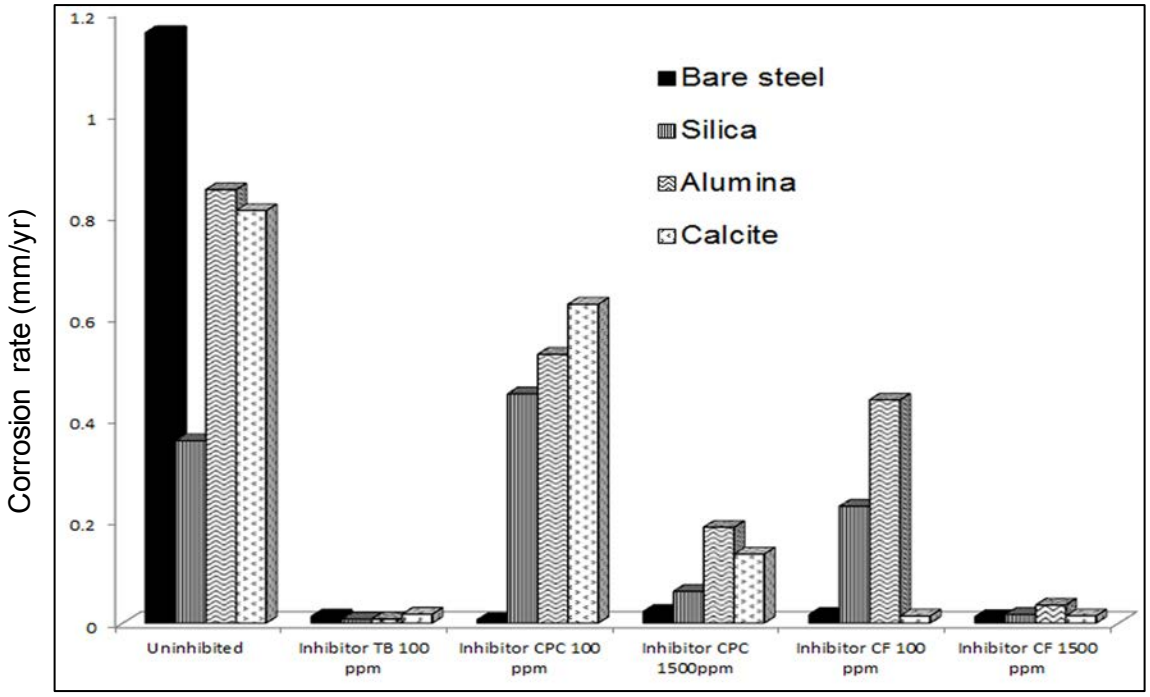

Figure 11: Corrosion rates from potentiodynamic polarization curves recorded after 24 h at OCP of bare steel and deposit-covered steels in CO_2 saturated uninhibited and inhibited test solutions at 30 °C

CONCLUSIONS

Three types of mineral deposits with different composition and particle geometries have been investigated for their influence on the corrosion of carbon steels under stagnant conditions in CO_2 saturated brine solution.

The results indicated that the bare steel surface in the test environment underwent uniform corrosion whereas the steels covered with silica, alumina and calcite deposits were susceptible to localized attack. Under uninhibited conditions, both electrochemical and weight loss data showed lower uniform corrosion rates for all deposit-covered steels compared to the bare steel, suggesting that the deposit layer acted as a diffusion barrier for corrosive ions. However, the surface observations showed that the steels beneath the deposits were affected by localized corrosion. The extent of the corrosion damage varied according to the deposit characteristics and significant surface structural differences were noticed in the steels corroded in the presence/absence of different deposits.

Comparing the inhibitor evaluation results of two pure organic corrosion inhibitors, thiobenzamide (TB) and cetylpyridinium chloride monohydrate (CPC) and a commercial inhibitor formulation (CF), we found that inhibitor performance at deposit-covered steels is dependent on the chemical nature of the inhibitor. The order of tested inhibitor's protective performance under deposits was TB > CF > CPC. Inhibitor TB exhibited the maximum inhibition effect at a low concentration of 100 ppm, irrespective of the presence of deposits. Inhibitor CPC at 100 ppm was ineffective at deposit-covered steels and offered only a minimum degree of inhibition even at the high concentration of 1500 ppm. The commercial inhibitor CF showed an increase in effectiveness as the dosage level was increased from 100 to 1500 ppm. CF provided similar level of inhibition at 1500 ppm as the inhibitor TB at 100 ppm and the penetration of CF through the deposit layer was faster if the initial concentration supplied was higher.

The accumulation of deposits in the pipeline is inevitable but determining the expected inhibitor adsorption at deposits present and predicting the corrosion rates under deposits is a useful approach to mitigate under-deposit corrosion of carbon steel in CO_2 environment.

ACKNOWLEDGEMENTS

The authors would like to thank Woodside Energy Ltd[9] for the financial support and permission to publish this work. We also acknowledge the support of the Western Australian Energy Research Alliance[10] (WAERA). One of us (V. P.) thanks the Curtin University for the Postgraduate Research Scholarship (CIPRS). K. L. thanks Curtin University for a Curtin Research Fellowship. We also thank the Centre for Materials Research (CMR) facility at Curtin University for SEM access.

REFERENCES

1. M. M. Salama, "Influence of sand production on design and operations of piping systems." CORROSION/ 00, paper no. 080 (Houston, TX: NACE, 2000).

2. B. R. Tian, Y. F. Cheng, "Electrochemical corrosion behavior of X-65 steel in the simulated oil sand slurry. I: Effects of hydrodynamic condition.", Corrosion Science 50(3) (2008), 773-779.

3. N. Tajallipour, Z. Zhu, P. J. Teevens, T. Place. "Parametric study of solids deposition in a heavy-oil transmission pipeline." in CORROSION/12, paper no.0001679 (Salt Lake City, UT: NACE, 2012).

4. K. Lepková, R. Gubner, "Development of standard test method for investigation of under-deposit corrosion in carbon dioxide environment and its application in oil and gas industry." CORROSION/10, paper no. 10331. (San Antonio, TX: NACE, 2010).

5. A. J. McMahon, L. J. Harris, J. W. Martin. "Effects of sand and interfacial adsorption loss on corrosion inhibitor efficiency." CORROSION/05, paper no. 274 (Houston, TX: NACE, 2005).

[9] Trade name.
[10] Trade name.

6. D. M. Drazic, L. J. Vracar, V. J. Drazic. “The kinetics of inhibitor adsorption on iron.” Electrochimica Acta 39 (8-9) (1994), 1165 -1170.

7. V. Pandarinathan, K. Lepková, R. Gubner, “Inhibition of CO_2 corrosion of 1030 carbon steel beneath sand-deposits.” CORROSION/11, paper no. 263. (Houston, TX: NACE, 2011).

8. K. Lepková, R. Gubner, “Study on corrosion processes at sand-deposited surfaces in a carbon dioxide media.” EUROCORR /10, (Moscow, Russia: Conference Proceedings, 2010).

9. ASTM G102 – 89 (2010) “Standard Practice for Calculation of Corrosion Rates and Related Information from Electrochemical Measurements”.

10. ASTM G1 – 03 (2011) “Standard Practice for Preparing, Cleaning, and Evaluating Corrosion Test Specimens”.

11. J. Toušek, “Theoretical aspects of the localized corrosion of metals”, (Aedermannsdorf, Switzerland: Trans Tech Publications, 1985).

12. V. Pandarinathan, K. Lepková, R. Gubner, “Thiobenzamide as inhibitor for under-deposit corrosion of carbon steel.” Manuscript in preparation.

13. A. Pedersen, K. Bilkova, E. Gulbrandsen, and J. Kvarekval. “CO_2 corrosion inhibitor performance in the presence of solids: Test method development.” CORROSION/08, paper no. 632 (Houston, TX: NACE, 2008).

14. K. S. Sorbie and N. Laing. “How scale inhibitors work: Mechanisms of selected barium sulphate scale inhibitors across a wide temperature range.” Proceedings of SPE International Symposium on Oilfield Scale, 1–10, Society of Petroleum Engineers, 2004.

15. R. Rong, “Adsorption of quaternary ammonium compounds onto activated sludge.” Journal of Water Resource and Protection 03, no. 02 (2011), 105–113.

Chapter III

V. Pandarinathan, K. Lepková and R. Gubner, Inhibition of CO_2 corrosion of 1030 carbon steel beneath sand-deposits, Corrosion 11, NACE International, paper no. 261, Houston, Texas (2011)

Original Reprint of the Publication

Paper No.
11261

NACE INTERNATIONAL CORROSION 2011 CONFERENCE & EXPO

INHIBITION OF CO_2 CORROSION OF 1030 CARBON STEEL BENEATH SAND-DEPOSITS

Vedapriya Pandarinathan, Kateřina Lepková and Rolf Gubner
Corrosion Centre for Education, Research and Technology
Department of Chemistry
Curtin University
Perth, Western Australia

ABSTRACT

The performance of three corrosion inhibitors was investigated at 1030 carbon steel surfaces in the presence and absence of a sand deposit. Potentiodynamic measurements showed that the inhibition efficiency to mitigate corrosion reactions decreases in the presence of sand deposit. In contrary, the inhibitor performance was found to increase with longer exposure time of the steel to the corrosive media, at sand deposited surfaces. The differences between the steels corroded with and without sand deposit in the presence of an inhibitor were confirmed using both potentiostatic polarisation technique and scanning electron microscopy. The inhibition activity of the studied compounds in mitigating under-deposit corrosion of carbon steel has been discussed.

Key words: Corrosion inhibitor, carbon dioxide, mild steel, under deposit.

INTRODUCTION

Investigation of CO_2 corrosion processes of 1030 carbon steel surfaces has been widely researched by numerous authors[1-7]. The impact of solid particles produced during oil and gas operations on the corrosion inhibition of the system is a major concern for the oil and gas industry[2,3]. CO_2 corrosion is enhanced in the presence of entrained sand particles in the pipelines leading to severe corrosion damage underneath the settled sand deposits[4,5]. It has been reported that under-deposit corrosion leads to localized corrosion and formation of pits on the metal surface[6]. In previous investigations, the mechanism of under-deposit corrosion has been related to a galvanic corrosion between surfaces with and without sand deposits [7-10]. However, the suggested principles have not been confirmed to date.

The control of under-deposit corrosion is currently being accomplished through methods such as pigging and the use of corrosion inhibitor chemicals. While the CO_2 corrosion inhibition of mild steel surfaces has been largely investigated, only limited studies have been undertaken to evaluate the inhibition efficiency under a produced sand layer. Little attention has been paid to the principles of inhibition offered by the applied corrosion inhibitors under circumstances where sand deposits are formed, but pigging is not possible[11,12]. It has been shown that the sand particles can adsorb the corrosion inhibitors applied to the system thereby reducing the activity of the inhibitor[13]. The organic compounds such as imidazolines, quaternary ammonium compounds, thiols, pyrimidine based

compounds, several mercaptans, phosphate esters etc. have been reported as potential CO_2 corrosion inhibitors for industrial applications[14-17].

The aim of this study is to evaluate the performance of a range of corrosion inhibitors under sand deposited carbon steel surfaces in CO_2 environment. Electrochemical investigations were conducted under potentiostatic and potentiodynamic conditions to determine the corrosion processes proceeding at the sand-deposited surfaces[18,19]. The estimated corrosion rates as a function of exposure time from the electrochemical test results and also from weight-loss immersion tests are presented. The surface morphology of the corroded structure plays an important role in determining the inhibition principles[20,21]. The surface characteristics of the corrosion scale formed in the presence and absence of sand deposits have been analysed using scanning electron microscopy. The influence of sand particles on the inhibition activity of the studied inhibitors has been discussed.

EXPERIMENTAL PROCEDURE

Test Materials

The electrochemical corrosion tests were conducted using 1030 grade carbon steel electrodes embedded in epoxy resin. Hastelloy and saturated silver/silver-chloride electrodes were used as counter electrode and reference electrode, respectively. Prior to each experiment, the samples were polished to 1200 grit SiC abrasive paper, washed with appropriate solvent and rinsed with ultra pure water (resistance – 18.2 MΩ cm) to remove any traces of the solvent. The samples were then dried and immediately placed into the test cell.

Acid-washed silica sand (Sigma-Aldrich) was used as a deposit. The nominal grain size of sand particles determined using laser diffraction analysis was 303.03 µm. The particle surface area of the sand was determined to be 0.062 m^2/g by applying the theory of Brunauer, Emmett and Teller (BET method).

Three different inhibitor chemicals (Sigma-Aldrich, 98%) were investigated. Two of the examined quaternary ammonium inhibitor compounds were cetyl pyridinium chloride monohydrate and dodecyl pyridinium chloride. They will be referred to as inhibitor A and B respectively. The third inhibitor referred to as C was 2-mercaptopyrimidine. The testing solution was 3% sodium chloride (NaCl; Ajax Finechem, analytical reagent, 99.9%) and 0.01% sodium hydrogen carbonate ($NaHCO_3$; Merck, 99.5%) prepared using ultra pure water. The appropriate inhibitor was added as required. The test solution was saturated with CO_2 for at least two hours before the experiments in a separate glass vessel. The pre-saturated solution was then pumped into the de-aerated experimental cell fitted with the electrodes. All experiments presented in this study were carried out under stagnant flow conditions with an inhibitor concentration of 200 ppm. Experiments were carried out at 30°C ±1°C.

Methods

The electrochemical tests were performed in a glass cell using a three-electrode system described elsewhere[26]. The working electrode was placed at the bottom of the cell and was covered with a layer of sand. A known amount of sand was used for each experiment ensuring a consistent sand layer height of ~7.5 mm deposited at the metal surface. The counter and reference electrodes were placed in close proximity to the working electrode. A Luggin capillary holding the reference electrode was placed within the sand layer to minimize the IR drop. The same distance between the Luggin capillary and working electrode was maintained for all experiments.

The electrochemical measurements, evaluating the three inhibitors were conducted using a Solatron SI 1287 potentiostat. The potentiodynamic polarization scans were run within the potential range of ±0.25 V vs open circuit potential (OCP) at a sweep rate of 0.1667 mVs^{-1}. The scan was

conducted after a 1 hour exposure period during which the samples were allowed to stabilize at OCP. The potentiodynamic measurements were also recorded after a 12 hour exposure period in order to determine the effect of the exposure time on the extent of corrosion.

The E-I responses were recorded using cyclic voltammetry at a sweep rate (dε/dt) of 10 mVs^{-1}. Prior to cyclic voltammetric experiments, a two step electrochemical pre-treatment was applied to the working electrode in order to ensure the same starting conditions for all experiments. The working electrode was held at a potential of -1.2 V vs. Ag/AgCl for 30 s. The electrode was then left to stabilize at the OCP for 300s (no potential was applied through the potentiostat at this step). After the above described electrochemical pre-treatment, the cyclic voltammetry measurement was started. The pre-treatment procedure was applied to the cyclic voltammetry measurements only.

The performance of inhibitor A was further analysed using the potentiostatic experimental technique. Following a 12 hour exposure period in the corrosive media containing inhibitor A, the bare steel samples were polarized at a constant potential of -0.5 V vs Ag/AgCl for 1800 seconds. The same tests were carried out with sand-deposited samples. After the potentiostatic measurements, the samples were washed with ultra pure water (the sand deposit was removed from the electrode surface), dried with nitrogen and stored under vacuum before performing the surface analysis.

The surface morphology of the samples exposed to corrosive media containing inhibitor A was analyzed using the Zeiss (Evo) scanning electron microscope (SEM). The samples were immersed in the inhibitor-containing solution for 12 hours prior to the potentiostatic polarization. The SEM analysis was carried out before and after the electrochemical polarization, one sample only was used for these measurements.

The weight loss measurements were performed at steel samples corroded in solutions containing inhibitor A in the presence and absence of sand deposits. Three carbon steel specimens with an exposed surface area of 7.5 cm^2 were immersed in the inhibited test solution for a period of 15 days (360 hours). Three coupons covered with a fixed sand layer were also immersed in the same test environment for the same time interval. The samples were weighed to an accuracy of ±0.5 mg before and after immersion. The corrosion rates (CR) were calculated from the average weight loss of the three representative samples[22] using Equation 1.

$$CR \text{ (in mm/y)} = (K \times W) / DAT$$

Eqn 1

where, constant $K = 8.76 \times 10^4$, W = weight loss in grams, D = metal density in g /cm^3, A = area of sample in cm^2, T = time of exposure of the metal sample in hours.

The corrosion rates were also determined by Tafel analysis of the potentiodynamically polarized samples in test solution containing inhibitor A in the presence and absence of sand layer. The corrosion rate was calculated from the estimated corrosion currents obtained from the intercept of the two linear segments of the respective Tafel plots[23] using Equation 2.

$$CR \text{ (in mm/y)} = (K_1 \times i_{corr} \times EW)/ \rho$$

Eqn 2

where, constant $K_1 = 3.27 \times 10^{-3}$ in mm g/µA cm yr, i_{corr} = corrosion current density in µA/cm^2 , EW = equivalent weight of the sample , ρ = density of the sample metal in g/cm^3.

RESULTS

Potentiodynamic polarization measurements at surfaces with and without sand deposits

Figure 1 shows the potentiodynamic curves for carbon steel surfaces under sand deposits in the testing solution without any inhibitor and with inhibitors A, B and C after 1 hour immersion. At the sand deposited surfaces, the quaternary ammonium compounds (inhibitors A and B) were found to have little influence on the corrosion mitigation. The polarization curves were displaced to a positive potential value of 33 mV and 44 mV for inhibitors A and B, respectively, in respect to the non-inhibited surfaces. Furthermore, only small decreases in current density in the cathodic region were observed in comparison to the inhibitor-free surface. Whereas the inhibitor compound C was found to perform better in mitigating the corrosion process under a sand layer; the overall current density considerably decreased. The corrosion potential was observed to shift to a more positive potential of 46 mV. The results of polarization scans revealed that the sand deposit has a negative impact on the performance of CO_2 corrosion inhibitors that otherwise provide sufficient corrosion protection to bare steel (Figure 2). The potential shift of bare sample surfaces with inhibitors A, B and C was 46 mV, 66 mV and 110 mV respectively in the positive potential direction. The greatest performance in terms of corrosion inhibition was observed for inhibitor C. The shift in corrosion potential was 110 mV in the positive direction for the bare samples in the test solution with inhibitor C. For the sand deposited samples, corroded under same conditions, the potential shift was only 46 mV which indicates insufficient inhibition by the same compound under the sand deposited surfaces. It can be speculated that this difference in the corrosion potential values between surfaces with and without deposits can enhance the corresponding overall corrosion rates[24]. The open circuit potentials (OCP) were monitored as a function of time during the immersion of samples before the potentiodynamic tests described above. The observed OCP variations for samples under sand deposits are shown in Figure 3. All the inhibited systems reached higher OCP values compared to the samples corroded in non-inhibited system. The OCP values stabilized after approximately 500 seconds of sample immersion in the test solutions.

Influence of immersion time on inhibitor performance

To evaluate the effect of exposure time on the performance of inhibitors, the potentiodynamic scans were measured after the introduction of samples in the test solution with inhibitors at a time interval of 12 hours. The corresponding curves are shown in Figure 4. The potential shift of sand-deposited sample surfaces with inhibitors A, B and C were 45 mV, 5 mV and 47 mV respectively in the positive direction. The corrosion potentials of samples in presence of inhibitor A and C were found to increase in positive direction when compared to the polarization curves obtained after one hour exposure which is illustrated in Figure 1. It can be seen that the performance of inhibitor B does not improve with time the same way as the inhibitors A and C. The decrease in corrosion current after 12 hours of exposure to inhibited solution shows the relation of inhibition activity of inhibitors A and C with time. This may be attributed to the fact that after longer exposure, the inhibitor molecules form protective layers which shield the metal surface from further corrosion[19]. The reduction in current density and the positive potential shift, in comparison to the measurements recorded after 1 hour immersion (Figure 1), indicate that inhibition is caused by the sorption of the inhibitor molecules to the active reaction sites on the corroding metal surface[14-17]. The inhibitor activity can be attributed either to physical adsorption or chemisorption of the inhibitor molecules onto the substrate metal. Thus the adsorbed molecules act as a barrier between the corroding steel surface and the corrosive medium.

Cyclic polarization measurements at sand-deposited surfaces

The cyclic voltammetry experiments were conducted to study the behaviour of the carbon steel samples in inhibited media saturated with CO_2. Figure 5 presents the anodic polarization scan from the sample corroded under sand in the test solution with inhibitor A. The E-I transients of the first two scans are presented. A steep increase in current density of the first scan is observed prior to the corresponding potential value of -0.4 V vs Ag/AgCl. The reduction in current density of the second scan

in the anodic potential region can be ascribed to the electrochemical pre-treatment step applied to the electrode before recording the voltammograms. A similar pre-treatment methodology has been previously applied and the reasoning for the change in current density with the subsequent number of scans has been reported elsewhere[26]. Further decrease in the current density values was also observed with the increasing number of scans. No hysteresis loop was observed at the positive end of the potential window in this measurement.

Figure 6 illustrates the voltammetric response from the surface corroded in test solution containing inhibitor B. The hysteresis loop observed in the second scan can be attributed to the localized attack proceeding at the polarized electrode surface[25]. Figure 7 shows the cyclic voltammogram obtained from the surface covered with sand deposits in the corrosive solution with inhibitor C. An opposite trend of gradual increase in the current density values with the increasing number of scans was observed in the presence of inhibitor C. This change in the voltammetric profile from other inhibitors studied can be related to the structural differences of the inhibitor compounds. The hysteresis loop seen in both the first and second scan indicates the onset of localized corrosion and formation of pits at the carbon steel surface under the sand layer. Previous investigations at surfaces without inhibition revealed similar electrochemical behaviour[26].

Potentiostatic polarization measurements with inhibitor A

The results of the potentiostatic experiments are shown in Figure 8. The variation in the nature of curves obtained from the bare steel surface and the surface covered with sand is apparent. For the samples corroded without sand deposit, the current density increased in the positive direction with time, at the applied potential and stabilised at approximately $4x10^{-3}$ A/cm^2. A similar trend in current density change for non-inhbited system has been reported elsewhere[27]. When the samples under sand-deposits were polarized at same potential, the current density decreased with time. It decayed to a constant value after a critical current density of $2x10^{-3}$ A/cm^2.

Surface characterization using scanning electron microscopy

The surface analysis of the carbon steel samples exposed for 12 hours in the presence of 200 ppm concentration of inhibitor A was undertaken to supplement the electrochemical test results. It was demonstrated that the sand deposits caused changes in the surface morphology of the corroded carbon steel surfaces. The surfaces without a deposit were reported to have a different texture under same testing conditions[22]. Figure 9a and 9b show the pre-corroded samples polarized at a constant potential of -0.5 V vs Ag/AgCl under the described experimental conditions. It is evident from the scanning electron micrographs that the samples polarized under sand exhibited greater corrosion damage than the bare samples.

Figure 10a and 10b present the representative images of the samples following the immersion for a period of 12 hours without sand and with sand respectively. These images were taken before the samples were polarized. It is interesting to note that the bare sample surface has no significant corrosion when compared to the surface which had been under the sand deposit. This indicates that the inhibitor offers protection against corrosion for the carbon steel surfaces after 12 hours of exposure to the corrosive test solution. Whereas the surface under sand shows the corroded structural features, demonstrating that the sand layer hinders the activity of inhibitor. The insufficient inhibition under sand deposits even at a high inhibitor concentration can be attributed to the adsorption losses of the active inhibitor molecules to the sand particles. Previous studies have reported that large concentration of corrosion inhibitors available to protect steel surfaces can be lost from bulk solution by adsorption onto the sand particle surfaces[13]. The adsorption experiments carried out by Durnie et al. [6] illustrates that the adsorption losses of the inhibitors to the sand particles leads to higher corrosion rates of the steel samples investigated.

Corrosion rate measurements

The weight loss of the carbon steel samples corroded in the test solution with inhibitor A for 15 days was measured. The mean weight loss of the bare carbon steel samples was 0.0103 g and that of the sand-deposited samples was 0.0948 g. The corrosion rates calculated from the weight loss measurements of bare surfaces and sand-deposited surfaces with inhibitor A were 0.0424 mm/y and 0.3907 mm/y respectively.

The corrosion rates were also calculated by Tafel extrapolation of the potentiodynamic polarization curves of the samples corroded in test solution containing inhibitor A. The current density values were calculated from the polarization plots obtained after 12 hours of sample immersion in the presence and absence of sand layer (Figure 4). The corrosion rates of bare surfaces and sand-deposited surfaces with inhibitor A were 0.0654 mm/y and 0.2287 mm/y respectively. The corrosion rates obtained from both the weight loss experiments and the Tafel analysis showed that higher corrosion rate values result from corrosion at the sand-deposited surfaces, when compared to the surfaces without deposits.

CONCLUSIONS

The performance of three corrosion inhibitors at sand-deposited carbon steel surfaces was investigated using electrochemical methods and a surface analysis technique. The studied inhibitors differed by their chemical composition. The inhibitor addition resulted in a lower corrosion current density and provided effective inhibition of the CO_2 corrosion in the absence of sand deposits. However, the same inhibitors did not provide the same level of corrosion protection in the presence of a sand layer at the steel surface. The results indicate that the inhibitor activity is diminished by the presence of sand deposits thereby accelerating the corrosion processes under deposits. The comparison of the potentiodynamic curves of the three inhibitors investigated showed that inhibitor C exhibits higher activity than inhibitors A and B at sand-deposited surfaces, at the inhibitor concentration evaluated. The differences in the inhibition efficiency can be related to the chemical nature and the adsorption characteristics of the respective compound. To gain a better understanding on the inhibitory action, further studies are being carried out to determine the adsorption behaviour of CO_2 corrosion inhibitors at sand-deposited surfaces.

REFERENCES

1. M. B. Kermani and A. Morshed, “Carbon dioxide corrosion in oil and gas production-a compendium”, Corrosion (2003) (59) 8, 659.
2. M. M. Salama, “Influence of Sand Production on Design and Operations of Piping Systems”, CORROSION/00, paper no. 00080. (Houston, TX: NACE, 2000).
3. B.R. Tian and Y.F. Cheng, “Electrochemical corrosion behavior of X-65 steel in the simulated oil sand slurry. I: Effects of hydrodynamic condition”, Corrosion Science 50(3), 773-779.
4. W. H. Durnie, M. A. Gough and J. A. M. de Reus, “Development of corrosion inhibitors to address under deposit corrosion in oil and gas production systems”, CORROSION/05, paper no. 05290. (Houston, TX: NACE, 2005).
5. J. Huang, B. Brown, X. Jiang, B. Kinsella and S. Nesic, “Internal CO_2 corrosion of mild steel pipelines under inert solid deposits”, CORROSION/10, paper no. 10379. (San Antonio, TX: NACE, 2010).
6. J.A.M. de Reus, E.L.J.A. Hendriksen, M.E. Wilms, Al-Habsi N. Yahya , W.H. Durnie and M.A. Gough “Test methodologies and field verification of corrosion inhibitors to address under deposit corrosion in oil and gas production systems”, CORROSION/05, paper no. 05288. (Houston, TX: NACE, 2005).
7. J. Han, Y. Yang, S. Nesic and B. N. Brown, “Roles of passivation and galvanic effects in localized CO_2 corrosion of mild steel”, CORROSION/08, paper no. 08332. (Houston, TX: NACE, 2008).

8. A. Pedersen, K. Bilkova, E. Gulbrandsen and J. Kvarekval, "CO_2 corrosion in inhibitor performance in the presence of solids: Test method development", CORROSION/08, paper no. 08632. (Houston, TX: NACE, 2008).
9. J. Marsh, J. W. Palmer and R. C. Newman, "Evaluation of inhibitor performance for protection against localized corrosion", CORROSION/02, paper no. 02288. (Houston, TX: NACE, 2002).
10. A. Turnbull, D. Coleman, A. J. Griffiths, P. E. Francis and L. Orkney, "Effectiveness of corrosion inhibitors in retarding the rate of propagation of localized corrosion", (2003), Corrosion 59(3):250.
11. A. Neville, C. Wang, S. Ramachandran and V Jovancicevic, "Understanding the action of inhibitors in mitigating erosion-corrosion in impinging flows". CORROSION/04, paper no. 04658. (New Orleans, LA: NACE, 2004).
12. W. Y. Mok, A. E. Jenkins, S. R. Keenan and C. G. Gamble, "Control of localized corrosion using green corrosion inhibitors", CORROSION/05, paper no. 05289. (Houston, TX: NACE, 2005).
13. A. J. McMahon, J. W. Martin and L. Harris, "Effects of sand and interfacial adsorption loss on corrosion inhibitor efficiency". CORROSION/05, paper no. 05274. (Houston, TX: NACE, 2005).
14. V.S. Reznik, V.D. Akamsin, Yu.P. Khodyrev, R.M. Galiakberov, Yu.Ya. Efremov and L. Tiwari, "Mercaptopyrimidines as inhibitors of carbon dioxide corrosion of iron", Corrosion Science 50 (2), 392-403.
15. V. Jovancicevic, S. Ramachandran and P. Prince, "Inhibition of CO_2 corrosion of mild steel by imidazolines and their precursors", CORROSION/98, paper no. 98018, (San Diego, CA: NACE, 1998).
16. T.M. Devine and P.H. Chou, "Corrosion inhibition of carbon steel in CO_2-saturated brine by phosphate monoester", ECS Transactions 1(9), 253-264.
17. K. Bilkova and N. Hackerman, "Inhibition of CO_2 corrosion of carbon steel by thioglycolic acid", CORROSION/02, paper no.02284, (Denver, CO: NACE, 2002).
18. S. Nesic, W. Wilhelmsen, S. Skjerve and S. M. Hesjevik, "Testing of inhibitors for CO_2 corrosion using the electrochemical techniques", Proceedings of the 8th European Symposium on Corrosion Inhibitors, Ann. Univ. Ferrara, N. S., Sez. V, Suppl. N. 10, 1995, p. 1163.
19. E. Gulbrandsen, S. Nesic, A. Stangeland, T. Burchardtt, B. Sundfaer, S. M. Hesjevik, and S. Skjerve, "Effect of precorrosion on the performance of inhibitors for CO_2 corrosion of carbon steel", CORROSION/98, paper no. 98013. (Houston, TX: NACE, 1998).
20. R. De Marco, W.H. Durnie, A. Jefferson and B. Kinsella, "Surface Analysis of Adsorbed CO_2 Corrosion Inhibitors" Corrosion 57(1), 9-18.
21. D. A. López, W. H. Schreiner, S. R. de Sánchez and S. N. Simison "The influence of inhibitors molecular structure and steel microstructure on corrosion layers in CO_2 corrosion - An XPS and SEM characterization", Applied Surface Science 236 (2004) 77-97.
22. ASTM G1 - 03 Standard Practice for Preparing, Cleaning, and Evaluating Corrosion Test Specimens.
23. ASTM G102 - 89(2010) Standard Practice for Calculation of Corrosion Rates and Related Information from Electrochemical Measurements.
24. K. Lepková and R. Gubner, "Development of standard test method for investigation of under-deposit corrosion in carbon dioxide environment and its application in oil and gas industry" CORROSION/10, paper no. 10331. (San Antonio, TX: NACE, 2010).
25. Toušek J, "Theoretical aspects of the localized corrosion of metals", (Aedermannsdorf, Switzerland: Trans Tech Publications, 1985).
26. K. Lepková and R. Gubner, "Investigation of corrosion processes at sand-deposited surfaces in a carbon dioxide environment" CORROSION & PREVENTION/10, (Adelaide, South Australia: ACA, 2010).
27. K. Lepková and R. Gubner, "Study on corrosion processes at sand-deposited surfaces in a carbon dioxide media" EUROCORR /10, (Moscow, Russia: CONFERENCE PROCEEDINGS, 2010).

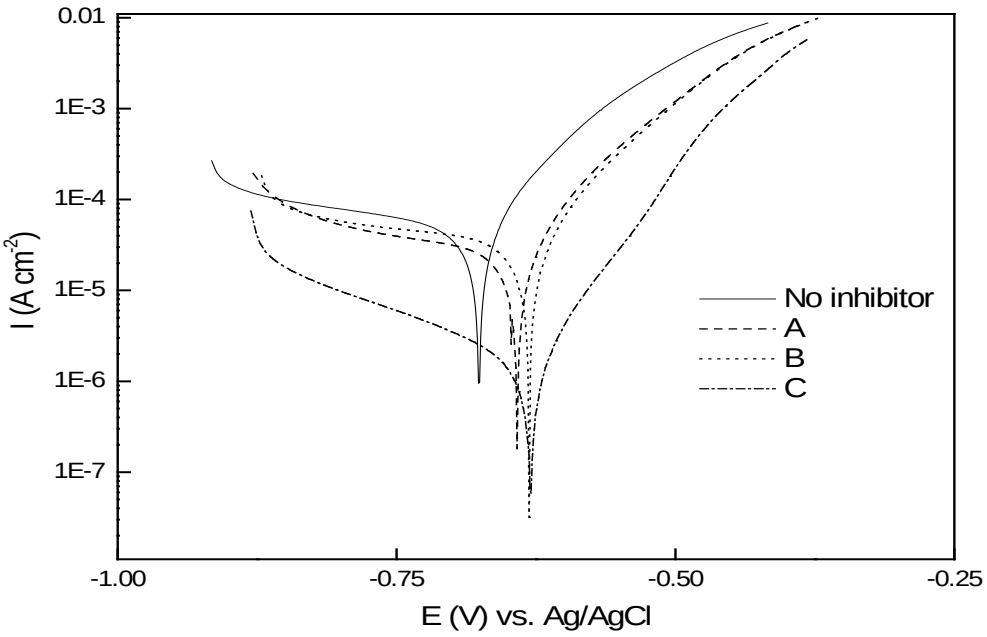

Figure 1: Potentiodynamic curves from surfaces with sand deposits without inhibitor and with inhibitors A, B and C after 1 hour immersion.

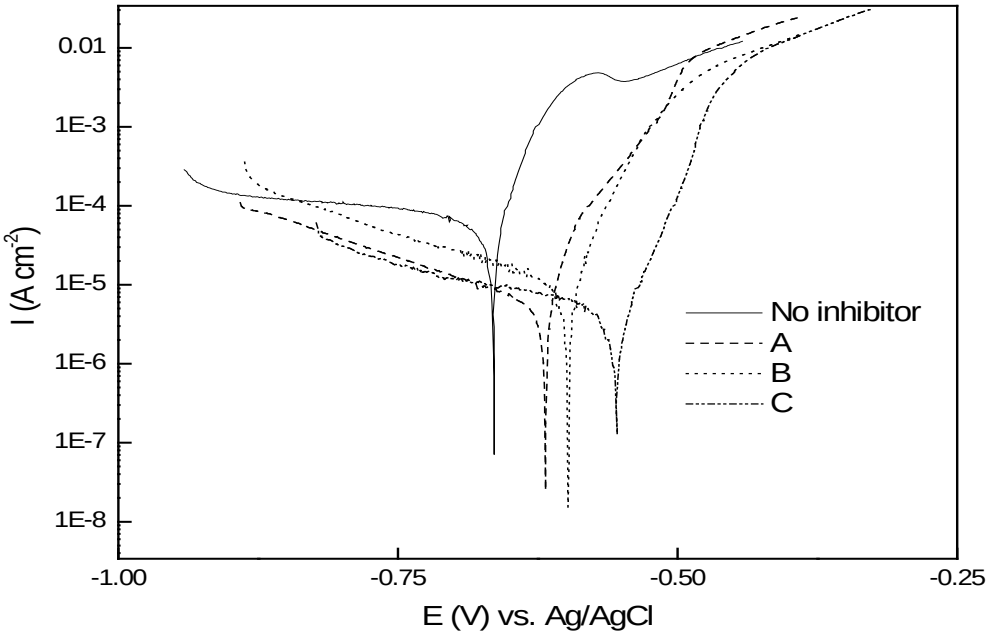

Figure 2: Potentiodynamic curves from bare surfaces without inhibitor and with inhibitors A, B and C after 1 hour immersion.

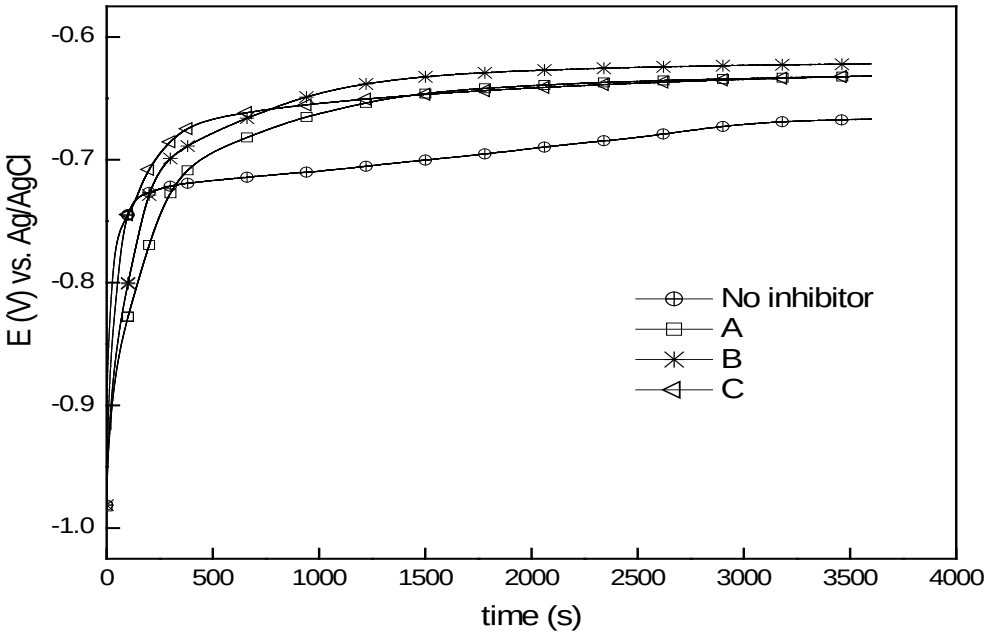

Figure 3: Open circuit potential measurements for surfaces with sand deposits and with inhibitors A, B and C.

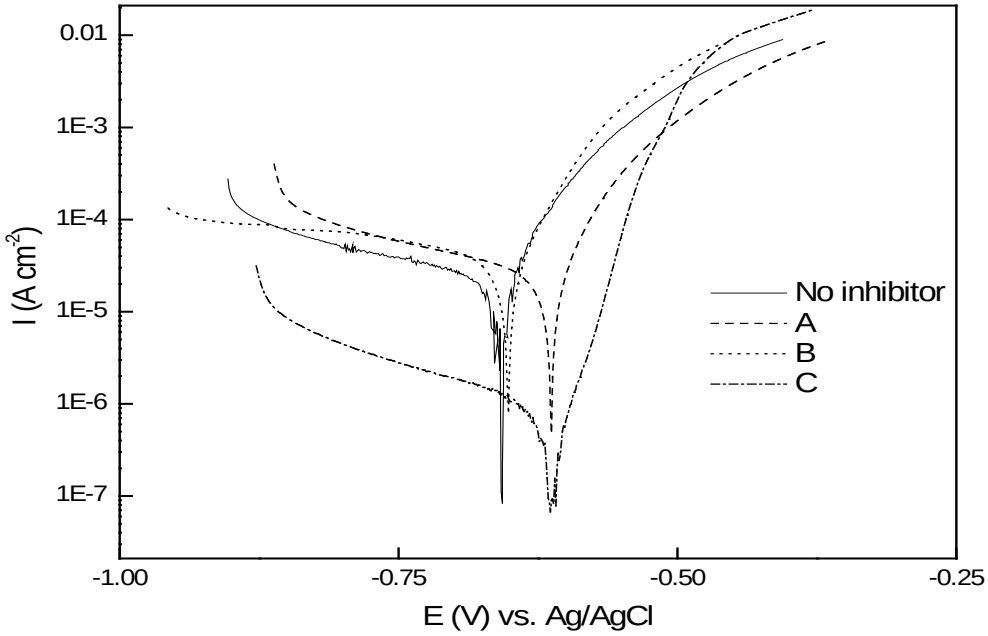

Figure 4: Potentiodynamic curves from surfaces with sand deposits without inhibitor and with inhibitors A, B and C after 12 hours immersion.

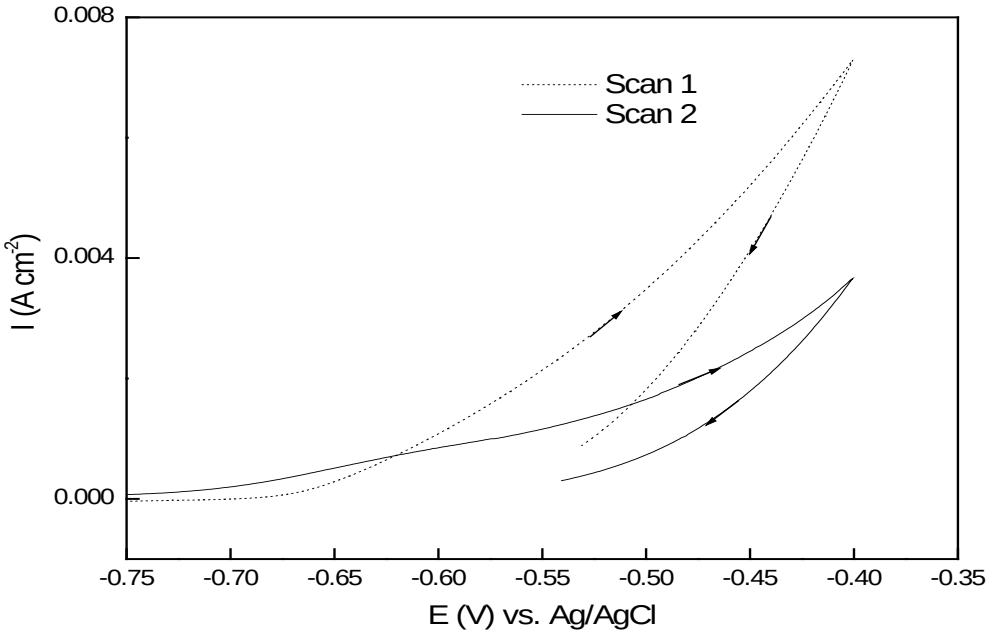

Figure 5: Cyclic voltammograms of surfaces with sand deposits and with inhibitor A. Scan 1-2.

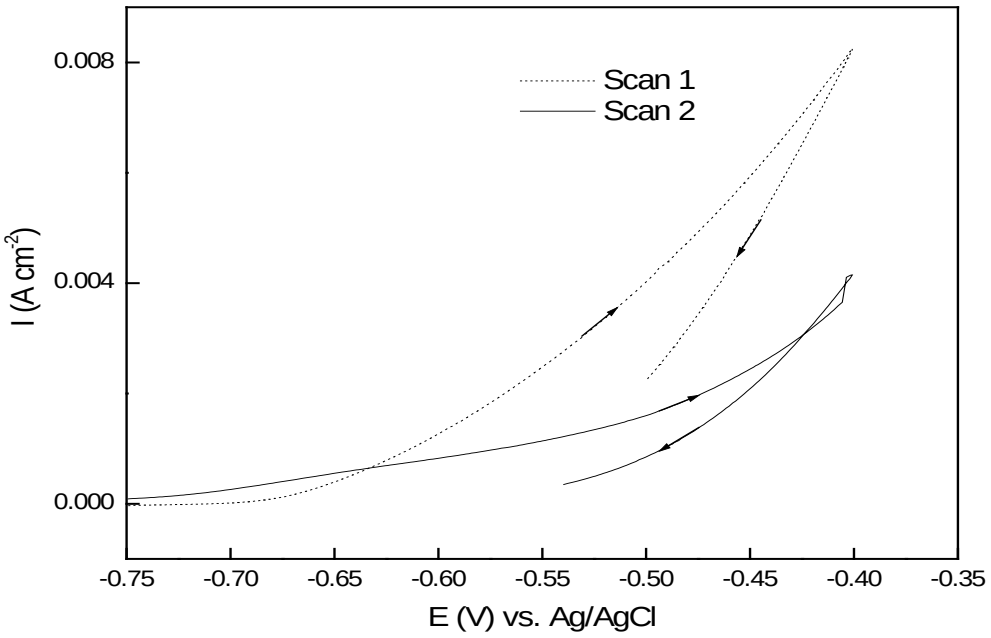

Figure 6: Cyclic voltammograms of surfaces with sand deposits and with inhibitor B. Scan 1-2.

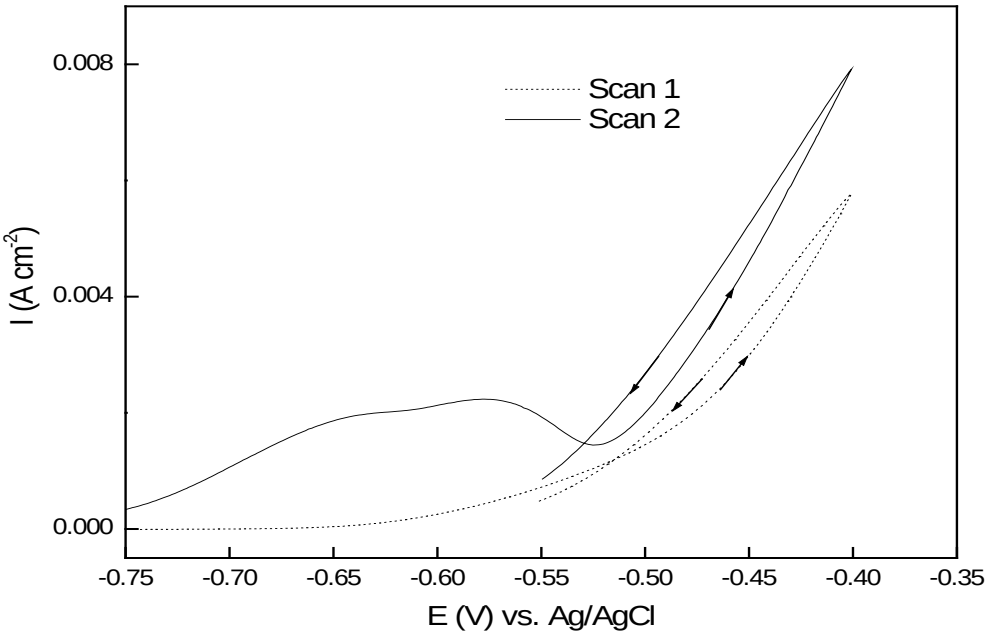

Figure 7: Cyclic voltammograms of surfaces with sand deposits and with inhibitor C. Scan 1-2.

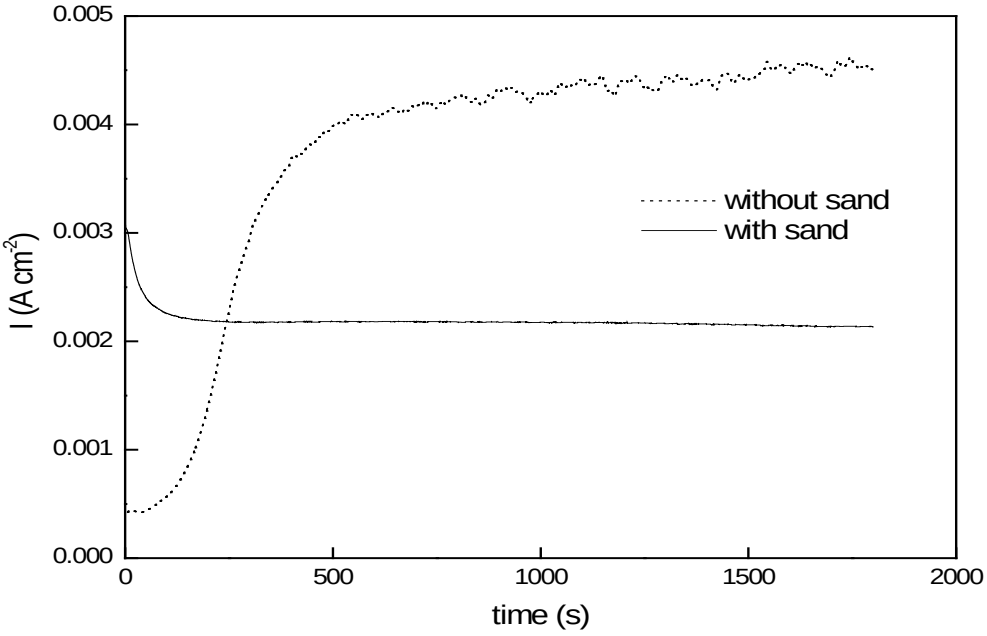

Figure 8: Potentiostatic transients at surfaces with and without sand deposits corroded at -0.5 V vs. Ag/AgCl. Inhibitor A present in the corrosive media.

9a **9b**

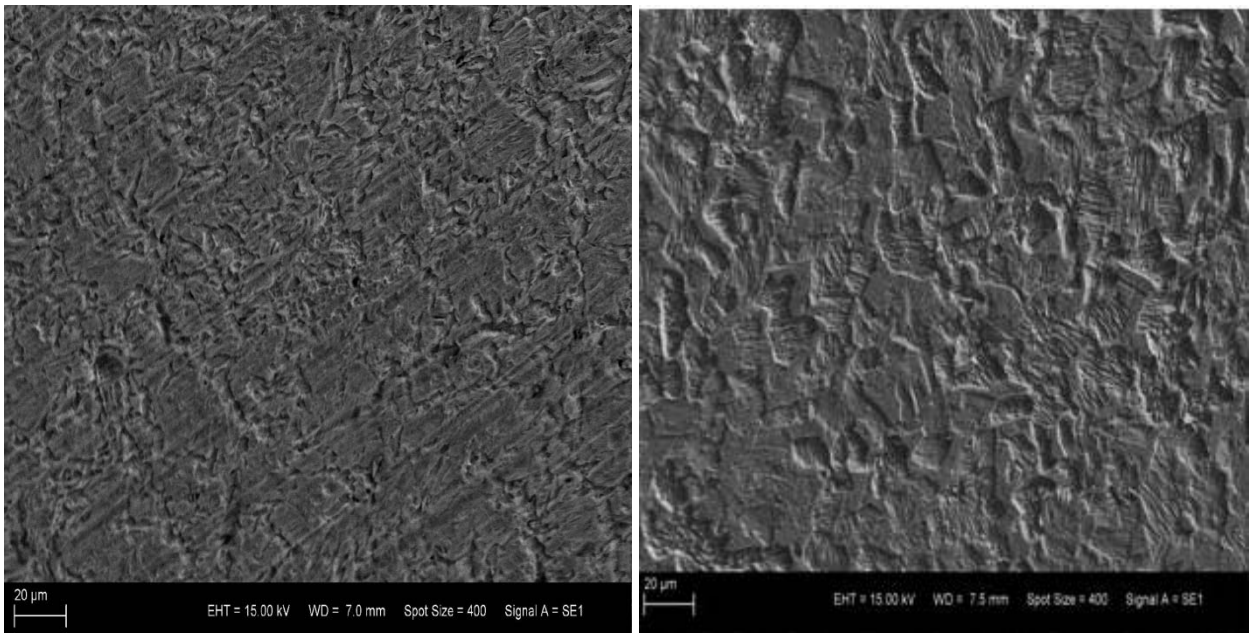

Figure 9: SEM images of carbon steel surfaces polarized in test solution with inhibitor A. 9a: bare sample surface; 9b: sample corroded under sand deposit.

10a **10b**

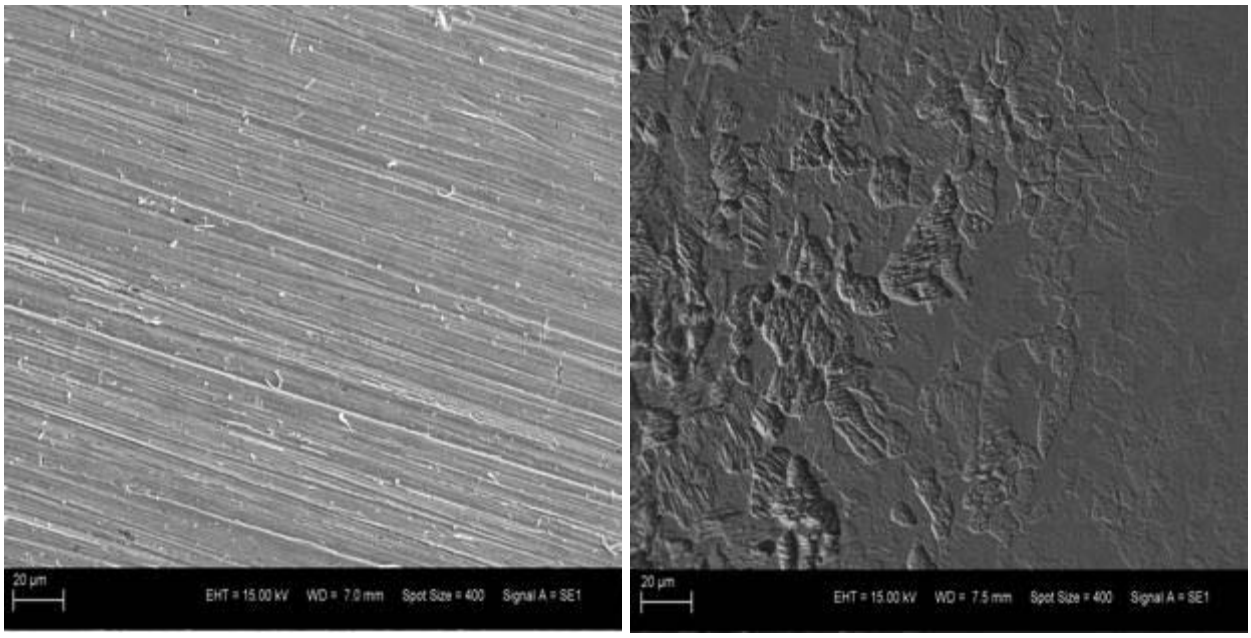

Figure 10: SEM images of carbon steel surfaces exposed to test solution with inhibitor A for 12 hrs. 10a: bare sample surface; 10b: sample corroded under sand deposit.

Chapter IV

V. Pandarinathan, K. Lepková, S.I. Bailey and R. Gubner, Evaluation of corrosion inhibition at sand-deposited carbon steel in CO_2-saturated brine, Corrosion Science, 72, 108-117 (2013)

Original Reprint of the Publication

Corrosion Science 72 (2013) 108–117

Contents lists available at SciVerse ScienceDirect

Corrosion Science

journal homepage: www.elsevier.com/locate/corsci

Evaluation of corrosion inhibition at sand-deposited carbon steel in CO_2-saturated brine

Vedapriya Pandarinathan, Kateřina Lepková *, Stuart I. Bailey, Rolf Gubner

Corrosion Centre for Education, Research and Technology, Department of Chemistry, Curtin University, Perth, WA 6845, Australia

ARTICLE INFO

Article history:
Received 16 November 2012
Accepted 4 March 2013
Available online 18 March 2013

Keywords:
A. Carbon steel
B. Polarization
B. EIS
C. Acid corrosion
C. Acid inhibition

ABSTRACT

The adsorption of four CO_2 corrosion inhibitors on silica sand and their subsequent inhibition activity at sand-deposited steel has been investigated. The presence of a sand deposit affects the performance of inhibitors at carbon steel due to their competitive adsorption on sand. Sulfur-containing organic compounds show minimal adsorption on sand compared to pyridinium surfactants and provide the highest inhibition efficiency at the sand-deposited steel. The extent of inhibitor adsorption onto sand is discussed in relation to their chemical structures. The significance of determining the adsorption affinity to sand in the selection of inhibitors to mitigate under-deposit corrosion is demonstrated.

1. Introduction

The CO_2 corrosion of carbon steel pipelines used in oil and gas production is exacerbated by the settling of deposits such as sand, resulting in the phenomenon known as under-deposit corrosion (UDC). UDC is often associated with localized attack and the formation of pits, which leads to severe corrosion problems in pipeline operations [1–4].

To mitigate the internal CO_2 corrosion of carbon steel structures, application of chemical inhibitors remains the most economical practice. Heterocyclic organic compounds containing one or more N, O, P and S atoms are commonly employed as corrosion inhibitors, among which the organic surfactants and S-containing compounds are reported as very effective inhibitors against internal pipeline corrosion of carbon steel in CO_2 environment [5–9]. The general inhibition principle is that the inhibitor molecules, which have a strong tendency to adsorb at metal surfaces, form a protective barrier against corrosion of steel. The inhibition efficiency depends on the chemical nature of the inhibitors.

An adequate quantity of a corrosion inhibitor is required at the steel surface to achieve the desired level of protection. However, inhibitors applied to the UDC-affected pipelines can adsorb to the sand deposits before reaching the underlying steel surface [10]. The inhibitor adsorption on sand, if not taken into account, can result in misinterpretation of the inhibition efficiency and of the corrosion rates of the sand-covered steel. In order to ensure effective corrosion control in the presence of the sand deposits, it is necessary to quantify the inhibitor adsorption to sand and the concentration remaining in the media for the protection of steel.

A number of chromatographic techniques such as high-performance liquid chromatography (HPLC), and thin layer chromatography (TLC) and spectroscopic techniques such as UV–Visible, Fourier transform infra-red (FTIR), and Raman spectroscopy are currently utilized for the quantitative analysis of inhibitor residuals in pipelines containing produced solids [11–16]. However, the chromatographic methods are all expensive and technically demanding compared to the UV–Visible spectroscopy, which has been shown to be a simple yet effective method for determination of corrosion inhibitor residuals in the oil field fluids [17–19].

The effect of sand deposits on the performance of corrosion inhibitors has been previously investigated using a combination of HPLC and UV–Visible spectroscopy [20,21]. It was established that the chemical structure of the inhibitors affects the extent of the adsorption on sand. The corrosion inhibitors which were not retained in significant quantity by the sand provided higher protection to the sand-deposited steel, as demonstrated by lower corrosion rates compared to the inhibitors highly-adsorbing on sand.

The aim of this study is to understand the extent of interaction between the corrosion inhibitors and sand deposit under CO_2 conditions. Corrosion inhibitors of different molecular structures, i.e. pyridinium surfactants and S-containing organic compounds, are investigated as they represent the main components of many inhibitor mixtures applied to protect carbon steel pipelines. Sand adsorption studies were performed using UV–Visible spectroscopy prior to inhibitor evaluation experiments at sand-deposited steel. The sand adsorption test results are compared with the corresponding corrosion rates obtained from electrochemical tests run

* Corresponding author. Tel.: +61 8 92667319; fax: +61 8 92662300.
E-mail address: K.Lepkova@curtin.edu.au (K. Lepková).

0010-938X/$ - see front matter © 2013 Elsevier Ltd. All rights reserved.
http://dx.doi.org/10.1016/j.corsci.2013.03.013

under simulated oil field conditions. Establishing a correlation between the adsorption values and the corrosion rates would facilitate the selection of corrosion inhibitors suitable for protecting steel against under-deposit corrosion.

2. Experimental

2.1. Test materials

The test solutions were prepared in ultra-pure water (Mili-Q system, resistivity 18.2 MΩ cm). The test brine solution (non-inhibited) consisted of 3% sodium chloride (NaCl; Ajax Finechem, analytical reagent, 99.9%) and 0.01% sodium hydrogen carbonate ($NaHCO_3$; Merck, 99.5%). The inhibited test solutions were prepared by adding the corrosion inhibitors in the concentration range of 5–200 ppm (ppm by weight) to the test brine solution. The chemical structures, names and abbreviations of the corrosion inhibitors studied are given in Table 1. All corrosion inhibitors were purchased from Sigma–Aldrich and used as received without any further treatment. The test solutions were saturated with CO_2 (oxygen content <10 ppb; pH-4.7) and used at temperature of 30 °C in all experiments.

Silica sand (SiO_2; Sigma–Aldrich) had the mean particle size of 303 μm (laser diffraction analysis) and specific surface area of 0.062 m^2/g (BET analysis). The sand was acid-washed and dried prior to use. The pH of the test solution was checked before and after addition of sand to ensure that no pH changes occurred due to the acid-wash procedure.

Carbon steel (1030 grade) had the following chemical composition by weight%: C (0.37%), Mn (0.80%), Si (0.282%), P (0.012%), S (0.001%), Cr (0.089%), Ni (0.012%), Mo (0.004%), Sn (0.004%), Al (0.01%), and Fe (balance). Carbon steel coupons with surface area of 0.196 cm^2 were embedded in epoxy resin, ground with SiC paper to 1200 grit, rinsed with ethanol and ultra-pure water, dried with nitrogen and placed into the test cell. Care was taken when handling the samples to minimize their exposure to air.

2.2. Test methods

2.2.1. UV–Visible spectrophotometry

The quantitative analysis of corrosion inhibitors was conducted by UV–Visible spectrophotometry using a Hewlett Packard 8452A diode array spectrophotometer (wavelength range 190–820 nm). The amount of inhibitor adsorbing on sand was determined by measuring the concentration of inhibitor in the test solutions before and after contact with sand.

8 g of silica sand was added to 100 mL of inhibited test solutions (10, 50 and 100 ppm) in glass bottles at 30 °C for an adsorption period of 96 h. The continuously CO_2 purged solutions in glass bottles were periodically shaken to ensure homogeneity. The volume of test solutions and the amount of sand were kept constant in all experiments. At the end of the test duration, the inhibited test solutions were centrifuged prior to the UV–Visible analysis in order to avoid any interference in the spectra from suspended sand particles. The UV absorbance of the test solutions was recorded every 24 h for a period of 96 h. No change occurred in the absorbance intensity of any of the solutions after 72 h of contact with sand.

The UV spectra of standard test solutions consisting of known concentrations (5–200 ppm) of the corrosion inhibitors were recorded to generate calibration plots. The correlation coefficient (r) of the linear calibration plots was greater than 0.98 for all inhibited test solutions, which confirms an acceptable calibration. The remaining concentration of each corrosion inhibitor after the sand adsorption experiments was calculated using the calibration data.

2.2.2. Electrochemical measurements

The electrochemical tests were performed using a working electrode (carbon steel coupon) placed at the bottom of glass cell and covered with a layer of sand (sand deposit). In all experiments, 8 g of sand was used ensuring a consistent height of ~7.5 mm of the sand deposit at the steel surface. The cell was de-aerated prior to the addition of the CO_2 saturated test solutions. The reference and counter electrodes were Ag/AgCl (3.5 M) and Hastelloy C, respectively. A Luggin capillary was used with the reference electrode to minimize the IR drop. The same distance between the reference and working electrode was maintained for all experiments. The carbon steel coupons were left to stabilize in the test solutions prior to the electrochemical analysis. All electrochemical measurements were run at 30 °C under stagnant conditions and ambient CO_2 pressure.

The potentiodynamic polarization tests were carried out in the potential range of ±0.25 V vs. open circuit potential (OCP) at a scan rate of 0.6 V/h using the Gamry Reference 600 potentiostat (Gamry Instruments, USA). The stabilization periods before potentiodynamic measurements were 1 h and 72 h, during which the OCP was continuously recorded. The corrosion rates (υ_{cor}) in mm y^{-1} were calculated from the estimated current densities (i_{corr}) obtained from the intercept of the two linear segments of the respective Tafel plots using the following equation [22]:

$$\upsilon_{cor} = 3.27 \times i_{corr} \times \frac{M}{\rho} \quad (1)$$

where i_{corr} is the corrosion current density in μA cm^{-2}, M is the molar mass of 1030 carbon steel in g mol^{-1}, ρ is the density in g $cm^{-3}$of 1030 carbon steel.

The % inhibition efficiency (η) from potentiodynamic test results was determined using the following equation:

Table 1
Chemical formulas and structures of corrosion inhibitors.

Corrosion inhibitor	Chemical formula	Chemical structure
Cetylpyridinium chloride monohydrate (CPC)	$C_{21}H_{38}ClN\cdots H_2O$	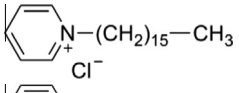
1-Dodecylpyridinium chloride hydrate (DPC)	$C_{17}H_{30}ClN\cdots H_2O$	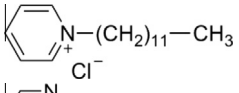
2-Mercaptopyrimidine (MPY)	$C_4H_4N_2S$	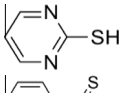
Thiobenzamide (TB)	$C_6H_5CSNH_2$	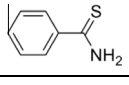

$$\eta = \left(\frac{i_{corr(brine)} - i_{corr(inhibitor)}}{i_{corr(brine)}}\right) \times 100 \quad (2)$$

where $i_{corr(brine)}$ and $i_{corr(inhibitor)}$ are the corrosion current densities in $\mu A\,cm^{-2}$ from the non-inhibited and inhibitor-containing test solution, respectively.

The electrochemical impedance spectroscopy (EIS) measurements were performed using the Gamry Reference 600 potentiostat. The stabilization period before EIS measurements was 1 h at OCP. The AC excitation amplitude of 10 mV over a frequency range of 10 kHz to 0.01 Hz at 10 points per decade was applied and the impedance spectra were analyzed using ZView software (Scribner Associates Inc.) to determine the corrosion rates. The % inhibition efficiency (η_z) from EIS measurements was determined using the following equation:

$$\eta_z = \left(\frac{R_{ct(inhibitor)} - R_{ct(brine)}}{R_{ct(inhibitor)}}\right) \times 100 \quad (3)$$

where $R_{ct(brine)}$ and $R_{ct(inhibitor)}$ are the charge transfer resistances in $\Omega\,cm^2$ from the non-inhibited and inhibitor-containing test solution, respectively.

3. Results and discussion

3.1. Evaluation of adsorption of corrosion inhibitors on sand

The UV spectra showing the wavelength of maximum absorption (λ_{max}) of different inhibitors (initial concentration C_i = 100 ppm) after 24 h contact with sand are presented in Fig. 1. The absorbance intensities (A) at the marked wavelengths (λ_{max}) were used to determine the final inhibitor concentrations (C_f) remaining in the solutions after the adsorption on sand. It is noteworthy that commercial inhibitor formulations often contain a mixture of several components. Fig. 1 shows that each inhibitor species does have a unique spectrum, and it is clear that advanced numerical methods could be applied to deconvolute the spectra of mixtures – however this would depend on the specific properties of each inhibitor component, and is beyond the scope of the present investigation.

3.1.1. Effect of contact time and initial inhibitor concentration

Fig. 2 shows the residual inhibitor concentration as a function of time (duration of contact with sand) calculated from the UV–Visible analysis (A at λ_{max}). The initial corrosion inhibitor concentrations before sand addition were 10, 50 and 100 ppm (mg/L) in a 100 mL test solution volume.

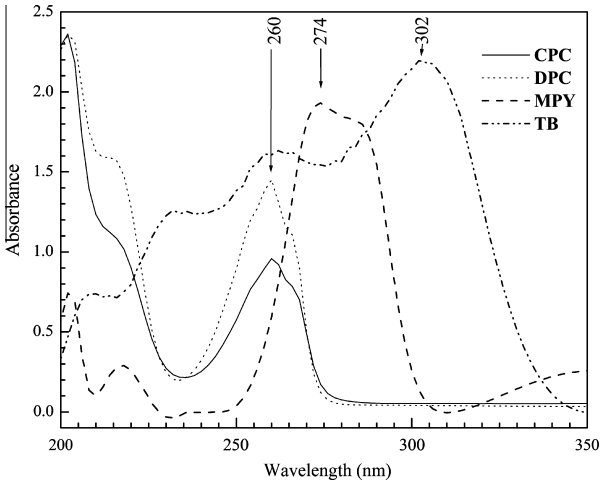

Fig. 1. UV absorbance spectra of CO_2 saturated inhibited test solutions at 30 °C after 24 h contact with sand, showing the absorption maxima of each corrosion inhibitor. Concentration of inhibitors before sand addition (C_i) is 100 ppm.

It can be seen that inhibitor CPC (Fig. 2A) undergoes a more significant concentration decrease due to sand addition, as compared to the rest of the inhibitors studied, and attains a steady value after 72 h. The concentration of DPC (Fig. 2B) decreases to a lesser extent compared to CPC. The major concentration decrease is observed in the first 24 h. It is to be noted that the critical micelle concentration (cmc) determined for CPC in the test electrolyte (3% NaCl) was <2 ppm and the concentration range studied always gives micellar solutions. Whereas the inhibitor DPC has a higher cmc value (~60 ppm) such that the studied concentration range includes both solutions below and above the cmc.

Only a minimal effect of sand, indicated by a negligible decrease in the inhibitor concentration, is observed for the S-containing compounds MPY and TB, irrespective of their initial concentrations. Steady concentration values are established within 24 h of the test duration for both the MPY (Fig. 2C) and TB (Fig. 2D).

The concentration decrease from the bulk solution represents the quantity of the inhibitor adsorbed (q_{ads}) on sand. The q_{ads} values are determined using the following equation [23]:

$$q_{ads} = \frac{((c_i - c_f) \times V)}{M} \quad (4)$$

where q_{ads} is the amount of corrosion inhibitor adsorbed in mg/g of sand, C_i is the initial inhibitor concentration before sand addition in ppm (mg/L), C_f is the final inhibitor concentration remaining in solution in ppm (mg/L), V is the volume of test solutions in L, M is the mass of adsorbent (sand) in g. The concentration values and the calculated q_{ads} are summarized in Table 2 for all the corrosion inhibitors studied.

The data for CPC (Table 2) reveal that the amount adsorbed (q_{ads}) on sand is dependent on the initial concentration (C_i) and increases with the increase in C_i. When C_i is raised from 10 to 100 ppm, the amount adsorbed increases from 0.07 to 1.14 mg/g respectively. This can be related to a greater number of molecules being available for the adsorption on the sand surface at the high C_i that subsequently results in higher q_{ads}. The DPC data show that there is a comparatively large quantity of DPC retained in the solution phase at each concentration after the test period of 72 h, compared to CPC, despite their similar molecular structure. The DPC does not show significant adsorption on sand compared to CPC at the higher C_i as can be seen from its adsorption amount at C_i of 50 and 100 ppm. At C_i of 10 ppm, the q_{ads} of CPC and DPC are closely similar. In contrast to CPC and DPC, it is apparent from the q_{ads} < 0.03 mg/g that initial concentration of the corrosion inhibitor has minimal influence on the adsorption of the two S-containing compounds, MPY and TB. The adsorption data were tested using Langmuir, Temkin and Freundlich isotherms, but no linear fit to these isotherms could be obtained for the sand-deposited steels in the concentration range studied.

The primary focus of this investigation is in determining the extent of adsorption of inhibitors on sand with respect to the chemical structure of the inhibitor. The mechanism of adsorption and the molecular orientation of the inhibitors at sand/steel surface are not addressed in detail. Nonetheless the differences in the adsorption behavior of the corrosion inhibitors used in this study can be attributed to the structural/molecular properties of the respective compounds. Previous studies showed that charged organic inhibitor molecules can adsorb on oppositely charged solid substrates (silica sand) by electrostatic interaction [23,24]. Hence, it is probable that the positive charge of the cationic-surfactant inhibitors CPC and DPC has an influence on the sand adsorption levels of these inhibitors. The hydrophilic quaternary ammonium head group of CPC and DPC are electrostatically attracted by the high density of acquired negative charges at the sand surface in

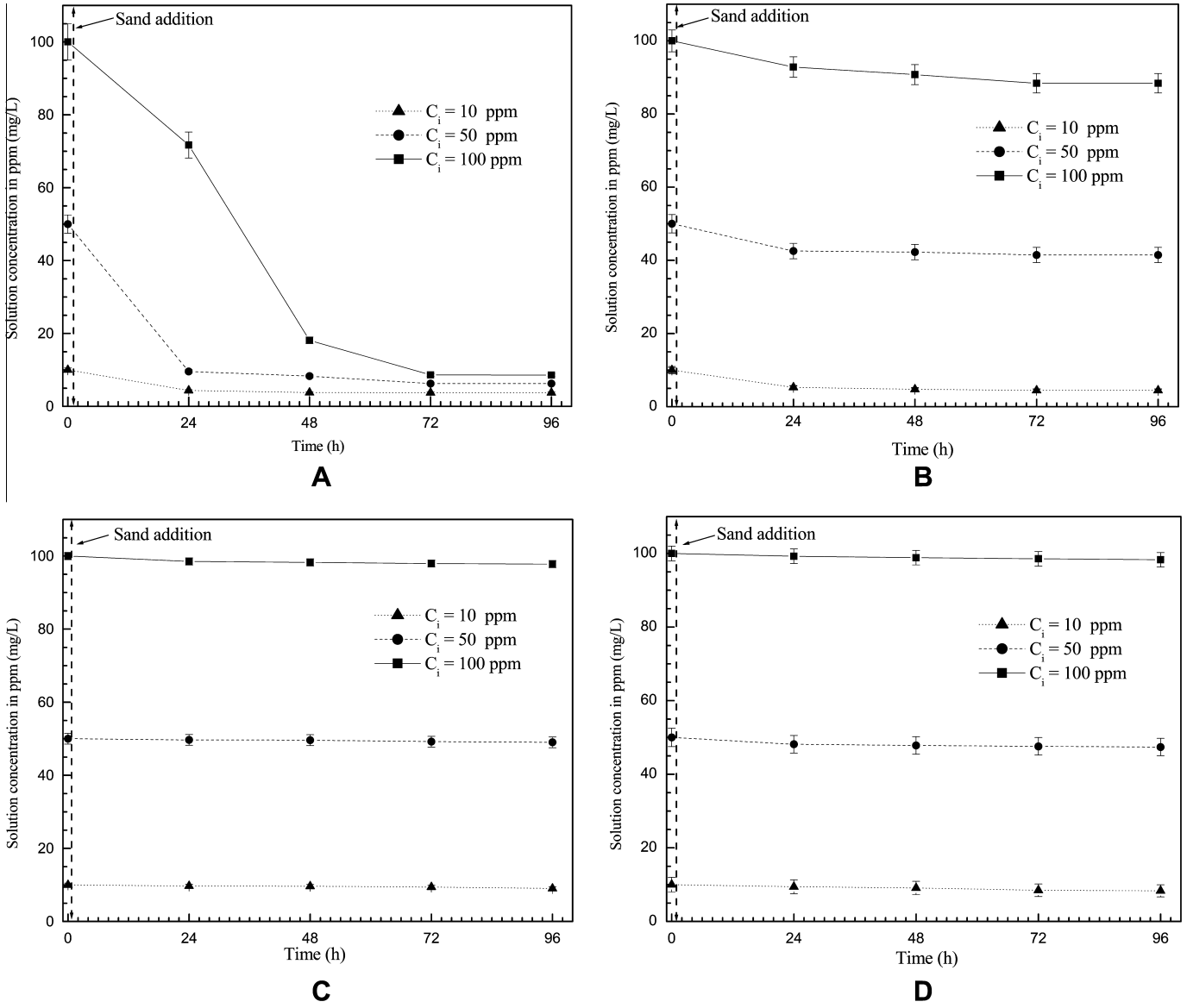

Fig. 2. Change in inhibitor concentration with time in CO_2 saturated inhibited test solutions containing different initial inhibitor concentrations due to sand adsorption; (A) CPC; (B) DPC; (C) MPY; and (D) TB.

Table 2
Amount of corrosion inhibitor adsorbed on sand after 72 h determined by UV–Visible analysis for different initial inhibitor concentrations in CO_2 saturated test solutions at 30 °C.

Inhibitors	C_i ppm (mg/L)	C_f ppm (mg/L)	q_{ads} mg/g
CPC	10	3.7	0.07
	50	6.2	0.54
	100	8.6	1.14
DPC	10	4.4	0.06
	50	41.4	0.10
	100	88.4	0.14
MPY	10	9.0	<0.02
	50	49.0	
	100	97.7	
TB	10	8.3	<0.03
	50	47.3	
	100	98.2	

aqueous solution. The fact that the surfactants' adsorption on sand predominantly involves electrostatic interactions is supported by our adsorption experiments carried out in aerated test solutions (dissolved oxygen content ~8.69 ppm) without any CO_2 (graphs not shown). The amount of inhibitor adsorbed on sand (q_{ads}) from aerated test solutions of pH ~ 7.58 were less than 0.03 mg/g for all the corrosion inhibitors tested. Comparing this to the q_{ads} values in Table 2 obtained from CO_2-saturated test solutions (pH ~ 4.7), it can be seen that the higher inhibitor adsorption on sand occurred under the CO_2 conditions (acidic pH range).

However, variation in the level of adsorption between CPC and DPC is observed, showing that CPC interacted more strongly with sand compared to DPC. This can be a reflection of the difference in the length of their alkyl chains. CPC possesses high hydrophobicity due to its longer alkyl chain, thus greater affinity for active sites on sand [25–29]. Thus, the inhibitor CPC with longer hydrophobic chain adsorbs more on sand than the shorter alkyl chain compound DPC, thereby the amount adsorbed is higher for CPC compared to DPC as demonstrated by the data in Table 2.

By contrast, the amounts of MPY and TB adsorbed on sand are significantly lower compared to the cationic-surfactants, CPC and DPC. The MPY and TB are polar molecules with the S- and N-atom

being the negative and positive end of the dipole, respectively. The strongly electronegative sulfur atom which is the adsorption centre of the two S-containing compounds exhibits less attraction to the negatively charged silica sand, hence the long persistence in the solution phase [20]. This suggests that MPY and TB at the concentration studied are good candidates for corrosion protection of steel underneath the sand deposit.

3.2. Effect of sand deposit on the CI performance on steel

3.2.1. Corrosion potential measurements

The open circuit potential (OCP) was monitored continuously for 72 h at the carbon steel samples under a sand deposit in CO_2 saturated test brine solution (non-inhibited) and inhibited test solution containing 100 ppm corrosion inhibitors, in order to determine the effect of the sand on the electrochemical potential of the underlying steel surface (Fig. 3). The exposure time of 72 h corresponds to the time needed for saturation of sand with the inhibitor as determined by sand adsorption (UV–Visible analysis) experiments (Fig. 2). The OCP reaches stable values after approximately 1 h exposure time and then remains constant in all tests except for that carried out with the CPC. Stable OCP values indicate that the formation of inhibitor film on the steel surface is causing the corrosion reactions to stabilize. The OCP of TB is more positive and that of CPC is more negative in respect to the non-inhibited sample, suggesting that TB offers superior protection among the corrosion inhibitors studied. The potential of sand-deposited steels in all the inhibited test solutions shifted towards the cathodic direction with respect to the non-inhibited sample. This indicates that the tested inhibitors could be regarded as mixed-type inhibitors, predominantly suppressing the cathodic reactions.

3.2.2. Polarization measurements

The effectiveness of corrosion inhibitors on the steel surfaces with and without sand deposit was evaluated after 1 h exposure to the inhibited (100 ppm inhibitor concentration) and non-inhibited test solutions using the potentiodynamic polarization technique. The results are presented graphically in Fig. 4. At sand-deposited surfaces, the potentiodynamic tests were also carried out after 72 h exposure to the test solutions, to evaluate the influence of exposure time on the inhibitor performance (curves not shown).

The corrosion potential (E_{corr}), corrosion current density (i_{corr}) and Tafel constants (βa, βc) were estimated from the Tafel extrapolation of the polarization curves in Fig. 4. The electrochemical parameters obtained from all potentiodynamic tests are summarized in Table 3.

The results show that the overall corrosion current densities decreased in inhibited test solutions, with respect to test brine solution (non-inhibited), at both steel with and without sand deposit.

At the steel surface with sand deposit (Fig. 4A, 1 h exposure time), the inhibitors CPC and DPC were found to have a moderate effect on corrosion mitigation, ascertained from the small decrease in i_{corr} in respect to the non-inhibited carbon steel. On the other hand, regardless of the sand deposit on the surface, the compounds MPY and TB were effective in corrosion inhibition as demonstrated by a considerable i_{corr} decrease in their presence. This can be ascribed to blockage of corroding sites on the metal surface by the MPY and TB molecules, thereby reducing the access to the corrosive species from the test solution [30]. The inhibition performance at steel surface with sand deposit is in the sequence MPY ≈ TB > DPC > CPC.

At steel surfaces without sand deposit (Fig. 4B, 1 h exposure time), introducing the inhibitors resulted in lower general corrosion rates depicted by a shift in potential with respect to non-inhibited surface. The observed anodic current densities of steels without sand were steeper which can be attributed to the active dissolution of the bare steel surface compared to sand-deposited

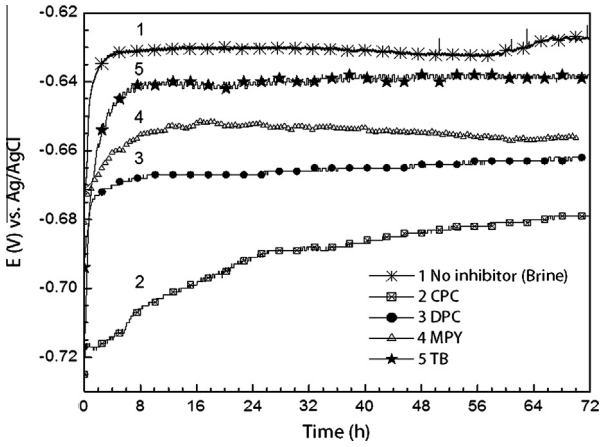

Fig. 3. OCP measurements of steel covered with a sand deposit in CO_2 saturated non-inhibited and inhibited test solutions for 72 h at 30 °C.

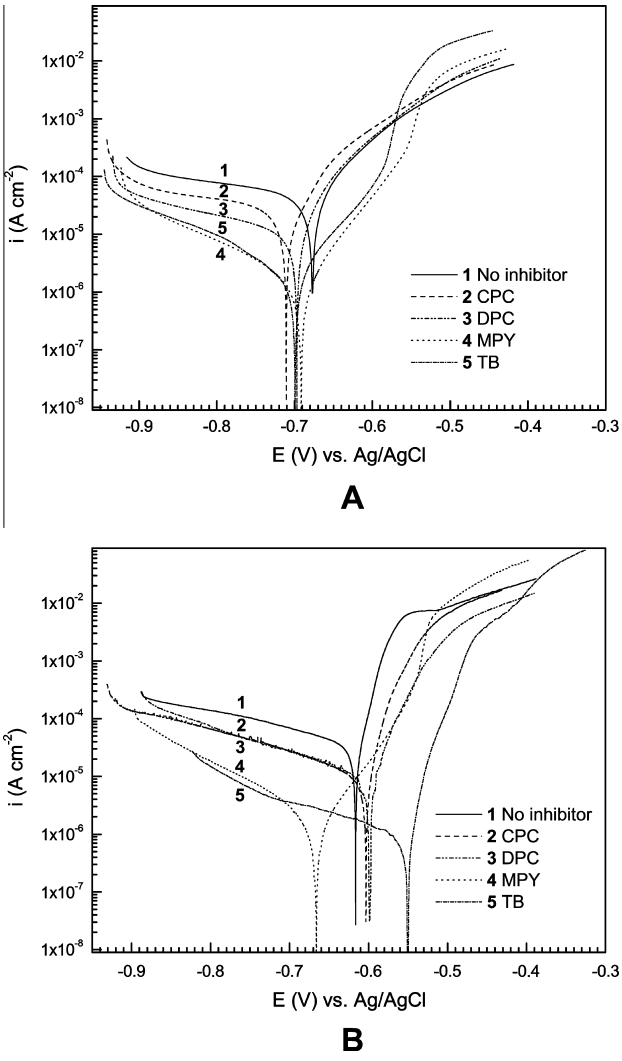

Fig. 4. Potentiodynamic polarization curves recorded at steel surfaces; (A) with sand deposit; (B) without sand deposit after 1 h exposure in CO_2 saturated non-inhibited (test brine) and inhibited test solutions at 30 °C.

Table 3
Electrochemical parameters derived from potentiodynamic polarization measurements of carbon steel with and without sand deposit in CO_2 saturated non-inhibited (test brine) and inhibited test solutions at 30 °C.

	Without sand deposit after 1 h exposure						With sand deposit								
							After 1 h exposure						After 72 h exposure		
	$-E_{corr}$ V vs. Ag/AgCl	i_{corr} μA cm^{-2}	βa V dec^{-1}	$-\beta c$	v_{cor} mm y^{-1}	η %	$-E_{corr}$ V vs. Ag/AgCl	i_{corr} μA cm^{-2}	βa V dec^{-1}	$-\beta c$	v_{cor} mm y^{-1}	η %	$-E_{corr}$ V vs. Ag/AgCl	i_{corr} μA cm^{-2}	v_{cor} mm y^{-1}	η %
No inhibitor	0.616	46.43 ± 0.07	0.025	0.393	0.52	–	0.675	45.87 ± 0.05	0.106	0.474	0.52	–	0.621	31.53 ± 0.04	0.36	–
CPC	0.603	9.92 ± 0.04	0.031	0.261	0.11	78.6	0.710	43.01 ± 0.07	0.103	0.324	0.49	6.2	0.750	38.42 ± 0.07	0.43	−21.8
DPC	0.598	5.87 ± 0.04	0.037	0.399	0.07	87.3	0.697	20.28 ± 0.05	0.088	0.308	0.23	55.8	0.687	14.91 ± 0.07	0.17	52.7
MPY	0.665	1.42 ± 0.02	0.057	0.120	0.016	96.9	0.691	1.33 ± 0.04	0.056	0.146	0.015	97.4	0.665	1.05 ± 0.03	0.012	96.6
TB	0.549	1.39 ± 0.03	0.042	0.363	0.015	97.0	0.699	2.15 ± 0.03	0.063	0.158	0.024	95.3	0.657	1.51 ± 0.03	0.017	95.2

steels. The polarization curves from the CPC and DPC-containing test solutions are identical on the cathodic domain and a slight shift in the E_{corr} in respect to the non-inhibited carbon steel was observed. There is no appreciable difference in their Tafel slopes, suggesting that the inhibition activity against the corrosion reactions is similar for both CPC and DPC [30]. The greatest inhibition performance is observed from S-containing compounds MPY and TB. Even though the current density decreases in both anodic and cathodic domains of the polarization curve of MPY, the negative shift in the E_{corr} observed at the MPY inhibited steel, in respect to the non-inhibited steel can be related to the suppression of the cathodic corrosion reaction primarily. It is evident from Fig. 4B that the compounds MPY and TB afford superior protection to the steel surface without sand deposit compared to rest of the inhibitors. The corrosion control performance of the inhibited steels without sand is in the same sequence as sand-deposited steels.

Comparing the electrochemical parameters obtained both from steel with and without a sand deposit after 1 h exposure (Table 3), the corrosion rates are higher at surfaces with sand deposit, indicating that the sand has a negative impact on the inhibitor performance. Similar observations for inhibited systems with sand have been reported previously [20,31–35] and the behavior was attributed to the sand deposit which influences the corrosion inhibitor activity at the steel by competing for adsorption sites. The data presented in Table 3 shows that the S-containing compounds MPY and TB imparts an inhibition efficiency >95% in the tests both with and without sand deposit, which is apparently greater than that of the cationic-surfactants, CPC and DPC. Among the cationic-surfactants, the inhibitor efficiency of DPC (55.8%) is significantly higher than that of CPC (6.2%) at steel with a sand deposit. The inhibitor most impacted by the sand is CPC, for which efficiency is reduced by a factor of 12 in the presence of sand deposit at the surface. This substantial difference in the inhibitor efficiencies at steel with and without a sand deposit can be associated with the possible affinity of CPC to sand preferred to the steel surface underneath.

The results from the potentiodynamic polarization tests carried out at the sand-deposited surfaces after 72 h exposure of the steel to the test solutions (Table 3) showed that the efficiency of the CPC decreased over time. CPC was found to provide no inhibition to the corrosion reactions of the steel surface after 72 h exposure. In contrast, no significant changes in the corrosion rates were observed in tests with DPC, MPY and TB after 72 h compared to that from 1 h exposure time. The saturation of the sand deposit with the inhibitor led to only a slight reduction in the corrosion rates and the inhibition efficiency at surfaces with sand deposit after 72 h follows the similar trend as observed after 1 h exposure (MPY ≈ TB > DPC > CPC).

3.3. Electrochemical impedance measurements

To confirm the observed corrosion behavior, EIS measurements were recorded at the steel samples with and without sand deposit (after 1 h at OCP) exposed to CO_2 saturated inhibited (100 ppm inhibitor concentration) and non-inhibited test solutions.

Fig. 5A and B shows the Nyquist plots of carbon steel with sand deposit in all test solutions and the inset shows the equivalent circuit used to fit the impedance data. As can be seen, a single depressed semicircle equivalent to charge transfer resistance (R_{ct}) is observed indicating that the corrosion reactions at both non-inhibited and inhibited solutions are charge transfer controlled. The R_{ct} increases in the sequence MPY ≈ TB > DPC > CPC, the same order as obtained from the potentiodynamic polarization results. The corresponding Bode plots are shown in Fig. 5C and it is evident that the impedance increased for all the inhibited steels when compared to the non-inhibited steel. The phase shift observed in the high

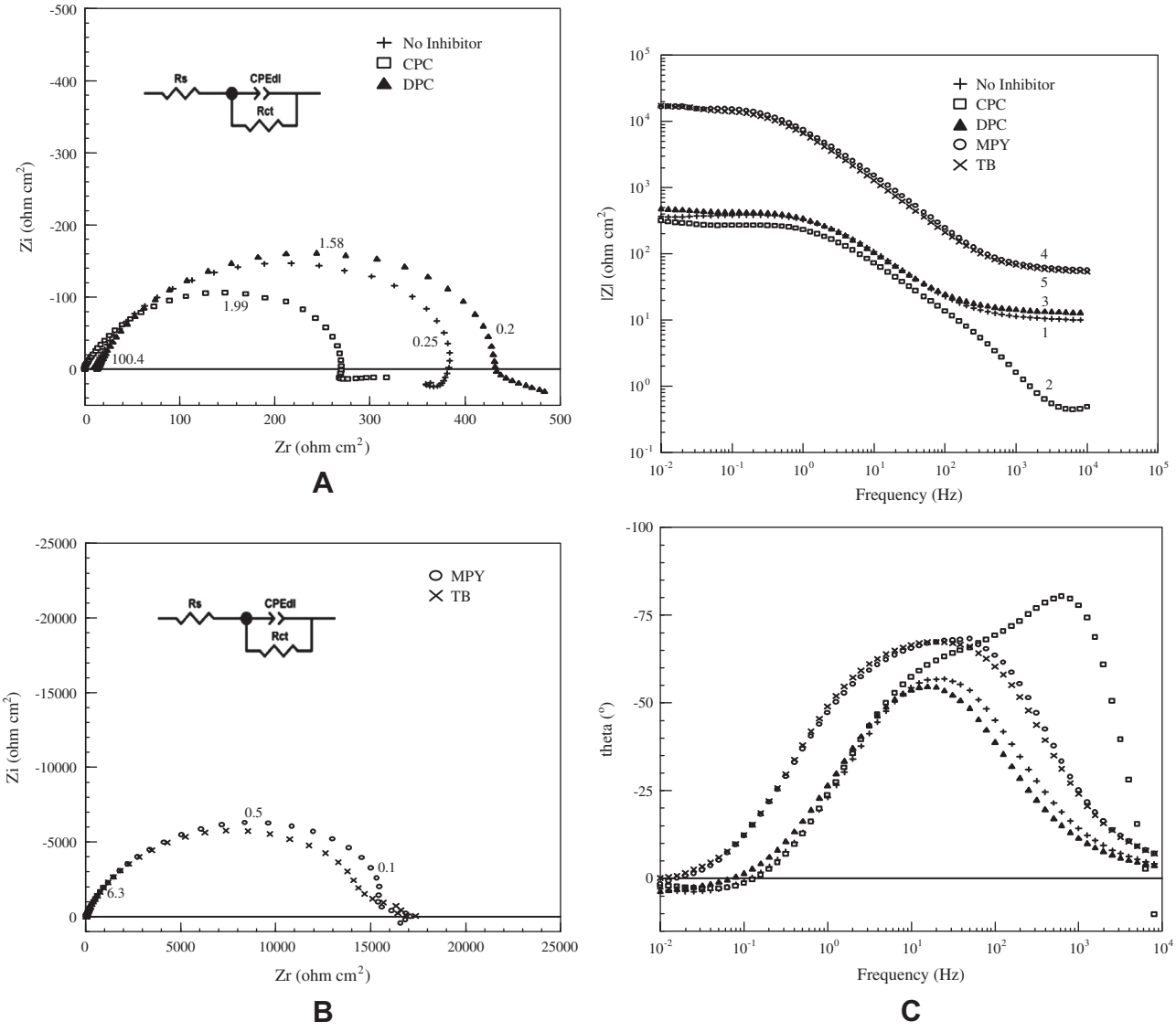

Fig. 5. Impedance spectra of steel surfaces with sand deposit after 1 h exposure in CO_2 saturated test solutions at 30 °C; (A) Nyquist plots for steels in solution containing no inhibitor, CPC and DPC; (B) Nyquist plots for steels in solutions containing MPY and TB; and (C) Bode plots from all test solutions; Fig. Inset – Randle's equivalent circuit model used to fit impedance data.

frequency domain for inhibited surfaces with respect to non-inhibited steel seen from the Bode phase plot indicates that the studied inhibitors protect the underlying steel surface.

Fig. 6A and B displays the Nyquist plots of carbon steel without sand deposit in all test solutions. The plots of MPY and TB in Fig. 6B are similar to those observed from steel with sand deposit seen in Fig. 5B; whereas the R_{ct} of CPC and DPC inhibited steel increased with respect to steel with sand deposit (Fig. 5). This indicates that the resistance to corrosion, and hence the effectiveness of the inhibitors is higher if there is no sand present. The corresponding Bode plots from steels without sand deposit are presented in Fig. 6C.

From Fig. 6B, it can be seen that the Nyquist plots from steels without sand in test solutions containing MPY and TB shows a poorly defined second time constant, which cannot be discriminated clearly from the Bode plot in Fig. 6C as well. Interestingly, the second time constant is much less pronounced in the presence of sand deposit at the steel surface (Fig. 5A–C). However, this feature does not affect the interpretation of the results in the way that they have been used, but it may suggest the formation of a strongly adsorbed inhibitor film on the bare steel surfaces without sand.

The calculated parameters from the equivalent circuit fit of the impedance data to Randle's circuit are shown in Table 4. The circuit elements are as follows: the solution resistance (R_s), the charge-transfer resistance (R_{ct}), and constant phase element (CPE) representing the interfacial capacitance [36,37]. The CPE was used instead of a pure capacitor because of the non-ideal frequency response seen from the Nyquist plots. This behavior can be ascribed to the non-homogeneities at the steel surface, arising due to surface roughness or pores in the sand deposit layer, which is typical for sand-covered steel. The obtained R_{ct} values were used to calculate the corrosion rates and inhibition efficiencies from EIS measurements and are summarized in Table 4.

The comparison of the four corrosion inhibitors investigated shows that the resistance offered by MPY and TB is much higher (~8 times) than that by the CPC and DPC to steel under a sand

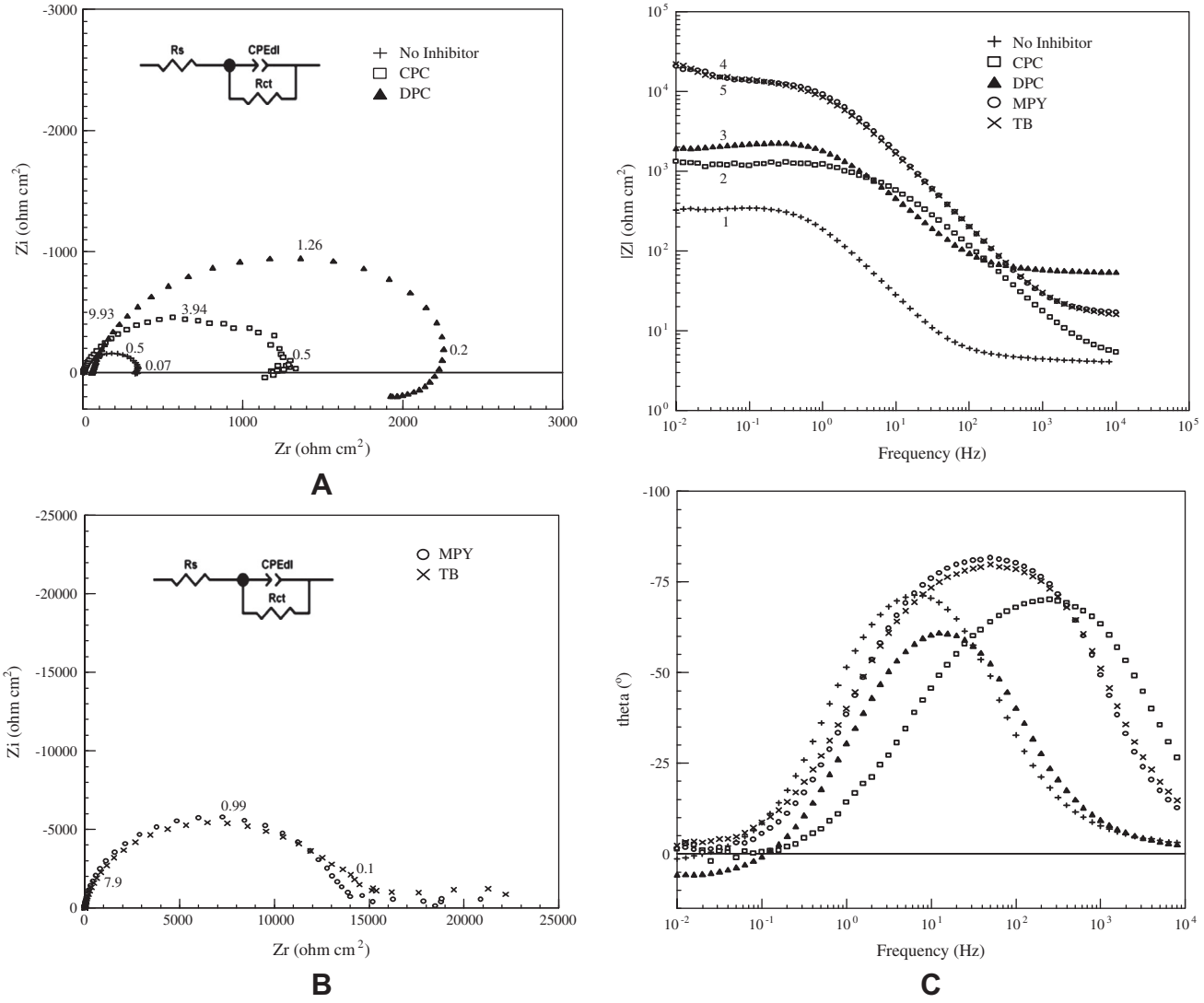

Fig. 6. Impedance spectra of steel surfaces without sand (bare steel) after 1 h exposure in CO_2 saturated test solutions at 30 °C; (A) Nyquist plots for steels in solution containing no inhibitor, CPC and DPC; (B) Nyquist plots for steels in solution containing MPY and TB; and (C) Bode plots from all test solutions; Fig. Inset – Randle's equivalent circuit model used to fit impedance data.

Table 4
Electrochemical parameters derived from impedance analysis of carbon steel with and without sand deposit in CO_2 saturated non-inhibited (test brine) and inhibited test solutions at 30 °C.

EIS recorded after 1 h exposure	R_s Ω cm^2	R_{ct} Ω cm^2	Error %	n^*	i_{corr} μA cm^{-2}	v_{cor} mm y^{-1}	η_z %
With sand deposit							
No inhibitor	9.87	395.3	0.83	0.81	65.77	0.74	–
CPC	0.44	261.9	1.70	0.87	46.4	0.52	–
DPC	12.92	445.6	0.84	0.79	22.4	0.25	11.29
MPY	54.83	16,499	0.76	0.82	1.08	0.01	97.60
TB	52.64	15,983	0.68	0.81	1.23	0.01	97.53
Without sand deposit							
No inhibitor	4.2	345.3	0.96	0.91	36.03	0.41	–
CPC	4.25	1243	0.68	0.83	9.79	0.11	72.22
DPC	15.18	2155	1.19	0.87	6.88	0.08	83.98
MPY	16.37	15,358	1.55	0.93	1.09	0.01	97.75
TB	15.03	15,779	1.76	0.90	1.04	0.01	97.81

* n is the exponent for constant phase element in the equivalent circuit used to fit impedance data.

deposit. This indicates that the CPC and DPC quantities in the test solutions are insufficient to inhibit the corrosion of steel surface under sand deposit. The EIS results are consistent with those from the potentiodynamic tests.

3.4. Correlation of adsorption on sand and inhibition efficiency at steel

The primary objective of this study is to investigate the relationship between the adsorption affinity of corrosion inhibitors to sand

and their effectiveness in providing protection to the steel surfaces deposited with sand.

The sand adsorption experiments have established that the amount adsorbed on sand varies for each corrosion inhibitor depending on its chemical nature, with cationic-surfactant inhibitors susceptible to adsorb in larger quantities compared to the S-containing inhibitors. The following sequence was obtained for the adsorbed amount (Table 2) of inhibitor on sand (q_{ads}): CPC > DPC > MPY ≈ TB. According to the proposed hypothesis, the preferential adsorption of inhibitors on sand would decrease the amount of the corrosion inhibitor available for the protection of the steels deposited with sand and result in enhanced corrosion rates. Thus, in this study the CPC was expected to have the lowest inhibition efficiency among the studied compounds. The cationic-surfactant CPC molecules that are bound to the sand presumably cannot diffuse to the active sites on steel surface and may be unavailable for any inhibition process at the steel interface. This can account for the high corrosion rates at sand-deposited steel applied with CPC as inhibitor.

The electrochemical tests (Section 3.2) showed that all the studied corrosion inhibitors provide protection to the steel surfaces without sand deposit with the $\eta > 75\%$ and that the sand deposit increases the corrosion rates observed in the presence of inhibitors. The corrosion rate of CPC increased from 0.11 to 0.48 mm y^{-1} due to the sand addition. For DPC there was an increase in corrosion rate from 0.07 to 0.23 mm y^{-1}. The MPY and TB inhibit corrosion to an acceptable extent, seen from their corrosion rates (0.015 and 0.024 mm y^{-1}) despite the presence of sand. The sequence of corrosion protection afforded by the inhibitors for steel covered with sand deposit is MPY ≈ TB > DPC > CPC.

The electrochemical test results are consistent with the sand adsorption analysis data demonstrating that the corrosion inhibitor (CPC) which experienced maximum adsorption at sand possessed minimum inhibition efficiency at the sand-deposited carbon steel surface. Likewise, the inhibitors (MPY and TB) with the lesser adsorption on sand were more efficient at the sand-deposited carbon steel surface. This can be attributed to less affinity for sand, and consequently more inhibitor molecules available at the steel surface. The data obtained from the UV–Visible spectroscopy and electrochemical tests confirm that the inhibitor adsorption on sand alters their protection efficiency at sand-deposited steel and the effect is dependent on the chemical nature of the corrosion inhibitor.

4. Conclusions

The effectiveness of a corrosion inhibitor to control UDC is affected by its affinity for the sand deposit and the sequence of affinity of studied corrosion inhibitors for sand is: CPC > DPC > TB ≈ MPY. The adsorption on sand results in the inhibitor not being available at the steel surface beneath.

Sand adsorption experiments showed that the chemical nature of corrosion inhibitors greatly influenced their tendency to preferentially adsorb on a sand deposit. Both the cationic surfactant type inhibitors adsorbed on silica sand to a relatively large extent due to charge attraction and alkyl group interactions under CO_2 saturated conditions. Conversely, the S-containing inhibitors adsorbed on sand to a lesser degree.

The observed relationship between the degree of adsorption and inhibitor properties was further supported by electrochemical studies. The corrosion rates of carbon steel in inhibited test solutions increases in the presence of sand deposit in the sequence CPC > DPC > TB ≈ MPY, consistent with the sand adsorption results. The most effective inhibitors at the sand-deposited steel were the S-containing compounds (MPY and TB).

The results suggest that a clear understanding of the inhibitor interaction with sand is necessary to predict its inhibition behavior at sand-deposited steel.

Acknowledgements

The authors would like to thank Woodside Energy Ltd. for the financial support and permission to publish this work. We also acknowledge the support of the Australian and Western Australian Governments, as well as the Western Australian Energy Research Alliance (WAERA). One of us (V.P.) thanks Curtin University for awarding the Curtin International Postgraduate Research Scholarship (CIPRS). K.L. thanks Curtin University for a Curtin Research Fellowship.

References

[1] B.R. Tian, Y.F. Cheng, Electrochemical corrosion behaviour of X-65 steel in the simulated oil sand slurry. I: Effects of hydrodynamic condition, Corros. Sci. 50 (2008) 773–779.
[2] E. Gulbrandsen, A. Pedersen, Alteration of sand wettability by corrosion inhibitors and its effect on formation of sand deposits, in: International Symposium on Oilfield Chemistry, SPE International, Houston, TX, 2007.
[3] M.A. Winters, P.S.N. Stokes, P.O. Zuniga, D.J. Schlottenmier, Real-time performance monitoring of fouling and under-deposit corrosion in cooling water systems, Corros. Sci. 35 (5–8) (1993) 1667–1675.
[4] M. Jeannin, D. Calonnec, R. Sabot, Ph. Refait, Role of a clay sediment deposit on the corrosion of carbon steel in 0.5 mol L^{-1} NaCl solutions, Corros. Sci. 52 (6) (2010) 2026–2034.
[5] P. Altoe, G. Pimenta, C.F. Moulin, S.L. Diaz, O.R. Mattos, Evaluation of oilfield corrosion inhibitors in CO_2 containing media: a kinetic study, Electrochim. Acta 41 (7–8) (1996) 1165–1172.
[6] D. John, A. Blom, S. Bailey, A. Nelson, J. Schulz, R. DeMarco, B. Kinsella, The application of neutron reflectometry in the study of inhibitor films, Phys. B: Phys. Condens. Matter 385–386 (2006) 924–926.
[7] V.S. Reznik, V.D. Akamsin, Yu P. Khodyrev, R.M. Galiakberov, Yu Ya Efremov, L. Tiwari, Mercaptopyrimidines as inhibitors of carbon dioxide corrosion of iron, Corros. Sci. 50 (2) (2008) 392–403.
[8] S.N. Raicheva, B.V. Aleksiev, E.I. Sokolova, The effect of the chemical structure of some nitrogen and sulphur-containing organic compounds on their corrosion inhibiting action, Corros. Sci. 34 (2) (1993) 343–350.
[9] M.P. Desimone, G. Gordillo, S.N. Simison, The effect of temperature and concentration on the corrosion inhibition mechanism of an amphiphilic amido-amine in CO_2 saturated solution, Corros. Sci. 53 (2011) 4033–4043.
[10] A. Pedersen, K. Bilkova, E. Gulbrandsen, J. Kvarekval, CO_2 corrosion inhibitor performance in the presence of solids: test method development, corrosion 08, NACE International, NewOrleans, LA, 2008.
[11] M.A. Gough, G.J. Langley, Analysis of oilfield chemicals by electrospray–mass spectrometry, Rapid Commun. Mass Spectrom. 13 (1999) 227–236.
[12] S. Weiss, T. Reemtsma, Determination of benzotriazole corrosion inhibitors from aqueous environmental samples by liquid chromatography-electrospray ionization-tandem mass spectrometry, Anal. Chem. 77 (2005) 7415–7420.
[13] E. Buck, Process for the detection and quantitation of corrosion and scale inhibitors in produced well fluids, U.S. Patent 5,152,177, 1992.
[14] M. Ghiaci, R.J. Kalbasi, H. Khani, A. Abbaspur, H. Shariatmadari, Free-energy of adsorption of a cationic surfactant onto Na-bentonite (Iran): inspection of adsorption layer by X-ray spectroscopy, J. Chem. Thermodyn. 36 (2004) 707–713.
[15] M. Sardashti, D. Blumer, Residual chemical monitoring system using surface enhanced Raman spectroscopy, U.S. Patent 7,982,872, 2011.
[16] J.F. Scamehorn, R.S. Schechter, W.H. Wade, Adsorption of surfactants on mineral oxide surfaces from aqueous solutions: I: Isomerically pure anionic surfactants, J. Colloid Interface Sci. 85 (2) (1982) 463–478.
[17] D.F. Brost, F.M. Rexach, G.A. Winslow, Optical methods for monitoring treating chemicals in oilfield water systems, in: Annual Technical Conference and Exhibition, SPE International, Dallas, TX, 1991.
[18] R.I. Kaplan, B.J. Strickland, Ultraviolet spectrographic monitoring of water soluble corrosion inhibitors, U.S. Patent 5,272,346, 1993.
[19] D. Doležal, T. Bolanca, Š.C. Stefanović, Development of UV/Vis spectrometric methodology for corrosion inhibitor residuals monitoring in oilfield brine, Materialwiss. Werkstofftech. 42 (3) (2011) 229–233.
[20] W.H. Durnie, M.A. Gough, J.A.M. de Reus, Development of corrosion inhibitors to address under deposit corrosion in oil and gas production systems, corrosion 05, NACE International, Houston, TX, 2005.
[21] J.A.M. de Reus, E.L.J.A. Hendriksen, M.E. Wilms, Y.N. Al-Habsi, W.H. Durnie, M.A. Gough, Test methodologies and field verification of corrosion inhibitors to address under deposit corrosion in oil and gas production systems, corrosion 05, NACE International, Houston, TX, 2005.
[22] ASTM G102-89, Standard Practice for Calculation of Corrosion Rates and Related Information from Electrochemical Measurements, ASTM International, 2010.

[23] C. Blachier, L. Michot, I. Bihannic, O. Barrès, A. Jacquet, M. Mosquet, Adsorption of polyamine on clay minerals, J. Colloid Interface Sci. 336 (2009) 599–606.
[24] S. Paria, K.C. Khilar, A review on experimental studies of surfactant adsorption at the hydrophilic solid–water interface, Adv. Colloid Interface Sci. 110 (3) (2004) 75–95.
[25] S. Paria, P.K. Yuet, Effects of chain length and electrolyte on the adsorption of n-alkylpyridinium bromide surfactants at sand–water interfaces, Ind. Eng. Chem. Res. 45 (2005) 712–718.
[26] J.L. Trompette, J. Zajac, E. Keh, S. Partyka, Scanning of the cationic surfactant adsorption on a hydrophilic silica surface at low surface coverages, Langmuir 10 (1994) 812–818.
[27] M. Chorro, C. Chorro, O. Dolladille, S. Partyka, R. Zana, Adsorption mechanism of conventional and dimeric cationic surfactants on silica surface: effect of the state of the surface, J. Colloid Interface Sci. 210 (1999) 134–143.
[28] T.P. Goloub, L.K. Koopal, B.H. Bijsterbosch, M.P. Sidorova, Adsorption of cationic surfactants on silica. Surface charge effects, Langmuir 12 (1996) 3188–3194.
[29] R. Atkin, V.S.J. Craig, E.J. Wanless, S. Biggs, Mechanism of cationic surfactant adsorption at the solid–aqueous interface, Adv. Colloid Interface Sci. 103 (2003) 219–304.
[30] C. Cao, On electrochemical techniques for interface inhibitor research, Corros. Sci. 38 (12) (1996) 2073–2082.
[31] X. Jiang, Y.G. Zheng, W. Ke, Effect of flow velocity and entrained sand on inhibition performances of two inhibitors for CO_2 corrosion of N80 steel in 3% NaCl solution, Corros. Sci. 47 (2005) 2636–2658.
[32] K. Lepková, V. Pandarinathan, R. Gubner, Investigation of corrosion processes at sand-deposited surfaces in a carbon dioxide environment, corrosion & prevention, Australasian Corrosion Association (ACA), Adelaide, South Australia, 2010.
[33] K. Lepková, R. Gubner, Study on corrosion processes at sand-deposited surfaces in a carbon dioxide media, in: The European Corrosion Congress (EUROCORR), Moscow, Russia, 2010.
[34] A.J. McMahon, L.J. Harris, J.W. Martin, Effects of sand and interfacial adsorption loss on corrosion inhibitor efficiency, corrosion 05, NACE International, Houston, TX, 2005.
[35] B.P. Binks, P.D.I. Fletcher, I.E. Salama, D.I. Horsup, J.A. Moore, Quantitative prediction of the reduction of corrosion inhibitor effectiveness due to parasitic adsorption onto a competitor surface, Langmuir 27 (2011) 469–473.
[36] I.M. Ritchie, S. Bailey, R. Woods, The metal–solution interface, Adv. Colloid Interface Sci. 80 (1999) 183–231.
[37] ASTM G106-89, Standard Practice for Verification of Algorithm and Equipment for Electrochemical Impedance Measurements, ASTM International, 2010.

Chapter V

V. Pandarinathan, K. Lepková, S.I. Bailey and R. Gubner, Inhibition of under-deposit corrosion of carbon steel by thiobenzamide, Journal of The Electrochemical Society, 160 (9) C432-C440 (2013)

Original Reprint of the Publication

Journal of The Electrochemical Society, **160** (9) C432-C440 (2013)
0013-4651/2013/160(9)/C432/9/$31.00 © The Electrochemical Society

Inhibition of Under-Deposit Corrosion of Carbon Steel by Thiobenzamide

Vedapriya Pandarinathan, Kateřina Lepková,[z] Stuart I. Bailey, and Rolf Gubner

Corrosion Centre for Education, Research and Technology, Department of Chemistry, Curtin University, Perth, WA 6845, Australia

The inhibition performance of thiobenzamide (TB) against the under-deposit corrosion of carbon steel in CO_2-saturated, chloride-containing environment has been investigated. TB concentrations were varied from 10 – 200 ppm and temperatures from 30°C to 60°C were tested. TB effectively inhibits corrosion at carbon steel surfaces with and without sand deposits, reducing the general corrosion rates below 0.1 mm y^{-1} in all cases studied. Electrochemical test results suggest that inhibition occurs via adsorption at the steel surface through the S atom of the TB molecule. Potentiodynamic polarization measurements show that the inhibition mechanism differs at surfaces with and without sand deposits with temperature change over the range of 30°C to 60°C. Surface analysis of the corroded steels showed that general corrosion takes place at surfaces without sand deposits, whereas localized corrosion proceeds at the surfaces underneath a sand deposit, both in the presence and absence of thiobenzamide.
 [DOI: 10.1149/2.078309jes]

Manuscript submitted April 29, 2013; revised manuscript received June 27, 2013. Published July 10, 2013.

Organic corrosion inhibitors are widely employed in the oil and gas industries as an effective and economical solution to protect carbon steel pipelines from CO_2 corrosion.[1–6] Numerous studies have been made on the use of corrosion inhibitors in a fluid phase in contact with steel,[1–6] but the under-deposit corrosion (UDC) of steel, caused by accumulated sand-deposits, necessitates attention as the deposits can interfere with the performance of corrosion inhibitors. Previous investigations have reported insufficient inhibition of steel beneath the sand-deposits.[7,8] The settled sand-deposits have been blamed for localized corrosion of the carbon steel pipelines and the reduction in efficiency of the applied CO_2 corrosion inhibitors. The intention of applying inhibitors is ultimately not successful if they do not reach the steel surface due to interaction with sand-deposits present in the transported fluids. Thus, the identification and development of appropriate inhibitors specific to UDC application is crucial for ensuring protection of sand-deposited pipelines.

Under-deposit corrosion has been related to the galvanic effect between deposit-covered and uncovered areas of the steel surfaces.[9,10] Han et al. proposed that galvanic corrosion takes place between the bare steel surface (cathode) and the steel surface covered with deposits (anode).[11] The initiation of localized corrosion has been attributed to the large cathode to anode ratio. Pedersen et al. also showed that galvanic effect might cause localized corrosion attack on the sand-deposited surfaces.[12] Other studies have examined the corrosion behavior of steel surfaces completely covered with deposits and found significant differences compared to deposit-free surfaces.[13–17]

The application of thiobenzamide (TB) to inhibit the UDC of 1030 carbon steel with and without sand deposit in a CO_2 saturated test environment has been investigated in this study. The choice of TB was based on our preliminary studies[18,19] conducted at sand-deposited carbon steel surfaces, in which higher inhibition efficiencies were obtained by employing thiobenzamide compared to other inhibitor compounds tested. Also, the molecular structure of thiobenzamide, consisting of a benzene ring, along with N and S atoms, is reported to facilitate adsorption on the steel surface, thus effectively mitigating corrosion of mild steel in acidic environments, with reported inhibition efficiencies of about 95%.[20–25]

The effect of TB concentration (10 to 200 ppm) and temperature (30°C – 60°C) on its protective performance against UDC has been evaluated using electrochemical polarization measurements and surface characterization techniques. The inhibition activity of the thiobenzamide against uniform CO_2 corrosion of carbon steel with and without a sand-deposit was estimated from electrochemical tests. Surface analysis is utilized to evaluate the inhibitor effectiveness with respect to general versus localized corrosion.

Table I. Chemical composition (weight%) of 1030 carbon steel.

C	Mn	Si	P	S	Cr	Ni	Mo	Sn	Al	Fe
0.37	0.80	0.282	0.012	0.001	0.089	0.012	0.004	0.004	0.01	balance

Experimental

Test materials.— 1030 carbon steel samples with an exposed surface area of 0.196 cm^2, embedded in epoxy resin, were used as working electrodes. The chemical composition of carbon steel is given in Table I. The carbon steel used had a ferritic-perlitic microstructure. The test brine (non-inhibited solution) consisting of 3% sodium chloride (NaCl; Ajax Finechem, analytical reagent, 99.9%) and 0.01% sodium bicarbonate ($NaHCO_3$; Merck, 99.5%) was prepared in ultra-pure water (resistivity – 18.2 MΩ.cm). The inhibited test solutions containing thiobenzamide (Figure 1) ($C_6H_5CSNH_2$; Sigma-Aldrich, 98%) were prepared in the concentration range of 10–200 ppm (ppm by weight) using test brine.

Prior to each experiment, the working electrode was ground with 1200 grit abrasive paper, rinsed thoroughly with ethanol and ultra-pure water, dried in nitrogen and immediately inserted into the de-aerated test cell. The test solutions were CO_2 saturated by pre-sparging for 2 h and the pH of CO_2-saturated solution was 4.7. The saturated solution was then pumped into the test cell, which was continuously purged with CO_2 at ambient pressure during the experiments. All the experiments were conducted under stagnant conditions, at temperatures of 30°C, 40°C and 60°C.

Silica sand (Sigma-Aldrich) with average particle size of 303 μm and specific surface area of 0.062 m^2/g was used as a deposit. Prior to use, the sand was acid-washed, dried and the pH of the solution was checked to ensure that it remained unaltered.

Electrochemical studies.— The experiments were carried out in a standard three electrode electrochemical cell setup described elsewhere.[18] Separate measurements were carried out at steel samples with and without a sand deposit. In all tests with a sand deposit at the steel surface, 8 g of sand was used to ensure a consistent sand layer height of ~7.5 mm above the steel surface. The amount of sand (8 g) was obtained from the sand volume and the known dry density of sand used. The Ag/AgCl (3.5 M) reference electrode was held in a Luggin

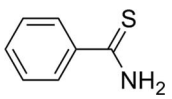

Figure 1. Chemical structure of thiobenzamide.

[z]E-mail: K.Lepkova@curtin.edu.au

capillary and the tip of the capillary was placed in close proximity to the steel surface within the sand layer in order to minimize errors due to iR drop. The electrolyte concentration used is high (30000 ppm of chloride) so the solution resistance within the sand layer will be minimized due to the high conductivity of the electrolyte. Hastelloy C was used as the counter electrode.

Linear Polarization Resistance (LPR) measurements were performed for 12 h under a CO_2 environment. After 100 minutes of pre-corrosion of the samples in test brine solution, required concentration of thiobenzamide solution was added to the test solution. LPR tests were conducted in the potential range of ±10 mV with respect to the open circuit potential (OCP), with a scan rate of 0.1667 mV/s using a Gill Potentiostat (ACM Instruments, UK). The corrosion rates from LPR measurements were calculated assuming the Stern-Geary constant of 26 mV.

Potentiodynamic polarization tests were conducted after 1 h exposure of the working electrode to the test solution in the potential range of ±0.25 V vs. OCP at a sweep rate of 0.1667 mV/s using Solartron SI 1287 potentiostat (Solartron Analytical, UK). The corrosion rates (CR) and inhibition efficiencies were calculated from the corrosion current densities (i_{corr}) estimated by Tafel extrapolation of the polarization curves.

The % inhibition efficiency (η) from the potentiodynamic tests at surfaces without sand deposit was determined using Eq. 1,

$$\eta = \left(\frac{i_{corr_{(brine)}} - i_{corr_{(inhibitor)}}}{i_{corr_{(brine)}}} \right) \times 100 \qquad [1]$$

where $i_{corr\ (brine)}$ and $i_{corr\ (inhibitor)}$ are the corrosion current densities in μA cm^{-2} from the non-inhibited and thiobenzamide-containing test solution, respectively.

At sand-deposited steels, % inhibition efficiency (η_s) was determined using Eq. 2,

$$\eta_s = \left(\frac{i_{corr_{(brine)sand}} - i_{corr_{(inhibitor)sand}}}{i_{corr_{(brine)sand}} \right) \times 100 \qquad [2]$$

where $i_{corr\ (brine)sand}$ and $i_{corr\ (inhibitor)sand}$ are the corrosion current densities in μA cm^{-2} from sand-deposited steels in the non-inhibited and thiobenzamide-containing test solution, respectively.

The electrochemical tests were carried out in triplicate to ensure reproducible results. No significant variation was found between the test repeats.

Surface analysis.— Steel samples of exposed surface area 1 cm^2 were subjected to immersion in the test brine and 200 ppm thiobenzamide-containing test solution for 29 days at 30°C. Separate immersion tests with and without sand deposits on the steel surface were conducted. After the immersion test period, the sand deposit was removed from those samples, the samples were dried with nitrogen gas and kept under vacuum until further analysis. The surface analysis of steels corroded in the immersion test was carried out using the Zeiss (Neon) field emission scanning electron microscope (FESEM) with an energy dispersive X-ray detector (EDS).

Visible-light microscopy was employed for the surface analysis of steels corroded by the potentiodynamic polarization tests using the Infinite Focus Microscope (Alicona Instruments, Austria). The samples after potentiodynamic polarization tests were dried in nitrogen gas and the visible-light micrographs of the surface, root mean square roughness parameter (*Rq*) and pit profiles on the entire sample surface area were acquired with the Alicona Infinite Focus 3.5 software.

Results and Discussion

Linear polarization measurements.— Figure 2 shows the corrosion rates from steel surfaces with and without sand deposit in CO_2 saturated test brine and solutions containing thiobenzamide at various concentrations.

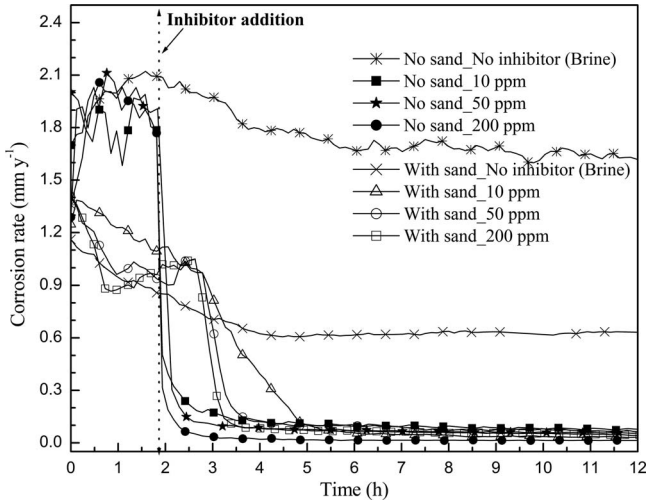

Figure 2. Corrosion rates of steels with and without sand deposits, before and after thiobenzamide addition to the CO_2 saturated test brine, obtained from LPR measurements at 30°C.

As an effect of inhibitor introduction, an immediate decrease in corrosion rate can be observed at the surfaces without sand. This can be attributed to the surface coverage by the inhibitor molecules forming a film on the surface.[26] The corrosion rates decrease below 0.1 mm y^{-1} within 2 h after the inhibitor addition demonstrating the efficiency of thiobenzamide to inhibit corrosion even at the lowest concentration supplied.

At the surfaces covered with sand deposit, the corrosion rates do not decrease immediately upon inhibitor addition and remain almost stable for approximately 1 h. This indicates that the sand-deposited steel surface is still not accessible to the inhibitor which does not provide corrosion protection at this time. Subsequently, the corrosion rates decreased gradually and stabilized at a final value below 0.1 mm y^{-1} after about 3.5 h (after the inhibitor addition) at all applied concentrations of thiobenzamide. A rapid decrease in the corrosion rates in the period of about 1 h (time 3-4 h in Figure 2) was observed for the TB concentrations of 50 and 200 ppm. This suggests that the duration of 1 h is sufficient for significant transport of the inhibitor through the sand deposit and for establishment of a protective layer at the underlying steel surface. The presence of a sand layer did not significantly decrease the amount of inhibitor available for the film-formation at the steel. This behavior can be attributed to the diffusion of inhibitor from the solution to steel surface being the transport mechanism through the deposit layer. It has been reported that thiobenzamide adsorbs at sand particles only in minimal amounts (<0.05 mg/g).[19] Since the adsorption process is influenced by the surface charge, the electrostatic repulsion between the negatively charged silica sand particles and the thiobenzamide molecule's electronegative adsorption center favors inhibitor diffusion through the deposit to reach an active site at the steel surface.

There is an apparent effect of the inhibitor concentration on the corrosion rates of sand-deposited steels, with the inhibition accomplished in shorter duration when treated with 50 and 200 ppm thiobenzamide concentration than with 10 ppm. However, it is clear that a sufficient inhibition is provided by thiobenzamide to the steels, both with and without sand deposits at all concentrations examined.

Potentiodynamic polarization measurements.— Figure 3 shows the potentiodynamic polarization curves of steels with and without sand deposits measured after 1 h exposure to non-inhibited (test brine) and inhibited test solutions containing different concentrations of thiobenzamide. The electrochemical parameters estimated by the Tafel extrapolation of the polarization curves are presented in Table II.

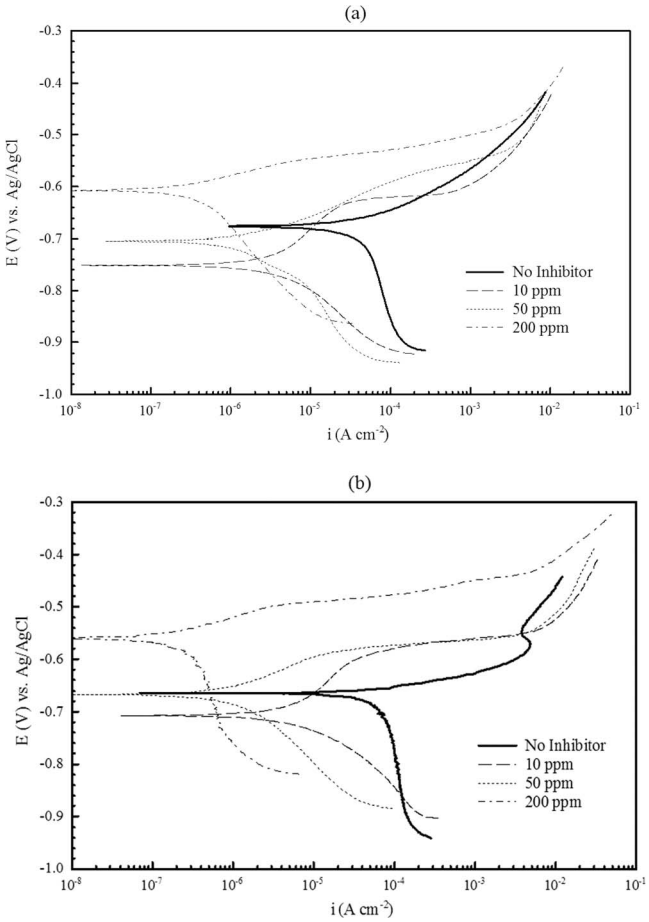

Figure 3. Polarization curves of steels in CO_2 saturated test brine and solutions with different concentrations of thiobenzamide at 30°C, a) with and b) without sand deposit.

The polarization curves under non-inhibited conditions (Figure 3) show that the corrosion current density (i_{corr}) of steel with sand deposit is lower than that of steel without sand. This indicates that the coverage of surface by deposit layer minimizes the uniform dissolution of steel. Also, a negative shift in corrosion potential (E_{corr}) of steel with sand deposit compared to steel without sand indicated that the cathodic reaction is predominantly suppressed in the presence of deposit at the surface. This corrosion behavior is attributed to the deposit layer acting as a diffusion barrier resulting in lower uniform dissolution of the sand-deposited steel.[27]

The potentiodynamic curves show apparent similarities between the surfaces with and without sand deposit in the inhibited test solutions. The corrosion potentials and corrosion current densities follow the same decreasing trend with increasing concentration of thiobenzamide at surfaces with and without sand deposit. Furthermore, the Tafel slope (b_a and b_c) values are similar for both surfaces at a given inhibitor concentration, implying that the inhibition principle of thiobenzamide is the same in presence/absence of sand deposit.

It was found that thiobenzamide concentration influences the corrosion rates as well as the type of inhibition effect. The corrosion rates decreased below 0.01 mm y^{-1} at both bare and sand-deposited surfaces with 200 ppm thiobenzamide concentration. The inhibition efficiencies as seen from Table II are greater than 90% in all cases studied, which is in agreement with the LPR test results. At all applied TB concentrations, the sharp reduction in both cathodic and anodic current densities compared to the non-inhibited surfaces is evident, indicating that TB inhibits both cathodic and anodic corrosion reactions. Simultaneous inhibition of both reactions is observed at the surfaces without sand deposit in the solution of 50 ppm thiobenzamide (Figure 3b where there is no shift in the E_{corr}) in respect to the non-inhibited surface. The remaining measurements with 10 and 50 ppm of TB showed a negative shift in E_{corr} which means that thiobenzamide has a predominant inhibition effect on the cathodic reaction. The E_{corr} shift and the Tafel slopes indicate that the inhibiting action at 10 and 50 ppm concentration is by a geometric blocking effect of inhibitor molecules, reducing the surface area available for cathodic reaction.[3,5,26] The anodic reaction of the corrosion process is predominantly affected in solutions with 200 ppm TB where the E_{corr} shifts in positive direction in respect to non-inhibited surface. The observed differences in corrosion potentials can be attributed to the fact that at lower concentrations, when there is not enough inhibitor molecules to block the steel surface, metal dissolution proceeds at the active sites on the steel. Whereas at higher concentration (200 ppm), the inhibition action can be related to the adsorption of TB molecules at most of the anodic sites on steel, forming a protective inhibitor film which reduces further dissolution.[26]

A comparison of polarization curves in Figure 3a and 3b suggests that thiobenzamide adsorbs at the steel surfaces and that the inhibition

Table II. Electrochemical parameters of the carbon steel surfaces derived from potentiodynamic polarization measurements in Figure 3.

TB concentration ppm	b_a mV dec^{-1}	$-b_c$ mV dec^{-1}	E_{corr} V	i_{corr} μA cm^{-2}	CR mm y^{-1}	η_s* %
	(a) With sand deposit					
0	113 ± 19	369 ± 41	−0.675 ± 0.002	45.87 ± 1.10	0.52	–
10	128 ± 7	145 ± 14	−0.751 ± 0.006	3.53 ± 0.12	<0.05	> 91
50	63 ± 1	133 ± 5	−0.706 ± 0.001	3.79 ± 0.08		
200	33 ± 2	122 ± 7	−0.607 ± 0.002	0.30 ± 0.10	<0.01	99.3
	(b) Without sand deposit					
	b_a	$-b_c$	E_{corr}	i_{corr}	CR	η
	mV dec^{-1}	mV dec^{-1}	V	μA cm^{-2}	mm y^{-1}	%
0	40 ± 9	728 ± 39	−0.664 ± 0.005	68.71 ± 0.87	0.77	–
10	111 ± 17	133 ± 3	−0.707 ± 0.010	1.66 ± 0.04		
50	62 ± 23	122 ± 2	−0.667 ± 0.005	0.96 ± 0.11	<0.02	>97
200	30 ± 5	119 ± 66	−0.561 ± 0.012	0.06 ± 0.07		

*Inhibitor efficiencies calculated with respect to current densities of non-inhibited surface (0 ppm TB in Table II) with and without sand deposit using Eq. 1 and Eq. 2.

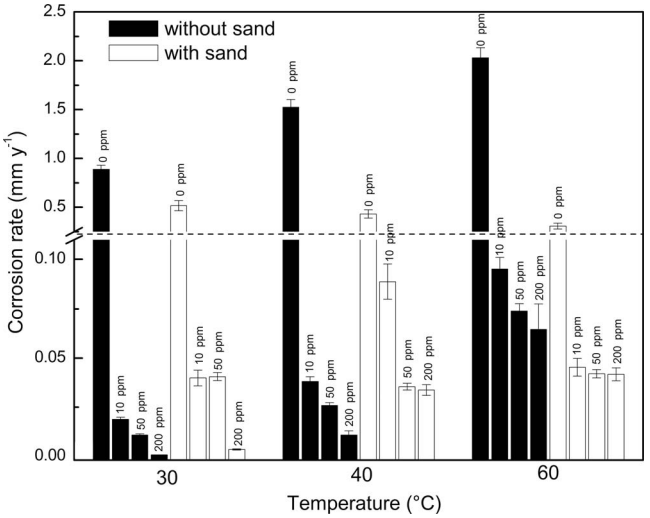

Figure 4. Corrosion rates of steels with and without sand deposits by Tafel analysis at various temperatures.

principle is similar for surfaces with and without sand deposit since no significant inhibitor loss to sand deposit occurred.

Effect of temperature.— Figure 4 presents the carbon steel corrosion rates in non-inhibited (test brine) and inhibited test solutions at different concentrations of TB over the temperature range of 30°C – 60°C. The corrosion rate values were derived from potentiodynamic polarization measurements conducted at steels with and without sand deposit.

At non-inhibited surfaces, the corrosion rates increase with increasing temperature for steels without sand, but the opposite trend is observed at the sand-deposited surfaces. This decrease in corrosion rate of sand-deposited steel with increasing temperature may be related to the variations in the composition and morphology of corrosion products formed at each temperature.[28]

In the absence of inhibitor, the steel with sand deposit exhibits lower general corrosion rates compared to steel without sand. This can be attributed to the sand deposit, which hinders the corrosion process by acting as a diffusion barrier for corrosive species in the test brine. The presence of sand-deposit at the surface also reduces the active surface area of steel available for corrosion, thereby reducing both anodic and cathodic corrosion current densities. The lower uniform corrosion rate of steel covered with sand deposit compared to steel without sand in the non-inhibited solution was also observed from the LPR test results at 30°C (see Figure 2).

The addition of thiobenzamide results in corrosion rates <0.1 mm y^{-1} at all studied concentrations, temperatures and surfaces (with and without sand). It clearly shows the ability of thiobenzamide to inhibit the CO_2 corrosion under these conditions. At surfaces without sand, the corrosion rates decrease with increase in inhibitor concentration at each individual temperature. Also, the corrosion rate increases with increasing temperature (at the same concentration of thiobenzamide). At the inhibited sand-deposited surfaces, the corrosion rates increase with increasing the temperature from 30°C to 40°C, but no further increase was observed at 60°C. This shows that the corrosion rates of the inhibited surfaces were independent of the applied inhibitor concentration. Interestingly, at 60°C, very similar corrosion rates were recorded regardless of the inhibitor concentration at the sand-deposited steel surfaces. This indicates that the general corrosion was inhibited sufficiently at the lowest concentration (10 ppm) and further concentration increase did not improve the inhibition behavior of thiobenzamide at sand-deposited steel at 60°C. It is also worth noting that only at 60°C are the corrosion rates from the sand-deposited inhibited surfaces lower than those from the surfaces without sand, at all concentrations.

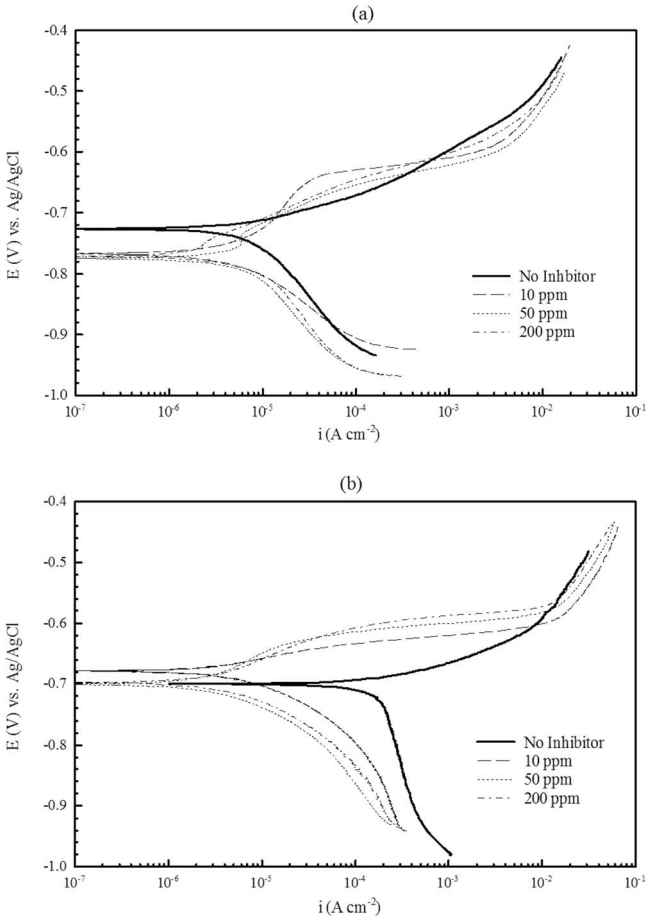

Figure 5. Polarization curves of steels in CO_2 saturated test brine and solutions with different concentrations of thiobenzamide at 60°C, a) with and b) without sand deposit.

To illustrate the inhibition activity of thiobenzamide at 60°C, the potentiodynamic curves from surfaces with and without sand deposit are plotted in Figure 5 and the corresponding Tafel parameters are presented in Table III. It can be seen in Figure 5a that inhibitor addition shifts E_{corr} to negative values, but the increase in concentration over the range from 10 to 200 ppm does not affect the corrosion reactions at sand-deposited surfaces. This can be related to the inhibitor effect. This was concluded to be geometric blocking at the concentrations of 10 and 50 ppm at low temperature (30°C), changing to complete chemisorption at 60°C, since the temperature increase accelerates the diffusion of the inhibitor species. At surfaces without sand (Figure 5b), the addition of thiobenzamide results in a slight increase of E_{corr} toward positive values, suggesting that a different inhibition mechanism takes place (compared to the surfaces with sand). This is also apparent from the differences in Tafel slopes (mainly b_c) from the surfaces with and without sand.

The results in Figure 5 suggest that the inhibition mechanism of thiobenzamide is not the same for surfaces with and without sand at 60°C. This is in contrast to the results obtained at 30°C where the same inhibition mechanism was shown for both surfaces with and without sand deposit (Figure 3). At 60°C, accelerated precipitation of iron carbonate and other corrosion products is expected to proceed.[29] It is reasonable to assume that the type and amount of the corrosion products differ for the two surfaces studied, due to the presence of a sand deposit. The corrosion product layers formed then influence the transport and adsorption of thiobenzamide at the steel surfaces. This could be the reason for the differences in the corrosion mechanism and the corrosion rates observed with increasing temperatures at the surfaces with and without sand deposits (Table II and III).

Table III. Electrochemical parameters of the carbon steel surfaces derived from potentiodynamic polarization measurements in Figure 5.

TB concentration	b_a	$-b_c$	E_{corr}	i_{corr}	CR
ppm	mV dec^{-1}	mV dec^{-1}	V	μA cm^{-2}	mm y^{-1}
			(a) With sand deposit		
0	68 ± 4	237 ± 6	−0.726 ± 0.010	27.31 ± 0.09	0.31
10	53 ± 38	166 ± 1	−0.767 ± 0.007	4.01 ± 0.13	< 0.05
50	43 ± 2	171 ± 1	−0.775 ± 0.004	3.7 ± 0.04	
200	49 ± 5	175 ± 14	−0.771 ± 0.007	3.69 ± 0.08	
			(b) Without sand deposit		
0	42 ± 8	581 ± 46	−0.699 ± 0.003	180.12 ± 1.01	2.03
10	40 ± 11	99 ± 28	−0.678 ± 0.013	8.44 ± 0.11	0.09
50	57 ± 14	106 ± 22	−0.700 ± 0.018	6.55 ± 0.18	0.07
200	57 ± 17	104 ± 9	−0.697 ± 0.006	5.73 ± 0.18	0.06

Galvanic corrosion effect.— The polarization curves shown in Figures 3 and 5 can be used to estimate a worst case scenario for possible galvanic corrosion of the steel surface beneath a sand deposit galvanically connected to the bare steel. In the worst case, it is assumed that the sand-deposited steel is fully polarized to the potential exhibited by the isolated bare steel. In fact, the effect should be substantially mitigated due to contributions from the polarization of the bare steel when coupled, and from the electrical resistance of the sand layer. Table IV presents the estimated galvanic current calculated by extrapolating the linear part of the anodic curve for the sand covered steel to the corrosion potential of the bare steel, for various concentrations of inhibitor. It is seen that a low level of galvanic corrosion may result because the bare steel is more noble than the sand-deposited steel. Nonetheless, the calculated rate of corrosion under the sand is still lowered (i.e. inhibited) compared to the corrosion rate with no inhibitor. The (maximum calculated) galvanic corrosion rate is suppressed compared to the non-inhibited system, but the level of inhibition is lower than for the corrosion of the bare and sand-deposited steel as measured (Table IV).

Adsorption studies.— The electrochemical results were fitted to adsorption isotherms to better understand the inhibition action of thiobenzamide on steel. The degree of surface coverage θ by the thiobenzamide molecules on the steel was calculated using Eq. 3

$$\theta = \left(\frac{i_{corr_{(brine)}} - i_{corr_{(inhibitor)}}}{i_{corr_{(brine)}}} \right) \quad [3]$$

Table IV. Estimated maximum galvanic corrosion current densities of the sand-deposited carbon steel surfaces derived from potentiodynamic polarization measurements.

T	TB concentration	$(E_{corr})_{sand}$	$(E_{corr})_{bare}$	$(i_{corr})_{sand}$	$(i_{corr})_{bare}$	$i_{galvanic}$
°C	ppm	V	V	μA cm^{-2}	μA cm^{-2}	μA cm^{-2}
30	0	−0.675	−0.664	45.87	68.71	72.40
	10	−0.751	−0.707	3.53	1.66	5.56
	50	−0.706	−0.667	3.79	0.96	5.03
	200	−0.607	−0.561	0.304	0.058	1.79
40	0	−0.709	−0.690	38.3	135.28	68.63
	10	−0.753	−0.715	7.87	3.38	7.34
	50	−0.710	−0.661	3.14	2.30	7.10
	200	−0.687	−0.648	2.99	0.96	2.94
60	0	−0.726	−0.699	27.31	180.06	63.81
	10	−0.767	−0.678	4.01	8.44	15.46
	50	−0.775	−0.700	3.72	6.55	9.39
	200	−0.771	−0.697	3.69	5.73	6.44

where $i_{corr\ (brine)}$ and $i_{corr\ (inhibitor)}$ are the corrosion current densities obtained from the polarization tests of steels exposed to non-inhibited (test brine) and thiobenzamide-containing test solution, respectively.

To demonstrate the adsorption phenomena, the experimental values were evaluated by fitting to Langmuir, Freundlich and Temkin isotherms. The Temkin isotherm provided the best linear regression fit for the surface coverage data at the steel surface without sand and is plotted in Figure 6. The correlation coefficient (r) is greater than 0.98 for all the plots which confirms the validity of this approach. It can be seen that the surface coverage increases with TB concentration at all the studied temperatures.

Since the adsorption data follows Temkin's isotherm, the slope (m) and the intercept (c) of the isotherm allow for calculating the thermodynamic properties using the Eq. 4 and Eq. 5[30]

$$\theta = \left(\frac{-RT}{\Delta H_{ads}} \right) ln\ K_{ads}\ C \quad [4]$$

$$\Delta G_{ads} = -RT\ ln\ K_{ads} \quad [5]$$

where θ is the fractional surface coverage, R is the universal gas constant in kJ K^{-1} mol^{-1}, T is the temperature in K, ΔH_{ads} is the enthalpy of adsorption in kJ mol^{-1}, ln K_{ads} is the adsorption equilibrium constant in L mg^{-1}, C is the molar concentration of thiobenzamide and ΔG_{ads} is the free energy of adsorption (kJ mol^{-1}). The estimated thermodynamic data are presented in Table V.

In general, an adsorption process can either be physical or chemical depending on the nature of the corrosion inhibitor and the test environment to which the steel is exposed. A positive ΔH_{ads} value is associated with an endothermic chemical adsorption process and a negative

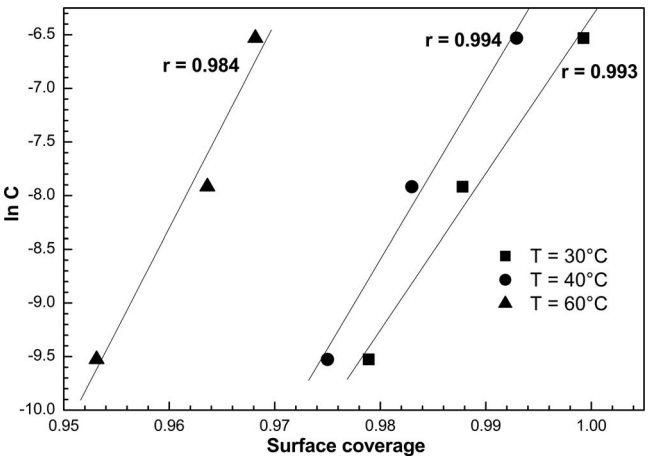

Figure 6. Temkin adsorption isotherms at different temperatures for thiobenzamide sorption at a steel surface without sand deposit, from polarization analysis.

Table V. Adsorption parameters from Temkin isotherm for thiobenzamide onto carbon steel surface.

Temperature°C	$ln\ K_{ads} = c/m$	ΔH_{ads} kJ mol^{-1}	ΔG_{ads} kJ mol^{-1}
30	1.04	17.3	−2.62
40	1.03	15.7	−2.68
60	1.00	14.5	−2.78

ΔH_{ads} value involves an exothermic adsorption process which may be either physisorption or chemisorption or both simultaneously.[14] The positive ΔH_{ads} values of thiobenzamide obtained in this study indicate that the adsorption is endothermic and is in accordance with the mode of thiobenzamide chemisorption onto a steel substrate proposed in the literature.[24]

The negative ΔG_{ads} values indicate spontaneous adsorption of inhibitor on steel, which can be interpreted by the S atoms (soft bases) of thiobenzamide sharing electrons with the Fe atoms (soft acids) on steel surface, eventually leading to chemical bonding between them, based on the hard and soft acid-bases concept.[21] Chemisorption is characterized by monolayer adsorption, which is consistent with the theoretical prediction that the adsorption is through the S atom of thiobenzamide. Hence, the isotherm supports the findings of both theoretical and electrochemical data that the TB molecules are held to the steel surface by a chemical bond that effectively retards corrosion.

For the steel surfaces covered with sand deposit, although thiobenzamide affords the desired level of protection as evidenced from the polarization curves, the adsorption data tested with different isotherm models were not linear at any of the conditions studied, over the range of thiobenzamide concentration from 10 – 200 ppm. The correlation coefficient values for the isotherm models to fit inhibitor concentration and fractional surface coverage were less than 0.8, hence further details of the fitting are not presented.

However, it can be considered that chemisorption takes place at surfaces with sand deposit at 30°C, since the corrosion mechanism appears to be the same as for the surfaces without deposit, based on the obtained electrochemical data.

In general, chemisorption is a highly specific and an irreversible process which involves the chemical bonding between specific molecular species. Thus, the mode of adsorption being chemisorption explains why the TB molecules (via S atoms) selectively adsorbs on the steel surface (Fe atoms) and does not have any affinity for the sand deposit (SiO_2 molecule), making it an effective inhibitor for under-deposit corrosion control.[19]

Surface analysis.— Previous investigations on under-deposit corrosion have reported that steel surfaces beneath the sand deposit are susceptible to localized corrosion.[12,31] To assess the effectiveness of thiobenzamide in this regard, surface examination of the carbon steels corroded by both electrochemical and immersion tests was conducted.

Visible light microscopy.— The optical micrographs of steel surfaces without sand (a, b) and with sand deposit (c, d) that were potentiodynamically polarized after 1 h immersion in CO_2 saturated test solution (samples from Figure 3) are shown in Figures 7 and 8.

It can be seen from Figure 7 that steels without sand deposit (a, b) exhibited uniformly corroded surface morphology both in the presence and absence of inhibitor and no localized attack could be detected. The inhibited surface without sand (b) appeared almost free from corrosion and the grinding marks were visible even after polarization. By contrast, at the steel surfaces covered with the sand deposit (c, d), numerous pits were noticed. This indicates that the presence of sand at steel surface promotes localized attack beneath the deposit.

Higher magnification micrographs of the corroded surfaces (Figure 8) show that the roughness (*Rq*) of the non-inhibited samples treated in test brine (a, c) is higher than that of the inhibited surfaces (b, d) due to higher metal dissolution in the absence of inhibitor. The very low roughness due to inhibition activity of thiobenzamide suggests that the corrosion damage is considerably reduced by its adsorption at the active sites on the steel surface.

The pit depths measured from different areas on the non-inhibited surface with sand deposit ranged from ~8 to 15 μm. The inhibited surface with sand deposit also exhibited localized defects, however, the pits were relatively less deep ranging from ~1.5 to 3 μm in depth. Also, the number of pits found at the inhibited surface was less than the non-inhibited surface, and the lower *Rq* value indicates that the surface is partially protected by thiobenzamide, even underneath the sand deposit.

It is evident from the optical micrographs that the susceptibility of the sand-deposited steels to both uniform and localized decreases in the presence of thiobenzamide.

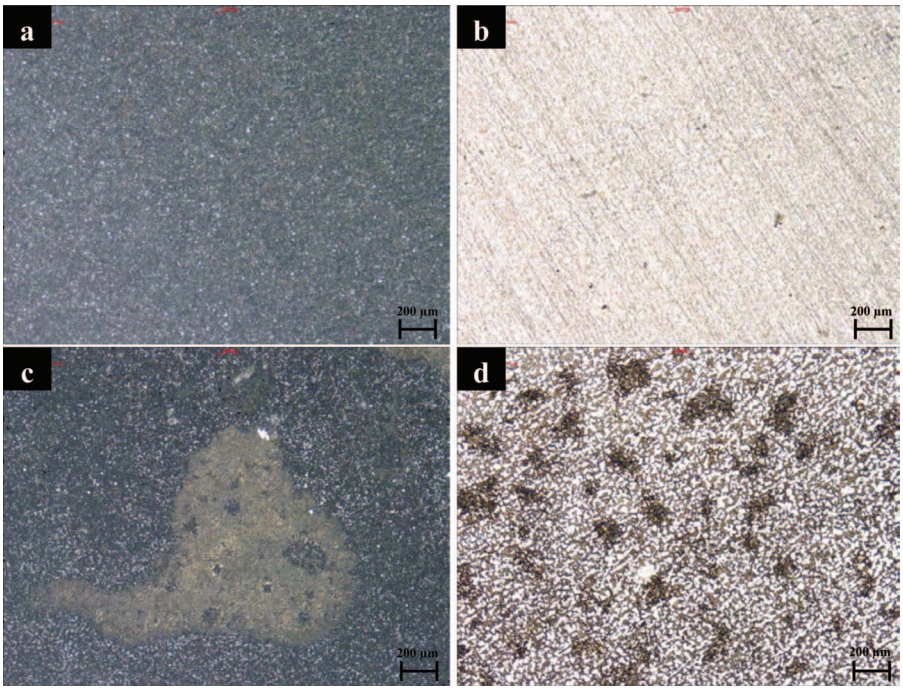

Figure 7. Visible light microscopy images (magnification 5x) of steels after potentiodynamic polarization test in a) test brine (non-inhibited) and b) 200 ppm thiobenzamide-containing solution without sand deposit; c) test brine (non-inhibited) and d) 200 ppm thiobenzamide-containing solution with sand deposit.

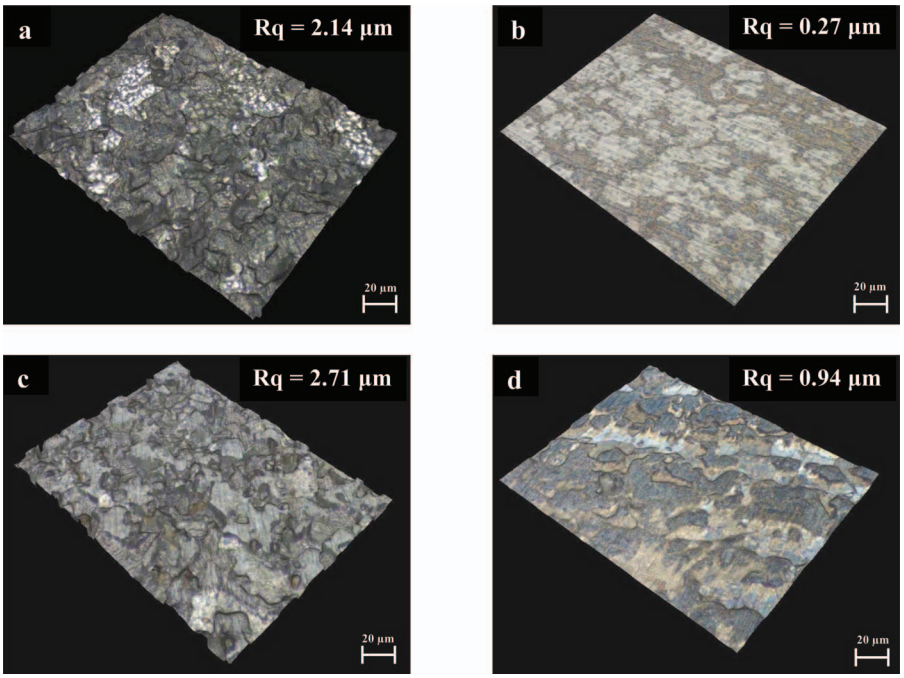

Figure 8. Visible light microscopy images (magnification 50x) of steels after potentiodynamic polarization test in a) test brine (non-inhibited) and b) 200 ppm thiobenzamide-containing solution without sand deposit; c) test brine (non-inhibited) and d) 200 ppm thiobenzamide-containing solution with sand deposit.

Scanning electron microscopy.— The FESEM/EDS analysis was performed to evaluate the localized corrosion susceptibility of the steels corroded with and without sand deposit, in the presence and absence of thiobenzamide. Figure 9 shows the scanning electron micrographs of the steels treated by long-term immersion (29 days) in the test brine and thiobenzamide-containing test solutions.

At the surfaces without sand deposit (a, b), the corrosion process results in severe metal dissolution at the non-inhibited surface (Figure 9a), which is significantly suppressed in the presence of inhibitor thiobenzamide (Figure 9b). No localized attack was observed at these surfaces, indicating that uniform corrosion proceeds in the sand-free environment.

The qualitative EDS analysis of the non-inhibited surface gave Fe, C and O peaks in the spectra, suggesting the formation of iron complexes as a result of corrosion reactions. The iron carbonates, hydroxides and oxyhydroxides have been proposed in the literature as possible corrosion products under CO_2 environment at low temperatures.[28] The EDS analysis of the inhibited surface showed the presence of a sulfur peak, indicating that inhibitor film is present at the surface. The C and O peaks were absent in the EDS spectrum from the inhibited steel surface indicating that few corrosion products were present. This can be attributed to the inhibitor adsorption resulting in a surface that is resistant to both general and localized corrosion.

The corroded steel surface in the presence of the sand deposit (c, d) shows grain boundaries due to dissolved crystallite phases suggesting that greater metal dissolution has occurred than in the absence of sand deposit. The micrographs also show pit formation at both non-inhibited and inhibited surfaces, with larger pits at the non-inhibited

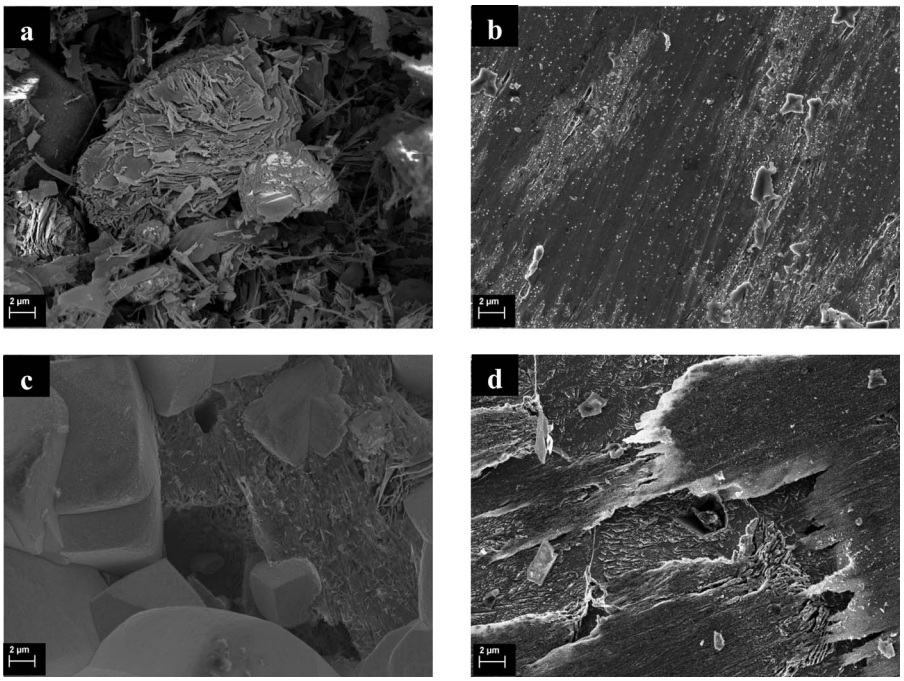

Figure 9. FESEM images of steels after 29 days immersion at 30°C in a) test brine (non-inhibited) and b) 200 ppm thiobenzamide-containing solution without sand deposit; c) test brine (non-inhibited) and d) 200 ppm thiobenzamide-containing solution with sand deposit.

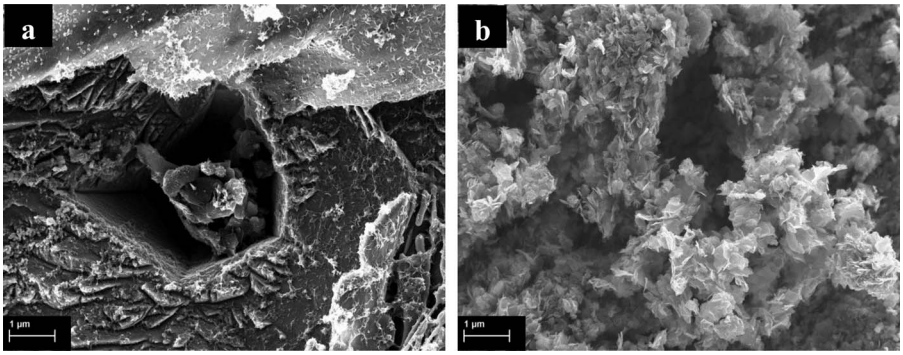

Figure 10. FESEM images of steel with sand deposit after 29 days immersion in inhibited test solution at 30°C a) an area of the inhibited surface with a pit, b) an area of the surface with adsorbed inhibitor.

surface (Figure 9c) compared to the pits at the inhibited surface (Figure 9d). The localized attack was seen on steel surfaces covered with sand deposits and not on the steel without sand. This can be related to the steel beneath the deposit layer being exposed to subtly different micro-environment, thereby localized corrosion takes place in presence of sand. We have also observed that the ferritic phase corroded preferentially resulting in the accumulation of undissolved iron carbide at the sand-deposited surfaces. The galvanic contact between the iron carbide and adjacent steel has been attributed to localized corrosion under deposits by accelerating the cathodic reaction of the corrosion process.[8] As seen in Figure 9c, the non-inhibited surface was covered with cubic crystalline corrosion products while no characteristic corrosion products were noticeable at the inhibited surface (Figure 9d). This is supported by the EDS analysis that showed the presence of Fe, C and O peaks at the non-inhibited surface and only Fe and S at the inhibited surface with sand deposit. The presence of the element sulfur suggests that thiobenzamide is adsorbed at the sand-deposited surface. Because of the semi-qualitative nature of the EDS, the elements present were not quantified, however, it was clear from the absence of C and O peaks for the inhibited steels that thiobenzamide inhibited corrosion.

Figure 10 presents the higher magnification FESEM images of sand-deposited steel surfaces corroded in thiobenzamide-containing solutions. The image (a) shows the area with a pit at the inhibited steel surface. Image (b) shows the inhibitor adsorbed at the area outside the surface indents.

The surface analysis results have demonstrated that thiobenzamide adsorbs at the steel regardless of the presence of the sand deposit, which correlates well with the low corrosion rates obtained from the electrochemical tests from the inhibited surfaces. However, the surface analysis results also show that localized corrosion takes place at the surfaces with sand deposits, even when inhibitor thiobenzamide is used.

Conclusions

- Thiobenzamide addition to the test brine resulted in corrosion rates <0.1 mm y^{-1} at carbon steel surfaces with and without sand deposit, in the studied temperature range (30°C – 60°C) and concentrations applied (10 – 200 ppm), as demonstrated by electrochemical tests. The results show that there is a sufficient amount of thiobenzamide reaching the steel surface without being depleted in the sand layer, which is an essential characteristic for the chemical to be a UDC inhibitor.
- The inhibition effect of thiobenzamide is temperature-dependent. At 30°C, the inhibition mechanism was found to be similar for steel surfaces irrespective of the sand deposit. The sand-deposited steels exhibited slightly higher corrosion rates than the steel without sand. At 60°C, a difference in the inhibition behavior between surfaces with and without sand deposit was observed. The corrosion rates were independent of concentration of inhibitor over the range 10 – 200 ppm at sand-deposited surfaces.
- The effectiveness of thiobenzamide increases with increase of its concentration and its adsorption follows the Temkin isotherm at surfaces without sand deposit. Thermodynamic parameters show that the adsorption process is spontaneous and endothermic. The mode of inhibition was found to be chemisorption at the active sites on steel, which is supported by high inhibition efficiencies observed even at low concentrations of thiobenzamide.
- Surface analysis using visible light and electron microscopy revealed the differences in the morphology of steel corroded with or without sand deposit (both in a spontaneous immersion and in an electrochemically accelerated test). The sand-deposited surfaces are susceptible to localized corrosion. Surface roughness of inhibited steels was very low in comparison with the non-inhibited steel, indicating that adsorbed thiobenzamide film protected the surface.
- Thiobenzamide provided high inhibition ($>$ 90%) to general CO_2 corrosion of carbon steel surfaces both with and without sand deposit. The results have demonstrated that thiobenzamide can be applied for inhibition of the under-deposit corrosion caused by sand deposit in aqueous CO_2 environment.

Acknowledgments

The authors thank Woodside Energy Ltd for the financial support and permission to publish this work and the Center for Materials Research (CMR) facility at Curtin University for FESEM access. We also acknowledge the support of the Australian and Western Australian Governments, as well as the Western Australian Energy Research Alliance (WAERA). One of us (V.P.) thanks the Curtin University for Postgraduate Research Scholarship (CIPRS). K. L. thanks Curtin University for a Curtin Research Fellowship.

References

1. J. A. Dougherty, *Corrosion 98*, NACE International, paper no. 15 (1998).
2. D. John, A. Blom, S. Bailey, A. Nelson, J. Schulz, R. De Marco, and B. Kinsella, *Phys. B*, **385–386**, 924 (2006).
3. S. Bailey, Y. J. Tan, and B. Kinsella, *Br. Corros. J.*, **32**, 49 (1997).
4. Y. J. Tan, B. Kinsella, and S. Bailey, *Br. Corros. J.*, **32**, 5 (1997).
5. Y. J. Tan, S. Bailey, and B. Kinsella, *Corros. Sci.*, **38**, 1545 (1996).
6. Y. J. Tan, S. Bailey, and B. Kinsella, *Corros. Sci.*, **38**, 1681 (1996).
7. J. A. M. de Reus, E. L. J. A. Hendriksen, M. E. Wilms, Y. N. Al-Habsi, W. H. Durnie, and M. A. Gough, *Corrosion 05*, paper no. 288 (2005).
8. K. Lepkova and R. Gubner, *Corrosion 10*, NACE International, paper no. 331 (2010).
9. J. R. Vera, D. Daniels, and M. H. Achour, *Corrosion 12*, NACE International, paper no. 1379 (2012).
10. R. Nyborg, *Corrosion 98*, NACE International, paper no. 48 (1998).
11. J. Han, Y. Yang, S. Nesic, and B. N. Brown, *Corrosion 07*, NACE International, paper no. 323 (2007).
12. A. Pedersen, K. Bilkova, E. Gulbrandsen, and J. Kvarekval, *Corrosion 08*, NACE International, paper no. 632 (2008).
13. M. Ramirez, A. Viloria, M. Castillo, and A. Balza, *Corrosion 03*, NACE International, paper no. 445 (2003).
14. W. H. Durnie, R. De Marco, B. Kinsella, A. Jefferson, and B. Pejcic, *J. Electrochem. Soc.*, **152**(1), B1 (2005).
15. J. Been, T. D. Place, and M. Holm, *Corrosion 10*, NACE International, paper no. 143 (2010).

16. J. Huang, B. Brown, X. Jiang, B. Kinsella, and S. Nesic, *Corrosion 10*, NACE International, paper no. 379 (2010).
17. W. H. Durnie, R. De Marco, A. Jefferson, and B. Kinsella, *J. Electrochem. Soc.*, **146**(5), 1751 (1999).
18. V. Pandarinathan, K. Lepková, and R. Gubner, *Corrosion 11*, NACE International, paper no. 261 (2011).
19. V. Pandarinathan, K. Lepková, S. I. Bailey, and R. Gubner, *Corros. Sci.*, **72**, 108 (2013).
20. J. J. Augsburger and R. K. Darlington, Corrosion inhibition of aqueous brines, *US patent 4,536,302,* (1985).
21. B. Donnelly, T. C. Downie, R. Grzeskowiak, H. R. Hamburg, and D. Short, *Corros. Sci.*, **14**, 597 (1974).
22. I. M. Ritchie, S. Bailey, and R. Woods, *Adv. Colloid Interface Sci.*, **80**, 183 (1999).
23. E. Lazarova, G. Petkova, T. Iankova, L. Ivan, and G. Neikov, *J. Appl. Electrochem.*, **38**, 1391 (2008).
24. G. E. Badr, *Corros. Sci.*, **51**, 2529 (2009).
25. B. G. Ateya, B. M. Abo-Elkhair, and I. A. Abdel-Hamid, *Corros. Sci.*, **16**, 163 (1976).
26. C. Cao, *Corros. Sci.*, **38**(12), 2073 (1996).
27. V. Pandarinathan, K. Lepková, S. I. Bailey, and R. Gubner, *Corrosion 13*, NACE International, paper no. 2579 (2013).
28. R. De Marco, Z. T. Jiang, B. Pejcic, and E. Poinen, *J. Electrochem. Soc.*, **152**(10), B389 (2005).
29. G. Schmitt and M. Horstemeier, *Corrosion 06*, NACE International, paper no. 112 (2006).
30. O. Hamdaoui and E. Naffrechoux, *J. Hazard. Mater.*, **147**, 381 (2007).
31. A. J. McMahon, J. W. Martin, and L. Harris, *Corrosion 05*, NACE International, paper no. 274 (2005).

Chapter VI

V. Pandarinathan, K. Lepková and W. van Bronswijk, Chukanovite ($Fe_2(OH)_2CO_3$) identified as corrosion product at sand-deposited carbon steel in CO_2-saturated brine, Corrosion Science, Article in Press

Accepted version of the Manuscript

Chukanovite ($Fe_2(OH)_2CO_3$) identified as corrosion product at sand-deposited carbon steel in CO_2-saturated brine

Abstract

Chukanovite ($Fe_2(OH)_2CO_3$) has been identified by synchrotron-sourced infrared microspectroscopy as the main corrosion product at sand-deposited carbon steel corroded in CO_2-saturated brine at 80 °C. Siderite has been shown as a minor corrosion product at the sand-deposited steel, and the only product at the sand-free steel. Sand-deposited steels have similar general corrosion rates as the sand-free steels, but were susceptible to localized corrosion. These differences are related to the presence of the sand-deposit at the surface that influences the local micro-environment and promotes the formation of the mixed layer of corrosion products (chukanovite and siderite) at the carbon steel.

Keywords: A. Carbon steel, B. IR spectroscopy, B. FESEM, B. Polarization.

1. Introduction

CO_2 corrosion of carbon steel in the presence of deposits such as sand has often been associated with localized corrosion taking place in the presence and absence of corrosion inhibitors at the sand-deposited steels [1-3]. Sand deposit reduces the active surface area of the steel and also acts as a diffusion barrier for corrosive species in the solution resulting in differences in the micro-environment at the deposit-covered steels compared to the deposit-free steels [4,5]. Previous studies have established that the sand-deposited steels show lower general corrosion rates compared to steels without deposits but are more susceptible to the localized attack [5,6]. This can be attributed to the type of corrosion products that form at the sand-deposited steels and are different from those at the sand-free surfaces. The type of corrosion products and the properties of the surface layer, such as thickness, porosity and uniformity are related to the protectiveness against corrosion [7,8].

The characterization of corrosion products on the heterogeneous surface of carbon steel is often limited by the low sensitivity of the analytical techniques. Synchrotron-sourced techniques with the very intense radiation allow identification of thin

corrosion product layers at the carbon steel surface as demonstrated in previous studies [9-11].

The main objective of this study is to identify the corrosion products formed at sand-deposited carbon steel surface corroded under CO_2-saturated environment. The surface morphology has been reported to differ for carbon steels corroded with and without sand deposit [3,5], but the composition of the surface layers formed under the sand have not been identified. Corrosion products expected to form on carbon steel corroded in CO_2-saturated brines are iron carbonates, oxides, hydroxides and oxyhydroxides [7,8]. In addition, ferrous hydroxy carbonate ($Fe_2(OH)_2CO_3$) also referred to as chukanovite was detected at carbon steel surface under CO_2 conditions by synchrotron X-ray diffraction technique as a precursor for the formation of siderite [9,10].

In this study, we used synchrotron-sourced infrared microspectroscopy and field-emission scanning electron microscopy to identify the corrosion products and to determine the morphology of the corrosion layers on carbon steels with and without sand deposits in CO_2-saturated brine at 80 °C. Electrochemical techniques were employed to assess the impact of the corrosion products on the corrosion rates. Determining the composition of the corrosion product layers and evaluating their effect on the corrosion processes advances the understanding of the under deposit corrosion (UDC) phenomena. This can potentially improve the UDC mitigation as the corrosion products are expected to either enhance or hinder the corrosion inhibitor performance depending on the inhibitors' adsorption on the corrosion products [12,13].

2. Experimental

2.1 Test materials

1030 carbon steel samples embedded in epoxy resin were ground with SiC paper upto 1200 grit, rinsed with ethanol and ultra-pure water and dried in nitrogen gas prior to use. The test solution consisted of 3 wt% sodium chloride (NaCl; Ajax Finechem; 99.9%), 0.01 wt% sodium hydrogen carbonate ($NaHCO_3$; Merck; 99.5%) and 56 ppm of 1-dodecyl pyridiniumchloride hydrate (DPC) prepared in ultra-pure water (resistivity 18.2 MΩ·cm). The inhibitor-containing test solution was saturated with CO_2 gas for 2 h prior to each experiment. The composition of this test solution closely resembles oilfield brines [14,15].

The deposit used was silica sand (SiO_2; Sigma-Aldrich) with average particle size of 303 μm (laser diffraction analysis) and specific surface area of 0.062 m^2g^{-1} (BET analysis). The sand was acid-washed, dried and the pH of the solution was checked to ensure that it remained unaltered.

2.2 Immersion tests

The carbon steel samples of 1 cm^2 exposed surface area were subjected to immersion in the CO_2-saturated test solution at 80 °C for 24 h. The immersion tests of steels with and without sand deposit were conducted separately. After the test period, the corroded steel samples were dried in nitrogen and kept under vacuum until surface analysis. The sand was removed from the sample surface before performing the surface analysis. Care was taken in handling the samples at all times to minimize their exposure to air.

2.3 Synchrotron Fourier-transform infrared microspectroscopy (FTIR)

Infrared spectroscopy was performed at the Australian Synchrotron, Infrared microspectroscopy beamline, using a Brüker Vertex 80v FTIR spectrometer with Hyperion 2000 microscope. The spectral analysis was performed using Opus 7 software (Brüker optics). The FTIR spectra were recorded using a germanium crystal in the Attenuated Total Reflectance (ATR) accessory at a resolution of 4 cm^{-1}, aperture size of 10 x 10 μm and a liquid nitrogen-cooled MCT detector. For each spectrum, 256 scans were collected in the wavenumber range of 3900-700 cm^{-1}. A total of 256 background scans were collected on untreated (non-corroded) steel surface followed by 256 scans on the test samples (corroded steel). Both the sample and the background were placed into an enclosed compartment surrounding the infrared microscope assembly. The compartment was continuously purged with nitrogen gas in order to reduce the atmospheric water vapour and carbon dioxide in the FTIR spectra. All the spectra presented are baseline corrected.

2.4 Field emission scanning electron microscopy (FESEM) and visible-light microscopy

The FESEM analysis was performed using a Zeiss Neon EsB focused ion beam scanning electron microscope (FIBSEM) with a field emission electron gun. The images were obtained at 5 kV accelerating voltage using the secondary electron and in-lens detectors in a 50%:50% ratio. The cross-sectional view of steel surface was obtained by milling using the focused ion beam (FIB).

Visible-light microscopy using an Infinite Focus Microscope (Alicona Instruments, Austria) was utilized to obtain the maximum pit depth value on the steel surface after cyclic voltammetry measurement.

2.5 Electrochemical measurements

Three electrochemical methods, namely linear polarization resistance (LPR), potentiodynamic polarization and cyclic voltammetry, were used to assess the steel surfaces for both general and localized corrosion. Each electrochemical method was applied separately (not in a sequence with other electrochemical methods) using a polished and cleaned carbon steel sample.

A three-electrode cell described by us previously [14] was used for all electrochemical measurements at steels with and without sand-deposits in CO_2-saturated test solution at 80 °C.

LPR measurements were performed for 24 h in the potential range of ±10 mV in respect to the open circuit potential (OCP), with a scan rate of 0.1667 mV/s using a Gill Potentiostat (ACM Instruments, UK). The corrosion rates from LPR measurements were calculated assuming the Stern-Geary constant of 26 mV.

Potentiodyanamic polarization measurements using a Solartron SI 1287 Potentiostat (Solartron Analytical, UK) were performed after 24 h immersion of the working electrode in the test solution in the potential range of ±0.25 V vs. OCP at a scan rate of 0.1667 mV/s.

Cyclic voltammetry measurements using a Solartron SI 1287 Potentiostat (Solartron Analytical, UK) were conducted at 10 mV/s scan rate. The working electrode was held at a potential of -1.2 V vs. Ag/AgCl reference electrode for 30 s. The electrode was then left to stabilize at OCP for 300 s prior to cyclic voltammetry measurement. The electrochemical pre-treatment was applied to the working electrode in order to remove any oxide layer from the electrode surface and to ensure the same starting conditions for all experiments.

3. Results and discussion

3.1 Synchrotron FTIR characterization

Fig. 1 shows a microscope image of the corroded steel surface. The steel was corroded in the presence of sand-deposit, which was removed prior to the surface analysis. The analysis points (10 x 10 µm) were randomly selected across the surface.

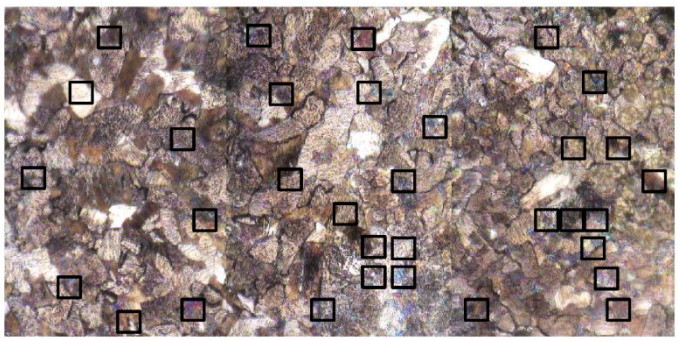

Fig. 1. Microscope image of steel surface after corrosion (corroded in the presence of sand deposit). Analysis point size is 10x10 µm.

Fig. 2 shows infrared spectra from the untreated (non-corroded) steel used as a background (spectrum a) and from steel corroded in the presence of sand-deposit (spectrum b). No background contamination giving rise to any spectral features was observed at spectrum a. The position of absorption bands in the infrared spectra obtained from different measurement points at the steel surface (Fig. 1) were identical to those shown in Fig. 2 (spectrum b). The assignment of the absorption bands is summarized in Table 1.

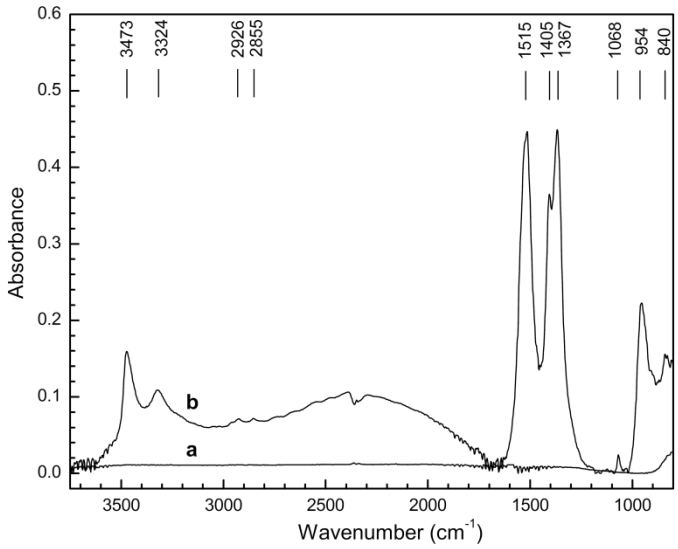

Fig. 2. Synchrotron ATR spectra of a) untreated (non-corroded) steel and b) corroded steel (corroded with sand deposit) after immersion in CO_2-saturated test solution at 80 °C for 24 h.

The absorption bands in the regions below 1700 cm^{-1} and above 3000 cm^{-1} are assigned to chukanovite ($Fe_2(OH)_2CO_3$). These absorption bands are an exact match to the chukanovite spectra published in literature [9,16,17]. The results show that

chukanovite is the dominant corrosion product formed at the sand-deposited steel surfaces. However, the presence of iron carbonate (siderite) typically formed at carbon steels in CO_2-saturated brines cannot be excluded. The absorption band characteristic of iron carbonate near 1420 cm^{-1} (antisymmetric stretching of CO_3^{2-}) could be overlapped by the intense absorption bands in the 1405-1515 cm^{-1} region. The two less intense absorption bands at 2926 cm^{-1} and 2855 cm^{-1} characteristic of the CH_2-symmetric and antisymmetric stretching vibrations are ascribed to the aliphatic chain of the corrosion inhibitor, 1-dodecyl pyridiniumchloride hydrate (DPC), present in the test solution and adsorbing at the corrosion products/steel surface [19].

Table 1. Band assignments of chukanovite ($Fe_2(OH)_2CO_3$) and 1-dodecylpyridinium chloride hydrate (DPC) *

Wavenumber (cm^{-1})	**Band assignment**
840	CO_3^{2-} bending vibrations
954	OH^- deformation vibrations
1068	CO_3^{2-} symmetric stretching vibrations
1367, 1405, 1515	CO_3^{2-} antisymmetric stretching vibrations
2855*	CH_2 symmetric stretching vibrations
2926*	CH_2 antisymmetric stretching vibrations
3324, 3473	OH^- stretching vibrations

Fig. 3 shows infrared spectra from the untreated (non-corroded) steel used as a background (spectrum a) and from steel corroded without sand deposit (spectrum b). The spectrum from the corroded steel exhibits a single intense band at 1410 cm^{-1} (CO_3^{2-} antisymmetric stretching vibrations) and a low intensity band at 896 cm^{-1} (CO_3^{2-} bending vibrations), both corresponding to siderite ($FeCO_3$) [18]. This is in good agreement with studies showing siderite as the main corrosion product on steel corroded in a CO_2 environment [7,8]. The weak absorption bands at 2926 cm^{-1} and 2854 cm^{-1} (Fig. 3 inset) are again assigned to DPC adsorbed at the corrosion products/steel surface. The results show that siderite is the main corrosion product at

the steel corroded without sand deposit and no absorption bands characteristic of chukanovite were recorded in the infrared spectra.

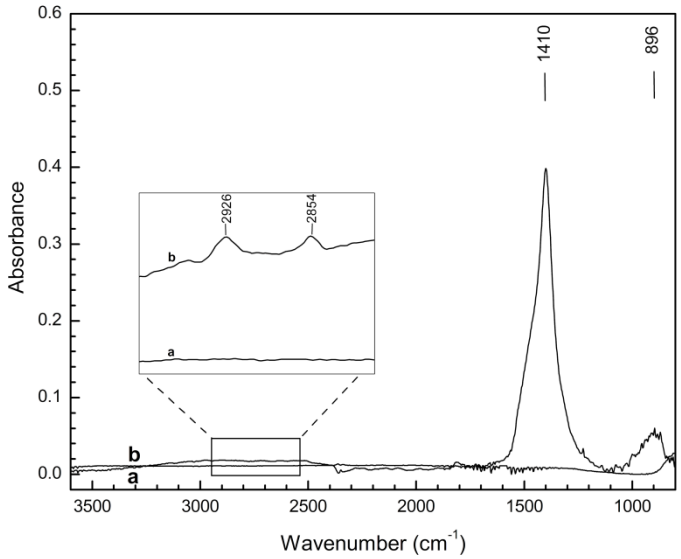

Fig. 3. Synchrotron ATR spectra of a) untreated (non-corroded) steel and b) corroded steel (corroded without sand) after immersion in CO_2-saturated test solution at 80 °C for 24 h.

The formation of corrosion products on carbon steel in CO_2 media is related to the interfacial concentrations of dissolved ions in the solution. The chemical reactions involving the formation of the Fe^{2+}, HCO_3^-/CO_3^{2-} and OH^- ions in oil field brines under CO_2-saturated conditions and their equilibrium constants have been well documented elsewhere [15]. These ions originate from iron dissolution (Fe^{2+}), dissociation of bicarbonate ion/carbonic acid (HCO_3^-/CO_3^{2-}) and direct reduction of water (OH^-) [15].

The corrosion process of carbon steel at high temperatures under CO_2-saturated conditions is generally regarded as the precipitation of iron carbonate (siderite) at the surface [7], which is a pH-dependent electrochemical process [15].

$$Fe^{2+} + CO_3^{2-} \rightarrow FeCO_3$$

At carbon steel surface in CO_2-saturated brine, chukanovite forms via the corrosion reactions [10],

$$2\,Fe_{(s)} + 2H_2O_{(l)} \rightarrow 2Fe(OH)^+_{(aq)} + 2H^+_{(aq)} + 4e^-$$

$$2\,Fe(OH)^+_{(aq)} + CO_3^{2-}{}_{(aq)} \rightarrow Fe_2(OH)_2CO_{3\,(s)}$$

The presence of both chukanovite and siderite, and the transformation of chukanovite to siderite have been reported for CO_2-saturated brines [10] and

carbonate-containing media [17,21]. The formation of chukanovite is controlled by the amount of iron and carbonate species in the solution and is promoted by the excess of either of these ions [17,22]. Preferential formation of chukanovite over siderite occurs at elevated pH, as the formation of siderite is hindered by alkaline conditions (excess of OH^-) [21,22].

Sand deposits at the steel surface act as a diffusion barrier for the transport of ions to and from the surface [4], resulting in changes in the micro-environment underneath the sand and giving rise to a local modification of pH at the interface. Furthermore, the transport of iron species between the steel surface and the electrolyte is restricted by the sand leading to iron-ion excess at the surface. Such conditions promote the observed formation of chukanovite at the sand-deposited surfaces in CO_2-saturated brine. It should also be considered that the presence and stability of the chukanovite layer at the sand-deposited surface in this work is likely to be influenced by the sand itself. Si-species have been shown to improve the stability of corrosion products (green rust) by interacting with its lateral faces thus influencing the transformation of iron oxidation products [23].

3.2 FESEM analysis

Fig. 4 presents FESEM images of a steel surface after corrosion in the presence of a sand-deposit. It can be seen that the surface is completely covered with corrosion products (Fig. 4a) dominated by needle-like, acicular to fibrous crystals characteristic of chukanovite (Fig. 4b) [16,17]. In addition, cubic iron carbonate crystals can also be found at the surface. Fig. 4c shows the association of chukanovite crystals into an iron carbonate crystal. This observation indicates the possibility of transformation of chukanovite to iron carbonate [10,21].

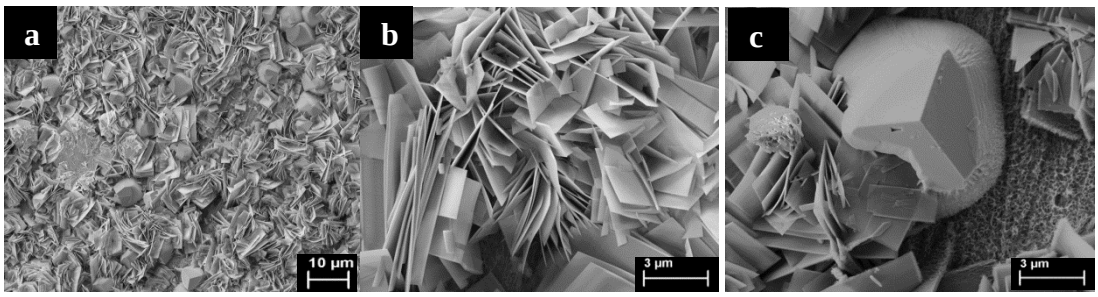

Fig. 4. FESEM images of corroded steel (corroded with sand deposit) after immersion in CO_2-saturated test solution at 80 °C for 24 h a) mixture of corrosion products, chukanovite and siderite; b) chukanovite crystals; c) transformation of chukanovite to siderite.

Fig. 5 shows FESEM images of the steel surface corroded without a sand deposit. The surface is uniformly corroded (Fig. 5a) and exhibits siderite morphology (Fig. 5b). Siderite precipitates at carbon steel surfaces when the ratio of dissolved ions exceeds the local super-saturation limit within the adjacent solution [7]. No morphology indicative of chukanovite can be seen at the surface corroded without a sand deposit, confirming that siderite is the main corrosion product in the absence of sand.

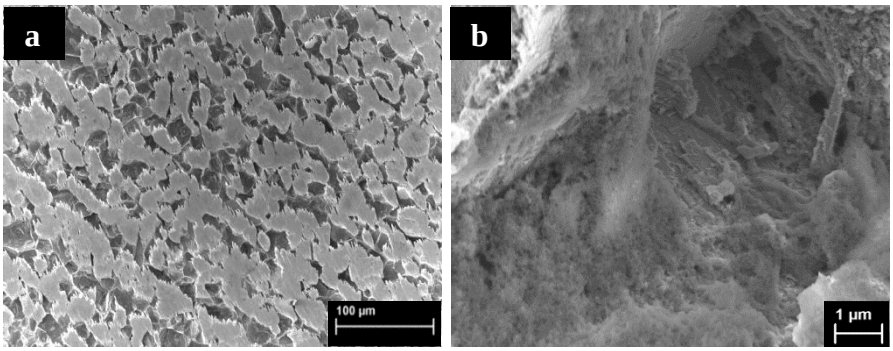

Fig. 5. FESEM images of corroded steel (corroded without sand deposit) after immersion in CO_2-saturated test solution at 80 °C for 24 h a) magnification 200x; b) magnification 3000x.

3.3 Electrochemical measurements

Electrochemical measurements were conducted to investigate the impact of the corrosion products and the sand deposit on the corrosion rates. General corrosion rates were shown to be lower at sand-deposited steels compared to deposit-free steels at low temperatures (less than 60 °C) in CO_2-saturated brines, which was related to the presence of the sand-deposit [5]. At 80 °C used in this study, it is expected that the corrosion rates will be further influenced by the protective corrosion products typically formed in CO_2-saturated brines at elevated temperatures [7].

3.3.1 Linear polarization resistance measurements

Fig. 6 shows the corrosion rates obtained from steels corroded with and without sand deposit for 24 h. At sand-deposited steel, the initial corrosion rate is lower than at the steel without sand due to the deposit layer reducing the active surface area of the steel and/or acting as a diffusion barrier to the transport of corrosive ions. Similar corrosion behaviour has been observed at sand-deposited steels at low temperature (30 °C) [5]. The initial corrosion rate of 1.2 mm y^{-1} decreased to 0.6 mm y^{-1} at the end of 24 h. This final corrosion rate is likely a result of the combined effect of the

sand deposit and the mixed layer of corrosion products (chukanovite and siderite) formed at the surface. The protectiveness of chukanovite against corrosion has been reported previously for mild steel and iron surfaces in CO_2 and carbonate-bicarbonate environments [24,25].

At steel without a sand deposit, the corrosion rate is high compared to sand-deposited steel for the initial 5 hours of exposure. This can be related to faster dissolution of active surface sites on the steel without sand. From about 5 h of exposure, the corrosion rates started to decrease and reached the final value of 0.8 mm y^{-1} at 24 h of test duration. The reduction of corrosion rates at temperatures above 60 °C is associated with the precipitation of siderite at the surface which forms a protective layer [7,8]. The presence of inhibitor DPC in the test solution (56 ppm) did not significantly influence the corrosion rates when compared to the values without inhibitor. The respective corrosion rates of sand-free steels recorded from solutions with and without DPC were 0.77 mm y^{-1} and 0.81 mm y^{-1}. This is consistent with previous study at low temperature (30 °C) which showed that a concentration of 100 ppm DPC was required to provide significant reduction in corrosion rate under CO_2 environment [14].

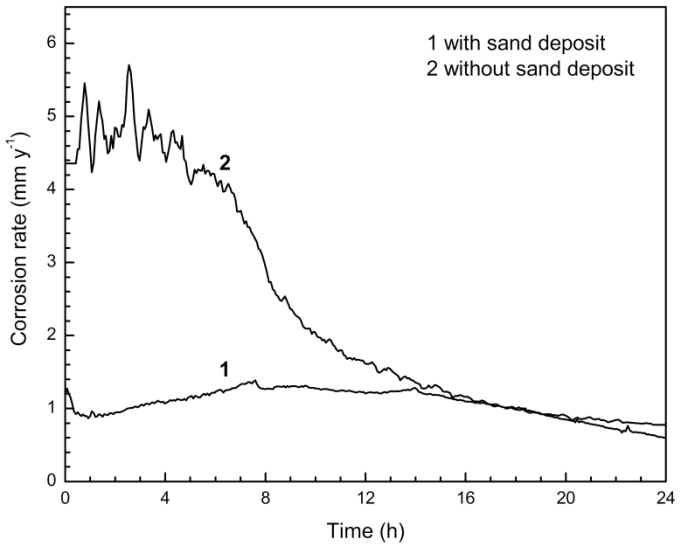

Fig. 6. Corrosion rates of steels with and without sand deposit immersed in CO_2-saturated test solution at 80 °C for 24 h from LPR measurements.

3.3.2 Potentiodyanamic polarization measurements

Fig. 7 shows the potentiodynamic polarization curves of steels with and without sand deposits measured after 24 h immersion in the test solution. The electrochemical

parameters obtained from Tafel extrapolation of the polarization curves are summarized in Table 2.

The results show that the corrosion current density (i_{corr}) is lower at the sand-deposited steel and the corrosion potential (E_{corr}) shifts in a negative direction compared to the steel without a deposit. The negative shift in E_{corr} of sand-deposited steel with respect to the sand-free steel can be associated with the cathodic reaction being predominantly suppressed in the presence of sand-deposit. This can be attributed to the sand-deposit and the corrosion products blocking the cathodic sites at the surface. The general corrosion rates (v_{corr}) are similar for both steels with and without sand deposit, which is in agreement with the linear polarization measurements.

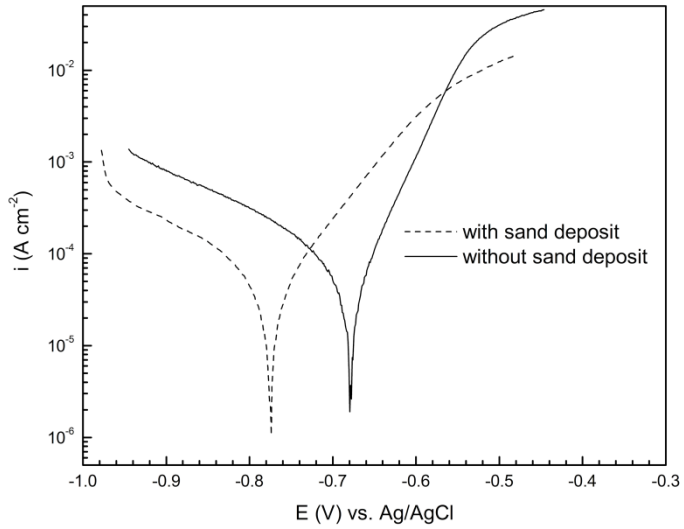

Fig. 7. Potentiodyanamic polarization curves from steels with and without sand deposit after 24 h immersion in CO_2-saturated test solution at 80 °C.

Table 2. Electrochemical parameters derived from potentiodynamic polarization analysis of carbon steel with and without sand deposit in CO_2-saturated test solution at 80 °C.

With sand deposit					**Without sand deposit**				
E_{corr}	i_{corr}	βa	$-\beta c$	v_{corr}	E_{corr}	i_{corr}	βa	$-\beta c$	v_{corr}
V vs. Ag/AgCl	µA cm^{-2}	V dec^{-1}	V dec^{-1}	mm y^{-1}	V vs. Ag/AgCl	µA cm^{-2}	V dec^{-1}	V dec^{-1}	mm y^{-1}
-0.775	51.4±1.9	0.101	0.183	0.58	-0.678	54.7±2.6	0.060	0.162	0.61

3.3.3 Cyclic voltammetry measurements

Fig. 8 shows the cyclic voltammograms recorded from steels with and without sand deposits. The measurements were carried out to assess the susceptibility of the steels to the localized corrosion that has been reported to occur beneath the sand-deposits and regarded as the most severe form of corrosion [15].

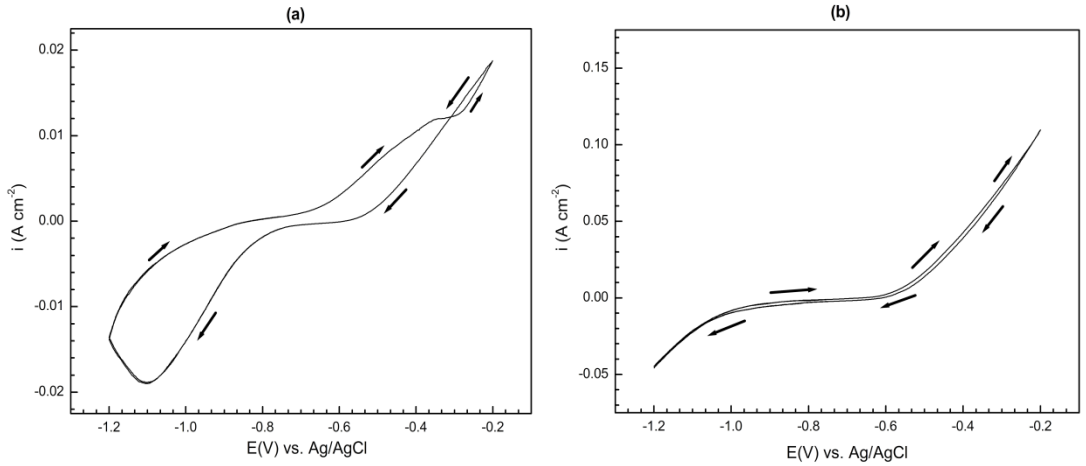

Fig. 8. Cyclic voltammograms after 300 s immersion in CO_2-saturated test solution at 80 °C from steels a) with and b) without sand deposit.

The cyclic voltammogram from steel with a sand deposit (Fig. 8a) exhibits a positive hysteresis loop at lower potentials indicating localized corrosion process at the surface [26]. The positive hysteresis loop is characterized by current densities that are higher in the reverse scan than in the forward scan, at the same potential. This response is indicative of an active electrochemical behaviour of the steel surface that impedes repassivation of an existing pit. No characteristics of localized attack were visible at the steel surface without sand (Fig. 8b), where the forward and reverse scans were almost identical in the potential window studied.

The susceptibility of the sand-deposited steel to localized corrosion can be attributed to the morphology and composition of the corrosion products formed at the surface. Defects in the corrosion product layers due to non-uniform growth have been shown to induce pitting [27]. The FESEM analysis (Fig. 4) revealed a mixed layer of corrosion products (chukanovite and siderite) at the sand-deposited surfaces. The layer consists mainly of chukanovite which can transform into siderite during the corrosion process. The mixed layer of corrosion products is likely to result in potential differences across the surface and hence promote the localized corrosion.

Conversely, a homogeneous layer of siderite formed at the steel surface corroded without a sand deposit (Fig. 5) did not induce localised corrosion.

Localized corrosion at the sand-deposited steel surface after the cyclic voltammetry measurement was further examined by milling the steel surface with focused ion beam (FIB) and imaged with FESEM. Fig. 9a shows the FESEM image of the pitted surface covered with corrosion products before the FIB milling. The maximum pit depth at this surface measured with visible-light microscopy was 5.6 µm. The localized corrosion observed at the surface corroded with sand deposit (Fig. 9a) is consistent with the cyclic voltammetry results (Fig. 8a) that showed positive hysteresis loop in the voltammogram. The cross-sectional FESEM image (Fig. 9b) shows a layer of corrosion products at the pitted area of the surface, confirming that localized attack proceeds underneath the corrosion products.

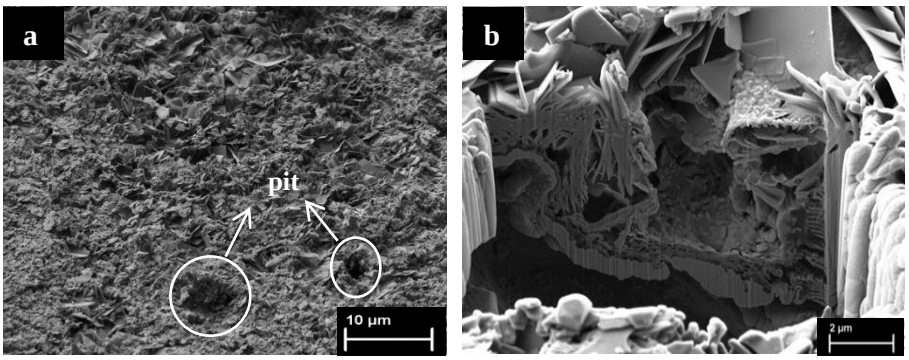

Fig. 9. FESEM images of corroded steel (corroded with sand deposit) in CO_2-saturated test solution at 80 °C a) glancing-angle view of pitted steel surface with corrosion products; b) cross-section of pit covered with corrosion product layer.

4. Conclusions

Corrosion products at steels corroded with and without a sand-deposit in CO_2-saturated brines at 80 °C were characterized using synchrotron infrared microspectroscopy and scanning electron microscopy. Chukanovite ($Fe_2(OH)_2CO_3$) and siderite ($FeCO_3$) were identified as the main corrosion products at sand-deposited and sand-free steels, respectively. Siderite was also found at the sand-deposited steel as a minor corrosion product formed by the transformation of chukanovite. Both sand-deposited and sand-free steels exhibited similar general corrosion rates ascribed to the sand-deposit and the corrosion products layers. Sand-deposited steels were susceptible to localized corrosion which has been attributed to the sand influencing the local micro-environment at the surface. A mixed layer of

corrosion products (chukanovite and siderite) is formed at the sand-deposited steel which promotes localised corrosion.

5. Acknowledgements

This research was undertaken on the Infrared microspectroscopy beamline at the Australian Synchrotron, Victoria, Australia. The assistance of Dr. Mark Tobin and Dr. Danielle Martin is greatly acknowledged. We thank the Centre for Materials Research (CMR) facility at Curtin University for FESEM access. One of us (V. P.) thanks the Curtin University for the Postgraduate Research Scholarship (CIPRS) and Woodside Energy Limited for the financial support. K. L. thanks Curtin University for a Curtin Research Fellowship.

6. References

[1] M.M. Salama, Influence of sand production on design and operations of piping systems, Corrosion 00, NACE International, paper no. 80 (2000).

[2] H. Xue, F.Y. Cheng, Z. Zhu, N. Tajallipour, P.J. Teevens, Internal pitting corrosion of X80 pipeline steel under deposited sand bed in CO_2-saturated solutions, Corrosion 11, NACE International, paper no. 264 (2011).

[3] K. Lepková, R. Gubner, Development of standard test method for investigation of under-deposit corrosion in carbon dioxide environment and its application in oil and gas industry, Corrosion 10, NACE International, paper no. 331 (2010).

[4] V. Pandarinathan, K. Lepková, S.I. Bailey, R. Gubner, Impact of mineral deposits on CO_2 corrosion of carbon steel, Corrosion 13, NACE International, paper no. 2579 (2013).

[5] V. Pandarinathan, K. Lepková, S.I. Bailey, R. Gubner, Inhibition of under-deposit corrosion of carbon steel by thiobenzamide, J. Electrochem. Soc. 160 (9) (2013) C432-C440.

[6] A. Pedersen, K. Bilkova, E. Gulbrandsen, J. Kvarekval, CO_2 corrosion inhibitor performance in the presence of solids: Test method development, Corrosion 08, NACE International, paper no. 632 (2008).

[7] A. Dugstad, Mechanism of protective film formation during CO_2 corrosion of carbon steel, Corrosion 98, NACE International, paper no. 31 (1998).

[8] J.L. Crolet, N. Thevenot, S. Nesic, Role of conductive corrosion products in the protectiveness of corrosion layers, Corrosion 54 (1998) 194-203.

[9] R. De Marco, Z.T. Jiang, B. Pejcic, E. Poinen, An in-situ synchrotron radiation grazing incidence X-ray diffraction study of carbon dioxide corrosion, J. Electrochem. Soc. 152 (10) (2005) B389-B392.

[10] R. De Marco, Z.T. Jiang, D. John, M. Sercombe, B. Kinsella, An in situ electrochemical impedance spectroscopy/synchrotron radiation grazing incidence X-ray diffraction study of the influence of acetate on the carbon dioxide corrosion of mild steel, Electrochim. Acta. 52 (2007) 3746-3750.

[11] B. Ingham, M. Ko, G. Kear, P. Kappen, N. Laycock, J.A. Kimpton, D.E. Williams, *In situ* synchrotron X-ray diffraction study of surface scale formation during CO_2 corrosion of carbon steel at temperatures up to 90 °C, Corros. Sci. 52 (2010) 3052-3061.

[12] M. Foss, E. Gulbrandsen, J. Sjöblom, Interaction of carbon dioxide corrosion inhibitors with corrosion products deposit, Corrosion 08, NACE International, paper no. 343 (2008).

[13] S. Ramachandran, V. Jovancicevic, M.B. Ward, Understanding interactions between corrosion inhibitors & iron carbonate films using molecular modeling, Corrosion 99, NACE International, paper no. 7 (1999).

[14] V. Pandarinathan, K. Lepková, S.I. Bailey, R. Gubner, Evaluation of corrosion inhibition at sand-deposited carbon steel in CO_2-saturated brine, Corros. Sci. 72 (2013) 108-117.

[15] S. Nešić, Key issues related to modelling of internal corrosion of oil and gas pipelines - A review, Corros. Sci. 49 (2007) 4308-4338.

[16] V.E. Erdos, H. Altorfer, Ein dem Malachit ahnliches basisches Eisenkarbonat als Korrosionsprodukt von Stahl, Werkst. Korros. 27 (1976) 304-312.

[17] C. Rémazeilles, Ph. Refait, Fe(II) hydroxycarbonate $Fe_2(OH)_2CO_3$ (chukanovite) as iron corrosion product: Synthesis and study by Fourier Transform Infrared Spectroscopy, Polyhedron, 28 (2009) 749-756.

[18] K. Lepková, W.V. Bronswijk, V. Pandarinathan, R. Gubner, Synchrotron infrared microspectroscopy study of the orientation of an organic surfactant on a microscopically rough steel surface, Vib. Spectrosc. 68 (2013) 204-211.

[19] B.C. Smith, Infrared Spectral Interpretation: A Systematic Approach, Taylor & Francis, 1999.

[20] Ph. Refait, J.A. Bourdoiseau, M. Jeannin, D.D. Nguyen, A. Romaine, R. Sabot, Electrochemical formation of carbonated corrosion products on carbon steel in deaerated solutions, Electrochim. Acta. 79 (2012) 210-217.

[21] I. Azoulay, C. Rémazeilles, Ph. Refait, Determination of standard Gibbs free energy of formation of chukanovite and Pourbaix diagrams of iron in carbonated media, Corros. Sci. 58 (2012) 229-236.

[22] M.L. Schlegel, C. Bataillon, C. Blanc, D. Pret, E. Foy, Anodic activation of iron corrosion in clay media under water-saturated conditions at 90 °C: Characterization of the corrosion interface, Environ. Sci. Technol. 44 (2010) 1503-1508.

[23] A.S. Sergent, F. Jorand, K. Hanna, Effects of Si-bearing minerals on the nature of secondary iron mineral products from lepidocrocite bioreduction, Chem. Geol. 289 (2011) 86-97.

[24] S. Al-Hassan, B. Mishra, D.L. Olson, M.M. Salama, Effect of microstructure on corrosion of steels in aqueous solutions containing carbon dioxide, Corrosion 54 (6) (1998) 480-491.

[25] J. Blengino, M. Keddam, J. Labbe, L. Robbiola, Physico-chemical characterization of corrosion layers formed on iron in a sodium carbonate-bicarbonate containing environment, Corros. Sci. 37 (4) (1995) 621-643.

[26] J. Toušek, Theoretical aspects of the localized corrosion of metals, Trans. Tech Publications, Aedermannsdorf, Switzerland, 1985.

[27] G. Schmitt, M. Horstemeier, Fundamental aspects of CO_2 metal loss corrosion – Part II: Influence of different parameters on CO_2 corrosion mechanisms in Corrosion 06, NACE International, paper no. 112 (2006).

Chapter VII

V. Pandarinathan, K. Lepková, S.I. Bailey, T. Becker and R. Gubner, Adsorption of corrosion inhibitor 1-dodecylpyridinium chloride on carbon steel surface by *in-situ* AFM and electrochemical methods, Industrial & Engineering Chemistry Research, Article in Press

Accepted version of the Manuscript

Adsorption of Corrosion Inhibitor 1-dodecylpyridinium chloride on Carbon Steel Studied by *in-situ* AFM and Electrochemical Methods

ABSTRACT

Corrosion rates are influenced by the formation of inhibitor aggregates at the steel surface. *In-situ* atomic force microscopy (AFM) was used to investigate the adsorbed structures of cationic surfactant, 1-dodecylpyridinium chloride (DPC) at a carbon steel surface in relation to its performance as a CO_2-corrosion inhibitor. An increase in the water contact-angle in the presence of DPC indicated its adsorption at the steel and *in-situ* AFM visualization confirmed the formation of DPC aggregates. The aggregates changed from hemispherical to cylindrical shape with increasing DPC concentration in CO_2-saturated brine, resulting in a decrease in corrosion rates as determined by electrochemical measurements. For comparison to the aggressive CO_2 environment, the inhibition behavior of DPC was monitored in less corrosive N_2-saturated solutions. Formation of cylindrical aggregates was quicker, and a lower corrosion rate was observed in brine saturated with N_2 compared to CO_2.

KEYWORDS: Carbon steel, Surfactant, Adsorption, AFM, Polarization, EIS

1. INTRODUCTION

Organic corrosion inhibitors are extensively used in the oil and gas industry to protect carbon steel pipelines against CO_2 corrosion.[1-4] The surfactant-type organic compounds inhibit corrosion by adsorbing as micelles at the steel-solution interface above a certain inhibitor concentration termed the critical micelle concentration (CMC).[5] The three main micellar shapes reported to form above the CMC in bulk surfactant solutions and at interfaces between the aqueous phase/solid substrate are spherical, cylindrical, and bilayers, based on the micelle curvature.[5,6] As surfactants are added in a majority of industrial CO_2 corrosion inhibitor formulations, it is valuable to characterize their adsorption behavior at steel surfaces for their successful application as inhibitors.

In-situ atomic force microscopy (AFM) and scanning tunneling microscopy (STM) are widely used for surfactant adsorption and thin surface layer studies, since the analysis can be performed directly at the substrate-solution interface with molecular level resolution.[7,8] Several *in-situ* AFM studies of surfactant adsorption at model substrates such as mica, quartz, copper and iron have been reported.[9-15] In contrast, only a few *ex-situ* and *in-situ* AFM investigations on real pipeline material, carbon steel, are available.[16-20] This is because carbon steel is a very reactive substrate that changes rapidly (typically in a time scale of seconds) under corrosive conditions. This causes difficulties in monitoring the surface processes on carbon steel by AFM where the time required to capture one image can be in the order of minutes.[21] Moreover, unlike the atomically smooth model surfaces, the roughness of carbon steel surface is very high which can affect the resolution of the AFM measurements of thin inhibitor layers forming at carbon steel. Thus, most of the AFM inhibitor adsorption research has been performed at homogeneous model surfaces under mildly corrosive conditions, whereas the carbon steel surfaces under severe corrosion conditions typical for oil and gas fields have largely not been investigated by *in-situ* AFM.

Adsorbed inhibitor structures are highly substrate-dependent.[22] Surface properties such as charge density, chemical composition, hydrophilicity/hydrophobicity, etc. differ for each substrate, both for model surfaces and between different alloys of steel. Hence examining the adsorption behavior at model substrates may not accurately predict an inhibitor's performance under field conditions. Furthermore,

AFM investigations at model surfaces do not accurately allow correlation between the adsorption activity at the surface and the corrosion rates.

The present study investigates the application of *in-situ* AFM on a carbon steel surface that is solution-deposited with a corrosion inhibitor, 1-dodecylpyridinium chloride hydrate (DPC) in CO_2-saturated brine. DPC is a surfactant-type organic compound that inhibits corrosion by forming a protective film at the steel surface. Our *in-situ* AFM experimental arrangement was equipped with a flow-through liquid cell assembly and an environmental chamber continuously purged with CO_2. This arrangement facilitated imaging of the inhibitor activity at a carbon steel surface in a controlled test environment closely resembling field conditions for the first time. The AFM analysis in combination with electrochemical and contact angle measurements is utilized to elucidate the adsorption behavior of DPC at a carbon steel surface.

2. MATERIALS AND METHODS

2.1 Substrate. 1030 carbon steel samples embedded in epoxy resin with an exposed surface area of 0.196 cm^2 were used as the substrate material. The chemical composition of carbon steel (weight %) was C (0.37), Mn (0.80), Si (0.282), P (0.012), S (0.001), Cr (0.089), Ni (0.012), Mo (0.004), Sn (0.004), Al (0.01), and Fe (balance). The steel samples were polished to < 1 μm surface finish using diamond suspensions, ultrasonically cleaned with ethanol for 1 min, rinsed with ultrapure water and dried in nitrogen gas before being mounted on the AFM liquid cell holder. The polishing procedure ensured a uniform and reproducible surface preparation for the inhibitor adsorption study at different concentrations. In addition, the sensitivity of the AFM technique requires a flat surface with submicrometer roughness.[10] The root-mean-square roughness determined by AFM of the untreated (bare) steel surface before contact with test solution was ~30 nm (at 10x10 μm^2 sample area).

2.2 Test Solutions. The tests were performed using standard brine solution with 30 g/L sodium chloride (NaCl; Ajax Finechem, 99.9%) and 0.1 g/L sodium hydrogen carbonate ($NaHCO_3$; Merck, 99.5%) prepared in ultrapure water (resistivity - 18.2 MΩ cm). The inhibitor investigated was a cationic surfactant, 1-dodecylpyridinium chloride monohydrate ($C_{17}H_{30}ClN.H_2O$; Sigma Aldrich; 98%) shown in Figure 1. The inhibitor DPC was used as received without further treatment.

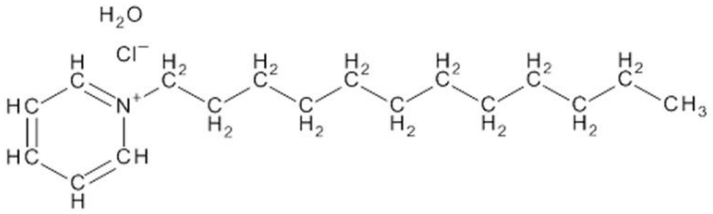

Figure 1. Chemical structure of 1-dodecylpyridinium chloride monohydrate.

The test solutions were saturated with the respective gases (CO_2 or N_2) by presparging for 2 h. This ensured that the dissolved oxygen level in the solutions was less than 20 ppb. The pH of the CO_2-saturated solution was 4.7 and that of N_2-saturated solution was 7.5. The saturated solutions were then pumped into the test cell which was continuously purged with CO_2 or N_2 at ambient pressure during the experiments.

The critical micelle concentration (CMC) of DPC in CO_2-saturated brine solution (pH 4.7) at room temperature (23 °C) was determined from surface tension measurements. The surface tension of aqueous DPC solutions in the concentration range of 5 to 100 ppm (ppm by weight) was measured using the pendant drop method (using KSV CAM 200 goniometer).[23] The CMC value for DPC determined from the surface tension versus concentration plot was 55.8 ppm.

2.3 Contact Angles on Steel Surfaces. Water contact angle measurements were conducted at steel surfaces corroded in CO_2-saturated brine in the presence and absence of DPC for 4 h at 23 °C. The treated steels were then dried with nitrogen gas, and the advancing contact angle of a drop of water on steel was measured by static sessile drop method.[24] A goniometer (KSV CAM 200) with image processing software was used to calculate the mean contact angle (θ) of three measurements to an accuracy of ±1°. No significant change in the water contact angles was observed after 4 h immersion period.

2.4 *In-situ* AFM Imaging. The *in-situ* AFM measurements were performed using the commercial Agilent Picoplus Scanning Probe Microscope system (Agilent Technologies, USA) held in a vibration isolation stage (Figure 2). A silicon nitride cantilever with a spring constant of 0.3 N m^{-1} was used and operated in soft contact mode. In soft contact mode, the tip is scanned over the substrate with an imaging force below the force required for breaking the adsorbed inhibitor film.[5] The standard environmental chamber was used to maintain the test apparatus in an

oxygen-free, controlled environment by purging the high purity (99.99 %) saturation gases (CO_2 or N_2) before and throughout the experiments.

The freshly polished and dried steel sample was placed in the sample holder of the flow-through liquid cell (Figure 3), and the untreated surface was scanned by AFM to assess the bare surface before contact with test solution. The test solution was then pumped through the capillary tube to the liquid cell. The photodetector of the AFM was readjusted and scanning of the steel sample in the test solution was started. The flow-through liquid cell allows for continuous recirculation of the test solution at a slow rate during the experiment. This minimizes any concentration polarization effect and ensures that the test solution does not evaporate over the course of time. The AFM topography and deflection images were recorded at 512x512 pixels resolution.

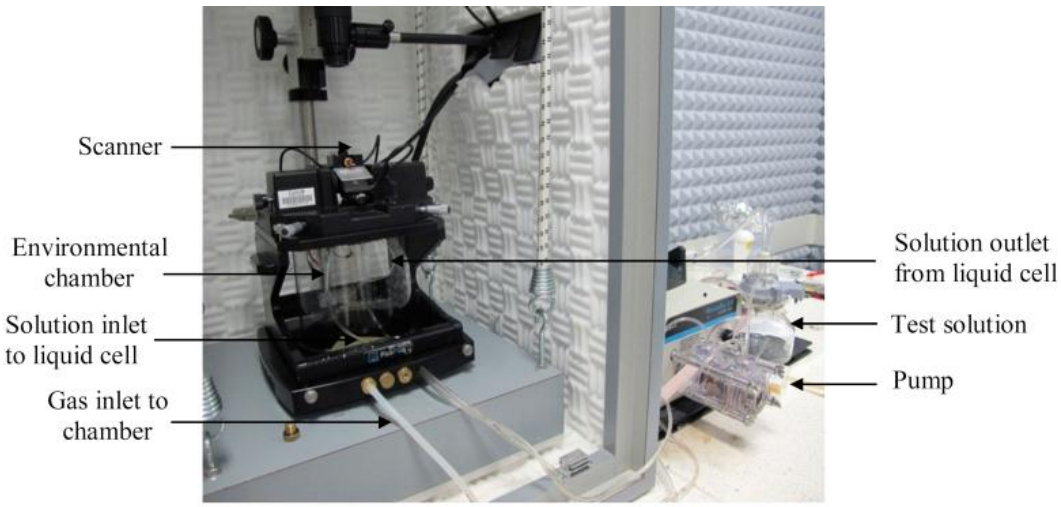

Figure 2. Experimental arrangement of *in-situ* AFM setup.

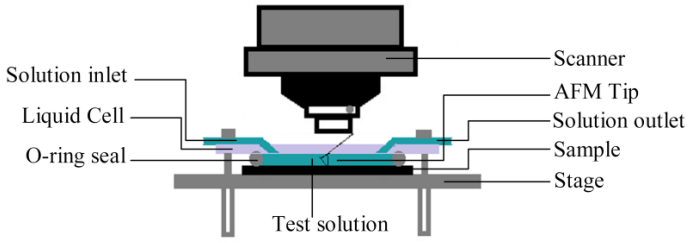

Figure 3. Schematic of the *in-situ* flow-through AFM liquid cell assembly.

Duplicate experiments were carried out for each test condition at 23 °C, and different areas on each sample were profiled to ensure reproducibility of the measurements reported. The sequence of representative AFM images recorded for a period of 4 h is shown for all the experiments. The test duration of 4 h corresponds to

the time sufficient to obtain a stable surface structure which remained unchanged thereafter.

2.5 Electrochemical Measurements. The steel surfaces were evaluated using linear polarization resistance (LPR) and electrochemical impedance spectroscopy (EIS) measurements conducted in a standard three electrode setup described elsewhere.[4] The carbon steel working electrodes were ground up to 1200 grit abrasive paper, ethanol-cleaned, rinsed with ultrapure water, and dried prior to use. Hastelloy C and saturated Ag/AgCl (3.5 M KCl) with a Luggin capillary were used as counter and reference electrodes, respectively. All electrochemical tests were conducted at 23 °C under stagnant conditions.

LPR measurements were conducted for 5 h in the potential range of ±10 mV with respect to the open circuit potential (OCP), at a scan rate of 0.1667 mV/s using an ACM Gill Potentiostat (ACM Instruments, UK).

EIS measurements were performed at applied AC excitation amplitude of 10 mV over a frequency range of 10 kHz to 0.01 Hz using Gamry Reference 600 Potentiostat (Gamry Instruments, USA). The impedance spectra were recorded after the steel samples were stabilized at the OCP for 4 h in the test solutions. The electrochemical parameters, charge transfer resistance (R_{ct}), solution resistance (R_s) and corrosion rate (v) were estimated from the Nyquist plots fitted to the Randle's equivalent circuit using ZView software (Scribner Associates Inc.).

3. RESULTS AND DISCUSSION

3.1 Contact Angle Measurements. The contact angle of water on carbon steel corroded in the presence and absence of DPC was measured to evaluate its adsorption at the surface. Figure 4 shows the contact angle of a water drop on steel surfaces corroded in CO_2-saturated test solutions for 4 h.

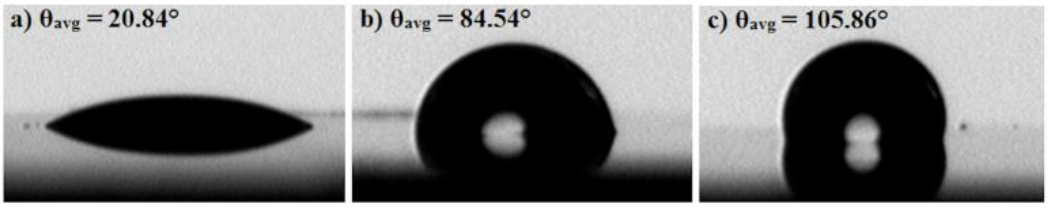

Figure 4. Contact angle of water at steel surfaces after 4 h immersion in CO_2-saturated solutions: a) uninhibited brine b) DPC in brine at CMC, and c) DPC in brine at 500 ppm.

It can be seen from Figure 4a that the water contact angle on the steel in uninhibited brine was low (20.84°) indicating that the corroded steel surface has strong affinity for water. This can be attributed to the presence of hydrophilic corrosion products at the uninhibited steel surface, which causes spreading of the water drop.[24]

Figures 4b and 4c show the water contact angles of the steels immersed in test solutions with DPC at the CMC (56 ppm) and 500 ppm concentrations, respectively. The contact angle of water drop on the inhibited steels was high (> 80°) compared to the uninhibited steel surface. When a drop of water is dispensed at the steel surface, molecules already adsorbed on the surface influence the adsorption of water molecules, depending on the hydrophilic/hydrophobic nature of the adsorbed layer present.[24] The observed increase in contact angle of inhibited steels thus indicates that the surface has become hydrophobic, which can be ascribed to DPC molecules adsorbing at the steel. Hence the water drop has less affinity for inhibited steel compared to the uninhibited surface. In addition, the contact angle increased with an increase in DPC concentration. This implies that hydrophobicity of the steel surface is influenced by the concentration of the inhibitor, where an increase in the inhibitor concentration increases the hydrophobic nature of the substrate.[25] From the contact angle observations, it is evident that the presence of inhibitor DPC in test solution has altered the surface wettability of steel by adsorbing at the steel surface.

3.2 Carbon Steel in CO_2-saturated Uninhibited Brine. Figure 5 shows the sequence of AFM 3D topography images obtained from the steel surface (10x10 μm^2 area) immersed in uninhibited brine. Figure 5a shows the image of untreated steel substrate before contacting the solution. Figure 5b is the topography after 5 min immersion in uninhibited brine. It can be seen that the steel surface immediately shows a rough texture indicating metal dissolution due to corrosion in the uninhibited brine. With prolonged immersion, the surface topography revealed the dissolved structure with grain boundaries (Figure 5d). The difference in surface structure before and after contact with uninhibited brine solution clearly shows that the carbon steel corrodes substantially under these conditions.

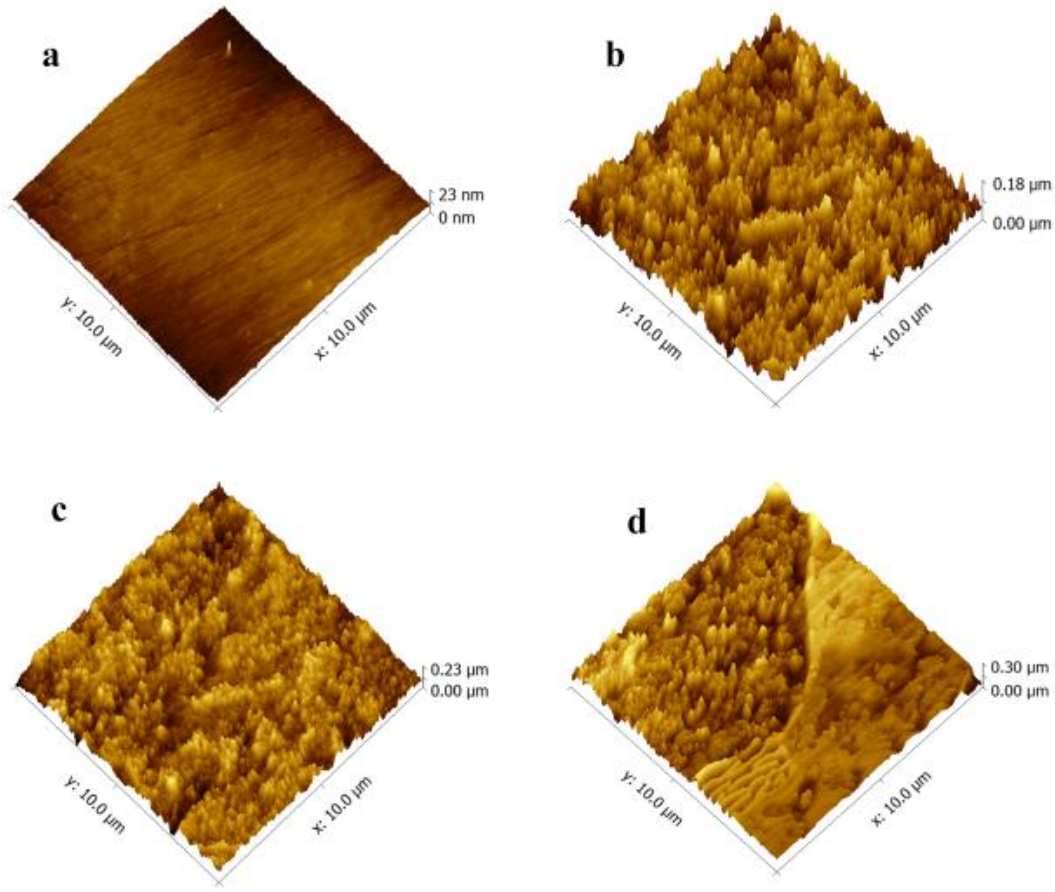

Figure 5. *In-situ* AFM topography of carbon steel in uninhibited brine. Sequence shows (a) untreated bare steel before immersion; and after immersion for (b) 5 min, (c) 30 min, and (d) 4 h.

3.3 Carbon Steel in CO_2-saturated Brine with DPC at the CMC. The time-dependent topography change of steel surface immersed in brine with inhibitor DPC at its CMC is presented in Figure 6. After 5 min of immersion (Figure 6b), hemispherical globules appear as projections on the surface. This can be attributed to DPC forming a surface layer at carbon steel instantly after contact with the inhibited test solution. The hemispherical shaped aggregates represent the most thermodynamically stable (low energy) micellar shape, and the formation of hemispherical interfacial aggregates on various substrates in contact with surfactant solutions has been reported previously.[6,7,9] The growth of the inhibitor aggregates with immersion time can be seen from Figures 6c and 6d, while the hemispherical shape is maintained.

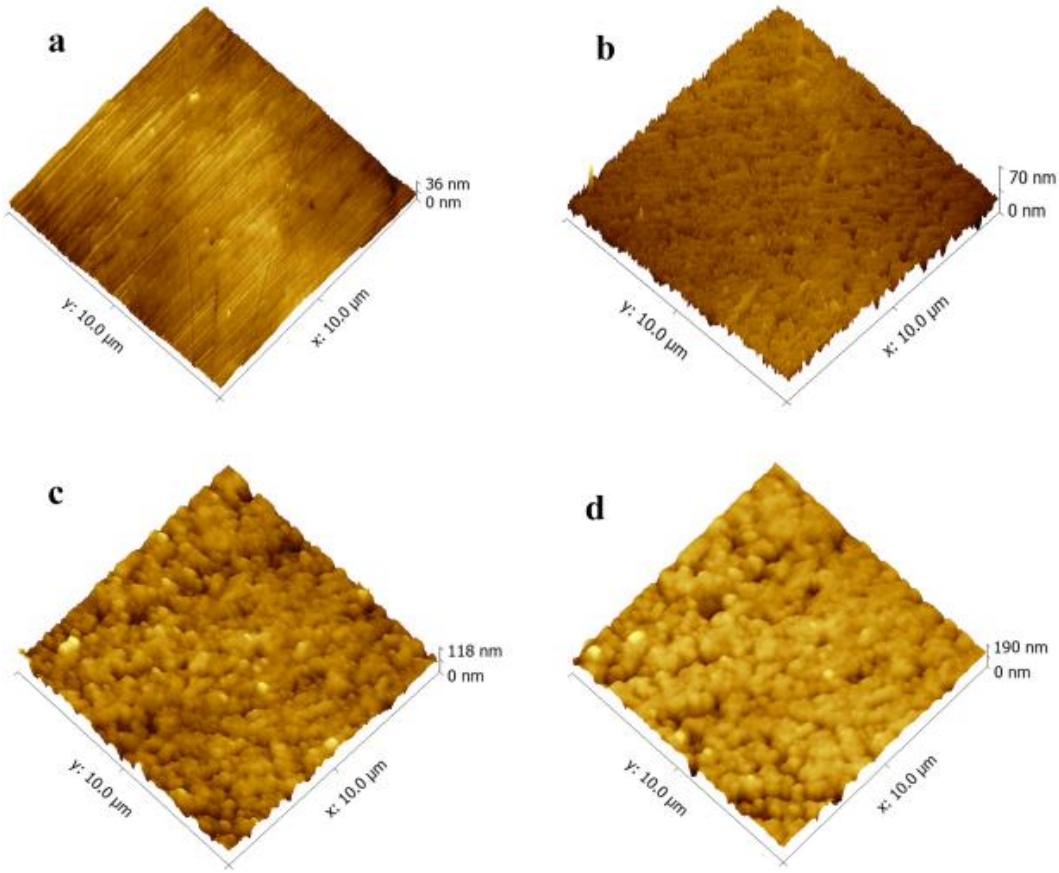

Figure 6. *In-situ* AFM topography of carbon steel in brine with DPC at the CMC. Sequence shows (a) untreated bare steel before immersion; and after immersion for (b) 5 min, (c) 30 min, and (d) 4 h.

It is evident from Figures 5 and 6 that the corroded surface structure under uninhibited condition is different from the aggregate structure formed at steel in the presence of DPC at the CMC. The difference can be ascribed to DPC in the test solution spontaneously forming aggregates at the steel surface.

3.4 Carbon Steel in CO_2-saturated Brine with DPC at 500 ppm. Figure 7 displays the topography images of steel immersed in brine with DPC at 500 ppm concentration. Figure 7a is the untreated steel surface. Within 5 min after the introduction of test solution, a thin layer of cylindrically shaped aggregates was observed at the surface (Figure 7b) with grinding marks remaining visible underneath the layer. This shows that inhibitor DPC adsorbs as cylindrical aggregates at higher concentration. With an increase in immersion time, the aggregate layer became dense (Figure 7c) and eventually the aggregates overlapped forming a relatively homogeneous film covering the surface (Figure 7d).

The increase in DPC concentration above the CMC resulted in the formation of cylindrical aggregates at the carbon steel surface (Figure 7), rather than hemispherical aggregates observed at the CMC concentration (Figure 6). With increasing DPC concentration, the number of inhibitor molecules associating to form aggregates increases (increase in aggregation number). Furthermore, the number of aggregates formed at the surface will be higher due to the compression of electrical double layer surrounding the ionic head groups. The aggregate structure aims to accommodate maximum number of inhibitor molecules into the interfacial layer. This leads to the formation of larger size aggregates, whereby DPC forms cylindrical shaped aggregates.

Patrick et al. showed the formation of cylindrical aggregates on a mica substrate immersed in an aqueous solution of a cationic surfactant at concentrations above CMC.[7] The transition of spherical surfactant aggregates to cylindrical shaped aggregates with an increase in surfactant concentration has been reported at different substrates.[7,13] Comparison of Figures 6 and 7 clearly suggests that the morphology of the inhibitor film formed is influenced by the inhibitor concentration applied.

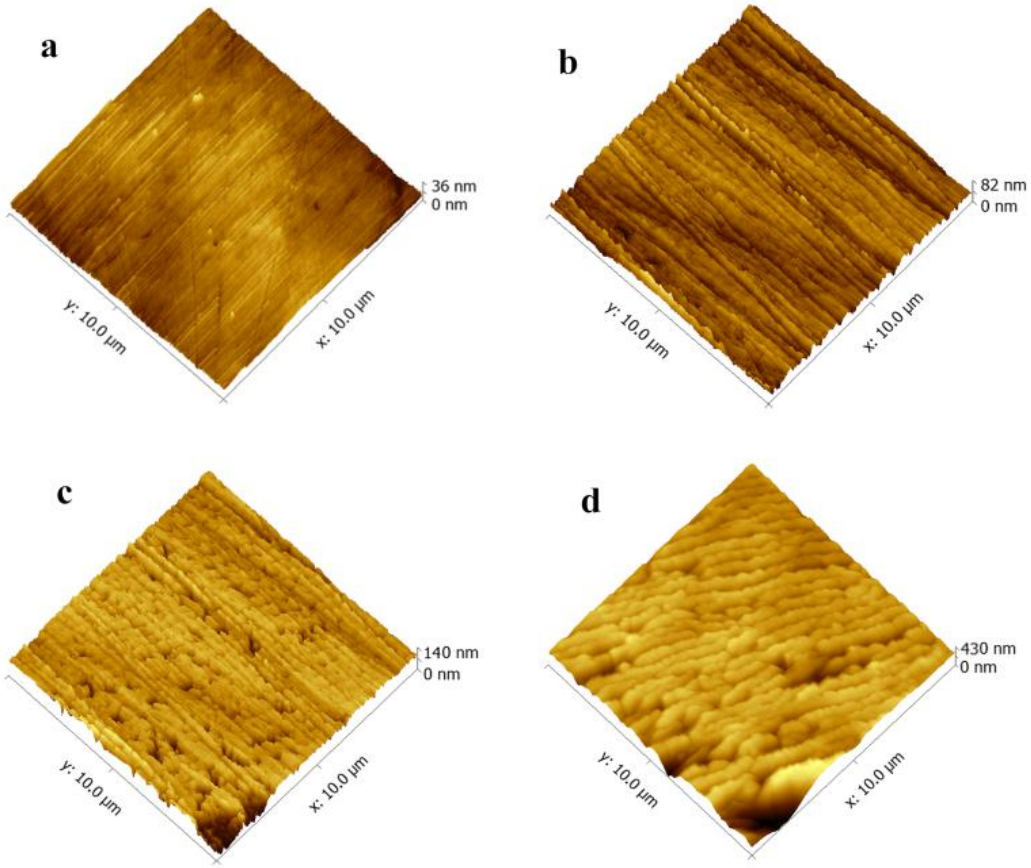

Figure 7. *In-situ* AFM topography of carbon steel in brine with DPC at 500 ppm. Sequence shows (a) untreated bare steel before immersion; and after immersion for (b) 5 min, (c) 30 min, and (d) 4 h.

High magnification imaging was conducted for the detailed visualization of inhibitor aggregates at the steel surface. The 2D deflection images obtained from steel immersed in brine with 500 ppm DPC recorded at a higher magnification (sample area reduced to 1x1 μm^2) is shown in Figure 8. The inhibitor adsorption is apparent after 5 min immersion (Figure 8b). The number of inhibitor aggregates increases with immersion time, along with the previously formed aggregates growing in size.

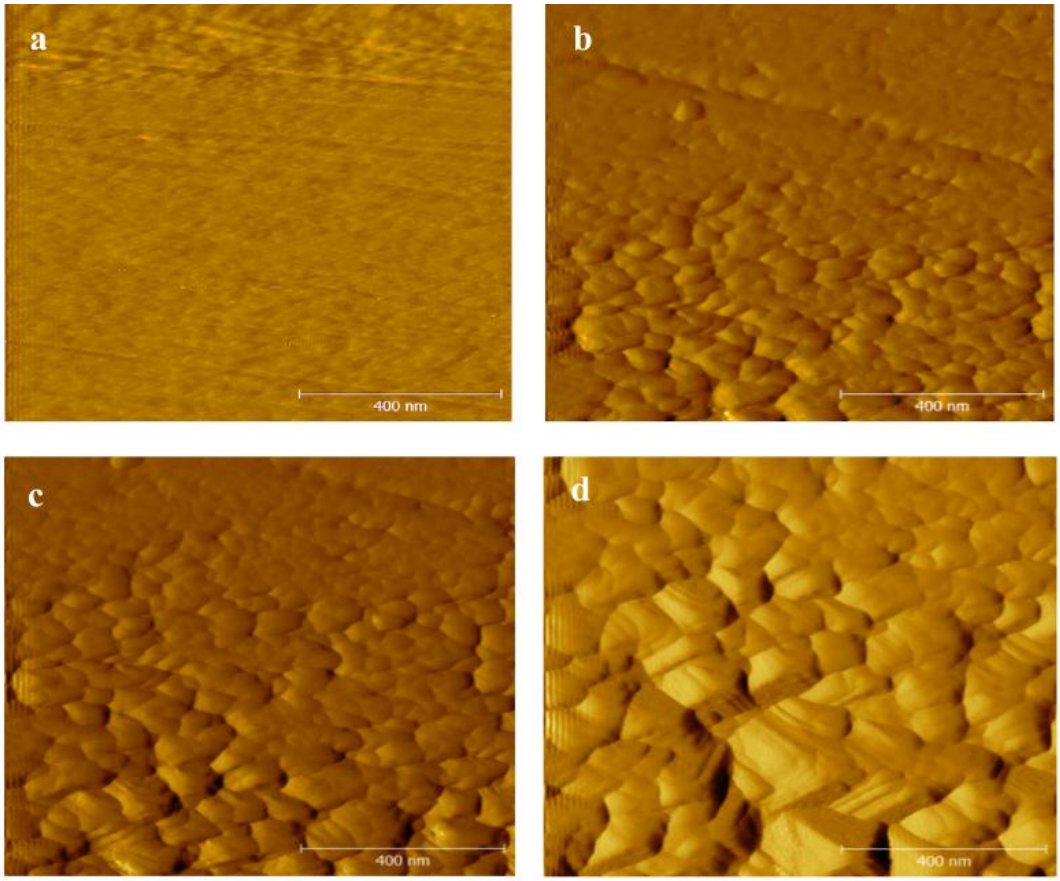

Figure 8. *In-situ* AFM deflection images of carbon steel in brine with DPC at 500 ppm. Sequence shows (a) untreated bare steel before immersion; and after immersion for (b) 5 min, (c) 30 min, and (d) 4 h.

3.5 Carbon Steel in N_2-saturated Brine with DPC at 500 ppm. In order to examine the effect of CO_2 on the inhibitor adsorption process, the carbon steel surface was investigated in N_2-saturated brine with DPC at 500 ppm concentration. The image sequence is shown in Figure 9.

Cylindrical inhibitor aggregates were readily seen at the surface in the N_2-saturated test solution (Figure 9b) and a stable adsorbed structure formed within 30 min of immersion (Figure 9c) compared to the 4 h required for complete film formation under CO_2 environment. At the same DPC concentration, this difference in adsorption behavior in N_2-saturated brine compared to CO_2-saturated brine can be attributed to the pH effect.[26] The pH of the test solution saturated with N_2 and CO_2 was 7.5 and 4.7, respectively. The higher pH in the N_2-saturated test solution means that the steel surface acquires a negative charge due to preferential adsorption of Cl^- ions at steel. The surface charge of mild steel and solution pH has been shown to be determining factors in simple amine inhibitor adsorption.[17] Therefore, the positively

charged cationic inhibitor aggregates spontaneously adsorb at the surface due to electrostatic interactions. The higher pH also minimizes the repulsion between adjacent aggregates, hence a stable, closely packed structure is formed in a shorter period of time than in the CO_2 environment. Whereas in the CO_2 media with a high density of H^+ ions at the surface the inhibitor adsorption is relatively slow. Previous investigations on adsorbed surfactant structures formed on model substrates have shown that surface charge of the substrate is one of the factors influencing the adsorption process.[22,26] When a cationic surfactant inhibitor is applied to a substrate of negative surface charge (such as carbon steel in a N_2 environment), the inhibitor adsorbs at the cathodic sites due to electrostatic attractions. Similarly, when there are counterions such as H^+ (such as carbon steel in a CO_2 environment) the adsorption of the cationic inhibitor is limited by the repulsive forces between the ions.

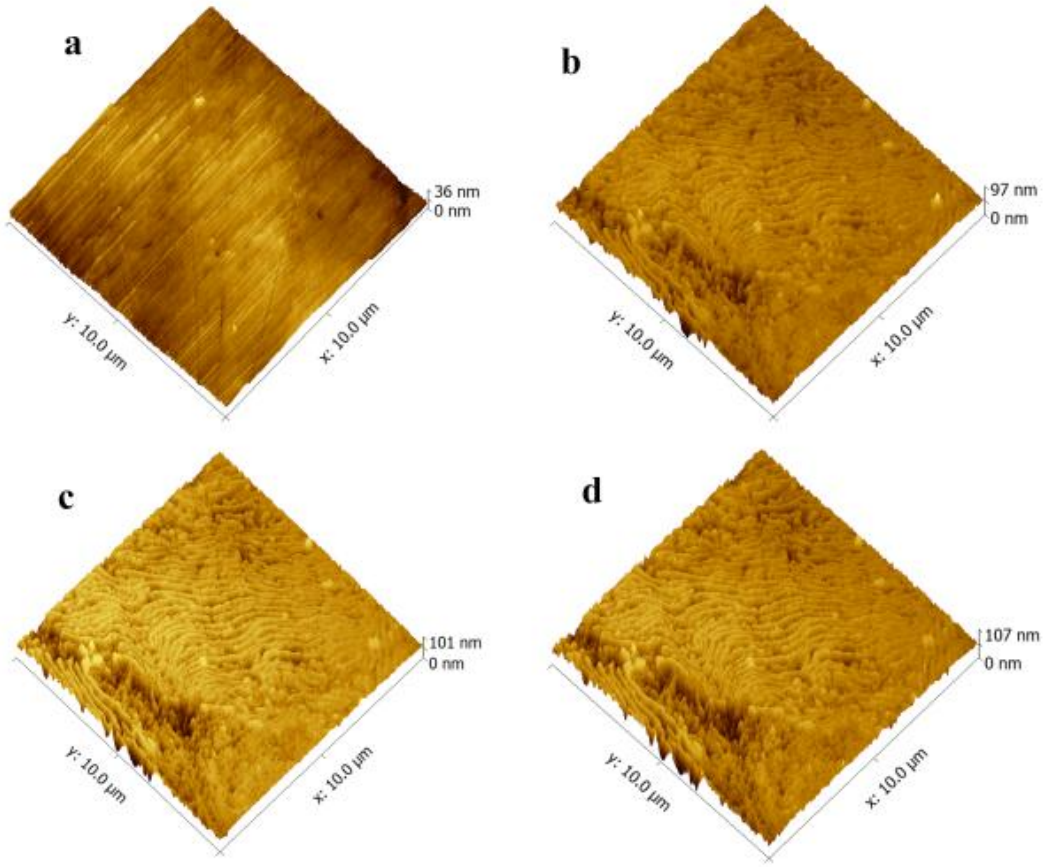

Figure 9. *In-situ* AFM topography of carbon steel in N_2-saturated brine with DPC at 500 ppm. Sequence shows (a) untreated bare steel before immersion; and after immersion for (b) 5 min, (c) 30 min, and (d) 4 h.

3.6 Influence of the Structure of Inhibitor Film on the Corrosion Rates. The electrochemical measurements at carbon steel surfaces were conducted to determine

if any correlation exists between inhibition performance of DPC at steel with the type of aggregates formed at the interface. The electrochemical tests were run under the same conditions as used in the *in-situ* AFM analysis.

3.6.1 LPR Measurements. Corrosion rates obtained from LPR measurements are presented in Figure 10. The curve (a) in Figure 10 of the steel in CO_2-saturated uninhibited brine exhibits a high corrosion rate as expected. This correlates well with AFM images taken at steel immersed in uninhibited solution where a dissolved steel structure was observed (Figure 5).

The curve (b) obtained from steel immersed in CO_2-saturated brine with DPC at CMC concentration shows a decrease in corrosion rate in respect to the uninhibited condition (curve (a)). This decrease is attributed to the adsorption of inhibitor molecules at the steel surface which prevents the corrosion reactions occurring on the underlying steel, as the protective iron carbonate film does not form at the temperatures studied in this work.[27] Hence, the observed lower corrosion rate in the presence of the inhibitor indicates DPC aggregation at the steel surface as shown by the AFM measurements (Figure 6).

The curve (c) corresponds to the corrosion rate of steel in CO_2-saturated brine with DPC at 500 ppm (concentration greater than CMC). The corrosion rate decreases rapidly for 30 min after immersion followed by a gradual decrease for a period of 2 h. The rapid decrease in the corrosion rate for the initial 30 min can be related to the inhibitor molecules diffusing from the bulk and adsorbing as cylindrical aggregates at the steel surface as seen from AFM topography (Figure 7). The subsequent gradual decrease in the corrosion rate can be associated to the duration for the adsorbed aggregates to grow and form a dense stable film. A final corrosion rate value less than 0.2 mm y^{-1} was attained within 4 h after immersion, and it remained reasonably constant thereafter. This can be ascribed to formation of a high-density adsorbed structure in 4 h, which effectively inhibits the steel surface from further corrosion. The corrosion rate trend is consistent with the changes in the surface topography of steel observed by AFM where the image sequence changed for 4 h, ascribable for the formation of cylindrical aggregates until the inhibitor aggregate structure was stable. Further immersion in solution after 4 h did not change the adsorbed structure, and consequently the corrosion rate can be expected to remain essentially constant, as was observed.

Comparing curves (b) and (c), the corrosion rate decreases considerably with an increase in DPC concentration from 55.8 ppm (CMC) to 500 ppm. This indicates that the adsorbed inhibitor film is more protective and the adsorption time for complete coverage is shorter when a higher DPC concentration is used. Relating these differences in the electrochemical behavior to the AFM observation, it can be supposed that the adsorbed structure composed of cylindrical aggregates (Figure 7) formed with 500 ppm DPC is more protective than the hemispherical aggregates observed with DPC at CMC (Figure 6). This can be related to the spherical aggregate structure allowing more access of corrosive ions to the steel surface due to its higher surface curvature morphology than a cylindrical aggregate layer would. Rabinovich et al. determined that when the surfactant aggregate structure changes from spherical to cylindrical shape, the mechanical properties such as elastic modulus, yield stress, etc. of surfactant aggregates formed are doubled.[28] Hence the very low corrosion rate (enhanced inhibition activity) with DPC at 500 ppm can be ascribed to the adsorbed structure impacting the corrosion behavior of the steel.

Curve (d) shows the corrosion rate of steel in N_2-saturated uninhibited brine. The corrosion rate can be seen to be much lower than in CO_2-saturated brine (curve (a)). This is attributed to the change in solution chemistry (less corrosive) when sparging with N_2. The curve (e) shows the corrosion rate of steel in N_2-saturated brine with 500 ppm DPC. The reduction in corrosion rate seen from curve (e) compared to the uninhibited condition (curve (d)) can be related to inhibitor activity at the steel surface.

At the same applied inhibitor concentration of 500 ppm, curve (e) shows a lower corrosion rate with respect to the CO_2 environment (curve (c)) and stabilizes in less than 1 h after immersion. The corresponding AFM images under the N_2 environment (Figure 9) demonstrated that adsorption is faster than under the CO_2 environment (Figure 7) where cylindrical aggregates appeared on the steel surface immediately after immersion. The entire steel surface was covered with a dense layer of inhibitor aggregates forming a protective barrier against corrosive ions (Figure 9). This improved inhibitor performance under N_2 conditions can be ascribed to the bare steel surface immersed in the N_2-saturated test solution exhibiting negative surface charge density, which electrostatically strongly interacts with the cationic surfactant DPC to form a protective film against corrosion.

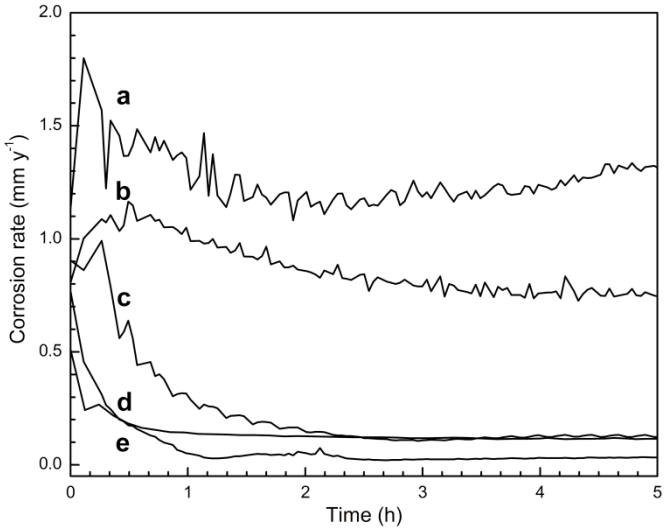

Figure 10. Corrosion rates from carbon steels immersed in CO_2-saturated brine a) uninhibited, b) with DPC at CMC, and c) with 500 ppm DPC and steels immersed in N_2-saturated brine d) uninhibited e) with 500 ppm DPC.

3.6.2 EIS Measurements. The corrosion behavior of carbon steel was further studied using EIS conducted after stabilization of the steel samples at the OCP for 4 h. Figure 11a shows the Nyquist plots of carbon steel surfaces immersed in CO_2-saturated brine in the presence and absence of DPC. Figure 11b presents the plot obtained from the steel surface immersed in N_2-saturated brine in the presence and absence of 500 ppm DPC. The calculated electrochemical parameters are shown in Table 1.

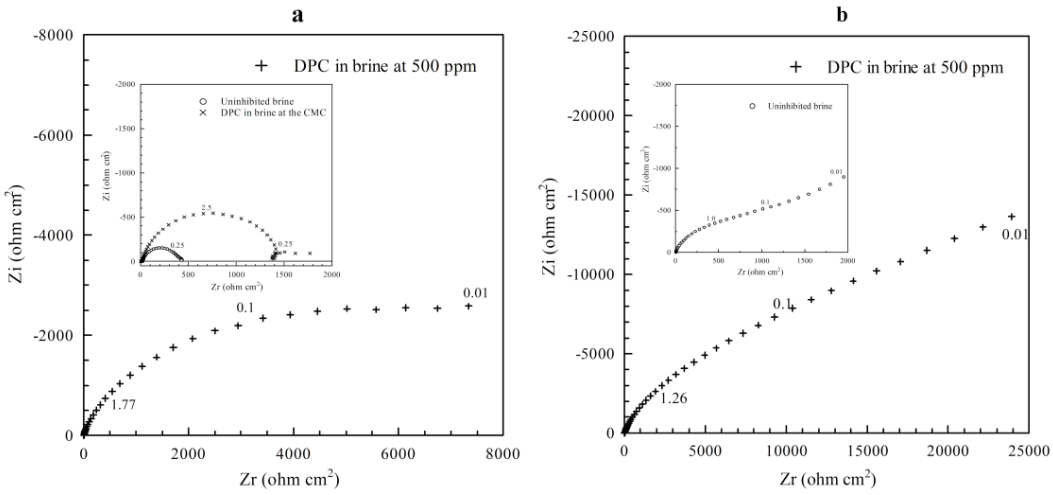

Figure 11. EIS Nyquist plots from carbon steels after 4 h immersion in a) CO_2-saturated brine with 500 ppm DPC (inset: uninhibited brine and DPC at the CMC) and b) N_2-saturated brine with 500 ppm DPC (inset: uninhibited brine).

Table 1. Estimated Corrosion Parameters from EIS Analysis of Carbon Steel

Saturation gas	Test solution	R_s	R_{ct}	*Error*	$i_{corr} = 26/R_{ct}$	v
		$\Omega\ cm^2$	$\Omega\ cm^2$	%	$\mu A\ cm^{-2}$	$mm\ y^{-1}$
CO_2	Uninhibited brine	14.25	410	4.5	63.38	0.72
	DPC in brine at CMC	11.07	1414	3.4	18.39	0.20
	DPC in brine at 500 ppm	2.98	7037	3.1	3.69	0.04
N_2	Uninhibited brine	2.44	1741	4.6	14.93	0.17
	DPC in brine at 500 ppm	10.96	23613	7.1	1.10	0.01

It can be seen from the impedance plots under CO_2-saturated conditions (Figure 11a) that R_{ct} is low for steel in uninhibited brine, and it increases with an increase in DPC concentration. This indicates inhibitor adsorption at steel resists the corrosive ions from reaching the steel surface, thus lowering the corrosion rate in the presence of DPC. At 500 ppm DPC concentration, R_{ct} increases significantly due to the enhanced adsorption of DPC at the steel surface at a concentration above the CMC. The decrease in solution resistance (R_s) with an increase in DPC concentration is attributed to the increase in ion concentration in the solution. The magnitude of R_{ct} is substantially higher for both inhibited and uninhibited N_2-saturated conditions (Figure 11b) with respect to the CO_2-saturated conditions due to less corrosion proceeding in the N_2 environment, consistent with both the LPR and AFM measurements.

The differences in the corrosion resistances observed under each test condition can be interpreted as a reflection of the morphological changes of adsorbed structure which in turn alters the surface coverage by inhibitor. The EIS results support the finding that a strong correlation exists between the corrosion rate and the adsorbed structure of inhibitor film formed at the surface.

4. CONCLUSIONS

The adsorption of corrosion inhibitor 1-dodecylpyridinium chloride (DPC) at the carbon steel surface has been confirmed by *in-situ* AFM, and the type of DPC aggregates influence the corrosion rates.

It was found that DPC adsorption increased the hydrophobicity of the steel surface, indicated by the increase in water contact angle from 20.84° to 105.8° upon addition of 500 ppm DPC to CO_2-saturated brine. The *in-situ* AFM revealed the formation of hemispherical and cylindrical aggregates in CO_2-saturated brine with 55.8 ppm (CMC) and 500 ppm DPC, respectively. The formation of cylindrical aggregates is enhanced under N_2-saturated conditions (high pH) compared to CO_2-saturated conditions (low pH).

The *in-situ* AFM results correlate well with the electrochemical measurements providing a relationship between the type of adsorbed aggregates and the corrosion rate of the steel. The corrosion rates decrease with increasing DPC concentration, which is relevant to the observation of hemispherical and cylindrical aggregates at low and high DPC concentrations, respectively. The enhanced formation of the cylindrical aggregates under N_2-saturated conditions (compared to CO_2) corresponds to lower corrosion rates observed in the N_2 environment.

The combination of *in-situ* AFM and electrochemical tests demonstrated that DPC adsorbs on the steel surface and its inhibition performance is dependent on the structure of the aggregates formed.

ACKNOWLEDGEMENTS

The authors would like to thank Woodside Energy Ltd. for the financial support and permission to publish this work. We also acknowledge the support of the Australian and Western Australian Governments, as well as the Western Australian Energy Research Alliance (WAERA). One of us (V.P.) thanks Curtin University for awarding the Curtin International Postgraduate Research Scholarship (CIPRS). K. L. thanks Curtin University for a Curtin Research Fellowship.

REFERENCES

(1) Dougherty, J.A. Controlling CO_2 corrosion with inhibitors, *Corrosion 98*, NACE International, San Diego, CA, **1998**.

(2) Okafor, P.C.; Liu, C.B.; Zhu, Y.J.; Zheng, Y.G. Corrosion and corrosion inhibition behavior of N80 and P110 carbon steels in CO_2-saturated simulated formation water by rosin amide imidazoline, *Ind. Eng. Chem. Res.* **2011**, *50* (12), 7273–7281.

(3) Tan, Y.J.; Bailey, S.; Kinsella, B. The monitoring of the formation and destruction of corrosion inhibitor films using electrochemical noise analysis (ENA), *Corros. Sci.* **1996,** *38,* 1681-1695.

(4) Pandarinathan, V.; Lepková, K.; Bailey, S.I.; Gubner, R. Evaluation of corrosion inhibition at sand-deposited carbon steel in CO_2-saturated brine, *Corros. Sci.* **2013**, *72,* 108-117.

(5) John, D. Mechanism of carbon-dioxide corrosion and inhibition under high flow - a jet impingement study, *PhD thesis*, Curtin University **2006**.

(6) John, D.; Blom, A.; Bailey, S.; Nelson, A.; Schulz, J.; DeMarco, R.; Kinsella, B. The application of neutron reflectometry in the study of inhibitor films, *Phys B (Amsterdam, Neth.)* **2006**, *385-386,* 924-926.

(7) Patrick, H.; Warr, G.G.; Manne, S.; Aksay, I.A. Surface micellization patterns of quaternary ammonium surfactants on mica, *Langmuir.* **1999**, *15,* 1685-1692.

(8) Massoud, T.; Maurice, V.; Klein, L.H.; Marcus, P. Nanoscale morphology and atomic structure of passive films on stainless steel, *J. Electrochem. Soc.* **2013**, *160,* C232–C238.

(9) Wolgemuth, J.L.; Workman, R.K.; Manne, S. Surfactant aggregates at a flat, isotropic hydrophobic surface, *Langmuir.* **2000**, *16,* 3077-3081.

(10) Schulz, J.; Warr, G.; Butler, P.; Hamilton, W. Adsorbed layer structure of cationic surfactants on quartz, *Phys. Rev. E.* **2001,** *63,* 041604.

(11) Telegdi, J.; Shaglouf, M.M.; Shaban, A.; Karman, F.H.; Betroti, I.; Mohai, M.; Kalman, E. Influence of cations on the corrosion inhibition efficiency of aminophosphonic acid, *Electrochim. Acta.* **2001**, *46*, 3791-3799.

(12) Paria, S.; Khilar, K.C. A review on experimental studies of surfactant adsorption at the hydrophilic solid-water interface, *Adv. Colloid Interface Sci.* **2004**, *110,* 75-95.

(13) Israelachvili, J.N. *Intermolecular and Surface Forces,* third ed., Academic Press, London, **2011**.

(14) Inoue, S.; Uchihashi, T.; Yamamoto, D.; Ando, T. Direct observation of surfactant aggregate behavior on a mica surface using high-speed atomic force microscopy, *Chem. Commun. (Cambridge, U. K.)* **2011**, *47*, 4974-4976.

(15) Chen, Z.; Huang, L.; Zhang, G.; Qiu, Y.; Guo, X. Benzotriazole as a volatile corrosion inhibitor during the early stage of copper corrosion under adsorbed thin electrolyte layers, *Corros. Sci.* **2012**, *65*, 214–222.

(16) Solmaz, R.; Kardaş, G.; Çulha, M.; Yazici, B.; Erbil, M. Investigation of adsorption and inhibitive effect of 2-mercaptothiazoline on corrosion of mild steel in hydrochloric acid media, *Electrochim. Acta.* **2008,** *53*, 5941–5952.

(17) Luo, H.; Guan, Y.C.; Han, K.N. Corrosion inhibition of a mild steel by aniline and alkylamines in acidic solutions, *Corrosion* **1998**, *54*, 721-731.

(18) Bosenberg, S.; John, D.; Becker, T.; Bailey, S.; De Marco, R. Resolving the structure of carbon dioxide corrosion inhibitors on surfaces, 47th Annual Conference of the Australasian Corrosion Association, Sydney, **2007**, 819-828.

(19) Zhang, F.; Pan, J.; Claesson, P.M. Electrochemical and AFM studies of mussel adhesive protein (Mefp-1) as corrosion inhibitor for carbon steel, *Electrochim. Acta*. **2011**, *56*, 1636-1645.

(20) Zhang, F.; Pan, J.; Claesson, P.M.; Brinck, T. Electrochemical, atomic force microscopy and infrared reflection absorption spectroscopy studies of pre-formed mussel adhesive protein films on carbon steel for corrosion protection, *Thin Solid Films.* **2012**, *520*, 7136-7143.

(21) Valtiner, M.; Ankah, G.N.; Bashir, A.; Renner, F.U. Atomic force microscope imaging and force measurements at electrified and actively corroding interfaces: challenges and novel cell design, *Rev. Sci. Instrum.* **2011,** *82*, 023703.

(22) Rosen, M.J.; Kunjappu, J.T. *Surfactants and Interfacial Phenomena*, fourth edition, John Wiley & Sons, **2012**.

(23) Lin, S.Y.; McKeigue, K.; Maldarelli, C. Diffusion-controlled surfactant adsorption studied by pendant drop digitization, *AIChE Journal.* **1990**, *36*, 1785-1795.

(24) Schmitt, G.; Stradmann, N. Wettability of steel surfaces at CO_2 corrosion conditions I. Effect of surface active compounds in aqueous and hydrocarbon media, *Corrosion 98*, Paper no 28, NACE International, San Diego, CA, **1998**.

(25) Li, C. Effect of corrosion inhibitor on water wetting and carbon dioxide corrosion in oil-water two phase flow, Ph.D. thesis, Ohio University, **2009**.

(26) Atkin, R.; Craig, V.S.J.; Wanless, E.J.; Biggs, S. Mechanism of cationic surfactant adsorption at the solid-aqueous interface, *Adv. Colloid Interface Sci.* **2003**, *103,* 219-304.

(27) Schmitt, G.; Horstemeier, M. Fundamental aspects of CO_2 metal loss corrosion - Part II: Influence of different parameters on CO_2 corrosion mechanisms, *Corrosion 06*, Paper no 112, NACE International, San Diego, CA, **2006.**

(28) Rabinovich, Y.; Vakarelski, I.U.; Brown, S.C.; Singh, P.K.; Moudgil, B.M. Mechanical and thermodynamic properties of surfactant aggregates at the solid-liquid interface, *J. Colloid Interface Sci.* **2004**, *270,* 29-36.

Appendix 1

V. Pandarinathan and K. Lepková, Investigation of generic inhibitors for general and localized corrosion of sand-deposited carbon steel surfaces under CO_2-saturated conditions, Manuscript to be submitted

Manuscript version to be Submitted

Investigation of generic inhibitors for general and localized corrosion of sand-deposited carbon steel surfaces under CO_2-saturated conditions

Abstract

The effectiveness of inhibitors to mitigate corrosion of carbon steel under sand-deposits in a CO_2-saturated environment was investigated. Sulphur-containing inhibitor showed excellent inhibition performance against both general and localized corrosion at sand-deposited steels. Quaternary ammonium inhibitors were less effective compared to the sulphur-containing inhibitor and the results revealed localized attack at the sand-deposited steels in their presence. Inhibition failure at surface sites on steel inaccessible to the inhibitor due to its adsorption to sand-deposits is supposed to promote localized corrosion.

Keywords: Carbon-dioxide, Carbon steel, Corrosion inhibitor, Sand-deposit, Polarization.

1. Introduction

CO_2 corrosion of the carbon steel pipelines is enhanced in the presence of sand-deposits causing under-deposit corrosion [1]. The sand-deposits are also a limiting factor for the performance of corrosion inhibitors applied to protect the steel surface [2-5]. In our previous study, it was found that the efficiency of corrosion inhibitors at sand-deposited steels was dependent on their adsorption affinity to sand-deposits [6]. Reduced inhibition effect at the steel surface was observed as a consequence of the adsorption loss to sand and was found to be dependent on the chemical structure of the inhibitors [6,7]. However, these results relate to the inhibition of general corrosion, while the primary concern in the presence of sand-deposits has been reported to be localized corrosion [8-10]. Therefore, it is important to assess the risk of localized corrosion while evaluating the effectiveness of corrosion inhibitors for under-deposit corrosion.

This study presents the activity of four generic inhibitors against both general and localized corrosion of carbon steel under CO_2-saturated conditions. The organic

inhibitors investigated were three quaternary ammonium compounds (surfactants) and a sulphur-containing compound. The selection of inhibitors was based on our previous studies which showed that these compounds provide sufficient inhibition to carbon steels against general CO_2 corrosion [6,11]. Immersion and electrochemical tests were conducted to determine the inhibitor performance at steels, followed by field emission scanning electron and visible-light microscopy analysis of the surface morphology. The study is expected to determine the inhibitors that can be used for both general as well as localized corrosion mitigation under sand-deposits.

2. Experimental

Test solutions consisted of 3 wt% sodium chloride (NaCl; Ajax Finechem; 99.9%) and 0.01 wt% sodium hydrogen carbonate ($NaHCO_3$; Merck; 99.5%) prepared in ultra-pure water (Milli-Q system, resistivity 18.2 MΩ.cm) and respective inhibitors at 200 ppm concentration. Table 1 shows the corrosion inhibitors evaluated in this study. The test solutions were CO_2-saturated at atmospheric pressure and the solution pH was 4.7. All the experiments were carried out at 30±1 °C under stagnant conditions.

Table 1. Generic corrosion inhibitors, their chemical formulas and structures.

Inhibitor	Chemical formula	Chemical structure
1-dodecylpyridinium chloride hydrate (DPC)	$C_{17}H_{30}ClN \cdot H_2O$	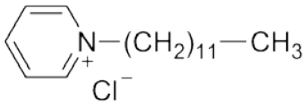
Cetylpyridinium chloride monohydrate (CPC)	$C_{21}H_{38}ClN \cdot H_2O$	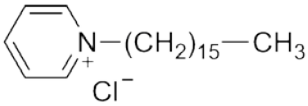
Benzyl dimethyl hexadecyl ammonium chloride (BDHAC)	$C_{25}H_{46}NCl$	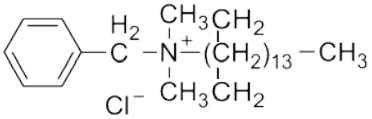
2-mercaptopyrimidine (MPY)	$C_4H_4N_2S$	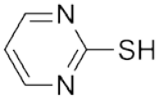

The composition of carbon steel was (wt %), C (0.37%), Mn (0.80%), Si (0.28%), P (0.01%), S (0.001%), Cr (0.08%), Ni (0.01%), Mo (0.004%), Sn (0.004%), Al (0.01%) and Fe (balance). Carbon steel samples were embedded in epoxy resin and the exposed surface area was 0.196 cm^2. Prior to the tests, samples were ground up

to 1200 grit SiC paper, washed in ethanol and ultra-pure water and dried in nitrogen gas.

Silica sand (SiO_2; Sigma-Aldrich) with the mean particle size of 303 μm and specific surface area of 0.062 $m^2\ g^{-1}$ was used as a deposit.

A three-electrode glass cell setup [11] was used to perform the electrochemical measurements (using a Gill Potentiostat, ACM Instruments, UK) at steels with and without sand-deposit.

Linear polarization resistance (LPR) measurements were conducted for 24 h in the potential range of ±0.01 V in respect to the open circuit potential (OCP). Potentiodynamic polarization measurements were conducted at steels stabilized at OCP for 24 h in the potential range of ±0.25 V vs. OCP at 10 mV min^{-1} sweep rate.

Cyclic voltammetry measurements (using a Solartron 1287 Potentiostat, Solartron Analytical, UK) were performed at 10 mV s^{-1} sweep rate after the steels were left to stabilise at OCP for 24 h. Electrochemical pre-treatment procedure was applied to the steels before the cyclic voltammetry measurements to ensure the same starting conditions of the surfaces and is described elsewhere [11].

Surface morphology of the steels after the cyclic voltammetry measurements, pit depth and root mean square surface roughness parameter (R_q) were analysed using visible-light microscopy (Alicona Infinite Focus Instruments, Austria).

Weight loss measurements were conducted at steels (exposed surface area 2.5 cm^2) after immersion for a period of 15 days. After the test period, the corrosion rates were determined as per the ASTM standard G1 [12].

Immersion tests were performed for a period of 29 days and the sample surfaces after immersion were examined using the Zeiss (Neon) field emission scanning electron microscopy (FESEM). Samples for FESEM analysis were not chemically cleaned to ensure that the surface remained unchanged.

3. Results and discussion

3.1 Linear polarization resistance measurements

The variation in general corrosion rates of uninhibited and inhibited steels with and without sand-deposit is shown in Fig.1. Table 2 presents the corrosion rates at 24 h test period.

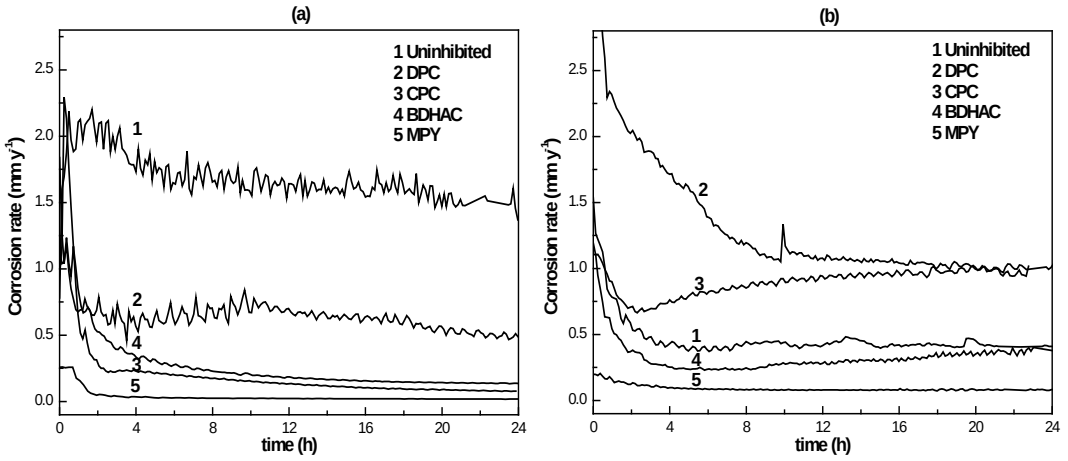

Fig. 1. Corrosion rates of steels in CO_2-saturated uninhibited and inhibited test solutions for 24 h at 30 °C, a) without sand-deposit and b) with sand-deposit, obtained from LPR measurements.

Table 2. Corrosion rates obtained from LPR measurements at 24 h.

Corrosion rate (mm y^{-1})	Uninhibited	DPC	CPC	BDHAC	MPY
Without sand-deposit	1.53	0.47	0.08	0.11	0.01
With sand-deposit	0.44	1.01	1.03	0.37	0.08

At steels without sand-deposit (Fig. 1a), the corrosion rate under uninhibited condition was high due to the dissolution of steel in the corrosive test environment. With the application of CPC, BDHAC and MPY, the corrosion rates decreased below 0.11 mm y^{-1} showing that these compounds sufficiently inhibited corrosion processes. In the presence of DPC, the corrosion rate remained relatively high (0.47 mm y^{-1}) compared to the rest of the inhibitors.

At steels with sand-deposit (Fig. 1b), the corrosion rate under uninhibited condition was lower than that observed at the steel without sand-deposit. This is attributed to the sand reducing the active surface area on steel and/or act as a diffusion barrier for the corrosive ions in the test solution [9]. With the application of MPY, considerable decrease in the corrosion rate was observed, irrespective of the deposit presence. However, with inhibitors DPC and CPC, the corrosion rates increased with respect to the uninhibited condition. In the presence of inhibitor BDHAC, the corrosion rate was similar to the uninhibited condition.

It has been reported that the cationic head group of the quaternary ammonium compounds have a strong affinity for sand-deposits, while sulphur-containing compounds have lesser affinity [6]. This is consistent with the observation in Fig. 1a in the present study, confirming that the sulphur-containing inhibitor MPY effectively inhibits general corrosion of the sand-deposited steel. The reduced inhibition performance of the quaternary ammonium inhibitors CPC, DPC and BDHAC compared to MPY is ascribable to their concentration loss to sand-deposits. The inhibition performance of quaternary ammonium compounds was in the sequence BDHAC > CPC > DPC. The better performance exhibited by BDHAC can be attributed to its chemical structure with a long alkyl chain. In the homologous series of quaternary ammonium compounds, an increase in chain length has been related to better surface coverage and corrosion inhibition [13].

Weight loss measurements were conducted at steels with and without sand-deposit to verify the inhibitor performance determined by the LPR measurements. The corrosion rates obtained from weight loss tests conducted for 15 days are shown in Table 3. The presence of inhibitor MPY results in very low corrosion rates of both steels with and without sand-deposit compared to the uninhibited condition. With the inhibitors DPC, CPC and BDHAC, the corrosion rates of steels with sand-deposit were higher than the steels without sand. This shows that the corrosion rate trend from weight-loss measurements is in good agreement with the LPR data.

Table 3. Corrosion rates obtained from weight loss measurements after 15 days.

Corrosion rate ($mm\ y^{-1}$)	Uninhibited	DPC	CPC	BDHAC	MPY
Without sand-deposit	0.88	0.08	0.06	0.06	0.02
With sand-deposit	0.52	0.26	0.29	0.21	0.02

3.2 Potentiodynamic polarization measurements

Potentiodynamic polarization curves recorded from steels with and without sand-deposit after 24 h immersion (at OCP) in uninhibited and inhibited test solutions are shown in Fig. 2. The electrochemical parameters calculated from the potentiodyanamic curves (Fig. 2) are summarized in Table 4.

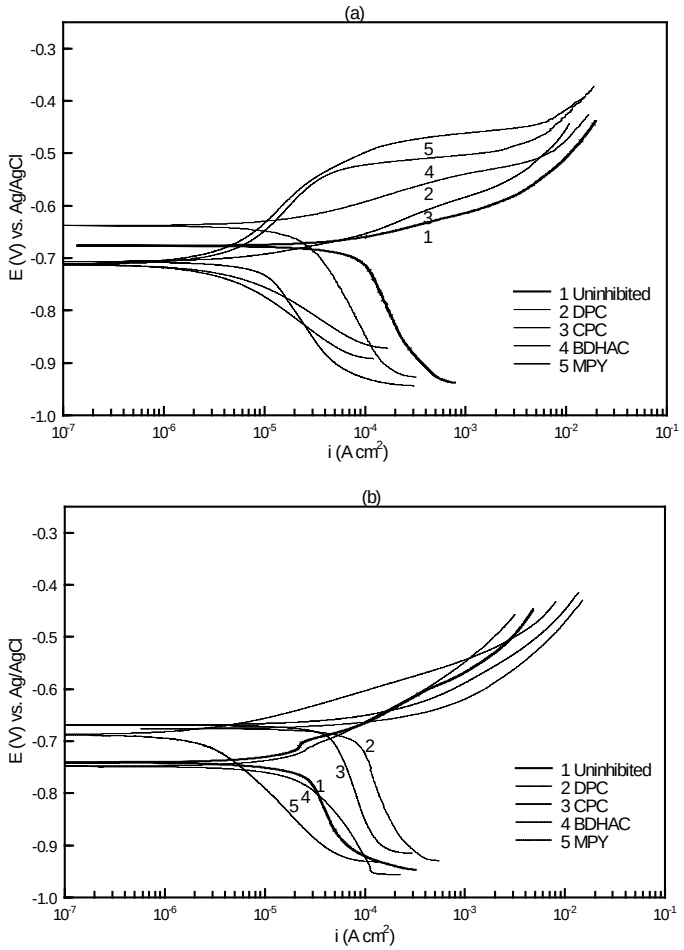

Fig. 2. Potentiodynamic curves of steels in CO_2-saturated uninhibited and inhibited test solutions after 24 h immersion at OCP at 30 °C, a) without sand-deposit and b) with sand-deposit.

Table 4. Electrochemical parameters of carbon steel surfaces derived from potentiodynamic polarization measurements in Fig. 2.

(a) Without sand-deposit	E_{corr} V vs. Ag/AgCl	ba mV dec^{-1}	-bc mV dec^{-1}	i_{corr} µA cm^{-2}	ν_{cor} mm y^{-1}	θ
Uninhibited	-0.676	62	475	100.50	1.13	-
DPC	-0.614	44	354	22.20	0.25	0.69
CPC	-0.711	66	570	14.70	0.16	0.72
BDHAC	-0.708	126	172	3.75	0.04	0.92
MPY	-0.712	161	104	3.54	0.03	0.98
(b) With sand-deposit	E_{corr} V vs. Ag/AgCl	ba mV dec^{-1}	-bc mV dec^{-1}	i_{corr} µA cm^{-2}	ν_{cor} mm y^{-1}	θ
Uninhibited	-0.740	126	481	30.36	0.34	-
DPC	-0.675	55	446	92.78	1.04	0.33
CPC	-0.684	64	561	49.36	0.56	0.38
BDHAC	-0.748	141	329	31.82	0.35	0.75
MPY	-0.687	58	243	3.76	0.04	0.94

At steels without sand-deposit (Fig. 2a), the corrosion current densities (i_{corr}) decreased in the presence of the inhibitors, with respect to the uninhibited condition. The sequence of the corrosion protection trend was MPY > BDHAC > CPC > DPC, similar to that obtained from the LPR measurements in Fig. 1.

At steels with sand-deposit (Fig. 2b), the corrosion current densities increased in the presence of inhibitors DPC, CPC and BDHAC with respect to the uninhibited condition. Among these three inhibitors, BDHAC possessed higher inhibition effect, same as determined from the LPR measurements. This suggests that the long alkyl chain of BDHAC may be responsible for its improved inhibition action. In the presence of inhibitor MPY, the corrosion current density decreased considerably compared to the other three inhibitors. The observed decrease in both cathodic and anodic current densities suggests that MPY inhibits both the cathodic and anodic corrosion processes.

From the corrosion current densities of uninhibited and inhibited steels, the surface coverage (θ) by the inhibitor was determined (Table 4). It can be seen that the surface coverage of the steels without sand-deposit by all four inhibitors is higher compared to the sand-deposited steels. At steels with sand-deposit, the surface coverage by MPY is the highest and for the quaternary ammonium inhibitors surface coverage increases with increase in alkyl chain length (BDHAC > CPC > DPC). This implies that the amount of quaternary ammonium inhibitors that reached the steel surface through the deposit layer was insufficient and can be related to the adsorption loss to the sand-deposits. Hence they afford less corrosion protection to the steel surface.

3.3 Field emission scanning electron microscopy (FESEM) analysis

The representative FESEM images of steels with and without sand-deposit, after 29 days immersion in uninhibited and inhibited test solutions are shown in Fig. 3.

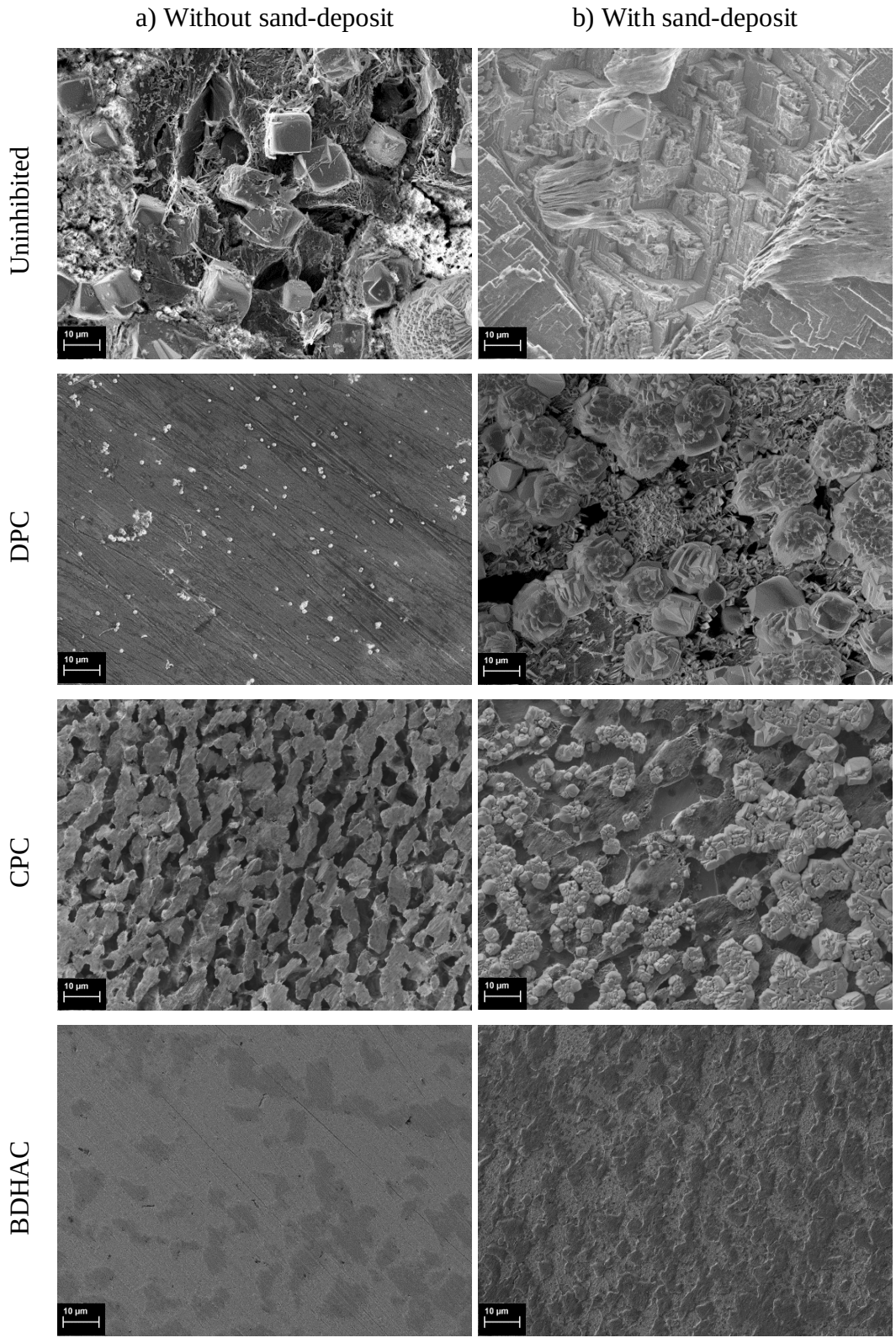
a) Without sand-deposit
b) With sand-deposit
Uninhibited
DPC
CPC
BDHAC
10 µm

MPY

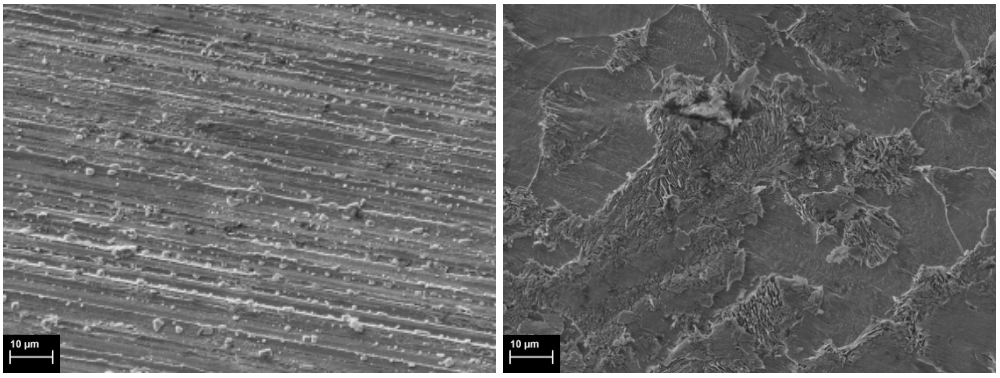

Fig. 3. FESEM images of steels in CO_2-saturated uninhibited and inhibited test solutions after 29 days immersion at 30 °C, a) without sand-deposit and b) with sand-deposit.

Dissolved surface morphology due to corrosion attack was observed under uninhibited conditions at both sand-free (Fig. 3a) and sand-deposited steels (Fig. 3b), with the corrosion products visible at the steel surface without sand-deposit.

At steels without sand-deposit (Fig. 3a), the inhibitors DPC, BDHAC and MPY offer good corrosion protection as seen from the grinding marks still visible at the inhibited steels. However, the CPC-inhibited steel shows a homogenously corroded surface indicating that CPC did not inhibit the steel to the same level as the other three compounds tested.

At steels with sand-deposit (Fig. 3b), a more-corroded surface structure compared to the steels without sand can be observed in the presence of all four inhibitors. This suggests that the inhibitor adsorption at steel beneath sand was hindered by the deposit layer and/or the adsorbed inhibitor film was less protective than that formed at steels without sand. The CPC and DPC-inhibited steels were corroded to a greater extent and corrosion products were visible at the surfaces. In contrast, the BDHAC and MPY-inhibited steels showed minimal general corrosion attack with preferential α-Fe dissolution leaving behind the iron carbide (Fe_3C) phase of the original steel. Accumulation of Fe_3C on the steel surface resulting in a decrease in corrosion rate due to physically restricted access of the corrosive ions to the steel surface has been reported for ferritic-pearlitic steels [14]. However, enhanced corrosion due to galvanic coupling between Fe_3C and the adjacent steel surface has also been shown [15].

3.4 Localized corrosion susceptibility

3.4.1 Cyclic voltammetry measurements

The cyclic voltammetry curves of steels with and without sand-deposit in uninhibited and inhibited test solutions are shown in Fig. 4. The curve from DPC-inhibited steel is displayed as a representative of the three quaternary ammonium compounds. The cyclic voltammetry curves from the other two quaternary ammonium compounds (CPC and BDHAC) showed similar E-i response in terms of localized corrosion evaluation to that obtained from the DPC-inhibited steels.

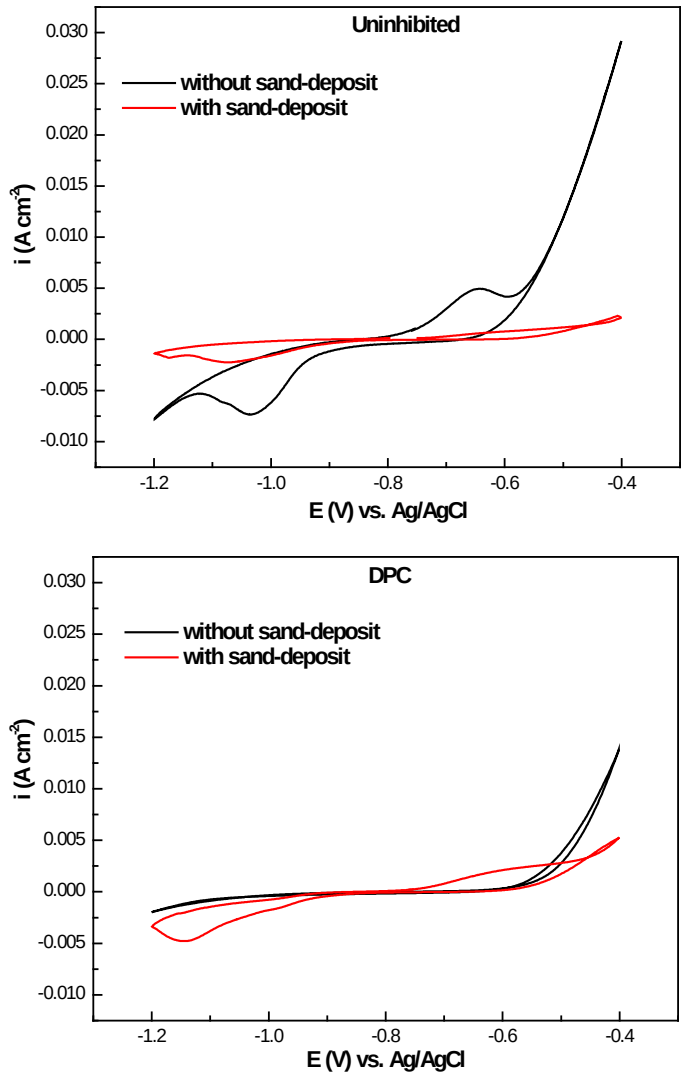

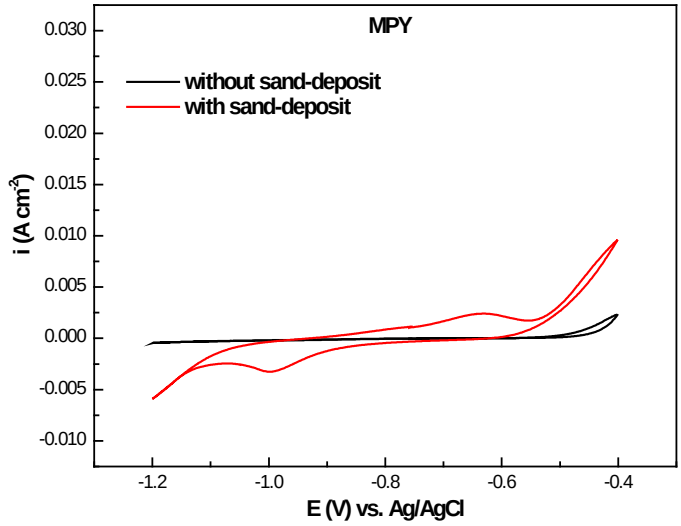

Fig. 4. Cyclic voltammetry curves of steels in CO_2-saturated uninhibited and inhibited test solutions recorded after 24 h immersion at OCP at 30 °C.

At steels without sand-deposit under uninhibited conditions, the electrode behaviour is typical of uniform corrosion process with the formation of corrosion products at the surface [7]. In the presence of inhibitors, the oxidation and the reduction current peaks diminished compared to the uninhibited condition. This indicates the suppression of corrosion reactions by the inhibitor film formed at the steel surface. Among the tested compounds, the lowest anodic current density was observed for the MPY-inhibited steel. This shows that the film formed by MPY has a more compact structure than the rest of the inhibitors, hence is more protective.

At steels with sand-deposit, the uninhibited surface revealed a positive hysteresis loop where the anodic current density is greater during the reverse scan than that observed in the forward scan. A positive hysteresis loop indicates localized attack at the surface [16]. However, no hysteresis loop was observed at the MPY-inhibited steel in the reverse scan. This indicates that localized corrosion does not proceed at the steel surface inhibited with MPY, irrespective of the presence of sand-deposits.

In contrast to MPY, a positive hysteresis loop was observed in the reverse scan of sand-deposited steels inhibited with all three quaternary ammonium compounds indicating localized corrosion and formation of pits. This can be attributed to the presence of sand-deposit altering the inhibitor film formation and/or reducing the film repassivation. The repassivation potential (E_r) represents the potential in the reverse scan, below which the pit growth will stop [16]. The more positive E_r, the

less likely it is that localized corrosion will occur. The E_r values from the cyclic voltammetry curves of sand-deposited steels are shown in Table 5. It should be noted that the E_r values are relevant to the measurement parameters and may vary with the applied scan rate. According to the E_r values, the sequence of resistance to localized corrosion offered by the quaternary ammonium compounds is BDHAC ≈ CPC > DPC.

Table 5. Repassivation potential (E_r) from cyclic voltammetry measurements in Fig.4.

Steels with sand-deposit	E_r V vs. Ag/AgCl
Uninhibited	-0.490
DPC	-0.456
CPC	-0.438
BDHAC	-0.437
MPY	-

3.4.2 Visible-light microscopy analysis

The visible-light microscopy images of uninhibited and inhibited steels with and without sand-deposit after the cyclic voltammetry measurements (Fig. 4) are shown in Fig. 5. Similar surface morphology was observed for the three quaternary ammonium compounds tested and only DPC-inhibited surfaces are shown.

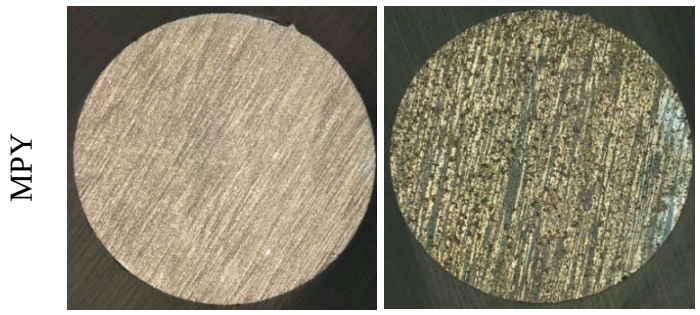

Fig. 5. Visible-light microscopy images of steels after cyclic voltammetry measurements in Fig. 4, a) without sand-deposit and b) with sand-deposit; magnification 5x.

At steels without sand-deposit (Fig. 5a) under uninhibited condition, the surface was covered with a dark film consistent with corrosion product formation. All the inhibited steels without sand-deposit exhibited uniformly corroded surface morphology. The surface roughness R_q of the untreated (non-corroded) steel surface was 1.5 µm. Compared to the non-corroded steel, the R_q of the uninhibited steel increased to 2.6 µm while that of the inhibited steels decreased to an average value of 1.4 µm. This indicates that the inhibitors form a protective film on the surface which mitigates corrosion and in turn reduces the surface roughness. No localized attack could be observed at the steels without sand-deposit both in the presence and absence of inhibitors.

At steels with sand-deposit (Fig. 5b) locally corroded areas (pits) were visible at uninhibited surface as well as surfaces inhibited with all three quaternary ammonium compounds. It is supposed that the presence of sand-deposits restricts the access of inhibitor molecules to the steel, resulting in the difference between the surface sites where the inhibitor molecules formed a film and the sites without inhibitor, thus promoting localized corrosion. The observed localized attack can be ascribed to the deposit layer hindering further transport of dissolved ions into the pits to repassivate. However, no localized corrosion at the sand-deposited steels was detected in the presence of MPY, suggesting that it is an effective inhibitor for carbon steel under sand-deposits.

Among the three quaternary ammonium compounds tested, the most significant localized damage was observed at the steel surface inhibited with DPC. Fig. 6 shows the area with the deepest pit observed on the DPC-inhibited surface and the cross-sectional pit profile. The estimated maximum pit depth values from the sand-

deposited steel surfaces are given in Table 6. It can be seen that the maximum pit depth decreased with increase in alkyl chain length of the inhibitor's structure. This is consistent with the inhibition performance of quaternary ammonium compounds increasing in the sequence BDHAC > CPC > DPC as determined by the electrochemical measurements.

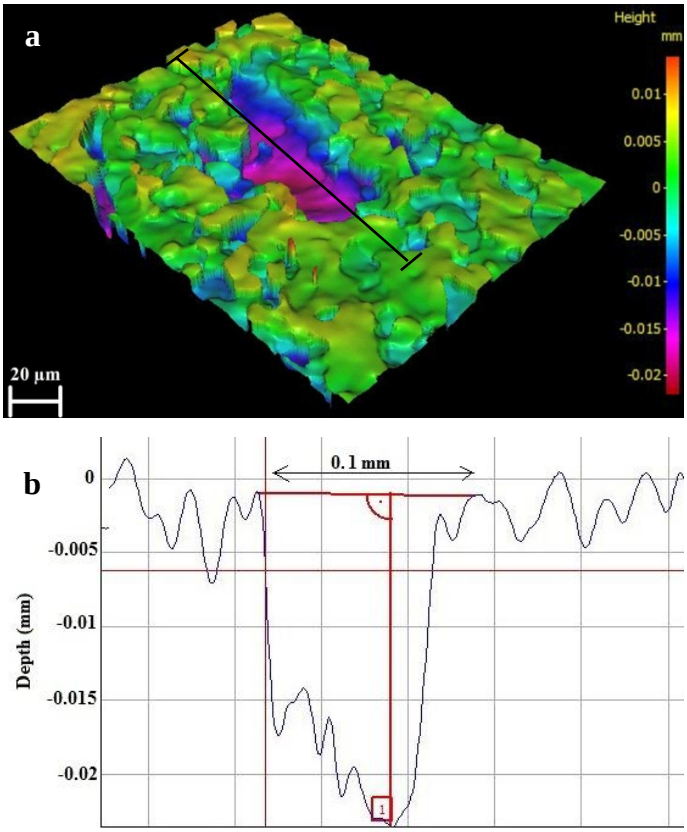

Fig. 6. Visible-light microscopy image of a) area with a pit at the DPC-inhibited sand-deposited steel surface; and b) pit depth profile.

Table 6. Estimated maximum pit depth at steel surfaces from visible-light microscopy analysis.

Steels with sand-deposit	Maximum pit depth µm
Uninhibited	13.2
DPC	22.5
CPC	15.3
BDHAC	11.9
MPY	-

Conclusions

CO_2 corrosion inhibitors, a sulphur-containing compound (2-mercaptorpyrimidine, MPY) and three quaternary ammonium compounds were assessed for their performance to mitigate both general and localized corrosion at the sand-deposited carbon steel surfaces.

The effectiveness of a corrosion inhibitor at sand-deposited steels was related to its chemical structure and the extent of surface coverage by the inhibitor. MPY was found to effectively inhibit the general and localized corrosion of steels, regardless of the presence of the sand-deposit. The inhibition performance of the quaternary ammonium compounds at the sand-deposited steels was found to increase with increasing alkyl-chain length in the inhibitor's structure. Localized corrosion proceeded at the sand-deposited carbon steels inhibited with all quaternary ammonium compounds tested, but the susceptibility to the localized attack decreased with increasing alkyl-chain length.

The results contribute to the understanding of the inhibitor selection for under-deposit corrosion and show that corrosion at sand-deposited steels can be minimized by using an appropriate inhibitor.

References

[1] M.M. Salama, Influence of sand production on design and operations of piping systems, Corrosion 00, NACE International, paper no. 80 (2000).

[2] W.H. Durnie, M.A. Gough, J.A.M. de Reus, Development of corrosion inhibitors to address under deposit corrosion in oil and gas production systems, Corrosion 05, NACE International, paper no. 290 (2005).

[3] J.A.M. de Reus, E.L.J.A. Hendriksen, M.E. Wilms, Y.N. Al-Habsi, W.H. Durnie, M.A. Gough, Test methodologies and field verification of corrosion inhibitors to address under deposit corrosion in oil and gas production systems, Corrosion 05, NACE International, paper no. 288 (2005).

[4] A. Pedersen, K. Bilkova, E. Gulbrandsen, J. Kvarekval, CO_2 corrosion inhibitor performance in the presence of solids: Test method development, Corrosion 08, NACE International, paper no. 632 (2008).

[5] K. Lepková, R. Gubner, Development of standard test method for investigation of under-deposit corrosion in carbon dioxide environment and its application in oil and gas industry, Corrosion 10, NACE International, paper no. 331 (2010).

[6] V. Pandarinathan, K. Lepková, S.I. Bailey, R. Gubner, Evaluation of corrosion inhibition at sand-deposited carbon steel in CO_2-saturated brine, Corros. Sci. 72 (2013) 108-117.

[7] V. Pandarinathan, K. Lepková, S.I. Bailey, R. Gubner, Impact of mineral deposits on CO_2 corrosion of carbon steel, Corrosion 13, NACE International, paper no. 2579 (2013).

[8] J. Han, Y. Yang, B. Brown, S. Nesic, Electrochemical investigation of localized CO_2 corrosion on mild steel, Corrosion 07, NACE International, paper no. 323 (2007).

[9] V. Pandarinathan, K. Lepková, S.I. Bailey, R. Gubner, Inhibition of under-deposit corrosion of carbon steel by thiobenzamide, J. Electrochem. Soc. 160 (9) (2013) C432-C440.

[10] J. Huang, B. Brown, S. Nesic, Localized corrosion of mild steel under silica deposits in inhibited aqueous CO_2 solutions, Corrosion 13, NACE International, paper no. 2144 (2013).

[11] V. Pandarinathan, K. Lepková, R. Gubner, Inhibition of CO_2 corrosion of 1030 carbon steel beneath sand-deposits, Corrosion 11, NACE International, paper no. 261 (2011).

[12] ASTM G1, Standard Practice for Preparing, Cleaning, and Evaluating Corrosion Test Specimens, ASTM International (2011).

[13] D. Schweinsberg, V. Ashworth, The inhibition of the corrosion of pure iron in 0.5 M sulphuric acid by n-alkyl quaternary ammonium iodides, Corros. Sci. 28 (1988) 539-545.

[14] R. Jasinski, Corrosion of N80-type steel by CO_2/water mixtures, Corrosion, (1987) 214–218.

[15] J.L. Crolet, N. Thevenot, S. Nesic, Role of conductive corrosion products in the protectiveness of corrosion layers, Corrosion, 54 (3) (1998) 194-203.

[16] J. Tousek, Theoretical aspects of the localized corrosion of metals, Trans. Tech Publications, 1985.

Appendix 2

V. Pandarinathan, K. Lepková, T. Becker and R. Gubner, *In-situ* electrochemical AFM study of CO_2 corrosion of carbon steel, CORSYM 13, NACE International and Gateway India Section, paper no. 38, Chennai, TN (2013)

Original Reprint of the Publication

In-situ electrochemical AFM study of CO_2 corrosion of carbon steel

Vedapriya Pandarinathan[1], Kateřina Lepková[1], Thomas Becker[2] and Rolf Gubner[1]

[1]Corrosion Centre for Education, Research and Technology

[2]Nanochemistry Research Institute

Department of Chemistry

Curtin University

Perth, Western Australia

Corresponding author e-mail: v.pandarinathan@curtin.edu.au

Abstract

CO_2 corrosion of carbon steel pipelines is a universal problem faced by the oil and gas industry and numerous investigations have been carried out to understand the corrosion process in order to develop effective inhibition measures.

This study presents the application of *in-situ* electrochemical atomic force microscopy (ECAFM) to examine the CO_2 corrosion process at carbon steel surface exposed to pH-stabilized sodium chloride solution at 60 °C. The experiments were conducted using temperature-controlled liquid-cell in a CO_2-saturated environment that resembled the field conditions.

The ECAFM technique allowed the simultaneous determination of the corrosion rates and direct observation of the steel-solution interface with molecular-level precision. The complimentary scanning electron microscopy (SEM) and energy dispersive spectroscopy (EDS) investigations of the corroded surface confirmed that iron carbonate ($FeCO_3$) forms as the main corrosion product.

The results demonstrate that the ECAFM is applicable to real-time monitoring of the corroding steel surfaces and thus improves the understanding of the corrosion process.

***Keywords*:** carbon dioxide, carbon steel, corrosion products, electrochemical atomic force microscopy

1. INTRODUCTION

CO_2 corrosion of carbon steel pipelines is one of the major corrosion problems faced by oil and gas industry[1]. Depending upon the operating conditions, the corrosion process and the nature of corrosion products formed at the steel surfaces varies substantially[2,3]. Hence, it is essential to characterize the steel surface in order to understand the severity of a corrosive environment and in turn device appropriate control measures.

Many of the techniques widely used to investigate corroded metal surfaces are *ex-situ* methods i.e. only the surface structure before and after exposure to corrosive environment can be examined. Whereas, *in-situ* analysis methods allow for the direct observation of the corroding metal-solution interface during the corrosion process.

The present study describes the application of *in-situ* electrochemical atomic force microscopy (ECAFM), which is a combination of electrochemical and atomic force microscopy (AFM) techniques, to evaluate the corrosion of carbon steel surface in CO_2 environment.

The AFM is one of the scanning probe microscopy techniques that operate by scanning an extremely sensitive probe (containing a sharp tip at the end of a cantilever) across the substrate surface under investigation[4]. The forces acting between the tip and the substrate are measured as the cantilever deflects according to the changes in surface topography. The cantilever displacement is detected via the beam deflection method, where a laser is focussed onto the back of the cantilever and reflected onto a photo detector. During scanning, the cantilever deflection and thus the contact force between probe and sample is maintained constant by the electronic feedback of the system and a three-dimensional surface profile of the substrate is obtained. Essentially, the working principle of *in-situ* AFM is same as that of *ex-situ* AFM, except that the scanning of substrate immersed in the test electrolyte is conducted directly. The benefit of *in-situ* AFM is that it can be performed in the desired environment such as carbon-dioxide media and at controlled temperatures resembling the actual field conditions. There is no requirement for the sample to be transferred between the test media and the AFM chamber for surface analysis.

In this study, the surface of 1030 carbon steel exposed to pH-stabilized sodium chloride solution at 60 °C has been investigated *in-situ* using the ECAFM technique. The objective is to demonstrate the applicability of the ECAFM technique to monitor the corrosion process of carbon steel surface in real-time.

2. EXPERIMENTAL

2.1 Test materials and apparatus

The experimental conditions are presented in Table 1. The 0.5 M brine consisted of 3% sodium chloride (NaCl; Ajax Finechem, analytical reagent, 99.9%) and 0.01% sodium hydrogen carbonate ($NaHCO_3$; Merck, 99.5%) prepared in ultra-pure water (resistivity 18.2 MΩ·cm) and with 30 mg/L of ferrous ions added as iron salt. The test solution was saturated with CO_2 and pH stabilized to 8 using a concentrated amine.

Table 1 Test conditions

Material	1030 carbon steel
Test solution	0.5 M brine
pH	8
Temperature	60 °C
Saturation gas	CO_2 (1 bar)

Figure 1a shows the *in-situ* ECAFM experimental arrangement and the three electrode setup mounted on the standard AFM sample plate is shown in Figure 1b.

a)

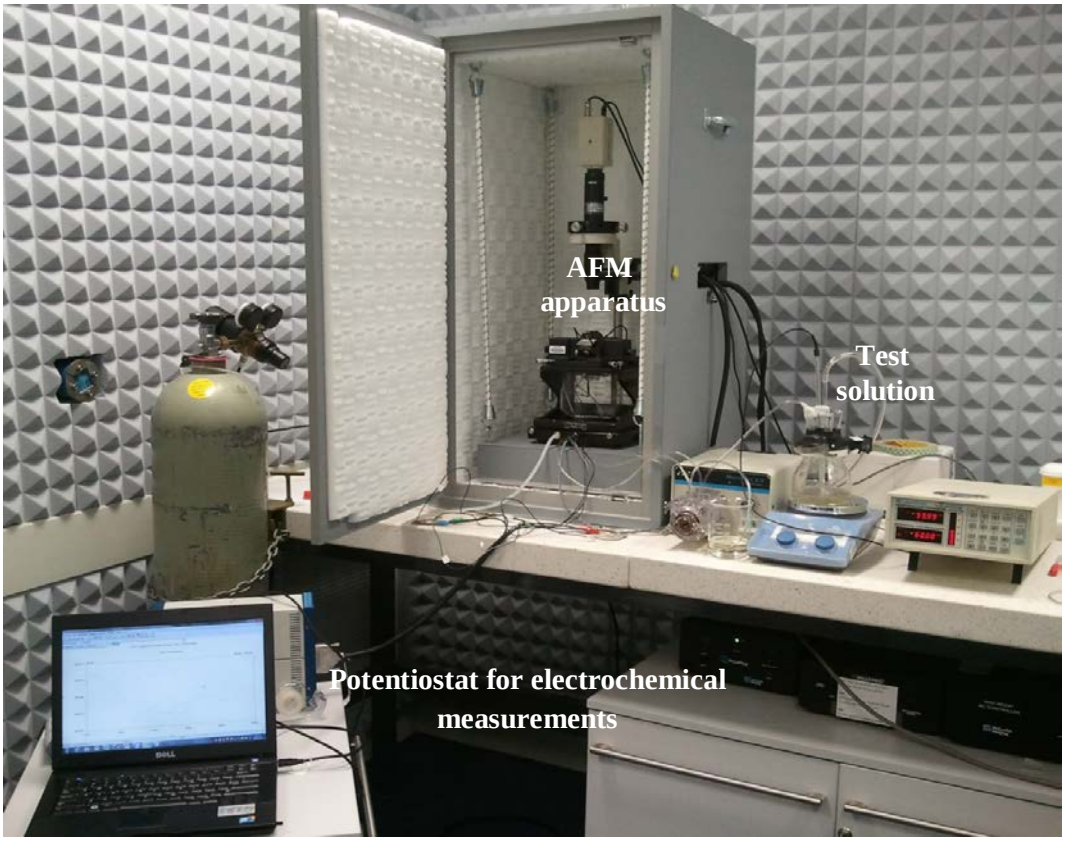

b)

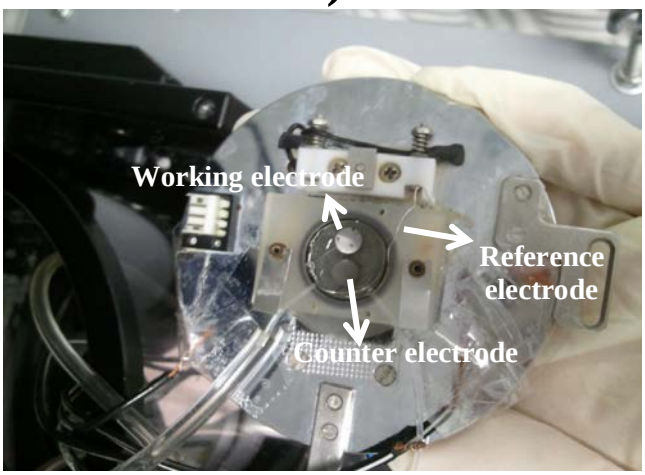

Figure 1 a) *in-situ* ECAFM experimental arrangement b) sample mounted on the AFM sample plate with heating stage and liquid cell

The 1030 carbon steel rods were used as working and counter electrodes and embedded in epoxy resin with the electrical connections drawn using thin copper wires. The Pt wire was used as pseudo-reference electrode. The surface area of the working electrode was 0.196 cm^2 and it was polished to < 1 µm using diamond suspension (Struers TegraPol). The polished sample was ultrasonically cleaned, rinsed with ultra-pure water and dried in nitrogen gas prior to analysis. The Pt

pseudo-reference (connected through the sample stage plate) was wound circularly and positioned in close proximity to the sample surface without any direct contact.

2.2 Preliminary electrochemical measurements

The Linear polarisation resistance (LPR) technique was applied to monitor the corrosion rates using ACM Gill potentiostat (ACM instruments, UK) in the potential range of ±10 mV in respect to open circuit potential (OCP), at a scan rate of 0.1667 mV/s and the detailed test procedure is described elsewhere[5].

2.3 In-situ ECAFM measurements

In the ECAFM experiments, the sequence of consecutive AFM images from a 10x10 µm area of the steel surface were recorded simultaneously with the potential of the surface being monitored using a potentiostat. AFM analysis was performed with a silicon nitride contact mode probe with a spring constant of 0.3 N/m (type DNP, Bruker) using an Agilent Picoplus Scanning Probe Microscope system (Agilent Technologies, USA) operating in contact mode. The temperature of the liquid cell with heating stage was maintained at 60 °C using the autotuning temperature controller of the SPM system (Lakeshore, USA). The test solution was circulated through the liquid cell at a constant flow rate during the experiment. Electrochemical measurements were conducted at ± 10 mV vs. OCP at a scan rate of 0.1667 mV/s using Gamry Ref 600 potentiostat (Gamry Instruments, USA). The results presented are from duplicate experiments and local AFM observations at different areas on the sample were also conducted to verify the homogeneity of the surface structure.

2.4 Iron count analysis

The test solution after the ECAFM experiment was analysed to determine the amount of soluble iron with standard FerroVer reagent using the Hach DR 3900 Benchtop Spectrophotometer (measured at 510 nm).

2.5 SEM/EDS surface analysis

The scanning electron microscope (SEM) (Zeiss, Evo) with an energy dispersive x-ray detector (EDS) was used to characterize the sample surface. The corroded steel samples (after ECAFM measurement) were dried in nitrogen and stored under vacuum until the SEM/EDS analysis.

3. RESULTS AND DISCUSSION

3.1 Preliminary electrochemical measurements

Prior to ECAFM tests, electrochemical measurements were conducted to determine the corrosion rates of carbon steel during the corrosion process under the test conditions shown in Table 1. Figure 2 shows the corrosion rates derived from linear polarization resistance (LPR) measurements carried out for 15 h at the carbon steel surface.

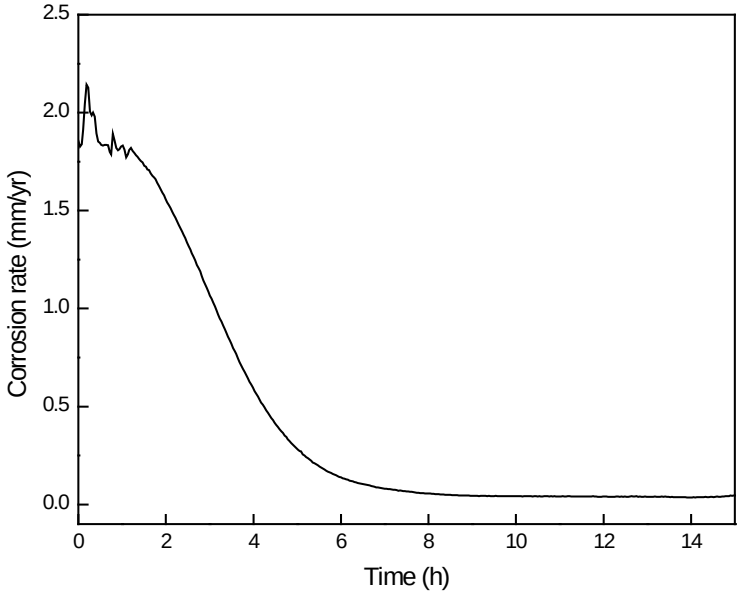

Figure 2 Corrosion rate of carbon steel surface exposed to CO_2 saturated test brine solution at 60 °C, from LPR measurements

As can be seen from Figure 2, the relatively high initial corrosion rate started to decrease gradually for a period of 6 h and stabilized at values less than 0.05 mm/yr at the end of 8 h exposure to the corrosive test solution. The observed trend in corrosion rate can be related to metal dissolution followed by precipitation of corrosion products at the surface when the iron ions exceed the saturation level in the test environment. The iron count at the end of 15 h from the spectrophotometric analysis of the test solution was 2.1 mg/L compared to the 30 mg/L at the beginning of the test. The considerable decrease in iron count and the corresponding low corrosion rates (below 0.05 mm/yr) can be related to the formation of protective iron carbonate film at the steel surface, which efficiently restricts further corrosion reactions. It is consistent with previous studies carried out at elevated temperatures and alkaline pH that have attributed the decrease in corrosion rate to the protective iron carbonate film formation under CO_2 saturated conditions[6,7].

3.2 In-situ ECAFM analysis

The corrosion process proceeding at carbon steel surface exposed to CO_2 saturated test brine solution is illustrated in the sequence of *in-situ* AFM topography images in Figure 3.

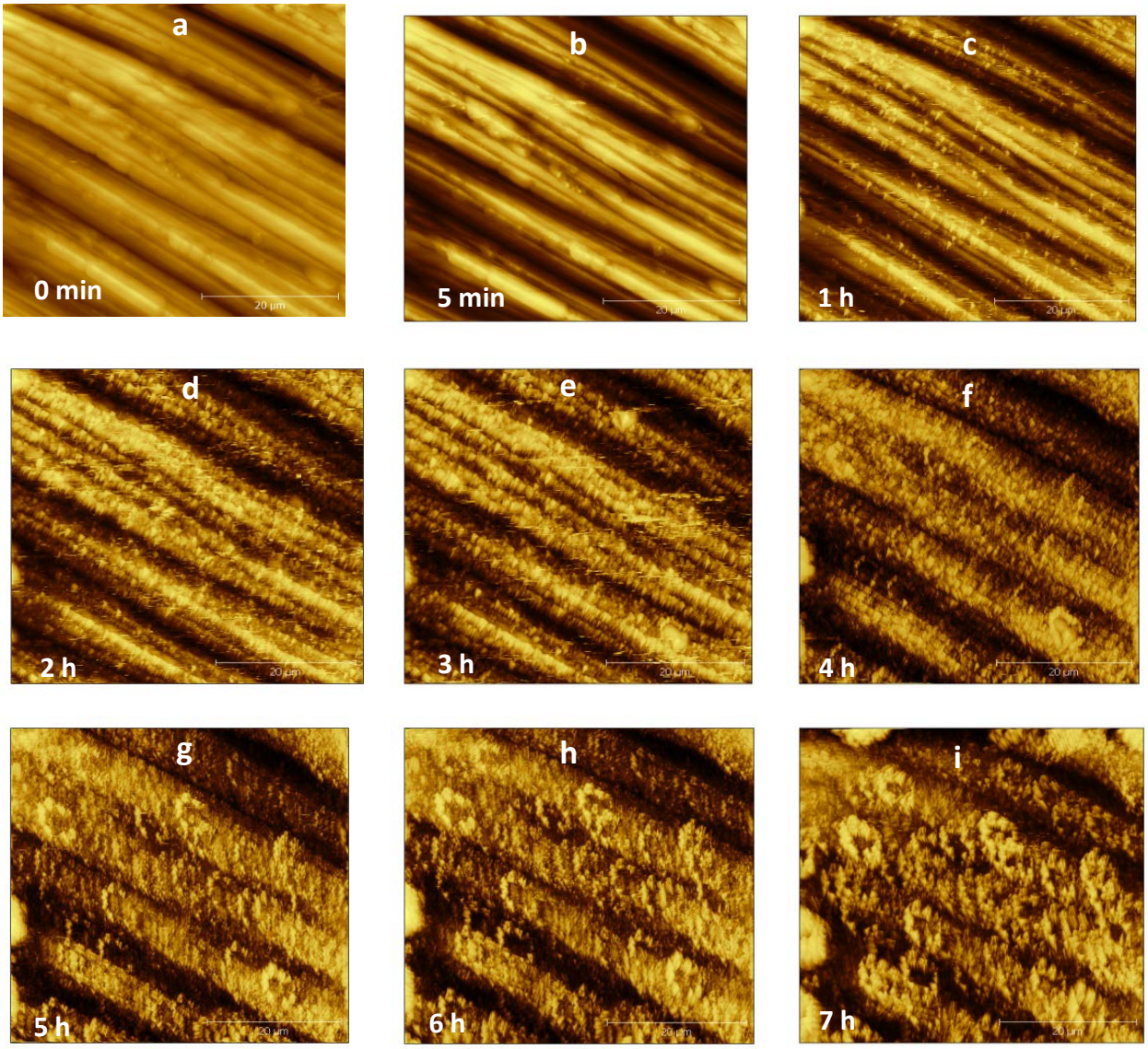

Figure 3 *In-situ* topography images of carbon steel surface exposed to CO_2 saturated test brine solution at 60 °C; (a) bare steel before contact with test solution; (b) to (i) steel after contact with test solution showing corrosion product formation

The image (a) shows the unexposed steel surface before contacting the test solution. After the test solution was introduced, there was no considerable change observed at the surface (image b) during the first hour. Subsequently, surface features began to appear at the image (c) recorded after 1 h exposure to the test solution. The surface

topography changed over time and spiky projections became apparent at the surface which can be associated to the formation of crystalline corrosion product(s). With further increasing exposure time, larger surface structures became visible at the surface, but there was no significant change in the images obtained after 6 h period. The linear polarization resistance (LPR) measurements were run simultaneously with the *in-situ* AFM analysis. The corrosion rates derived from the LPR data are shown in Figure 4.

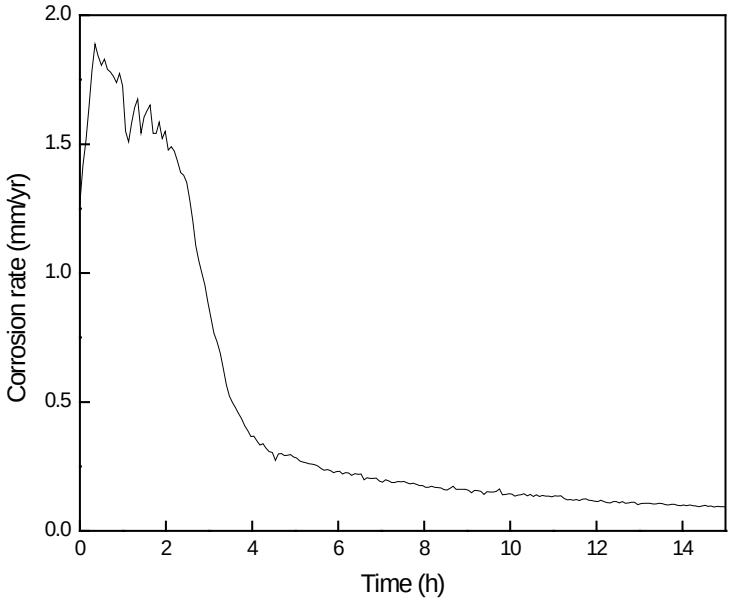

Figure 4 Corrosion rates of carbon steel surface exposed to CO_2 saturated test brine solution at 60 °C, from LPR measurements

The decrease in corrosion rate with time supports the AFM observation and confirms the formation of protective corrosion product film at the steel. Consistent with the preliminary electrochemical measurements (Figure 2), the *in-situ* ECAFM demonstrated the corrosion product formation under the studied conditions. Investigations on iron corrosion products have reported the formation of iron carbonate as major corrosion product under similar test conditions[3].

The amount of iron ions determined spectrophotometrically in the test solution after 15 h test duration was 4.7 mg/L. The decrease in soluble iron count by a factor of 6 from the initial value of 30 mg/L in the test solution can be ascribed to the precipitation of iron carbonate at the steel surface, consequently reduced level of dissolved iron ions in the solution.

3.3 SEM/EDS analysis

Figure 5a shows SEM image of the surface morphology of the corroded steel (after the ECAFM experiment) and Figure 5b shows the EDS spectrum obtained from the corroded steel.

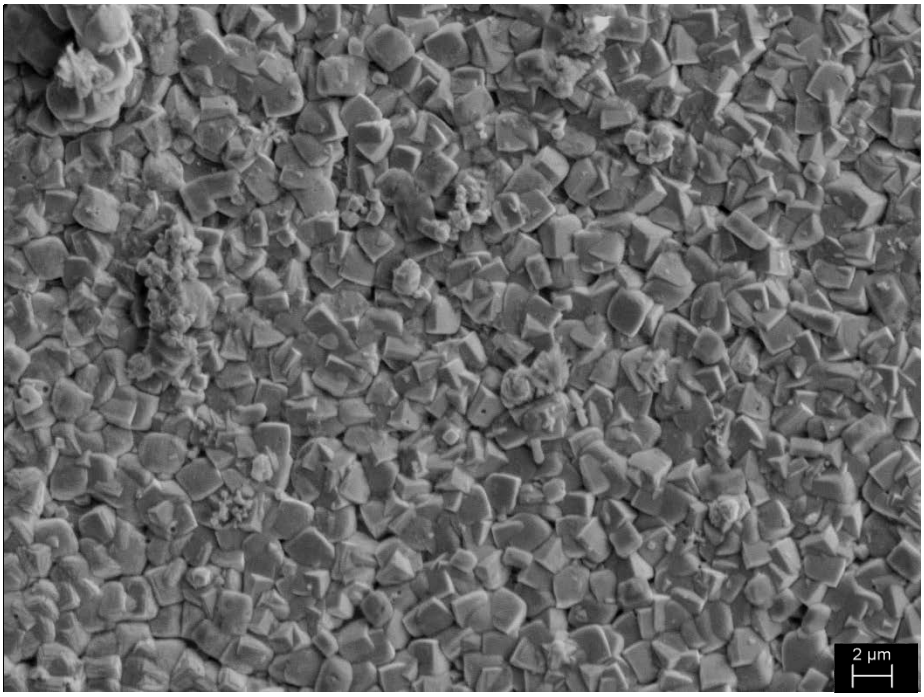

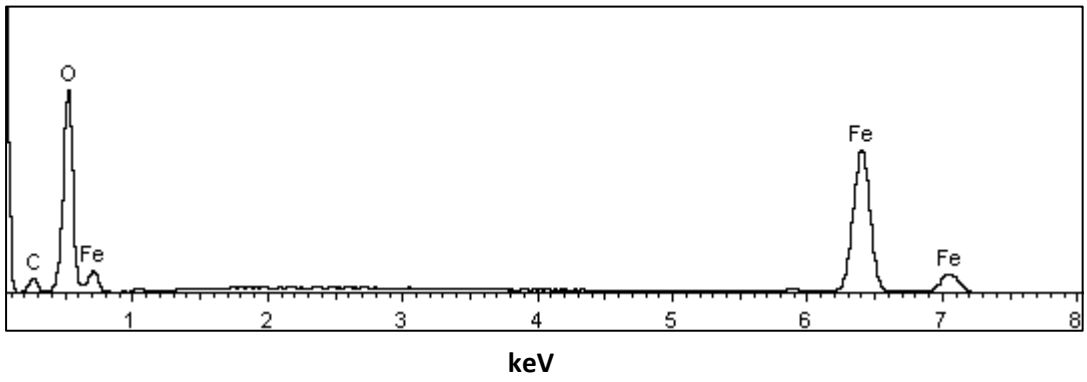

Figure 5 a) Representative SEM image from carbon steel surface exposed to CO_2 saturated test brine solution at 60 °C; b) EDS spectrum from the steel surface

As can be seen from Figure 5, iron carbonate ($FeCO_3$) was identified by the SEM/EDS analysis to be the dominant corrosion product at the steel surface under the studied test conditions. Iron carbonate has been previously reported as the predominant iron corrosion product in high pH CO_2 environment and its formation has been related to the decrease in solubility of iron[8]. However, formation of other

iron complexes as minor corrosion products can also be expected under the CO_2 saturated conditions.

From Figure 5a, it can be seen that the highly crystalline stacks of iron carbonate formed are closely-packed and adherent to the surface. Since the structure of the corrosion product film influences the corrosion process, it can be inferred that the adherent iron carbonate film formed under the studied conditions, hindered the corrosion reactions resulting in the decrease in corrosion rates.

4. SUMMARY

In-situ ECAFM technique was utilized to investigate the 1030 carbon steel surface exposed to pH-stabilized sodium chloride solution under CO_2 saturated conditions at 60 °C, a corrosive test environment closely resembling actual field conditions. The technique enabled the real-time visualization of corrosion product formation at the steel surface and simultaneous evaluation of the corrosion rates. The results showed the topographic changes at the steel surface during the corrosion process, indicating the formation of crystalline corrosion products. The observed decrease in corrosion rates is attributed to the protective nature of the formed surface film. The SEM/EDS characterization was complementary to ECAFM results and iron carbonate was identified as the major corrosion product formed at the steel surface.

The ECAFM technique was found suitable for *in-situ* investigations of the corroding carbon steel surfaces.

ACKNOWLEDGEMENTS

The authors would like to thank Woodside Energy Ltd for the financial support and permission to publish this work. We also acknowledge the support of the Australian and Western Australian Governments, as well as the Western Australian Energy Research Alliance (WAERA). We thank the Centre for Materials Research (CMR) facility at Curtin University for SEM access. One of us (V.P) thanks the Curtin University for the Postgraduate Research Scholarship (CIPRS). K. L. thanks Curtin University for a Curtin Research Fellowship.

REFERENCES

1. M. B. Kermani, A. Morshed, Carbon dioxide corrosion in oil and gas production - A compendium, Corrosion 59(8), 659-683 (2003).
2. G. Schmitt, Fundamental aspects of CO_2 corrosion, Advances in CO_2 corrosion, Corrosion/84, paper no. 10, NACE International, Houston, Texas (1984).
3. K. Videm, A. Dugstad, Corrosion of carbon steel in an aqueous carbon dioxide environment. Part 1: film formation, Materials Performance 28(4), 46–50 (1989).
4. P. Marcus, F. Mansfeld, Analytical methods in corrosion science and engineering, Taylor & Francis Group, (2006).
5. H. J. Butt, B. Cappella, M. Kappl, Force measurements with the atomic force microscope: Technique, interpretation and applications, Surface Science Reports 59, 1–152 (2005).
6. V. Pandarinathan, K. Lepková, R. Gubner, Inhibition of CO_2 corrosion of 1030 carbon steel beneath sand-deposits, Corrosion/11, paper no. 263, NACE International, Houston, Texas (2011).
7. A. Dugstad, Mechanism of protective film formation during CO_2 corrosion of carbon steel, Corrosion/98, paper no. 31, NACE International, San Diego, California (1998).
8. A. Dugstad, M. Seiersten, pH-stabilisation, a reliable method for corrosion control of wet gas pipelines, SPE paper 87560 (2004).

Appendix 3

K. Lepková, W. van Bronswijk, V. Pandarinathan and R. Gubner, Synchrotron infrared microspectroscopy study of the orientation of an organic surfactant on a microscopically rough steel surface, Vibrational spectroscopy, 68, 204-211 (2013)

Original Reprint of the Publication

Vibrational Spectroscopy 68 (2013) 204–211

Contents lists available at ScienceDirect

Vibrational Spectroscopy

journal homepage: www.elsevier.com/locate/vibspec

Synchrotron infrared microspectroscopy study of the orientation of an organic surfactant on a microscopically rough steel surface

Kateřina Lepková *, Wilhelm van Bronswijk, Vedapriya Pandarinathan, Rolf Gubner

Corrosion Centre for Education, Research and Technology, Department of Chemistry, Curtin University, Perth, WA 6845, Australia

ARTICLE INFO

Article history:
Received 3 February 2013
Received in revised form 30 July 2013
Accepted 1 August 2013
Available online 11 August 2013

Keywords:
Infrared microspectroscopy
Synchrotron
Steel
Molecular orientation
Organic surfactant
Corrosion.

ABSTRACT

The performance of organic surfactants as corrosion inhibitors is influenced by the mechanism of adsorption and the resulting molecular orientation on the substrate. The molecular orientation of 1-dodecylpyridinium chloride (DPC) deposited on non-corroded 1030 mild steel and after corrosion in a carbon dioxide environment has been investigated using synchrotron infrared microspectroscopy. DPC mitigates the corrosion process by adsorbing at the steel surface and forming a protective layer.

Infrared spectra analogous to polarized grazing angle spectra were obtained from a microscopically rough surface using a synchrotron source. The appearance of negative and positive absorption bands in the spectra, when using synchrotron radiation, is discussed in terms of the optical system used. The presence of the DPC surfactant at the steel surface is shown by the CH_2 and CH_3 infrared absorption bands of the aliphatic chain of the DPC molecule. The infrared spectra provide direct evidence on the orientation of DPC at the steel substrate. The aliphatic chain of the surfactant is tilted orthogonally, but not perpendicular to the substrate plane. The absence of significant absorption bands characteristic of the pyridinium ring of DPC indicates its orientation parallel to the substrate plane, and an adsorption mechanism involving π-bonding with the steel.

This study demonstrates the applicability of synchrotron infrared microspectroscopy to the investigations of thin organic films on microscopically rough steel surfaces, and can facilitate further investigations of thin films on metallic surfaces and monolayer studies in general.

1. Introduction

Organic surfactants which adsorb on a variety of substrates have been used in numerous applications, such as ore flotation, stabilization of foams and emulsions, wetting control and corrosion inhibition [1,2]. In corrosion inhibition, organic surfactants are used to mitigate corrosion reactions by adsorbing on the metallic substrates and forming a protective layer. The performance of organic surfactants as corrosion inhibitors depends on their bonding and molecular orientation towards the substrate. It has been suggested, for example, that chemisorbed organic surfactants are more persistent than physisorbed organic surfactants, and are therefore preferred as batch-treatment corrosion inhibitors [3].

Reflection-absorption infrared spectroscopy is a suitable technique for determining the molecular orientation of organic compounds on metallic substrates. Previous studies have established that at high angles of incidence thin surface layers exhibit high absorption of infrared radiation that is polarized perpendicular to the reflection plane (metallic substrate). In this arrangement, with application of the metal surface selection rule, only molecular vibrations perpendicular to the reflection plane absorb the infrared light and thus appear in the spectra. Since the recorded absorption bands are related to the different parts of the organic compound, the molecular orientation at the surface can be determined [4–6].

Detailed information on the nature of the surface layers is required in order to elucidate the exact mechanisms of the corrosion inhibition. However, when examining organic layers at corroded metallic substrates, determining the absorption of infrared radiation is often complicated due to the topography of the corrosion-roughened surface, and the limited thickness and heterogeneity of the surface layer.

To test the applicability of synchrotron-sourced infrared microspectroscopy to analyze such complex surfaces, we have studied a carbon steel surface that had been immersed in a 1-dodecylpyridinium chloride (DPC) solutions in nitrogen or carbon dioxide saturated media. Many oil and gas systems operate in carbon dioxide environments where corrosion is caused by carbonic acid. Pyridinium-based surfactant molecules with a long alkyl chain, such as DPC, are used as oil-well corrosion inhibitors [3], and pyridinium compounds efficiently inhibit corrosion reactions

* Corresponding author at: Department of Chemistry, Curtin University, G.P.O. Box U1987, Perth, WA 6845, Australia. Tel.: +61 892667319, fax: +61 892662300.
E-mail address: k.lepkova@curtin.edu.au (K. Lepková).

0924-2031/$ – see front matter © 2013 Elsevier B.V. All rights reserved.
http://dx.doi.org/10.1016/j.vibspec.2013.08.002

at iron surfaces in acidic media [7]. It has been proposed that DPC adsorbs at a metal surface through the aromatic ring, with the hydrophobic aliphatic chain oriented into the solution [3,8]. However, no direct evidence of the molecular orientation of DPC has been presented and the exact mechanism of the DPC adsorption is unknown.

A complementary method for studying the orientation and absorption mechanism of pyridine and pyridinium compounds on surfaces is surface enhanced Raman spectroscopy (SERS). SERS studies of pyridine/pyridinium adsorption at non-modified steel surfaces (iron–carbon alloys with original crystalline structure) have not been performed as the modification of the substrate (surface roughness) is required for quality SER spectra. Furthermore, the SERS technique is not sensitive to π-bonded organic compounds and can only detect pyridinium compounds that are bonded to the substrate through the nitrogen atom [9]. Hence, infrared spectroscopy can provide additional information on the surface orientation of the organic compounds. From SERS data of pyridine and pyridinium compounds adsorbed on iron-deposited silver substrates two different adsorption mechanisms were proposed: (1) coordination bonding between the nitrogen atom of the aromatic ring and the metal (σ-bond) resulting in non-parallel orientation of the aromatic ring at the substrate [10,11], and (2) π-electron interaction between the aromatic ring and the metallic substrate, which results in parallel orientation of the aromatic ring at the substrate. The π-electrostatic interaction can be influenced by the presence of halide ions that pre-adsorb at the surface [10–12]. It has also been proposed that an individual compound can adsorb through both of the mechanisms, depending on the nature of the substrate and the composition of the corrosive solution [12].

In this study, we use a strongly polarized synchrotron source infrared beam and a Cassegrain objective to record infrared spectra without a polarizer in the beam that are equivalent to those obtainable from flat metallic and non-conductor surfaces when a polarizer is used. The data allow the surface orientation of the organic surfactant to be determined. If the pyridinium ring and aliphatic chain of the DPC molecule are oriented non-parallel with respect to the steel surface then both parts of the molecule would interact with infrared radiation. This would be indicative of the σ-bonding of the pyridinium ring at the substrate through the nitrogen atom. On the other hand, parallel orientation of the pyridinium ring to the steel surface would not result in its interaction with infrared radiation. Therefore, the absence of the in-plane ring absorption bands in the infrared spectra would be indicative of π-bonding of the pyridinium ring at the substrate.

2. Materials and methods

2.1. Materials

The carbon steel studied had the following elemental composition (wt%): C 0.37, Mn 0.80, Si 0.28, Cr 0.09, P 0.01, Ni 0.01, Fe balance. Steel samples (20 mm diameter) were ground with SiC paper to 1200 grit and then polished to a surface finish of 1 μm using diamond suspensions. This polishing method consistently results in carbon steel surfaces with average surface roughness (root mean square, R_q) of ~ 0.4 μm, confirmed with visible light microscopy using an Alicona Infinite Focus (Alicona Imaging GmbH, Austria). The polished samples were cleaned with methanol and ultra-pure deionised water and dried with nitrogen prior to immersion in the test solution. The samples were dried with nitrogen after the test and stored under vacuum until further analysis. Care was taken when handling the samples to minimize their exposure to air.

The testing solutions were (1) 500 ppm of 1-dodecylpyridinium chloride hydrate ($C_{17}H_{30}ClN.xH_2O$; Sigma–Aldrich, 98%) in deionised ultra-pure water saturated with nitrogen; and (2) 500 ppm of 1-dodecylpyridinium chloride hydrate ($C_{17}H_{30}ClN.xH_2O$; Sigma–Aldrich, 98%) in brine, consisting of 0.5 M sodium chloride (NaCl; Ajax Finechem, 99.9%) and 1×10^{-3} M sodium hydrogen carbonate ($NaHCO_3$; Merck, 99.5%), saturated with high-purity carbon dioxide (99.99%) before and during the experiments. The chemical structure of the DPC molecule is given in Fig. 1.

Two types of samples are used in this study and differ by the degree of corrosion. The non-corroded samples were prepared by immersion into solution (1) at ambient temperature (20 °C) for 20 min. These conditions were expected to have little effect on the surface properties of the steel, such as roughness and reflectivity. Therefore these samples are referred to as non-corroded for the purpose of this study. The corroded samples were prepared in solution (2) at 60 °C for 24 h, i.e. the corrosion took place in the presence of the inhibitor, as it would in its industrial environment.

The DPC-treated steel samples and untreated (plain) steel, used for a background measurement, were placed into an enclosed compartment surrounding the infrared microscope assembly, which was continuously purged with dry nitrogen. After positioning the sample, the atmosphere inside the compartment was left to stabilize for 30 min. before the infrared analysis. This procedure minimized the amount of water vapour and carbon dioxide appearing in the recorded spectra.

The infrared spectrum of the DPC powder was recorded using Attenuated Total Reflectance and a Perkin-Elmer Spectrum 100 spectrometer. The DPC powder was used as received.

The corroded samples were also analyzed with a Hyperion 3000 microscope with a Focal Plane Array (FPA) detector and conventional infrared source. The aperture size was 100 μm × 100 μm. The untreated (plain) steel was used as a background for the FPA analysis.

2.2. Atomic force microscopy (AFM) measurement and analysis

In situ AFM analysis was carried out using an Agilent Picoplus AFM Multimode apparatus in a soft contact mode. A silicon nitride cantilever (type DNP) with a spring constant of 0.32 Nm^{-1} was used. The samples were mounted on the AFM liquid cell holder and the test solution (1) was continuously recirculated through the cell during the experiment.

2.3. Surface coverage measurement

The coverage of the corroded steel surface with DPC was determined from corrosion rates obtained from linear polarization resistance (LPR) analysis. A standard three-electrode system and solution (2) with and without DPC were used, and the steel samples were polarized in the potential range of ±10 mV vs. open circuit potential in a sweep rate of 0.6 V h^{-1} using a Gill Potentiostat (ACM Instruments, UK). The corrosion rates from the LPR measurements were calculated according to the standard procedure given elsewhere [13].

2.4. Corroded steel roughness measurement

The roughness of the corroded steel surfaces was measured using an Alicona Infinite Focus visible light microscope (Alicona Imaging GmbH, Austria) with 50× magnification objective. A surface roughness parameter R_q (root mean square) was calculated from the surface heights using the Alicona IFM 3.5 software. The samples were briefly exposed to air during the surface roughness

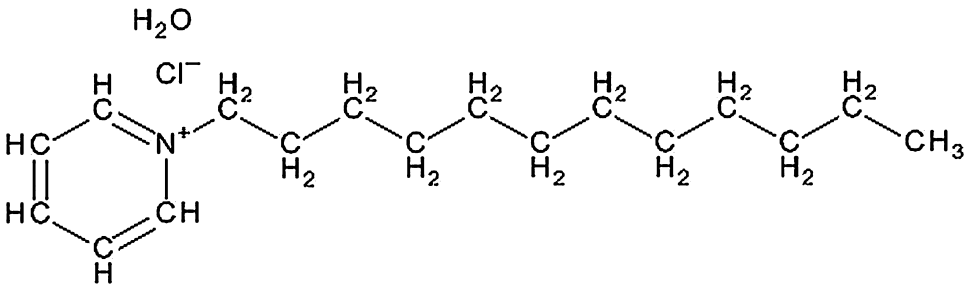

Fig. 1. Chemical structure of 1-dodecylpyridinium chloride hydrate.

measurements, which followed the infrared spectroscopy analysis.

2.5. Synchrotron infrared spectral measurement and analysis

Infrared spectroscopy was performed on the infrared microspectroscopy beamline at the Australian Synchrotron using a Brüker Hyperion 2000 microscope coupled to a Vertex V80v FTIR spectrometer. A Cassegrain objective with 36× magnification was used and the aperture of the microscope was set at 20 μm × 20 μm. Spectra acquisition and processing was performed using Opus 6.5 software (Brüker optics).

The FTIR spectra were recorded in reflectance mode with a resolution of 4 cm^{-1}, using a liquid nitrogen-cooled MCT detector. For each spectrum, 256 scans were collected in the range of 3800–800 cm^{-1}. A total of 256 background scans were collected on untreated (plain) steel of the same elemental composition as the test samples. 256 scans were also collected using a gold mirror to obtain an absorbance spectrum of the untreated steel. The untreated steel and gold mirror were placed in the nitrogen-purged compartment at the same time as the test samples to ensure identical environmental conditions for collection of the background and the sample spectra. The spectra are presented in terms of $-\log(I/I_0)$, where I and I_0 are the absorption intensities in the single channel spectra obtained from the test sample and the untreated steel, respectively.

2.5.1. Optical parameters

The Australian Synchrotron IR microscope beamline uses only the bending magnet radiation. The polarization ellipse of this radiation is not significantly affected by the optical path of the microscope [14]. Infrared spectra were acquired with a predominantly *p*-polarized synchrotron beam (parallel (*p*): perpendicular (*s*) ~4:1), but without a polarizer in the beam. A reverse Cassegrain objective was used and hence the polarized synchrotron infrared beam's incidence angle approaching the surface changes within the hollow cone, which is approximately 30°, i.e. the incident beam will have both a *p* and an *s* component relative to the microscope plane. Infrared spectroscopy with a synchrotron source applied in polarization studies, particularly in transmission mode showed that orientation information could be obtained with the use of the intrinsic synchrotron source and without a polarizer [15,16].

At optically flat metallic surfaces that are reflective (conductors), *p*-polarization has non-zero strength and interacts with vibrations perpendicular to and at the surface, whereas *s*-polarization has zero field strength and does not interact. The intensity of the absorption bands from thin surface films at metallic substrates increases with increasing angle of incidence, with maximum absorbance obtained at a grazing angle of 88° [17]. At low angles of incidence, such as used in this work, the surface enhancement of the adsorbed molecules on the steel surface is not achieved however absorption bands with lower intensity to those recorded at the optimum grazing angles can be observed [17,18]. The position and shape of the absorption bands recorded from thin surface films are expected to be independent of the angle of incidence and sensitive to the substrate orientation on the metal surface [17]. In the case of the pyridinium compound with aliphatic chain (1-dodecylpyridinium chloride) used in this study, only vibrations non-parallel to the steel surface are expected to be detected in the infrared spectra.

For a rough surface, the polarization of the beam and the angle of incidence in relation to a particular surface facet cannot be established. A schematic presentation of the reverse Cassegrain optical path used in this study and applied in analysis of a topographically uneven (corrosion-roughened) steel surface is given in Fig. 2. The angle of incidence will vary due to the local topography of the surface and may be anywhere between 0° and 90°. Therefore, it is reasonable to assume that both polarizations of the beam, parallel (*p*) and perpendicular (*s*) are encountered in the course of the analysis (with multiple measurement points over a large surface area) and that there will be instances where a *p* or *s* component of the polarized beam relative to the surface facet is dominant.

The formation of corrosion products at steel surface and the consequent increased roughness results in decreased reflectivity of the surface. Corroded metallic surfaces are at best semi-reflective and behave as semiconductors or non-conductors in terms of the reflection-absorption spectroscopy. At the semi-reflective and non-conductor surfaces, both *s* and *p*-polarizations have non-zero components in the electric field and vibrations in any direction (*x*, *y*, *z*) in respect to the surface can be detected. The optimal sensitivity of the absorption bands is observed at incidence angles of 60–80° (*p*-polarization) and close to the surface normal (*s*-polarization). Furthermore, both positive and negative absorption bands can occur in the infrared spectra from a semiconductor or non-conductor, depending on the angle of the incidence beam with respect to the Brewster angle. With *p*-polarization, a maximum positive absorbance occurs just below the Brewster angle and maximum negative absorbance just above the Brewster angle. For *s*-polarization only negative absorbance occurs and is at a maximum at the normal angle of incidence. The presence of the positive or negative absorption bands in the spectra can provide information on the orientation of molecules in thin surface films [17].

3. Results and discussion

Atomic force microscopy (AFM) was used to investigate the adsorption of DPC at the steel surface. Fig. 3 shows images of the untreated (plain) steel (A) and DPC-treated steel (B) with a surface film of a well-defined structure. It should be noted that the roughness of the untreated steel is approximately 0.45 μm. This may have implications for the infrared analysis as the surface roughness affects the local incidence angle of the infrared beam, as discussed previously.

The formation of the surface layer began immediately after immersion of the steel to the DPC-containing solution (1). The layer

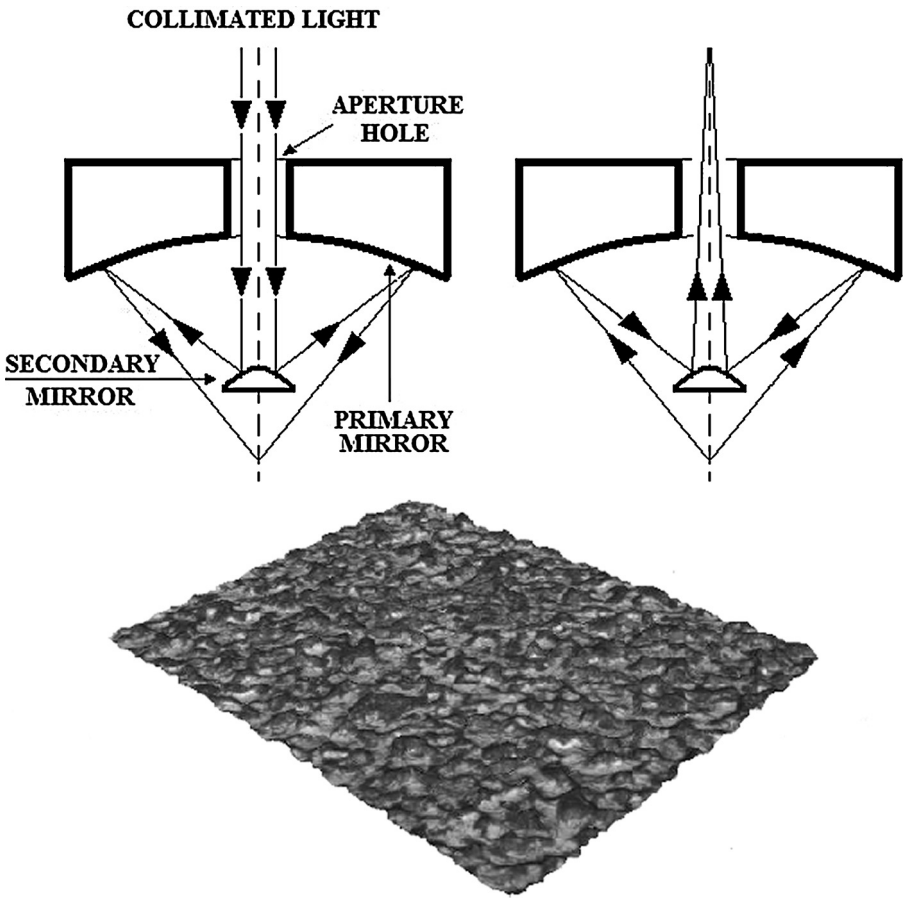

Fig. 2. Schematic presentation of reverse Cassegrain design objective used in analysis of topographically rough steel surface. The surface shown is a representative version of the highly complex corroded surface.

was fully formed after approximately 3 h exposure (shown in Fig. 3) and no further changes in its structure were observed. The AFM results clearly demonstrate that DPC adsorbs at the steel surface and that the surface film can be prepared by solution-deposition.

The presence of DPC at the steel surface is further confirmed by linear polarization resistance analysis carried out in the presence and absence of the DPC in the corrosive testing solution (2). The respective corrosion rates measured in the presence and absence of DPC after 3 h exposure (consistent with the AFM data) were 1.9 and 4.9 mm y^{-1}, equivalent to 61% surface coverage with DPC. After 24 h immersion, the surface coverage increased to final value of 72%, calculated from the stabilized corrosion rates of 1.1 and 3.9 mm y^{-1}.

3.1. Infrared spectral analysis of DPC-deposited non-corroded steel

Fig. 4 shows infrared spectra from the untreated (plain) steel, bulk DPC powder and DPC-deposited non-corroded steel. Spectrum A is from the untreated steel and it is used as a background spectrum. It clearly shows that background contamination does not give rise to any spectral features. Spectrum B represents bulk powder of 1-dodecylpyridinium chloride hydrate (DPC). The absorption bands below 1650 cm^{-1} and in the region 3100–3010 cm^{-1} can be assigned to vibrations of the pyridinium ring and the aliphatic chain in the DPC molecule. The pyridinium ring C—H stretches occur between 3086 cm^{-1} and 3008 cm^{-1} and have medium intensity.

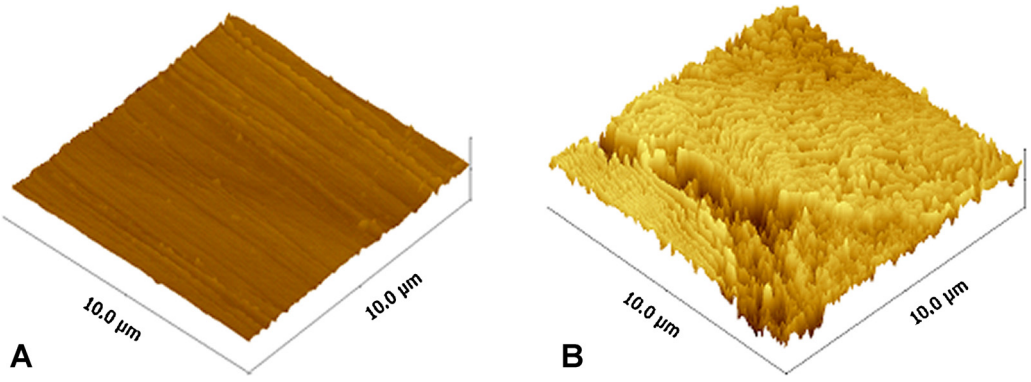

Fig. 3. AFM images of untreated (plain) steel (A) and DPC-deposited non-corroded steel (B).

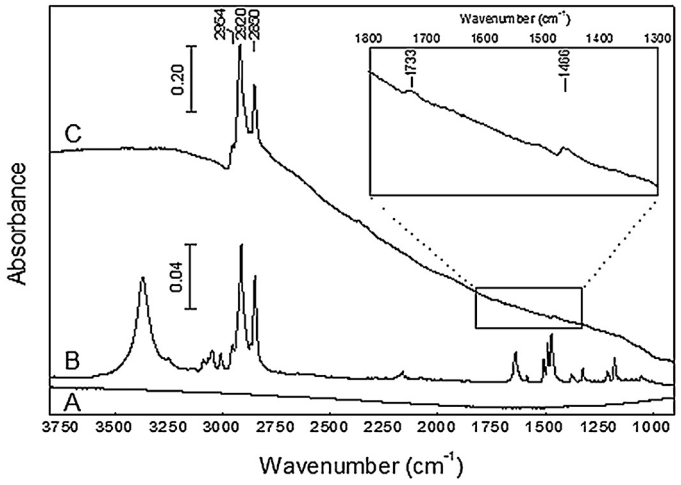

Fig. 4. Synchrotron infrared reflectance spectra of untreated steel (background spectrum, (A)), DPC powder (B) and DPC-deposited non-corroded steel (C). Band assignments are given in Table 1. Spectra are off-set for clarity.

The strong absorption bands at 2915 cm^{-1} and 2848 cm^{-1} represent C—H antisymmetric and symmetric stretching vibrations of the CH_2 groups of the aliphatic chain, respectively. The less intense absorption band at 2952 cm^{-1} is assigned to antisymmetric stretching of the CH_3 group of the aliphatic chain. The 3370 cm^{-1} band can be attributed to the O-H stretch of the water of crystallization of the hydrated form of DPC used [19]. A detailed assignment of the absorption bands of the DPC molecule below 1650 cm^{-1} is included in Table 1. Spectrum C is obtained from the DPC-deposited non-corroded steel. All the spectra obtained at more than 50 randomly selected measurement points at non-corroded steel and non-corroded areas of corroded samples were near identical in positions and relative intensities of the main absorption bands, suggesting that the micro-roughness of the surface did not influence these spectra. The most intense absorption bands are characteristic of CH_2 antisymmetric and symmetric stretching (2920 cm^{-1} and 2850 cm^{-1}) of the aliphatic chain of the DPC molecule. The CH_3 antisymmetric stretching (2954 cm^{-1}) is also evident. Much less intense absorption bands (inset in Fig. 4) were found below 1800 cm^{-1}. The band at 1466 cm^{-1} is attributed to aliphatic chain C—H deformation vibrations (antisymmetric) and/or —CH_2— scissor vibrations [19]. The absorption band at 1733 cm^{-1} was detected at non-corroded areas of corroded samples and is attributed to C=O stretching vibrations of carbonic acid (H_2CO_3) and/or bicarbonate (HCO_3^-) [20] adsorbed at the steel surface treated in CO_2 media [21]. Overall, the absorption bands in spectrum C are attributed to the DPC molecule and confirm its presence at the steel surface. It is important to note that the C—H stretching vibrations of the pyridine ring in the DPC molecule, typically found in the wavelength region 3100–3000 cm^{-1}, were not observed in spectrum C from the DPC-deposited non-corroded steel. The C=C and C=N stretches of the ring at 1636 cm^{-1} and 1585 cm^{-1} were also not observed. As *s*-polarization has zero electric field intensity at a conductor surface, the positive absorbance bands observed in spectrum C are due to incident *p*-polarization radiation interacting with a molecule adsorbed on steel.

Table 1
Assignment of absorption bands shown in Fig. 4 from 1-dodecylpyridinium chloride hydrate (DPC) powder (spectrum B) and DPC-deposited non-corroded steel (marked with "*") (spectrum C) [19,20].

Wavenumber (cm^{-1})	Band assignment
1178, 1211	Pyridine ring C—H deformation vibrations (in-plane)
1325, 1377	Aliphatic chain C—H symmetric deformation vibrations
1466*	Aliphatic chain C—H antisymmetric deformation vibrations Aliphatic chain —CH_2— scissor vibration band
1471–1506	Pyridine ring stretching vibrations (C=C and C=N) Aliphatic chain —CH_2— scissor vibration band
1585, 1636	Pyridine ring stretching vibrations (in plane, C=C and C=N)
1733*	C=O stretching vibrations of carbonic acid (H_2CO_3) and/or bicarbonate ion (HCO_3^-)
2848 (2850*)	Aliphatic chain C—H symmetric stretching of CH_2 group
2915 (2920*)	Aliphatic chain C—H antisymmetric stretching of CH_2 group
2952 (2954*)	Aliphatic chain C—H antisymmetric stretching of CH_3 group
3008–3086	Pyridine ring C—H stretching vibrations
3370	O—H stretching, water of crystallization

It is worth noting that we have been unable to obtain meaningful spectra using a conventional (glow bar) infrared source and grazing angle accessory. Presumably because over to 25 mm × 50 mm area used in those attempts the samples are either too rough or not sufficiently flat, or both, or the source has insufficient intensity. These are not an issue with a 20 μm × 20 μm microscope aperture and ~8 μm synchrotron beam. A focal plane array FTIR microscope with aperture size of 100 μm × 100 μm and a conventional infrared source allowed detection of the absorption bands at the corroded steel surface. The spectral features obtained from these measurements were analogous to those shown in spectrum C in Fig. 4 and confirmed the presence of DPC at the surface.

3.1.1. *Proposed orientation of DPC molecules at the steel surface*

The spectrum of the DPC-deposited non-corroded substrate (Fig. 4C) was compared to that obtained from the bulk DPC compound (Fig. 4B) in order to determine the orientation of DPC at the steel surface. The absorption bands of the pyridinium ring would be expected in the regions below 1650 cm^{-1} and above 3010 cm^{-1}. However, the absorption bands detected in the region studied (3800–800 cm^{-1}) at the DPC-deposited steel surface are solely due to the aliphatic chain and out-of-plane C—H ring vibrations of the DPC molecule. The absence of absorption bands characteristic of in-plane vibrations of the pyridinium ring indicates that this part of the molecule is oriented flat (face-on/parallel) to the steel surface. In such an arrangement, the dipole transition moments of the aromatic C—H and pyridine ring stretches are parallel to the steel substrate, in which case no infrared absorption is observed.

The adsorption mechanism, resulting in a flat orientation of the pyridinium ring at the substrate, can be explained by π-electron interaction between the aromatic ring and the iron substrate and/or by π-electrostatic interaction of the negatively charged steel surface and positively charged pyridinium ion, that can be enhanced by halide ions pre-adsorbed at the substrate [10–12]. The proposed orientation of the aromatic ring of the DPC molecule at the steel substrate is consistent with literature published on the adsorption mechanism and orientation of pyridine and pyridinium compounds at modified metallic surfaces under similar conditions, mainly investigated with SERS [10–12,22].

The data in Fig. 4 also provides information on the orientation of the aliphatic chain of the DPC molecule in relation to the steel substrate. The presence and intensity of both the CH_2 symmetric and antisymmetric stretching vibrations in the spectra indicates that the aliphatic chain is tilted upwards from the steel substrate but is not perpendicular to it because a perpendicular aliphatic chain (in relation to the substrate) would result in absorption by the antisymmetrical C—H stretching only [23]. The weak band at 1466 cm^{-1} (Fig. 4C) appears due to some parts of the chain giving a CH_2 deformation dipole change normal to the surface.

Additional information on the tilt angle between the aliphatic chain axis and the steel (and therefore the pyridinium ring oriented parallel to the substrate) can be derived from a comparison of the absorbance intensities of the aliphatic chain bands. A constant relative ratio of the absorption intensities of the aliphatic chain bands would imply a specific orientation of the aliphatic chain within the adsorbed layer relative to the steel surface [23,24]. In the current work, the ratio of the intensities of the CH_2 antisymmetric and symmetric vibrations were almost identical at all measurement points. The absorption bands and their relative intensities were also found to be almost identical to the spectra of the pure DPC compound (Fig. 4B). This suggests that there is a similar orientation of the aliphatic chain within the adsorbed layer on this microscopically rough surface as in DPC crystals. The crystallography of the pure DPC compound shows that the structure relationship between the planes of aromatic rings and the aliphatic chain is 79.16°, with a mean deviation of 0.005 Å [25]. This orientation of the chains is thus most likely to be the one that occurs in the DPC layer adsorbed at the steel substrate (Fig. 5).

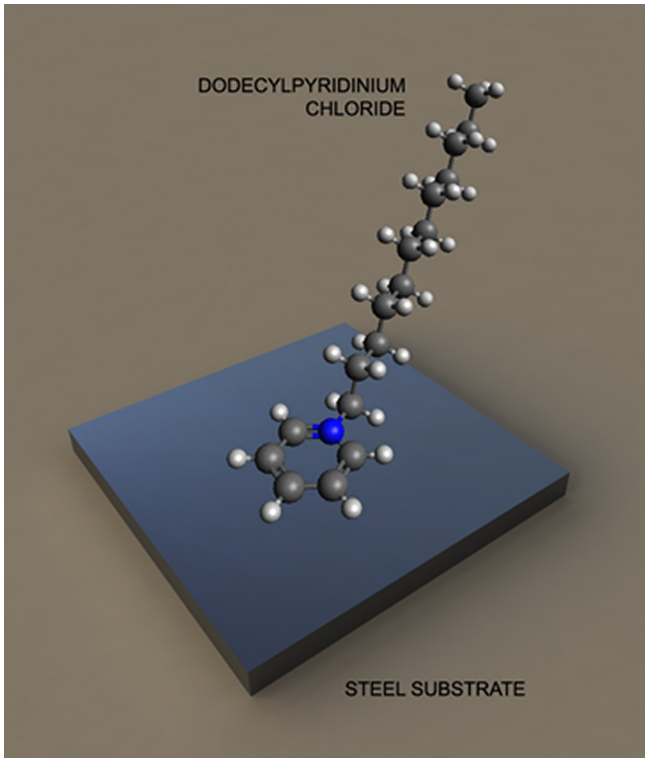

Fig. 5. Schematic presentation of the proposed orientation of the 1-dodecylpyridinium chloride molecule at the steel substrate.

3.2. Infrared spectral analysis of DPC-deposited corroded steel

Fig. 6 shows a microscope image of the DPC-deposited steel corroded in CO_2-saturated brine and the corresponding infrared spectra recorded at the analysis points indicated on the image. The surface is heterogeneous as a result of dissolution of the metal and/or the formation of the corrosion products, in addition to the DPC-deposition at the surface. More extensive corrosion appears at the darker area (surface inclusion) of the image (around measurement points 1–4) which is generally associated with high surface roughness. The roughness values (R_q) were approximately 0.53 μm at the less corroded areas and up to 1.28 μm at the more corroded areas (surface inclusions). The number, position and intensity ratios of the absorption bands from the corroded steel are essentially identical to those recorded from the non-corroded steel (Fig. 4C). The absorption bands at 2954, 2920 and 2850 cm^{-1} (Fig. 6) are therefore again assigned to the DPC molecule at the steel surface. These results also suggest that the orientation of the DPC molecule at the surface is relatively unaffected by the degree of corrosion and that the proposed orientation, involving π-interaction between the pyridinium ring and the surface, applies to the DPC-deposited corroded steels.

The data in Fig. 6 show that the amount of adsorbed DPC varies across the studied surface. The higher absorbances recorded at the more corroded analysis areas (1–4) are indicative of a greater DPC adsorption than that which occurs on the less corroded analysis area (5–9). The greater DPC adsorption can be associated with the higher surface roughness and/or the preferable adsorption of DPC to corrosion products at the more corroded areas. The formation of iron oxide/hydroxide/carbonate species can be expected in carbon dioxide media [26,27] but in this study no absorption bands characteristic of corrosion products are evident in the spectra in Fig. 6 nor observed in the 1800–800 cm^{-1} region. More interestingly, one of the spectra (4) in Fig. 6 showed negative absorbance bands.

Polarization of the infrared beam and its angle of incidence with respect to the Brewster angle define whether positive or negative spectra are observed. The effect of surface topography and

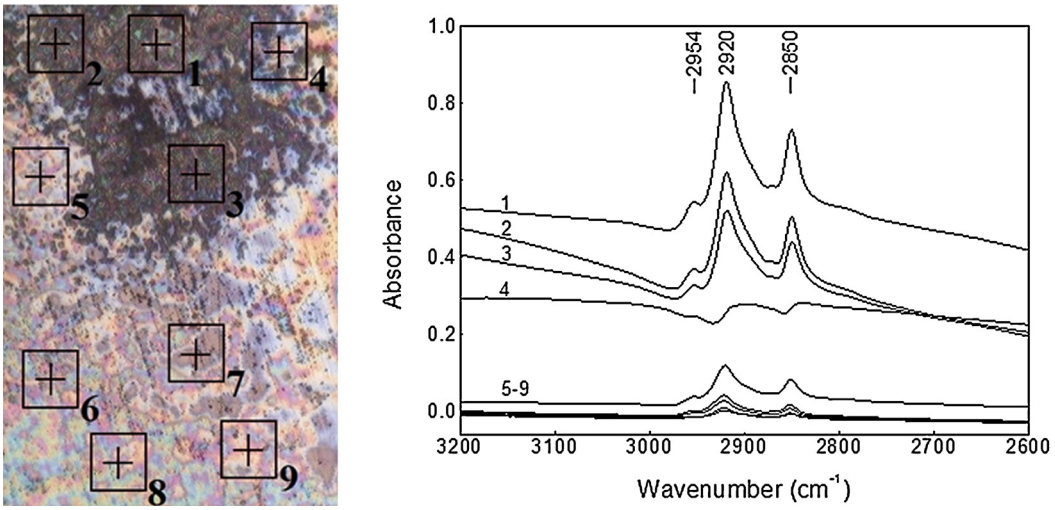

Fig. 6. Microscope image of DPC-deposited corroded steel with marked analysis points (20 μm × 20 μm) and the corresponding infrared reflectance spectra. Spectra are shown as recorded.

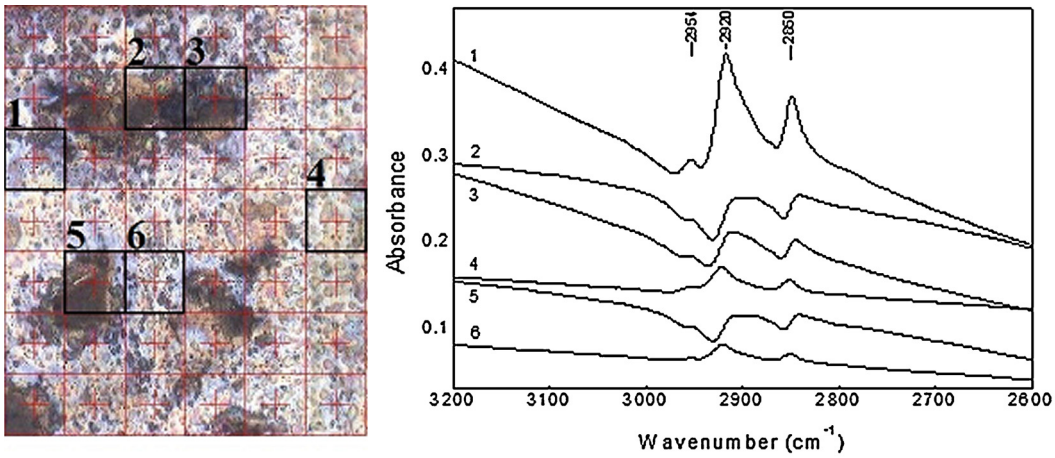

Fig. 7. Microscope image of DPC-deposited corroded steel with marked analysis points (20 μm × 20 μm) and the corresponding infrared reflectance spectra, positive (1, 4, 6) and negative (2, 3, 5). Spectra are off-set for clarity.

reflectivity on the appearance of the positive or negative absorption bands is further demonstrated in Fig. 7, which shows the grid map of analysis points of a larger area of the DPC-deposited corroded steel compared to that in Fig. 6. It was found that positive spectra (analysis points 1, 4 and 6) are recorded across almost the entire surface irrespective of the degree of corrosion, whereas the negative spectra (analysis points 2, 3 and 5) are specific to the more corroded areas (surface inclusions) or their close proximity. The appearance of both the positive and negative spectra at the more corroded areas can be explained by a combined effect of having both conductor (steel) and non-conductor (corrosion products) and a wider variation in the local angle of incidence as a function of increased roughness. The positive bands arise from the interaction of the *p*-polarized radiation with DPC adsorbed at a steel (conducting surface). The negative bands arise from the interaction of *p*-polarized radiation at angles greater than the Brewster angle, or *s*-polarized radiation, with DPC adsorbed on corrosion products (non-conducting). As we did not observe any in-plane C—H stretches nor in-plane pyridine ring vibrations it suggests that the negative bands arise from *p*-polarized radiation.

The observation of negative and positive infrared bands for corroded steel surfaces is analogous to variable angle polarized infrared beam measurements with a plane surface. In this instance it definitively confirms the π-bonded adsorption orientation of DPC on steel indicated by the non-corroded surface data. This orientation most probably also occurs on the corrosion products.

4. Conclusions

Synchrotron infrared microspectroscopy has been applied to study the adsorption of 1-dodecylpyridinium chloride (DPC) on non-corroded mild steel and mild steel corroded in carbon dioxide media. These complex surfaces represent real-life systems and are used to demonstrate the applicability of the infrared method to the analysis of organic film at a microscopically rough metal surface. Infrared spectra, analogous to polarized grazing angle spectra at varying angles of incidence were recorded. Positive and negative absorption intensities are observed at different measurement locations. These intensity changes are interpreted in terms of optical effects, their variation due to the uneven topography of the surface and a change from conductor to non-conductor substrates.

The presence of DPC at the steel surface is confirmed by the C—H stretching vibrations of the CH_2 and CH_3 groups of the aliphatic chain in the infrared spectra. The proposed surface orientation of DPC is derived from the presence and absence of absorption bands characteristic of the aliphatic chain and pyridinium ring, respectively, in the infrared spectra. The pyridinium ring of the DPC molecule is oriented flat at the surface and its aliphatic chain is tilted upwards from the substrate at ∼79°, i.e. not perpendicular to it. The DPC adsorption mechanism proposed involves π-electron interaction between the aromatic ring and the steel substrate.

Acknowledgments

This research was undertaken on the Infrared microspectroscopy beamline at the Australian Synchrotron, Clayton, Australia. The assistance of Dr. Mark Tobin and Dr. Danielle Martin is greatly acknowledged. The authors thank Curtin University for a Curtin Research Fellowship (K. L.) and a Curtin International Postgraduate Research Scholarship (V. P.).

References

[1] R. Atkin, V.S.J. Craig, E.J. Wanless, S. Biggs, Advances in Colloid and Interface Science 103 (3) (2003) 219–304.
[2] C.C. Nathan, Corrosion Inhibitors, National Association of Corrosion Engineers, Houston, TX, 1981.
[3] W. Durnie, R. de Marco, A. Jefferson, B. Kinsella, Journal of The Electrochemical Society 146 (5) (1999) 1751–1756.
[4] S.A. Francis, A.H. Ellison, Journal of the Optical Society of America 49 (2) (1959) 131–138.
[5] R.G. Greenler, Journal of Chemical Physics 44 (1) (1966) 310–315.
[6] P.R. Griffiths, J.A. de Haseth, Fourier Transform Infrared Spectrometry. Chemical Analysis, vol. 83, J. Wiley & Sons, NY, 1986.
[7] A. Frigani, F. Zucchi, C. Monticelli, British Corrosion Journal 18 (1) (1983) 19–24.
[8] C.C. Nathan, in: C.C. Nathan (Ed.), Corrosion Inhibitors, National Association of Corrosion Engineers, Houston, TX, 1981, pp. 42–54.
[9] H. Yamada, Y. Yamamoto, Surface Science 134 (1) (1983) 71–90.
[10] K. Aramaki, J. Uehara, Journal of the Electrochemical Society 136 (5) (1989) 1299–1303.
[11] K. Aramaki, M. Ohi, J. Uehara, Journal of the Electrochemical Society 139 (6) (1992) 1525–1529.
[12] J. Uehara, H. Nishihara, K. Aramaki, Journal of the Electrochemical Society 137 (9) (1990) 2677–2683.
[13] ASTM G102-89, Standard Practice for Calculation of Corrosion Rates and Related Information from Electrochemical Measurements, ASTM International, 2010.
[14] G. Santoro, I. Yousef, F. Jamme, P. Dumas, G. Ellis, Review of Scientific Instruments 82 (2011) 033710.
[15] G. Ellis, M.A. Gomez, C. Marco, Journal of Macromolecular Science, Part B: Physics 43 (1) (2005) 191–206.
[16] G. Ellis, C. Marco, M. Gomez, Infrared Physics & Technology 45 (2004) 349–364.
[17] J.A. Mielczarski, Journal of Physical Chemistry A 97 (11) (1993) 2649–2663.
[18] G.T. Merklin, P.R. Griffiths, The Journal of Physical Chemistry B 101 (1997) 7408–7413.
[19] G. Socrates, Infrared Characteristic Group Frequencies. Tables and Charts, 2nd edn., J. Wiley & Sons, Chichester, 1994.

[20] W. Hage, A. Hallbrucker, E. Mayer, Journal of the American Chemical Society 115 (1993) 8427.
[21] A. Wieckowski, E. Ghali, M. Szklarczyk, J. Sobkowski, Electrochimica Acta 28 (1983) 1619.
[22] W. Durnie, R. de Marco, A. Jefferson, B. Kinsella, Surface and Interface Analysis 35 (6) (2003) 536–543.
[23] G.A. Salensky, M.G. Cobb, E.S. Everhart, Industrial and Engineering Chemistry – Product Research Development 25 (2) (1986) 133–140.
[24] W.G. Golden, C.D. Snyder, B. Smith, Journal of Physical Chemistry A 86 (24) (1982) 4675–4678.
[25] K. Vongbupnimit, K. Noguchi, K. Okuyama, Acta Crystallographica C51 (1995) 1940–1941.
[26] M.B. Kermani, A. Moshed, Corrosion 59 (8) (2003) 659–683.
[27] R. de Marco, Z.-T. Jiang, B. Pejcic, E. Poinen, Journal of the Electrochemical Society 152 (10) (2005) B389–B392.

Appendix 4 - Copyright Statements

The rights granted by NACE International to reproduce the published material that form **Chapter II and Chapter III** of this thesis.

The rights granted by Elsevier to reproduce the published material that forms **Chapter IV**.

The rights granted by Electrochemical Society to reproduce the publication that forms **Chapter V**.

The rights granted by Elsevier to reproduce the published material in **Appendix 3**.

Permission to Publish NACE International Copyrighted Paper/Article

NACE International
1440 South Creek Drive
Houston, TX 77084
Tel: 281-228-6219
Fax: 281-228-6319

Date: 26/04/2013

Name: Vedapriya Pandarinathan Title: Miss.

Company ("Publisher"): Curtin University

Address: Kent Street, Bentley, Perth, Western Australia - 6845.

Tel: +61425118815 Fax: +61892667221

Email: v.pandarinathan@curtin.edu.au

Publication Media: PhD Thesis

Circle the source: *Materials Performance* *CORROSION* (Conference Paper) Standards

Paper/Article Title: Impact of mineral deposits on CO_2 corrosion of carbon steel

Conference Paper No: C2013-2579 Year: 2013

Authors: V. Pandarinathan, K. Lepková, S. I. Bailey, R. Gubner

NACE International ("NACE") hereby grants to "Publisher" the right to publish the Work utilizing the Publication Media elected above. To the extent the Publication Media is a Periodical, the publication right is limited to publication in the specific Issue identified above of the Periodical identified above and this right shall automatically terminate upon the date of issue of the particular Issue of the Periodical, whether or not such Work is actually published. To the extent the Publication Media is a Web Site, the publication right is limited to publication at the specific Web Site identified above. Any right granted herein is a limited, non-transferable, non-exclusive right. No other rights in the Work are granted herein. The Publisher agrees to hold NACE harmless and indemnify NACE against any and all legal action and expenses arising out of the Publisher's use and editing of NACE material.

Notwithstanding the foregoing, Publisher may edit or otherwise modify the Work as reasonably necessary to accommodate the style and size requirements of the specific publication so long as the published Work that will appear in the Publication remains substantially similar to the original Work. Any such permitted edit or modification shall maintain the integrity of the overall original Work.

Publisher shall obtain a copy of the original Work directly from NACE International and shall not utilize copies of the Work from other sources, including the author(s). Publisher shall include on the published version of the Work the names of all authors listed on the original Work.

The Publisher shall include the following applicable Copyright notation with any publication of the Work:*

A. Conference Paper
Reproduced with permission from NACE International, Houston, TX. All rights reserved. Paper NUMBER presented at CORROSION/YEAR, City, State. © NACE International YEAR.

B. Magazine/Journal Article
Reproduced with permission from NACE International, Houston, TX. All rights reserved. Published in the MONTH, YEAR issue of JOURNAL. © NACE International YEAR.

C. Standards
STANDARDS/TECHNICAL COMMITTEE REPORT NAME. © NACE International YEAR. All rights reserved by NACE. Reprinted with permission. NACE standards are revised periodically. Users are cautioned to obtain the latest edition; information in an outdated version of the standard may not be accurate.

* Modifications to Notations: Other reference wording can be used, but must be approved by NACE in writing *in advance*.

As between NACE and Publisher, Publisher acknowledges that NACE owns all rights in the Works. Publisher shall not be entitled to any compensation for its efforts in promoting the Work.

THE WORK IS PROVIDED "AS IS." ALL EXPRESS OR IMPLIED COVENANTS, CONDITIONS, REPRESENTATIONS OR WARRANTIES, INCLUDING ANY IMPLIED WARRANTY OF MERCHANTABILITY OR FITNESS FOR A PARTICULAR PURPOSE OR CONDITIONS OF ACCURACY, COMPLETENESS OR QUALITY AND THOSE ARISING BY STATUTE OR OTHERWISE IN LAW, ARE HEREBY DISCLAIMED.

IN NO EVENT WILL NACE BE LIABLE FOR ANY DIRECT, INDIRECT, PUNITIVE, SPECIAL, INCIDENTAL OR CONSEQUENTIAL DAMAGES IN CONNECTION WITH OR RELATED TO THIS AGREEMENT (INCLUDING LOSS OF PROFITS, USE, DATA, OR OTHER ECONOMIC ADVANTAGE), HOWSOEVER ARISING.

This Agreement and the rights granted herein may be terminated immediately by NACE upon breach of this Agreement by Publisher. Unless earlier terminated, this Agreement and the rights granted herein will automatically terminate 6 months from the Date set forth above. If the Work has not been published within that time period, a new Agreement must be obtained.

Publisher may not, directly or indirectly, sell, assign, sublicense, lease, rent, distribute, or otherwise transfer this Agreement or any rights granted herein, without the prior written consent of NACE.

If any provision of this Agreement is found to be unenforceable, then this Agreement shall be deemed to be amended by modifying such provision to the extent necessary to make it legal and enforceable while preserving its intent. The remainder of this Agreement shall not be affected by such modification.

This Agreement does not create, and shall not be construed to create, any employer-employee, joint venture or partnership relationship between the parties. No officer, employee, agent, servant or independent contractor of either party shall at any time be deemed to be an employee, servant, agent or contractor of any other party for any purpose whatsoever.

This Agreement shall be governed by, and construed and enforced in accordance with, the laws of the State of Texas, without regard to the choice of law provisions of that State.

This Agreement shall only be effective if signed by authorized representatives of both parties. This Agreement constitutes the entire Agreement between the parties with respect to the subject matter of this Agreement. Any change, modification or waiver hereto must be in writing and signed by authorized representatives of both parties.

Other Terms & Conditions: _____

Publisher hereby requests permission to publish the paper/article described above and agrees to comply with all Terms and Conditions listed above.

Request submitted by:

Vedapriya Pandarinathan
Printed Name

Miss
Title


Signature

26/04/2013
Date

Request approved by NACE:

Brenda Mitz
Printed Name

Books Coordinator
Title

Linda Mitz
Signature

April 26, 2013
Date

Request agreed to by:

Vedapriya Pandarinathan
Lead Author Printed Name

Miss.
Lead Author Title


Lead Author Signature

26/04/2013
Date

Permission to Publish NACE International Copyrighted Paper/Article

NACE International
1440 South Creek Drive
Houston, TX 77084
Tel: 281-228-6219
Fax: 281-228-6319

Date: 26/04/2013

Name: Vedapriya Pandarinathan Title: Miss.

Company ("Publisher"): Curtin University

Address: Kent Street, Bentley, Perth, Western Australia - 6845

Tel: +61425118815 Fax: +61892667221

Email: v.pandarinathan@curtin.edu.au

Publication Media: PhD Thesis

Circle the source: *Materials Performance* *CORROSION* (Conference Paper) Standards

Paper/Article Title: Inhibition of CO_2 corrosion of 1030 carbon steel beneath sand-deposits

Conference Paper No: C2011-11261 Year: 2011

Authors: V. Pandarinathan, K. Lepková, R. Gubner

NACE International ("NACE") hereby grants to "Publisher" the right to publish the Work utilizing the Publication Media elected above. To the extent the Publication Media is a Periodical, the publication right is limited to publication in the specific Issue identified above of the Periodical identified above and this right shall automatically terminate upon the date of issue of the particular Issue of the Periodical, whether or not such Work is actually published. To the extent the Publication Media is a Web Site, the publication right is limited to publication at the specific Web Site identified above. Any right granted herein is a limited, non-transferable, non-exclusive right. No other rights in the Work are granted herein. The Publisher agrees to hold NACE harmless and indemnify NACE against any and all legal action and expenses arising out of the Publisher's use and editing of NACE material.

Notwithstanding the foregoing, Publisher may edit or otherwise modify the Work as reasonably necessary to accommodate the style and size requirements of the specific publication so long as the published Work that will appear in the Publication remains substantially similar to the original Work. Any such permitted edit or modification shall maintain the integrity of the overall original Work.

Publisher shall obtain a copy of the original Work directly from NACE International and shall not utilize copies of the Work from other sources, including the author(s). Publisher shall include on the published version of the Work the names of all authors listed on the original Work.

The Publisher shall include the following applicable Copyright notation with any publication of the Work:*

A. Conference Paper
Reproduced with permission from NACE International, Houston, TX. All rights reserved. Paper NUMBER presented at CORROSION/YEAR, City, State. © NACE International YEAR.

B. Magazine/Journal Article
Reproduced with permission from NACE International, Houston, TX. All rights reserved. Published in the MONTH, YEAR issue of JOURNAL. © NACE International YEAR.

C. Standards
STANDARDS/TECHNICAL COMMITTEE REPORT NAME. © NACE International YEAR. All rights reserved by NACE. Reprinted with permission. NACE standards are revised periodically. Users are cautioned to obtain the latest edition; information in an outdated version of the standard may not be accurate.

* Modifications to Notations: Other reference wording can be used, but must be approved by NACE in writing *in advance*.

As between NACE and Publisher, Publisher acknowledges that NACE owns all rights in the Works. Publisher shall not be entitled to any compensation for its efforts in promoting the Work.

THE WORK IS PROVIDED "AS IS." ALL EXPRESS OR IMPLIED COVENANTS, CONDITIONS, REPRESENTATIONS OR WARRANTIES, INCLUDING ANY IMPLIED WARRANTY OF MERCHANTABILITY OR FITNESS FOR A PARTICULAR PURPOSE OR CONDITIONS OF ACCURACY, COMPLETENESS OR QUALITY AND THOSE ARISING BY STATUTE OR OTHERWISE IN LAW, ARE HEREBY DISCLAIMED.

IN NO EVENT WILL NACE BE LIABLE FOR ANY DIRECT, INDIRECT, PUNITIVE, SPECIAL, INCIDENTAL OR CONSEQUENTIAL DAMAGES IN CONNECTION WITH OR RELATED TO THIS AGREEMENT (INCLUDING LOSS OF PROFITS, USE, DATA, OR OTHER ECONOMIC ADVANTAGE), HOWSOEVER ARISING.

This Agreement and the rights granted herein may be terminated immediately by NACE upon breach of this Agreement by Publisher. Unless earlier terminated, this Agreement and the rights granted herein will automatically terminate 6 months from the Date set forth above. If the Work has not been published within that time period, a new Agreement must be obtained.

Publisher may not, directly or indirectly, sell, assign, sublicense, lease, rent, distribute, or otherwise transfer this Agreement or any rights granted herein, without the prior written consent of NACE.

If any provision of this Agreement is found to be unenforceable, then this Agreement shall be deemed to be amended by modifying such provision to the extent necessary to make it legal and enforceable while preserving its intent. The remainder of this Agreement shall not be affected by such modification.

This Agreement does not create, and shall not be construed to create, any employer-employee, joint venture or partnership relationship between the parties. No officer, employee, agent, servant or independent contractor of either party shall at any time be deemed to be an employee, servant, agent or contractor of any other party for any purpose whatsoever.

This Agreement shall be governed by, and construed and enforced in accordance with, the laws of the State of Texas, without regard to the choice of law provisions of that State.

This Agreement shall only be effective if signed by authorized representatives of both parties. This Agreement constitutes the entire Agreement between the parties with respect to the subject matter of this Agreement. Any change, modification or waiver hereto must be in writing and signed by authorized representatives of both parties.

Other Terms & Conditions: _____

Publisher hereby requests permission to publish the paper/article described above and agrees to comply with all Terms and Conditions listed above.

Request submitted by:

Vedapriya Pandarinathan
Printed Name

Miss
Title


Signature

26/04/2013
Date

Request approved by NACE:

Brenda Nitz
Printed Name

Books Coordinator
Title


Signature

April 26, 2013
Date

Request agreed to by:

Vedapriya Pandarinathan
Lead Author Printed Name

Miss.
Lead Author Title


Lead Author Signature

26/04/2013
Date

ELSEVIER LICENSE
TERMS AND CONDITIONS

Jul 03, 2013

This is a License Agreement between vedapriya pandarinathan ("You") and Elsevier ("Elsevier") provided by Copyright Clearance Center ("CCC"). The license consists of your order details, the terms and conditions provided by Elsevier, and the payment terms and conditions.

All payments must be made in full to CCC. For payment instructions, please see information listed at the bottom of this form.

Supplier	Elsevier Limited The Boulevard,Langford Lane Kidlington,Oxford,OX5 1GB,UK
Registered Company Number	1982084
Customer name	vedapriya pandarinathan
Customer address	40 A, Marchamley Street, Carlisle Perth, 6101
License number	3181231009199
License date	Jul 03, 2013
Licensed content publisher	Elsevier
Licensed content publication	Corrosion Science
Licensed content title	Evaluation of corrosion inhibition at sand-deposited carbon steel in CO2-saturated brine
Licensed content author	Vedapriya Pandarinathan,Kateřina Lepková,Stuart I. Bailey,Rolf Gubner
Licensed content date	July 2013
Licensed content volume number	72
Licensed content issue number	
Number of pages	10
Start Page	108
End Page	117
Type of Use	reuse in a thesis/dissertation
Portion	full article
Format	electronic
Are you the author of this Elsevier article?	Yes
Will you be translating?	No
Order reference number	
Title of your thesis/dissertation	Investigation of inhibition processes at sand-deposited surfaces

Expected completion date	Oct 2013
Estimated size (number of pages)	150
Elsevier VAT number	GB 494 6272 12
Permissions price	0.00 USD
VAT/Local Sales Tax	0.00 USD / 0.00 GBP
Total	0.00 USD
Terms and Conditions	

INTRODUCTION

1. The publisher for this copyrighted material is Elsevier. By clicking "accept" in connection with completing this licensing transaction, you agree that the following terms and conditions apply to this transaction (along with the Billing and Payment terms and conditions established by Copyright Clearance Center, Inc. ("CCC"), at the time that you opened your Rightslink account and that are available at any time at http://myaccount.copyright.com).

GENERAL TERMS

2. Elsevier hereby grants you permission to reproduce the aforementioned material subject to the terms and conditions indicated.

3. Acknowledgement: If any part of the material to be used (for example, figures) has appeared in our publication with credit or acknowledgement to another source, permission must also be sought from that source. If such permission is not obtained then that material may not be included in your publication/copies. Suitable acknowledgement to the source must be made, either as a footnote or in a reference list at the end of your publication, as follows:

"Reprinted from Publication title, Vol /edition number, Author(s), Title of article / title of chapter, Pages No., Copyright (Year), with permission from Elsevier [OR APPLICABLE SOCIETY COPYRIGHT OWNER]." Also Lancet special credit - "Reprinted from The Lancet, Vol. number, Author(s), Title of article, Pages No., Copyright (Year), with permission from Elsevier."

4. Reproduction of this material is confined to the purpose and/or media for which permission is hereby given.

5. Altering/Modifying Material: Not Permitted. However figures and illustrations may be altered/adapted minimally to serve your work. Any other abbreviations, additions, deletions and/or any other alterations shall be made only with prior written authorization of Elsevier Ltd. (Please contact Elsevier at permissions@elsevier.com)

6. If the permission fee for the requested use of our material is waived in this instance, please be advised that your future requests for Elsevier materials may attract a fee.

7. Reservation of Rights: Publisher reserves all rights not specifically granted in the combination of (i) the license details provided by you and accepted in the course of this licensing transaction, (ii) these terms and conditions and (iii) CCC's Billing and Payment terms and conditions.

8. License Contingent Upon Payment: While you may exercise the rights licensed immediately upon issuance of the license at the end of the licensing process for the transaction, provided that you have

disclosed complete and accurate details of your proposed use, no license is finally effective unless and until full payment is received from you (either by publisher or by CCC) as provided in CCC's Billing and Payment terms and conditions. If full payment is not received on a timely basis, then any license preliminarily granted shall be deemed automatically revoked and shall be void as if never granted. Further, in the event that you breach any of these terms and conditions or any of CCC's Billing and Payment terms and conditions, the license is automatically revoked and shall be void as if never granted. Use of materials as described in a revoked license, as well as any use of the materials beyond the scope of an unrevoked license, may constitute copyright infringement and publisher reserves the right to take any and all action to protect its copyright in the materials.

9. Warranties: Publisher makes no representations or warranties with respect to the licensed material.

10. Indemnity: You hereby indemnify and agree to hold harmless publisher and CCC, and their respective officers, directors, employees and agents, from and against any and all claims arising out of your use of the licensed material other than as specifically authorized pursuant to this license.

11. No Transfer of License: This license is personal to you and may not be sublicensed, assigned, or transferred by you to any other person without publisher's written permission.

12. No Amendment Except in Writing: This license may not be amended except in a writing signed by both parties (or, in the case of publisher, by CCC on publisher's behalf).

13. Objection to Contrary Terms: Publisher hereby objects to any terms contained in any purchase order, acknowledgment, check endorsement or other writing prepared by you, which terms are inconsistent with these terms and conditions or CCC's Billing and Payment terms and conditions. These terms and conditions, together with CCC's Billing and Payment terms and conditions (which are incorporated herein), comprise the entire agreement between you and publisher (and CCC) concerning this licensing transaction. In the event of any conflict between your obligations established by these terms and conditions and those established by CCC's Billing and Payment terms and conditions, these terms and conditions shall control.

14. Revocation: Elsevier or Copyright Clearance Center may deny the permissions described in this License at their sole discretion, for any reason or no reason, with a full refund payable to you. Notice of such denial will be made using the contact information provided by you. Failure to receive such notice will not alter or invalidate the denial. In no event will Elsevier or Copyright Clearance Center be responsible or liable for any costs, expenses or damage incurred by you as a result of a denial of your permission request, other than a refund of the amount(s) paid by you to Elsevier and/or Copyright Clearance Center for denied permissions.

LIMITED LICENSE

The following terms and conditions apply only to specific license types:

15. **Translation**: This permission is granted for non-exclusive world **English** rights only unless your license was granted for translation rights. If you licensed translation rights you may only translate this content into the languages you requested. A professional translator must perform all translations and reproduce the content word for word preserving the integrity of the article. If this license is to re-use 1 or 2 figures then permission is granted for non-exclusive world rights in all languages.

16. **Website**: The following terms and conditions apply to electronic reserve and author websites:
Electronic reserve: If licensed material is to be posted to website, the web site is to be password-protected and made available only to bona fide students registered on a relevant course if:
This license was made in connection with a course,
This permission is granted for 1 year only. You may obtain a license for future website posting,
All content posted to the web site must maintain the copyright information line on the bottom of each image,
A hyper-text must be included to the Homepage of the journal from which you are licensing at http://www.sciencedirect.com/science/journal/xxxxx or the Elsevier homepage for books at http://www.elsevier.com , and
Central Storage: This license does not include permission for a scanned version of the material to be stored in a central repository such as that provided by Heron/XanEdu.

17. **Author website** for journals with the following additional clauses:

All content posted to the web site must maintain the copyright information line on the bottom of each image, and the permission granted is limited to the personal version of your paper. You are not allowed to download and post the published electronic version of your article (whether PDF or HTML, proof or final version), nor may you scan the printed edition to create an electronic version.
A hyper-text must be included to the Homepage of the journal from which you are licensing at http://www.sciencedirect.com/science/journal/xxxxx . As part of our normal production process, you will receive an e-mail notice when your article appears on Elsevier's online service ScienceDirect (www.sciencedirect.com). That e-mail will include the article's Digital Object Identifier (DOI). This number provides the electronic link to the published article and should be included in the posting of your personal version. We ask that you wait until you receive this e-mail and have the DOI to do any posting.

Central Storage: This license does not include permission for a scanned version of the material to be stored in a central repository such as that provided by Heron/XanEdu.

18. **Author website** for books with the following additional clauses:
Authors are permitted to place a brief summary of their work online only.
A hyper-text must be included to the Elsevier homepage at http://www.elsevier.com . All content posted to the web site must maintain the copyright information line on the bottom of each image.
You are not allowed to download and post the published electronic version of your chapter, nor may you scan the printed edition to create an electronic version.

Central Storage: This license does not include permission for a scanned version of the material to be stored in a central repository such as that provided by Heron/XanEdu.

19. **Website** (regular and for author): A hyper-text must be included to the Homepage of the journal from which you are licensing at http://www.sciencedirect.com/science/journal/xxxxx. or for books to the Elsevier homepage at http://www.elsevier.com

20. **Thesis/Dissertation**: If your license is for use in a thesis/dissertation your thesis may be submitted to your institution in either print or electronic form. Should your thesis be published commercially, please reapply for permission. These requirements include permission for the Library and Archives of Canada to supply single copies, on demand, of the complete thesis and include permission for UMI to supply single copies, on demand, of the complete thesis. Should your thesis

be published commercially, please reapply for permission.

21. **Other Conditions**:

v1.6

If you would like to pay for this license now, please remit this license along with your payment made payable to "COPYRIGHT CLEARANCE CENTER" otherwise you will be invoiced within 48 hours of the license date. Payment should be in the form of a check or money order referencing your account number and this invoice number RLNK501057262. Once you receive your invoice for this order, you may pay your invoice by credit card. Please follow instructions provided at that time.

Make Payment To:
Copyright Clearance Center
Dept 001
P.O. Box 843006
Boston, MA 02284-3006

For suggestions or comments regarding this order, contact RightsLink Customer Support: customercare@copyright.com or +1-877-622-5543 (toll free in the US) or +1-978-646-2777.

Gratis licenses (referencing $0 in the Total field) are free. Please retain this printable license for your reference. No payment is required.

Request for Permission to Reproduce or Re-Publish ECS Material

Please fax this form to: The Electrochemical Society (ECS), Attn: Permissions Requests, 1.609.730.0629. You may also e-mail your request to: copyright@electrochem.org. Include all the information as required on this form. Please allow 3-7 days for your request to be processed.

I am preparing a (choose one): ☐ paper ☐ chapter ☐ book ☑ thesis

entitled: INVESTIGATION OF INHIBITION PROCESSES AT SAND-DEPOSITED SURFACE

to be published by: CURTIN UNIVERSITY, AUSTRALIA

in an upcoming publication entitled: _____

I request permission to use the following material in the publication noted above, and request nonexclusive rights for all subsequent editions and in all foreign language translations for distribution throughout the world.

Description of material to be used—Indicate what material you wish to use (figures, tables, text, etc.) and give the full bibliographic reference for the source publication. You may attach a separate list, organized by ECS title.

FULL ARTICLE

"INHIBITION OF UNDER-DEPOSIT CORROSION OF CARBON STEEL BY THIOBENZAMIDE" J. ELECTROCHEM. SOC., 2013, VOLUME 160, ISSUE 9, C432-C440

AUTHORS: VEDAPRIYA PANDARINATHAN, KATERINA LEPKOVA, STUART I. BAILEY, ROLF GUBNER

Signature: Ved P Date: 2/08/2013

Name: VEDAPRIYA PANDARINATHAN

Address: DEPARTMENT OF CHEMISTRY, CURTIN UNIVERSITY, G.P.O BOX U1987, KENT STREET, BENTLEY, PERTH WA 6845, AUSTRALIA

Telephone: +61 8 9266 2063 Fax: +61 8 9266 7221

E-mail: V.pandarinathan@curtin.edu.au

Permission is granted to include the above-referenced paper in your thesis, provided that you obtain permission of the other individual authors. In the thesis, please acknowledge the authors and the citation given above, and include the words: "Reproduced by permission of ECS — The Electrochemical Society."

Aug. 5, 2013 Ann F Goedkoop

Date Ann F. Goedkoop, Director of Publications

ELSEVIER LICENSE
TERMS AND CONDITIONS

Nov 09, 2013

This is a License Agreement between vedapriya pandarinathan ("You") and Elsevier ("Elsevier") provided by Copyright Clearance Center ("CCC"). The license consists of your order details, the terms and conditions provided by Elsevier, and the payment terms and conditions.

All payments must be made in full to CCC. For payment instructions, please see information listed at the bottom of this form.

Supplier	Elsevier Limited The Boulevard,Langford Lane Kidlington,Oxford,OX5 1GB,UK
Registered Company Number	1982084
Customer name	vedapriya pandarinathan
Customer address	40 A, Marchamley Street, Carlisle Perth, 6101
License number	3265151296942
License date	Nov 09, 2013
Licensed content publisher	Elsevier
Licensed content publication	Vibrational Spectroscopy
Licensed content title	Synchrotron infrared microspectroscopy study of the orientation of an organic surfactant on a microscopically rough steel surface
Licensed content author	Kateřina Lepková,Wilhelm van Bronswijk,Vedapriya Pandarinathan,Rolf Gubner
Licensed content date	September 2013
Licensed content volume number	68
Licensed content issue number	
Number of pages	8
Start Page	204
End Page	211
Type of Use	reuse in a thesis/dissertation
Portion	full article
Format	electronic
Are you the author of this Elsevier article?	Yes
Will you be translating?	No
Title of your thesis/dissertation	Investigation of inhibition processes at sand-deposited surfaces
Expected completion date	Nov 2013

Estimated size (number of pages)	150
Elsevier VAT number	GB 494 6272 12
Permissions price	0.00 USD
VAT/Local Sales Tax	0.00 USD / 0.00 GBP
Total	0.00 USD
Terms and Conditions	

INTRODUCTION

1. The publisher for this copyrighted material is Elsevier. By clicking "accept" in connection with completing this licensing transaction, you agree that the following terms and conditions apply to this transaction (along with the Billing and Payment terms and conditions established by Copyright Clearance Center, Inc. ("CCC"), at the time that you opened your Rightslink account and that are available at any time at http://myaccount.copyright.com).

GENERAL TERMS

2. Elsevier hereby grants you permission to reproduce the aforementioned material subject to the terms and conditions indicated.

3. Acknowledgement: If any part of the material to be used (for example, figures) has appeared in our publication with credit or acknowledgement to another source, permission must also be sought from that source. If such permission is not obtained then that material may not be included in your publication/copies. Suitable acknowledgement to the source must be made, either as a footnote or in a reference list at the end of your publication, as follows:

"Reprinted from Publication title, Vol /edition number, Author(s), Title of article / title of chapter, Pages No., Copyright (Year), with permission from Elsevier [OR APPLICABLE SOCIETY COPYRIGHT OWNER]." Also Lancet special credit - "Reprinted from The Lancet, Vol. number, Author(s), Title of article, Pages No., Copyright (Year), with permission from Elsevier."

4. Reproduction of this material is confined to the purpose and/or media for which permission is hereby given.

5. Altering/Modifying Material: Not Permitted. However figures and illustrations may be altered/adapted minimally to serve your work. Any other abbreviations, additions, deletions and/or any other alterations shall be made only with prior written authorization of Elsevier Ltd. (Please contact Elsevier at permissions@elsevier.com)

6. If the permission fee for the requested use of our material is waived in this instance, please be advised that your future requests for Elsevier materials may attract a fee.

7. Reservation of Rights: Publisher reserves all rights not specifically granted in the combination of (i) the license details provided by you and accepted in the course of this licensing transaction, (ii) these terms and conditions and (iii) CCC's Billing and Payment terms and conditions.

8. License Contingent Upon Payment: While you may exercise the rights licensed immediately upon issuance of the license at the end of the licensing process for the transaction, provided that you have disclosed complete and accurate details of your proposed use, no license is finally effective unless and until full payment is received from you (either by publisher or by CCC) as provided in CCC's

Billing and Payment terms and conditions. If full payment is not received on a timely basis, then any license preliminarily granted shall be deemed automatically revoked and shall be void as if never granted. Further, in the event that you breach any of these terms and conditions or any of CCC's Billing and Payment terms and conditions, the license is automatically revoked and shall be void as if never granted. Use of materials as described in a revoked license, as well as any use of the materials beyond the scope of an unrevoked license, may constitute copyright infringement and publisher reserves the right to take any and all action to protect its copyright in the materials.

9. Warranties: Publisher makes no representations or warranties with respect to the licensed material.

10. Indemnity: You hereby indemnify and agree to hold harmless publisher and CCC, and their respective officers, directors, employees and agents, from and against any and all claims arising out of your use of the licensed material other than as specifically authorized pursuant to this license.

11. No Transfer of License: This license is personal to you and may not be sublicensed, assigned, or transferred by you to any other person without publisher's written permission.

12. No Amendment Except in Writing: This license may not be amended except in a writing signed by both parties (or, in the case of publisher, by CCC on publisher's behalf).

13. Objection to Contrary Terms: Publisher hereby objects to any terms contained in any purchase order, acknowledgment, check endorsement or other writing prepared by you, which terms are inconsistent with these terms and conditions or CCC's Billing and Payment terms and conditions. These terms and conditions, together with CCC's Billing and Payment terms and conditions (which are incorporated herein), comprise the entire agreement between you and publisher (and CCC) concerning this licensing transaction. In the event of any conflict between your obligations established by these terms and conditions and those established by CCC's Billing and Payment terms and conditions, these terms and conditions shall control.

14. Revocation: Elsevier or Copyright Clearance Center may deny the permissions described in this License at their sole discretion, for any reason or no reason, with a full refund payable to you. Notice of such denial will be made using the contact information provided by you. Failure to receive such notice will not alter or invalidate the denial. In no event will Elsevier or Copyright Clearance Center be responsible or liable for any costs, expenses or damage incurred by you as a result of a denial of your permission request, other than a refund of the amount(s) paid by you to Elsevier and/or Copyright Clearance Center for denied permissions.

LIMITED LICENSE

The following terms and conditions apply only to specific license types:

15. **Translation**: This permission is granted for non-exclusive world **English** rights only unless your license was granted for translation rights. If you licensed translation rights you may only translate this content into the languages you requested. A professional translator must perform all translations and reproduce the content word for word preserving the integrity of the article. If this license is to re-use 1 or 2 figures then permission is granted for non-exclusive world rights in all languages.

16. **Website**: The following terms and conditions apply to electronic reserve and author websites:
Electronic reserve: If licensed material is to be posted to website, the web site is to be

password-protected and made available only to bona fide students registered on a relevant course if:
This license was made in connection with a course,
This permission is granted for 1 year only. You may obtain a license for future website posting,
All content posted to the web site must maintain the copyright information line on the bottom of each image,
A hyper-text must be included to the Homepage of the journal from which you are licensing at http://www.sciencedirect.com/science/journal/xxxxx or the Elsevier homepage for books at http://www.elsevier.com , and
Central Storage: This license does not include permission for a scanned version of the material to be stored in a central repository such as that provided by Heron/XanEdu.

17. **Author website** for journals with the following additional clauses:

All content posted to the web site must maintain the copyright information line on the bottom of each image, and the permission granted is limited to the personal version of your paper. You are not allowed to download and post the published electronic version of your article (whether PDF or HTML, proof or final version), nor may you scan the printed edition to create an electronic version.
A hyper-text must be included to the Homepage of the journal from which you are licensing at http://www.sciencedirect.com/science/journal/xxxxx . As part of our normal production process, you will receive an e-mail notice when your article appears on Elsevier's online service ScienceDirect (www.sciencedirect.com). That e-mail will include the article's Digital Object Identifier (DOI). This number provides the electronic link to the published article and should be included in the posting of your personal version. We ask that you wait until you receive this e-mail and have the DOI to do any posting.

Central Storage: This license does not include permission for a scanned version of the material to be stored in a central repository such as that provided by Heron/XanEdu.

18. **Author website** for books with the following additional clauses:
Authors are permitted to place a brief summary of their work online only.
A hyper-text must be included to the Elsevier homepage at http://www.elsevier.com . All content posted to the web site must maintain the copyright information line on the bottom of each image.
You are not allowed to download and post the published electronic version of your chapter, nor may you scan the printed edition to create an electronic version.

Central Storage: This license does not include permission for a scanned version of the material to be stored in a central repository such as that provided by Heron/XanEdu.

19. **Website** (regular and for author): A hyper-text must be included to the Homepage of the journal from which you are licensing at http://www.sciencedirect.com/science/journal/xxxxx. or for books to the Elsevier homepage at http://www.elsevier.com

20. **Thesis/Dissertation**: If your license is for use in a thesis/dissertation your thesis may be submitted to your institution in either print or electronic form. Should your thesis be published commercially, please reapply for permission. These requirements include permission for the Library and Archives of Canada to supply single copies, on demand, of the complete thesis and include permission for UMI to supply single copies, on demand, of the complete thesis. Should your thesis be published commercially, please reapply for permission.

21. **Other Conditions**:

v1.6

If you would like to pay for this license now, please remit this license along with your payment made payable to "COPYRIGHT CLEARANCE CENTER" otherwise you will be invoiced within 48 hours of the license date. Payment should be in the form of a check or money order referencing your account number and this invoice number RLNK501155451. Once you receive your invoice for this order, you may pay your invoice by credit card. Please follow instructions provided at that time.

Make Payment To:
Copyright Clearance Center
Dept 001
P.O. Box 843006
Boston, MA 02284-3006

For suggestions or comments regarding this order, contact RightsLink Customer Support: customercare@copyright.com or +1-877-622-5543 (toll free in the US) or +1-978-646-2777.

Gratis licenses (referencing $0 in the Total field) are free. Please retain this printable license for your reference. No payment is required.

Appendix 5 - Written statements from the co-authors of the publications forming the chapters in this thesis.

To Whom It May Concern,

I, Vedapriya Pandarinathan, contributed by conducting the research, interpreting and writing up the results reported in the publication entitled "**Impact of mineral deposits on CO_2 corrosion of carbon steel**".

Signature of Candidate

I, as a Co-Author, endorse that this level of contribution by the candidate indicated above is appropriate.

Kateřina Lepková	
Full Name of Co-Author 1	Signature of Co-Author 1
Stuart I. Bailey	
Full Name of Co-Author 2	Signature of Co-Author 2
Rolf Gubner	
Full Name of Co-Author 3	Signature of Co-Author 3

To Whom It May Concern,

I, Vedapriya Pandarinathan, contributed by conducting the research, interpreting and writing up the results reported in the publication entitled "**Inhibition of CO_2 corrosion of 1030 carbon steel beneath sand-deposits**".

Signature of Candidate

I, as a Co-Author, endorse that this level of contribution by the candidate indicated above is appropriate.

Kateřina Lepková
Full Name of Co-Author 1

Signature of Co-Author 1

Rolf Gubner
Full Name of Co-Author 2

Signature of Co-Author 2

To Whom It May Concern,

I, Vedapriya Pandarinathan, contributed by conducting the research, interpreting and writing up the results reported in the publication entitled "**Evaluation of corrosion inhibition at sand-deposited carbon steel in CO_2-saturated brine**".

Signature of Candidate

I, as a Co-Author, endorse that this level of contribution by the candidate indicated above is appropriate.

Kateřina Lepková
Full Name of Co-Author 1

Signature of Co-Author 1

Stuart I. Bailey
Full Name of Co-Author 2

Signature of Co-Author 2

Rolf Gubner
Full Name of Co-Author 3

Signature of Co-Author 3

To Whom It May Concern,

I, Vedapriya Pandarinathan, contributed by conducting the research, interpreting and writing up the results reported in the publication entitled "**Inhibition of under-deposit corrosion of carbon steel by thiobenzamide**".

Signature of Candidate

I, as a Co-Author, endorse that this level of contribution by the candidate indicated above is appropriate.

Kateřina Lepková
Full Name of Co-Author 1

Signature of Co-Author 1

Stuart I. Bailey
Full Name of Co-Author 2

Signature of Co-Author 2

Rolf Gubner
Full Name of Co-Author 3

Signature of Co-Author 3

To Whom It May Concern,

I, Vedapriya Pandarinathan, contributed by conducting the research, interpreting and writing up the results reported in the submitted manuscript entitled "**Chukanovite ($Fe_2(OH)_2CO_3$) identified as corrosion product at sand-deposited carbon steel in CO_2-saturated brine**".

Signature of Candidate

I, as a Co-Author, endorse that this level of contribution by the candidate indicated above is appropriate.

Kateřina Lepková
Full Name of Co-Author 1

Signature of Co-Author 1

Wilhelm van Bronswijk
Full Name of Co-Author 2

Signature of Co-Author 2

To Whom It May Concern,

I, Vedapriya Pandarinathan, contributed by conducting the research, interpreting and writing up the results reported in the manuscript under review entitled "**Adsorption of corrosion inhibitor 1-dodecylpyridinium chloride on carbon steel surface by *in-situ* AFM and electrochemical methods**".

Signature of Candidate

I, as a Co-Author, endorse that this level of contribution by the candidate indicated above is appropriate.

Kateřina Lepková
Full Name of Co-Author 1

Signature of Co-Author 1

Stuart I. Bailey
Full Name of Co-Author 2

Signature of Co-Author 2

Thomas Becker
Full Name of Co-Author 3

Signature of Co-Author 3

Rolf Gubner
Full Name of Co-Author 4

Signature of Co-Author 4

To Whom It May Concern,

I, Vedapriya Pandarinathan, contributed by conducting the research, interpreting and writing up the results reported in the publication entitled "***In-situ* electrochemical AFM study of CO_2 corrosion of carbon steel**".

Signature of Candidate

I, as a Co-Author, endorse that this level of contribution by the candidate indicated above is appropriate.

Kateřina Lepková
Full Name of Co-Author 1

Signature of Co-Author 1

Thomas Becker
Full Name of Co-Author 2

Signature of Co-Author 2

Rolf Gubner
Full Name of Co-Author 3

Signature of Co-Author 3